Structural elucidation of Microcystins [DMAdda^{5}]MC-LR and [DMAdda^{5}]MC-LHar by Nuclear Magnetic Resonance spectroscopy

Kristian Wiedicke Trovik

Thesis submitted for the degree of
Master of Science in Organic Chemistry
30 credits

Department of Chemistry
Faculty of Mathematics and Science

UNIVERSITY OF OSLO

12 / 2018

2018

Structural elucidation of Microcystins [DMAdda^{5}]MC-LR and [DMAdda^{5}]MC-LHar by Nuclear Magnetic Resonance Spectroscopy

Kristian Wiedicke Trovik

http://www.duo.uio.no/

Print: Reprosentralen, University of Oslo

Abstract

Multiple NMR techniques were utilized in an attempt to determine the complete structure of two low concentration samples. The atom sequence was determined, but the bulk of NOE-data remains to be interpreted. The atom sequences for sample 1 and 2 respectively indicate that they contain [DMAdda^{5}]MC-LR and [DMAdda^{5}]MC-LHar.

Preface

The presented work was performed at the Department of Chemistry at the University of Oslo from August 2018 to December 2018.

I would like to take this opportunity to express my gratitude towards my supervisors Prof. Frode Rise and Prof.Em. Alistair L. Wilkins as well as Ph.D. Cristopher O. Miles for making this project possible. Your continued support, guidance, availability and willingness to answer my questions has taught me so much about the scientific process, has made the project fun and has made me a more competent spectroscopist with a sense of achievement.

I would like to thank Amanda Foss for providing me with the materials used in the project.

I would like to thank Ph.D. Per Eugen Kristiansen for numerous fruitful consultations regarding the project and the opportunity to learn about new IT-tools which may be utilized in structure elucidation.

I am grateful to the staff for maintaining the NMR Lab and thus making the project possible.

Finally I would like express gratitude to my family and friends who have supported me throughout my degree.

I'm truly grateful for the joint effort of so many individuals and organizations to facilitate this degree.

Kristian Wiedicke Trovik, 24.12.2018

Abbreviations

AA	amino acid
COSY	correlation spectroscopy
DEPT	distortionless enhancement by polarization transfer
DEPTQ	distortionless enhancement by polarization transfer with retention of quaternaries
DIPSI-2	decoupling in the presence of scalar interaction
ES	excitation sculpting
FID	free induction decay
GARP	globally-optimised, alternating-phase rectangular pulses
HMBC	heteronuclear multiple-bond correlation
HSQC	heteronuclear single quantum correlation
INEPT	insensitive nuclei enhanced by polarization transfer
NMR	nuclear magnetic resonance
MC	microcystin
Mdha	N-Methyl dehydroalanine
MLEV	Malcolm Levitt's composite-pulse decoupling
NOE	nuclear Overhauser effect
NS	number of scans
ppm	parts per million
PFG	pulsed field gradient
PR	continuous wave presaturation

Preset NOESY	presaturated nuclear Overhauser spectroscopy
ROESY	rotating-frame nuclear Overhauser effect
SelTOCSY	selective total correlation spectroscopy
SelROESY	selective rotating-frame nuclear Overhauser effect spectroscopy
TD	time domain
TOCSY	total correlation spectroscopy
TMS	tetamethylsilane
WALTZ	wideband, alternating-phase, low-power technique for residual splitting
WATERGATE	water suppression by gradient-tailored excitation
WDW	window function
WHO	World Health Organization

Table of contents

1 Introduction

Blue-green algae has been a concern for drinking water and irrigation supplies for decades, reaching back to at least 1974 where Schindler did an experiment to determine which nutrients produced microflora that turned lakes green.[1-4] The green color is arises from the presence cyanobacteria[5] and is a symptom of eutrophication.[6-10] However it is not the bacteria itself that is harmful, but the toxins they create. Most notably; microsystins (MCs) and nodularins. Blooms of cyanobacteria have occurred all over the world[11-17] and has caused the death of many people[5], livestock (and fish)[2, 8, 13, 14, 18, 19] and wildlife[6, 17] which has resulted in the endangerment of Lesser Flamingo (*Phoeniconaias minor*).[8, 17] MCs are known to inhibit protein phosphatase I and II2A[9, 13, 14, 16, 17, 20, 21], suspected of promoting liver tumor formation[5, 6, 13] and having carcinogenic effects.[5, 13] Thus the World Health Organization (WHO) has issued a guideline of 1 µg/L[13], however numerous published works show that the analytical methods used do not account for the many different MCs with non-uniform toxicity and being vulnerable to false positives and negatives, making the true toxicity still undetermined.[3, 4, 8, 18, 22] The state of Ohio has been criticized for misinterpretation or over interpretation of the guideline.[23] WHO's report from 1999 states that "the implications of protein phosphatase inhibition in humans, due to low level chronic exposure to microcystins are not known" and most studies are based on mouse or phosphatase bioassay with a thousand factor applied to the no-observed-adverse-effect level.[13, 23] Thus there has been great effort to determine the toxicity of MCs. At least 243 different MCs have been reported.[24] They are cyclopeptides consisting of seven amino acids (AA), where the two and four position frequently exchanges, but are always L-type AAs.[25]

Many analytical tools have been utilized to determine presence, nature of and toxicity of the different MC species, however all methods are with drawbacks such as time, cost, limit of detection, limit of quantification and discrimination between MCs.[3, 8, 26] Nuclear magnetic resonance (NMR) spectroscopy may be a good analytical tool to differentiate between MCs and elucidate their exact structure and configuration. This elucidation is beneficial to scientists seeking to exploit the similar and/or different properties of MCs or determine its toxicity. Thus the aim of the thesis is to elucidate the structure of a set of samples containing isolated MCs.

2 Theory

2.1 NMR

2.1.1 Spin in NMR

NMR spectroscopy is a bundle of spectroscopic methods that exploit spin properties to elucidate structure of chemical compounds. Spin is an intrinsic property of fermions[27] and is best understood with quantum theory, but can be described using classical mechanics. This text will utilize both sets of theory.

All nuclei have a spin quantum number, *I*, which is a half integer equal to or greater than 0. It may be used to determine the amount of quantized spin states a fermion may inhabit and is exploited when placed in a magnetic field. The amount of spin states is determined by eq 1.

$$No.of\ spin\ states = 2I + 1 \tag{1}$$

All spin-states for fermions are multiples of ½. Every nucleus discussed in this thesis possess I = ½, meaning the available spin states are +½ or -½ unless otherwise specified. Nuclei with I = 0 possess no spin and are termed 'NMR silent'. These nuclei are isotopes with even atom number and atomic mass.

Nuclei possess charge and an angular momentum, which gives rise to the magnetic moment, μ. Those of interest are those with more than one spin state and are thus not NMR silent. Their operator and mathematical relation is given in eq. 2, where γ is the magnetogyric ratio and $\hat{I}$ is the operator for nuclear-spin angular momentum. The magnetogyric ratio is constant for any given nucleus. When such a nucleus is placed in a static magnetic field, the spin will align parallel or anti-parallel to it. Parallel and anti-parallel are respectively appointed (and termed) +½ (α) and -½ (β).

$$\hat{\mu} = \gamma\hat{I} \tag{2}$$

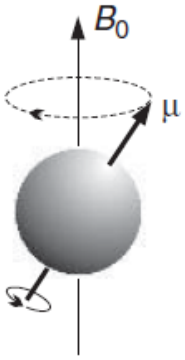

Figure 1: Nucleus with spin quantum number ½ in a static magnetic field, B_0, which applies a torque the magnetic moment, μ to produce Larmor precession. The circular path that the tip of the μ-vector exhibit is indicated by the dashed circle.

When nuclei are placed in a magnetic field, they arrange themselves relative to the field. Then Larmor precession ensues. This can be described in terms of classical mechanics. The static field applies a torque on the moment, making the tip of the magnetic vector take a circular path orthogonal to the static magnetic field. Such movement of a vector, as a whole, is known as precession, but in NMR the movement of the magnetic vector is more precisely termed the Larmor precession. The motion may be clockwise or anti-clockwise, but is always the same for any given nuclide. The movement is shown in figure 1. The Larmor precession may be described as a fluctuation and is then given in Hz and termed Larmor frequency (ν). The angular velocity (ω in rad s^{-1}) determines the rate of precession. Their relation is shown in eq. 3.[27]

$$\omega = -\gamma B_0 \quad \text{or} \quad \nu = \frac{\gamma B_0}{2\pi} \tag{3}$$

The Hamiltonian is the energy operator and is given in eq 4 for a magnetic field along the z-axis. The operator for nuclear-spin angular momentum in the z-direction: $\hat{I}_z = m_I \hbar$.[27]

$$\hat{H} = -\gamma B_0 \hat{I}_z = -\gamma B_0 m_I \hbar \tag{4}$$

The energy of the nuclei is dependent on the magnetic field and the gyromagnetic ratio. Their relation is shown in eq. 5, where h is Planck's constant and$\hbar = (h/2\pi)$.[27]

$$E_{m_I} = h\nu m_I = \frac{h\gamma B_0 m_I}{2\pi} = \hbar\gamma B_0 m_I \tag{5}$$

The α- and β-nuclei are lower and higher in energy relative to each other. The energy is given by eqs 6 and the energy difference, ΔE_{m_I}, is thus:

$$\Delta E_{m_I} = E_{-1/2} - E_{+1/2} \qquad \text{or} \qquad \Delta E_{m_I} = E_\beta - E_\alpha \tag{6}$$

By substituting E_{m_I} of eq. 6 for both spin states with E_{m_I} from eq. 5, eq. 7 is produced.

$$\Delta E_{m_I} = \tfrac{1}{2}\gamma\hbar B_0 - \left(-\tfrac{1}{2}\gamma\hbar B_0\right) = \gamma\hbar B_0 \tag{7}$$

Because of this energy difference, the states are not equally populated. They are Boltzmann distributed (eq. 8).

$$\frac{N_\alpha}{N_\beta} = e^{\Delta E_{ml}/k_B T} \tag{8}$$

$N_{\alpha,\beta}$ represents the number of nuclei in the spin orientation, k_B the Boltzmann constant, T the temperature in Kelvin. Due to the small energy difference between states, the population is very similar across states. This makes NMR insensitive relative to other spectroscopic methods as it is the population difference that gives rise to signals in an NMR spectrum. The population difference will be in the α-state's favor. From eq. 7 and 8 it is shown which parameters affect the population ratio and effect by their manipulation. The energy difference trend, arising from the magnetic field, between α and β is illustrated in figure 2. Temperature is not illustrated.[27]

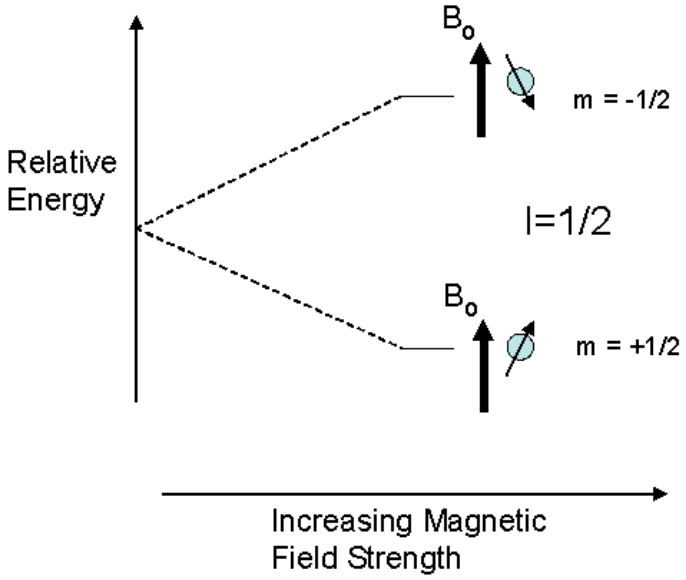

Figure 2: The energy difference between nuclei possessing two spin states, +½ and –½, is shown to increase with increasing field strength. It is also depicted that the spin aligned against the magnetic field is higher in energy relative to the other spin state.

2.1.2 Chemical shift and multiplicity/fine structure

Chemical shift

Not all nuclei resonate at the same frequency. The nuclei are surrounded (shielded) by core and valence electrons. Shielding is conventionally written as in eq 9.

$$\delta B = -\sigma B_0 \tag{9}$$

In a magnetic field, the valence electrons are caused to circulate which generates a counter magnetic field that interacts with the static magnetic field. Opposing and complying interaction caused by the resulting current is respectively called diamagnetic (σ_d) and paramagnetic (σ_p) contribution:

$$\sigma_{local} = \sigma_d + \sigma_p \tag{10}$$

The sum of which is termed the local contribution. With an empirical approach, the shielding constant (σ) is the sum of the local, neighbor and solvent contribution:

$$\sigma = \sigma_{local} + \sigma_{neighbor} + \sigma_{solvent} \tag{11}$$

This causes the nuclei to experience slightly different magnetic (chemical) environments. The total local magnetic field is given in eq 12.

$$B_{loc} = B_0 + \delta B = B_0 - \sigma B_0 = (1 - \sigma)B_0 \tag{12}$$

From eq 13 the nuclear Larmor frequency of a nuclide becomes:

$$\nu = \frac{\gamma B_0}{2\pi}(1 - \sigma) \tag{13}$$

Eq 13 describes the different environments make the nuclei resonate at different frequencies. [27]

The measurement of a nucleus' frequency is hard to measure, thus it is common practice to add a reference compound to the sample and all frequencies are measured relative to the reference compound. To make spectral data between instruments of different magnetic field strength more easily interpretable, the frequencies are treated as in eq 14 where the entities;

ν_{shift}, δ and $\nu_{spectrometer\ frequency}$ are given in, respectively, units of Hz, parts per million (ppm) and MHz.

$$\delta = \frac{\Delta\nu_{shift}}{\nu_{spectrometer\ frequency}} = \frac{\nu_{sample}-\nu_{ref}}{\nu_{ref}}10^6 \qquad (14)$$

The δ-values are uniform for all NMR instruments. The standard reference compound is tetamethylsilane (TMS) and is set to 0 ppm. A signal's δ-value is known as its chemical shift. By substituting eq 13 into 14 it becomes apparent that chemical shift increases with decreasing shielding as shown in eq 15.[28]

$$\delta = \frac{\nu_{sample}-\nu_{ref}}{\nu_{ref}}10^6 = \frac{\frac{\gamma B_0}{2\pi}[(1-\sigma_{sample})-(1-\sigma_{ref})]}{\frac{\gamma B_0}{2\pi}(1-\sigma_{ref})}10^6 = \frac{\sigma_{ref}-\sigma_{sample}}{1-\sigma_{ref}}10^6 \qquad (15)$$

An overview of typical chemical shift values for ^{1}H-NMR and ^{13}C-NMR in $CDCl_3$ is given in figure 3 and 4:

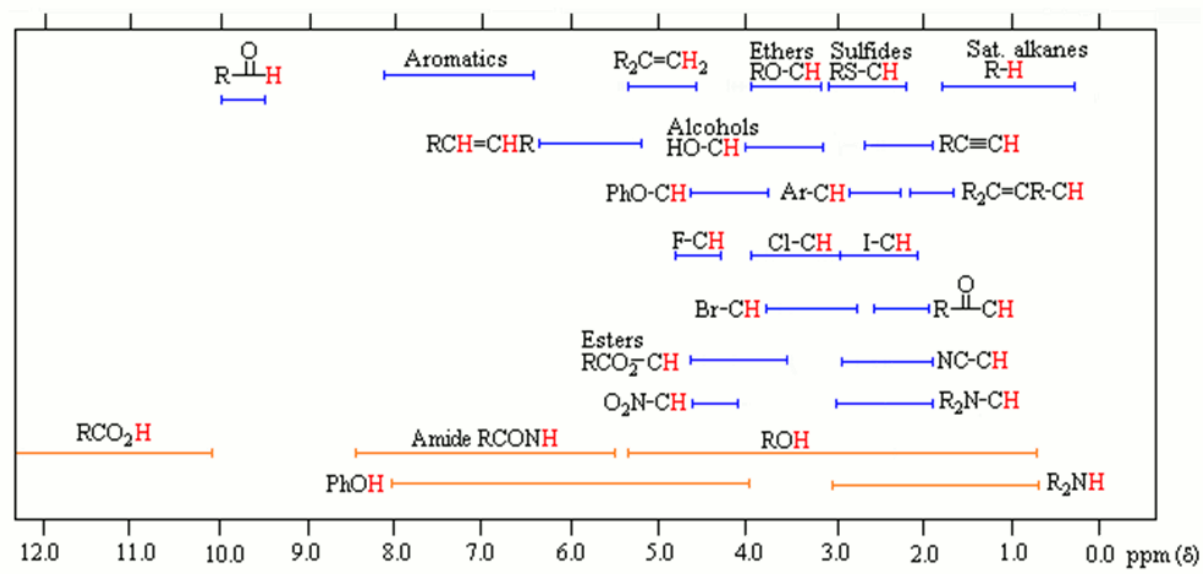

Figure 3: A solvent independent overview of typical chemical shift values for protons. Highlighted in orange are species which may hydrogen-bond thus exhibit a wide range of typical chemical shifts.

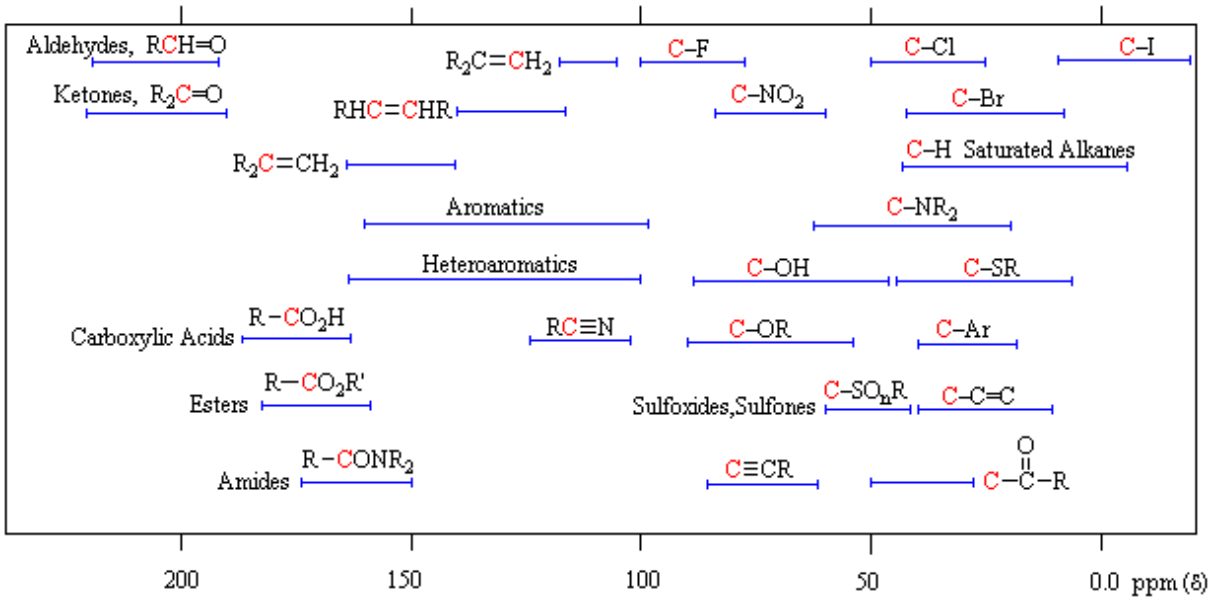

Figure 4: A solvent independent overview of typical chemical shift values for carbon isotope ^{13}C.

The chemical shift values in figure 3 and 4 show that the nuclides ^{1}H and ^{13}C resonate over very different intervals and signals from them appear over a range of values pending shielding from neighbors and solvent. The interval difference between nuclides is due to the gyromagnetic ratio for nuclides are different. The gyromagnetic ratio of ^{1}H and ^{13}C is about 4 to 1. Nuclides are typically grouped into high and low spin nuclides.[29] A selection of nuclei grouped in high-γ and low-γ are shown in table 1:

Table 1: Overview of high- and low-spin nuclei.

High-γ	Low-γ
^{1}H, ^{19}F, ^{31}P	^{13}C, ^{15}N, ^{29}Si

The trend that conjugated π-bonds increase the chemical shift of atoms at the ends of them, is due to the constructive contribution from the electrons in the π-bond. A notable peculiarity, however, is that triple bonds produces a lower chemical shift. Electrons forming double bonds are more deshielding than those in triple bonds. In a magnetic field double- and triple-bond electrons contribute constructively and destructively, respectively, with the static magnetic field. These are para- and diamagnetic currents in their respective cases. These deshielding and shielding contributions are what produces their chemical shifts. An illustration of the phenomena is found in figure 5 for frequently occurring π-systems.[28, 29]

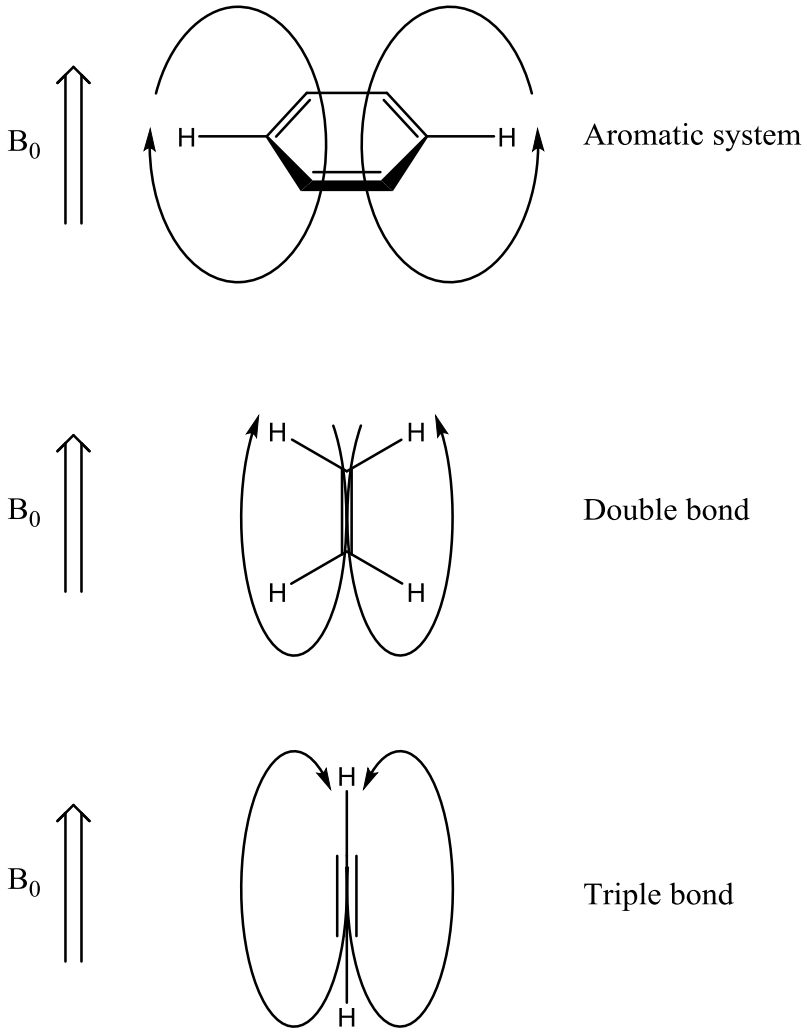

Figure 5: Constructive contribution of the π-electrons are shown for π-systems with one or more double bonds. Destructive contribution of the π-electrons is shown for a π-system consisting of a triple bond.

Scalar coupling, multiplicity and coupling constants

The Dirac nuclear-electronic spin model[27, 30] is a good tool to describe scalar couplings. Spin information is transferred between nuclei by electrons in the intervening orbitals. The nuclear spin interacts through electronic spins to reach the other nucleus. An electron near the nucleus has the lowest energy if its spin is also paired with the nuclear spin. Such an energy state is demonstrated in figure 6 for a ^{1}J coupling. Note that the electrons follow Pauli's exclusion principle which dictates that "When the labels of any two identical fermions are exchanged, the total wave function changes sign; when the labels of any two identical bosons are exchanged, the sign of the total wave function remains the same"[27, 31] is followed.

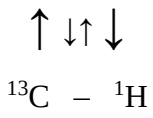

Figure 6: The configuration of the spin between two fermions which are σ-bonded that produces the lowest energy state.

As the couplings occur through chemical bonds, their configuration becomes important. This type of coupling is called a scalar coupling and is so called because the energy of interaction is a scalar product of the two interacting spins, seen in eq 16 (and remembering that $\hat{I}_z = m_l \hbar$). The energy is dependent on their relative orientations.

$$E_{m_1 m_2} = \frac{hJ}{\hbar^2} I_1 \cdot I_2 = hJ m_1 m_2 \tag{16}$$

The most favorable configuration of nuclear spins for a ^1J and ^2J coupling are antiparallel and parallel, respectively. When one nucleus is excited the paring orientation is broken, the energy of interaction is increased. By increasing the energy, the frequency also changes, as seen by inspection of eqs 7 and 17. For a two nuclei system, AX, the energy expression (including coupling) becomes:

$$E_{m_A m_X} = -h\nu_A m_A - \nu_X m_X + hJ m_A m_X \tag{17}$$

With $\Delta m_A = 1$ and $\Delta m_B = 0$ there are two possible transitions; $\beta_A \leftarrow \alpha_A$ when X is either α or β. Eq 17 simplifies to 18 when the energy difference of transitions for A are considered.[27]

$$\Delta E = h\nu_A \pm hJ \tag{18}$$

For an AX_N system, the X resonance will be split in two (doublet), divided by J. If N > 1 the A resonance will be split in two, where these signals will again be split, each time by frequency *J*. This process will occur N times and result in N+1 signals in the NMR spectrum. Thus the Pascal's triangle and the N+1 rule appears as all but the edge resonances will overlap with other resonances from the same splitting "sequence". Two schemes of Pascal's triangle is given in figure 6.[27, 28]

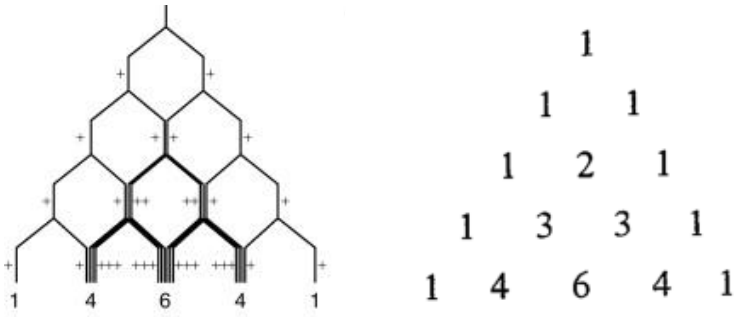

Figure 6: Two representations of Pascal's triangle where splitting (both), overlapping resonances (left) and intensities (right) are highlighted.

This type of splitting pattern is very commonly observed in NMR spectroscopy and are termed in table 2.

Table 2: Overview of terminology and multiplicity arising from an AX_N-system.

Number of lines	Intensity ratio of lines	Term for peak	Number of coupling neighbors
1	1	Singlet (s)	0
2	1:1	Doublet (d)	1
3	1:2:1	Triplet (t)	2
4	1:3:3:1	Quartet (q)	3
5	1:4:6:4:1	Quintet	4
6	1:5:10:5:1	Sextet	5
7	1:6:15:20:15:6:1	Septet	6

The coupling constant, *J*, is not always the same value for all coupling partners, nor is it always positive. The magnitude of *J* depends how much the other nucleus is affected by excitation of the original nucleus. This depends on the electronic orbital overlap(s) between nuclei which may be affected by dihedral angle (for ^3J) as well as bond length, valence angles and electronegativity of substituents. The Karplus curve[27, 28] shown in figure 7 makes perfect according to the Dirac model. Higher order coupling also depend on these factors. They are typically too small to see. This is mainly due to small orbital overlaps across bonds. Thus we typically only see them for π-systems (allylic and propargylic couplings), though couplings through planar W- and U-bound configurations of atoms also exist.[29]

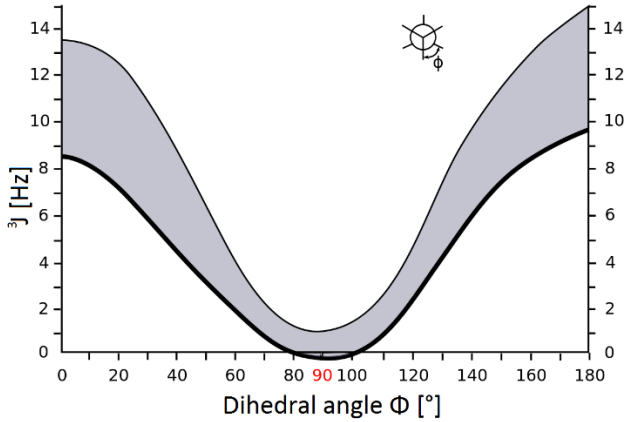

Figure 7: The Karplus curve which determines the scalar coupling, ^{3}J, based on the dihedral angle. The grey area is the interval for which frequency they may have.

In a coupling H_a-^{12}C-H_b system there arises a $^{2}J_{ab}$ coupling. The α-spin of H_a polarizes the electron, e_α, and is likely to be found close to ^{12}C. Hund's rule[27] applies here, and the most energetically favorable arrangement is for the α-electron in the other chemical bond to also reside close to the ^{12}C nucleus. Note that Hund's rule[27] applies for all ^{N}J-couplings (for N > 1). Then the Pauli exclusion principle[27] dictates that the other electron will have opposite spin, which in turn will interact with the nucleus through either a fermi contact interaction or a dipolar interaction. Thus in a ^{2}J coupling the spin-active nuclei and electrons furthest away from the spin-active nuclei will have parallel spin and the lowest energy configuration is for the spin active nuclei to have opposite spin of their closest electron. This is shown in figure 8.[27]

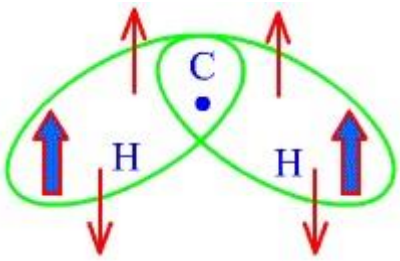

Figure 8: The proton-nuclei have parallel spin (α) in their lowest energy configuration because they polarize their respective parallel spin electron (α). This is in line with Hund's rule because the two electrons close to the carbon have parallel spin. This also follows Pauli's exclusion principle because the electrons in a bond have opposite spin.

When values for J are reported, the absolute value, $|J|$, is reported rather than $\pm J$. The sign of J indicates whether the coupling nuclei have parallel or antiparallel orientation of spins. As a rule of thumb, the sign alternates with scalar coupling length: $^{1}J > 0$, $^{2}J < 0$, $^{3}J > 0$ et cetera.

Another rule of thumb is that the magnitude of *J* depends on the orbital overlap between the nuclei.[27-29]

This causes *J* to follow an increasing trend with increasing s-character (hybridization).[27] Should the coupling constant differ between nuclei with Larmor frequency ν_A (or chemical shift value A), less common coupling patterns may arise. Some are given in figures 9 and 10.[28]

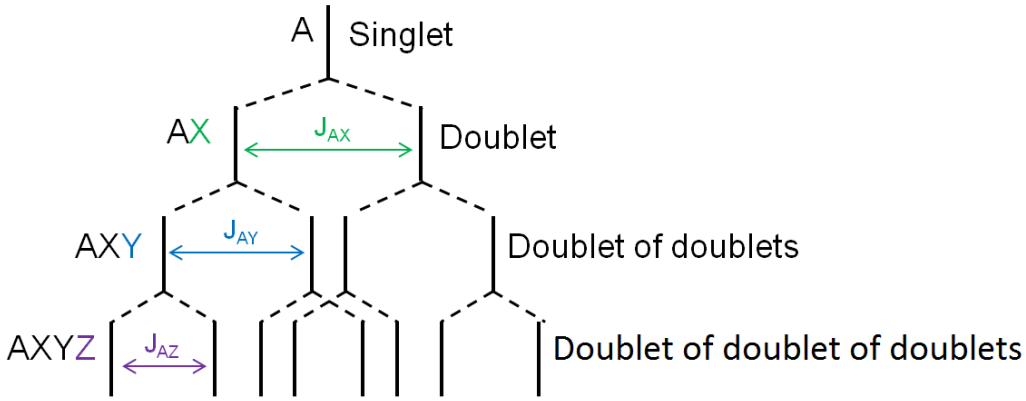

Figure 9: A resonance is split in 2 three times by different coupling partners with different magnitude of the couplings. This results in a doublet of doublet of doublets.

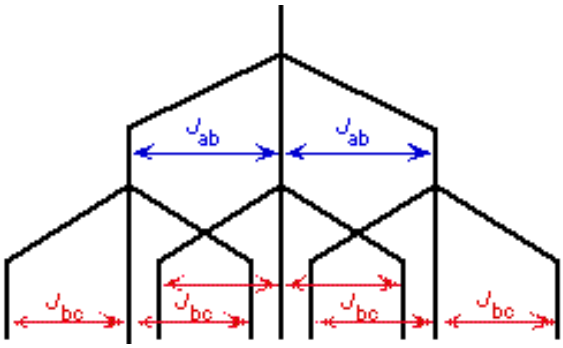

Figure 10: A resonance is split in 3 twice by different coupling partners with different magnitude of the couplings. This results in a triplet of triplets.

However, magnetically equivalent nuclei couple, but this has no effect on the appearance of the spectrum. This can be qualitatively explained by "all allowed nuclear spin transitions are collective reorientations of groups of equivalent nuclear spins that do not change the relative orientations of the spins within the group."[27] Since the relative orientations of the nuclei has not been changed, the couplings are not detectable. Nuclei that are not strictly magnetically equivalent may appear so because of rapid rotation around certain bonds e.g. the protons in $-CH_3$ rotate at such a rate around the 4th methyl bond that the differences average

out. To be magnetically equivalent they must be isochronous and must have equal coupling to all other nuclei in the molecule.[27]

2.1.3 The vector model (Bloch) and pulses

Having covered precession and a spin-active nucleus' behavior in a (static) magnetic field, the vector model and its frames; the rotating and laboratory frame, should be readily understood.

A sample usually consists of many spin-active nuclei, meaning there are many magnetic moments and precessions. For simplicity, the vector model collects all magnetic moment vectors of a certain nuclide in origo seen in figure 11a. By adding all the vectors together produces the resultant magnetic vector seen in figure 11b. The resultant magnetic vector will point directly along the z-axis (longitudinal plane) since the number of nuclei is large and they are distributed randomly along the precession path, making their transverse components cancel each other out.[28, 29]

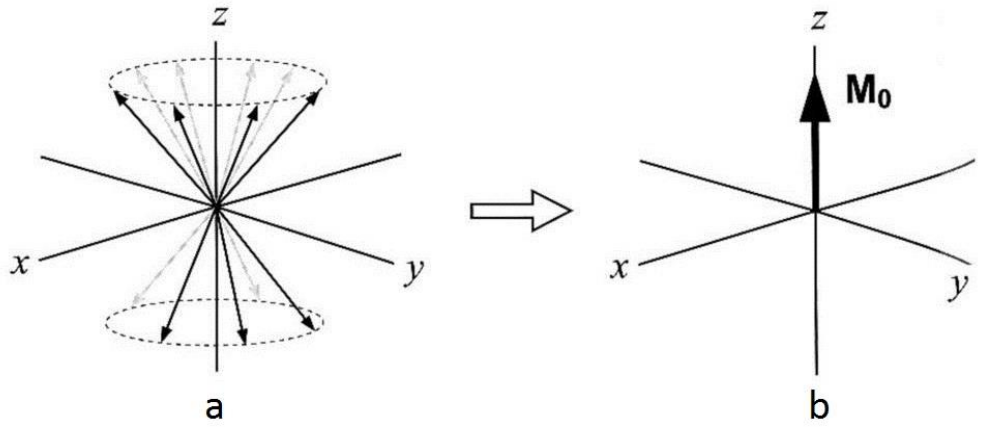

Figure 11: a) All the magnetic moments precessing in a sample are collected to originate from one origin, origo. b) All vectors in a) have been added together to form the resultant magnetic vector, M_0.

When subjected to an electromagnetic pulse, some of the nuclei become excited and all become phase coherent. When the nuclei become excited and turn against the static magnetic field, longitudinal component of M_0 decreases. The sample becomes phase coherent due to the magnetic component of the pulse creating magnetism in the transverse plane and is seen in figure 12.

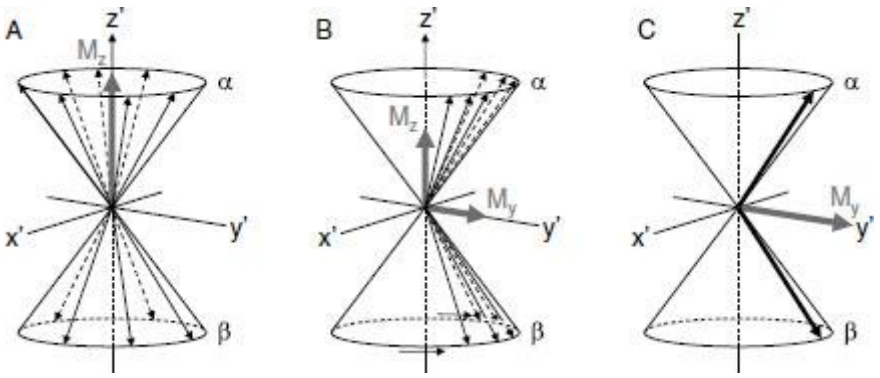

Figure 12:A) The sample's precessing magnetic moments are randomly distributed in the transverse plane and Boltzman distributed across spin states. B) The sample is subjected to electromagnetic radiation. The sample is becoming more phase coherent due to the magnetic component of the applied magnetic field, and the population of spin states is being evened out. C) The precessing magnetic components of the nuclei are perfectly phase coherent and there is an equal number of nuclei in both spin states.

As the pulse is applied along the positive x-axis, the magnetic component of the pulse concentrates the precessions along the positive y-axis, making the nuclei phase coherent. As seen in figure 13, the resultant magnetic vector will then have a component in the transverse plane as well. By applying a 90° pulse (termed flip angle) along the positive x-axis, M_0 will only have a component in the transverse plane. This is shown in figures 12C and 13.[28, 29]

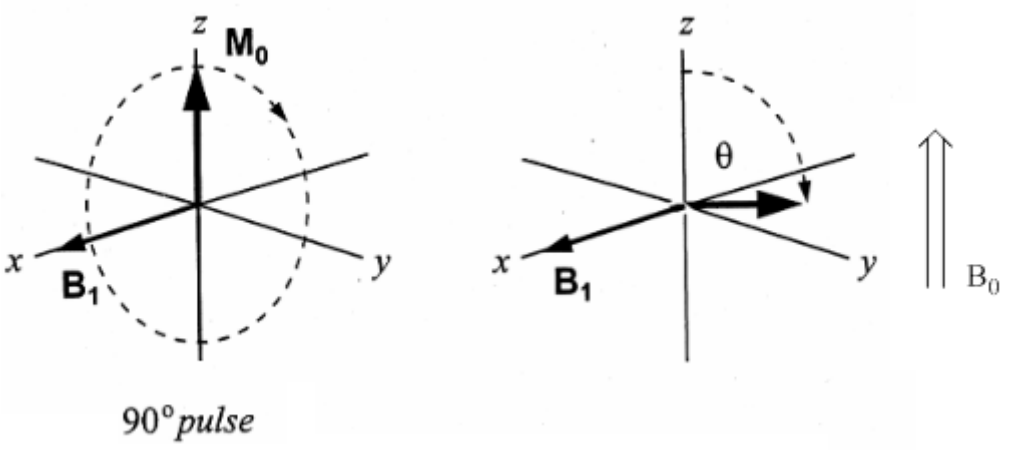

Figure 13: A 90° pulse (θ = 90°) is applied along the positive x-axis. This causes the resultant magnetic vector to align with the positive y-axis.

From this point, ignoring several factors to be covered later, the resultant magnetic vector will revolve around the center. So far, all the figures, except figure 12 and 13, have been shown from a bystander's point of view. This is known as the 'laboratory frame'. However, if one were to observe from the center of the coordinate system, rotating with the same frequency of the resultant magnetic vector, one would be observing from the 'rotating frame'. This is well illustrated in figure 14 (next page) as the rotating frame will make M_0 appear stationary (b), while the laboratory frame (a) will show the revolutions of M_0.[29]

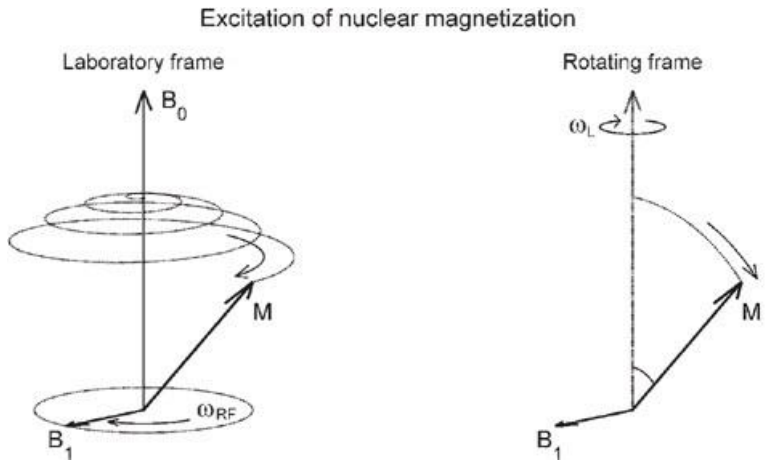

Figure 14: The laboratory frame (left) shows the resultant magnetic vector, M, precess while exposed to an electromagnetic pulse. In the rotating frame (right) the coordinate system rotates with the precession of the resultant magnetic vector.

With reference to chapters 2.1.2 it is then possible, using the rotating frame, to observe the chemical shifts protrude as well as the evolution of couplings when the resultant magnetic vectors of the different species in the sample precess at different speeds. Since they precess at different speeds, the nuclei of different chemical environments will separate. The multiplicity of each chemical shift will also separate, as the energy difference caused by orientations of spin directly affects precession. Evolution of chemical shift is illustrated in figure 15 where the rotating frame is set equal to the frequency of nucleus A, while evolution of multiplicity is shown in figure 16 is set to the frequency of the chemical shift ν_0. The rotating frame is used throughout the thesis unless otherwise specified.[29]

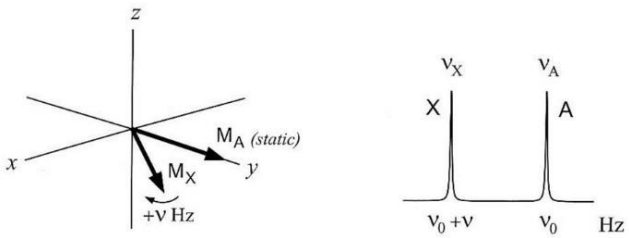

Figure 15:The two nuclei A and X precess with different frequencies. Nucleus X precesses somewhat faster than A and is thus seen to move away from A in the rotating frame (left). This difference in frequency is then detected and the signal is processed into two resonances with different chemical shifts.

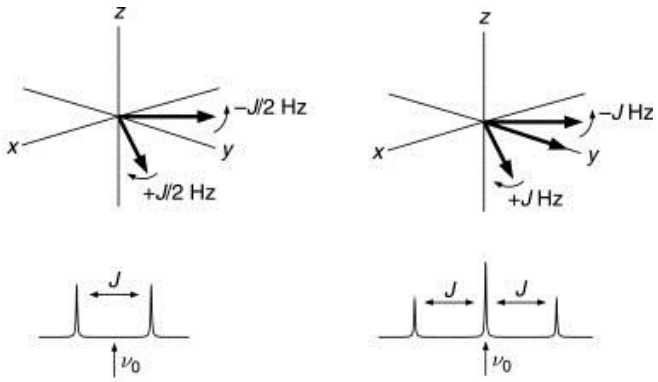

Figure 16: The different orientations of spin in the coupling nuclei cause them to precess at different frequencies (ref. subchapter 2.1.2 Scalar coupling, multiplicity and coupling constants). The higher energy orientation of spins will precess faster than the lower energy orientation. This is seen by the vectors moving away from each other. The evolving couplings (top) are seen for an AX system (left) and an AX_2 system (right). The differences in frequency are then detected and after processing, make up a doublet for the AX system (bottom left) and a triplet for the AX_2 system (bottom right).

Relaxation: T_1 and T_2

From pervious chapters it is known that the nuclei align when exposed to a 90° pulse and the resultant magnetic vector's z-component decreases as they become excited and align against the field. From this point on, if not exposed to further magnetization, the nuclei will revert back to equilibrium by relaxation. This means that the nuclei will flip back into equilibrium (longitudinal relaxation) and be Boltzmann distributed. The time constant utilized in the mathematical expression (not shown) for this to occur is termed T_1. Longitudinal relaxation is illustrated in figure 17. The individual vectors that make up the resultant magnetic vector will also fan out in the transverse plane and become randomly distributed over the entire precession movement. The time required for this to occur is termed T_2^* (effective T_2). Transverse relaxation is shown in figure 17 and 18. The relaxation process does not occur by itself. That would take between several deciseconds up to several hours. The relaxation occurs naturally through collisions between the nuclei and may result in heating of the sample. This can be problematic under decoupling and pulse sequences containing spin-lock which is described in subchapter 2.1.5.[28, 29]

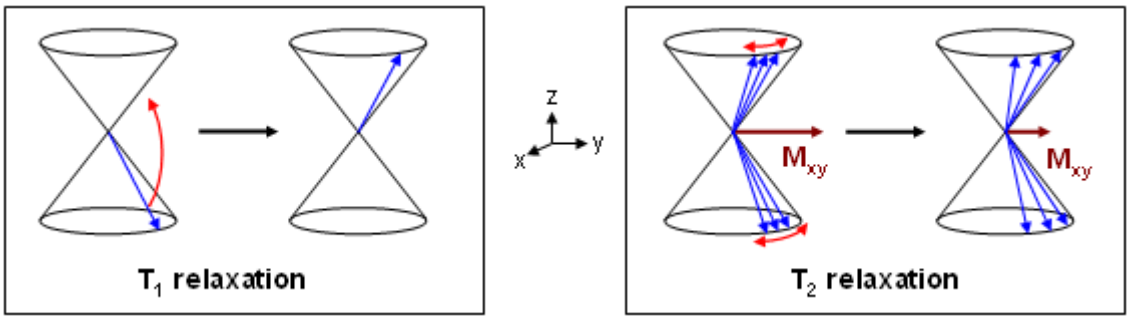

Figure 17: Longitudinal relaxation (left) is shown where the nuclei revert back to their original spin state. Transverse relaxation is shown where the individual magnetic moments fan out and become randomly distributed.

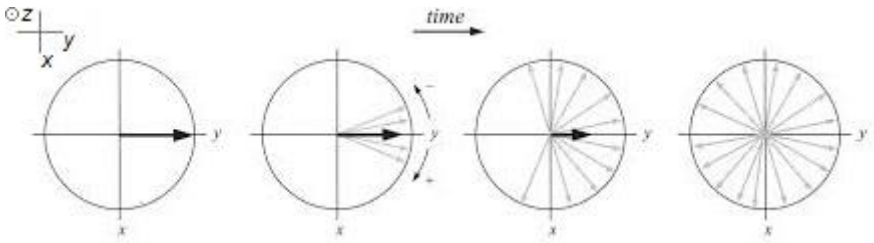

Figure 18: Transverse relaxation (in xy-plane) illustrated from the z-axis point of view.

During acquisition, the in-phase precession causes the detection. When the sample is in phase, the sample exhibits a small magnetic field from the in-phase nuclei. This causes a current in the listening coil which is acts as a transducer. The signal is then amplified and then digitized in the analog-to-digital-converter.[29]

2.1.4 General overview of NMR experiments

With respect to previous chapters, the reader should be equipped to understand 2D experiments. In basic 1D experiments, the sample is excited and then listened to. An example of such a pulse program is shown in figure 19 and a representative spectrum in figure 20.

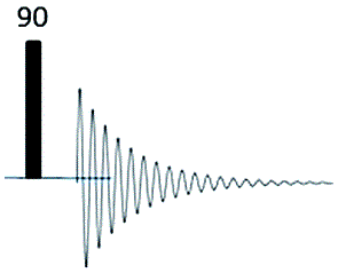

Figure 19: Simple illustration of a 1D experiment's pulse sequence.

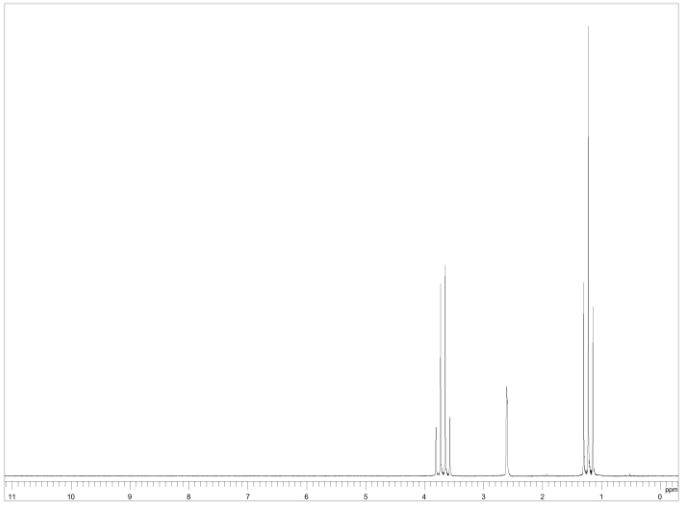

Figure 20: An illustration of the resulting spectrum after acquisition and signal processing of the recorded signal. The spectrum is of ethanol.

2D experiments are performed in a similar fashion. The general scheme for any 2D experiment is given in figure 21.

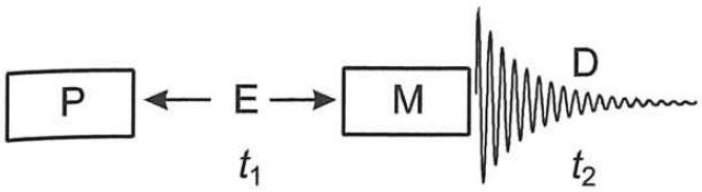

Figure 21: A general scheme of a 2D experiment is shown. The experiment is initiated by excitation in the preparatory stage (P), couplings are permitted to evolve during the evolution stage (E or t_1) and the sample is again exposed to electromagnetic radiation in the mixing stage (M) before aquisition (D or t_2).

The pulse program is initiated (prepared) by exciting the sample with electromagnetic radiation as seen with the vector model in previous chapters. The sample is then allowed to precess (evolve) for a time, t_1, where couplings evolve before being introduced to additional electromagnetic irradiation in the mixing time. Finally the sample's behavior is recorded during the acquisition time. An illustrative 2D correlation spectroscopy (COSY) spectrum is shown in figure 22.

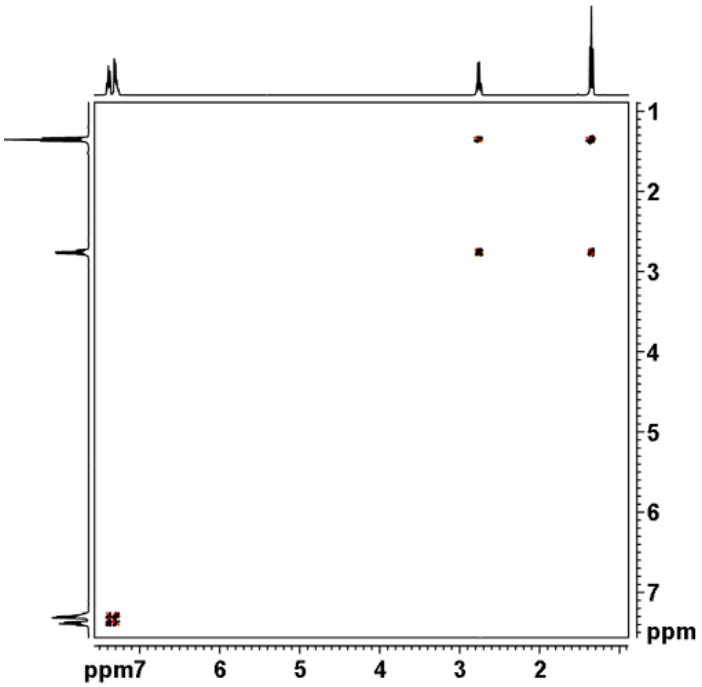

Figure 22: A 2D COSY spectrum of ethyl benzene is shown.

The second dimension arises by manipulation of the evolution time, t_1. The pulse program is run with t_1 changed incrementally where the signals (FIDs: free induction decay) from each increment of t_1 are stored separately. Each incremental change of t_1 may be recorded many times and is determined by the number of scans (NS). How many increments of t_1 is determined by the parameter "Time domain" (TD). The time required to run an experiment is thus equal to NS multiplied by TD; NSxTD. The sample is partially of fully allowed to revert back to equilibrium between scans.[29]

2.1.5 Pulse sequence tools (and phenomena)

To understand the remaining subchapters of the theory section, familiarity with symbols utilized in NMR experiments is beneficial. Therefore an overview is given here, in figure 23.

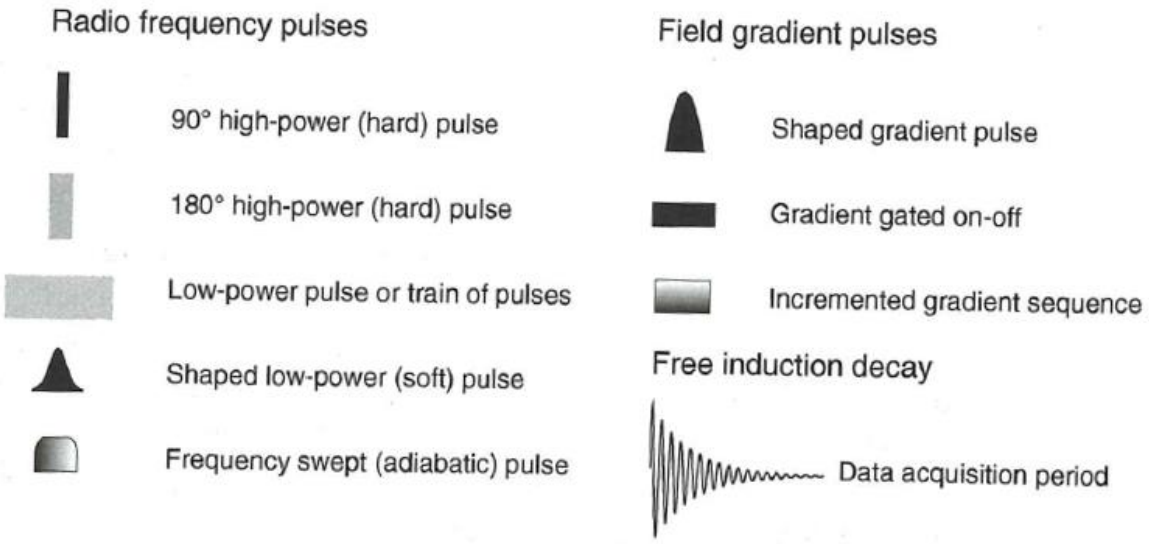

Figure 23: Overview of symbols utilized in pulse programs for NMR experiments.[29]

Refocusing

Utilizing the vector model and the knowledge of how chemical shift and coupling evolves from previous chapters, fundamental building blocks of NMR, such as spin-echoes, may now be described. By applying a pulse sequence, such as typically illustrated in figure 24 or shown in figure 25 where the vector model is used, one may refocus the chemical shift. The initial 90°_{x} pulse forces the resultant magnetic vector into the transverse plane where the chemical shifts will evolve for a time, Δ, as X is precessing faster than A. By application of a 180°_{y} pulse, the faster precessing chemical shift will be moved radially behind the slower precessing chemical shift and refocus after another equal time, Δ. [29]

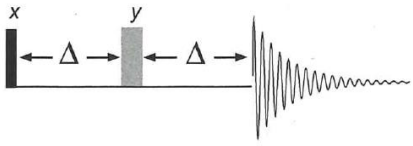

Figure 24: Typical illustration of a pulse sequence. The pulse sequence applies a 90°_{x} pulse followed by a 180°_{y} before acquisition. These three entities are separated by a time interval Δ and results in the refocusing of chemical shifts along the positive y-axis.

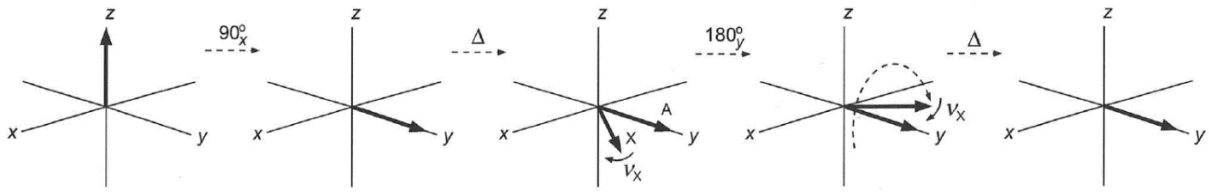

Figure 25: An illustration of refocusing of chemical shift utilizing the vector model.

Scalar couplings do not behave as chemical shift. Furthermore, if the two nuclei in question are the same element or not, the evolution of couplings may be different. The evolution of a homonuclear coupling continues to evolve even when subjected to a spin-echo pulse sequence. Heteronuclear couplings may however refocus uniform to the chemical shift or continue to evolve as homonuclear couplings do. This is because the option of selective excitation is available for a heteronuclear coupling.[29]

A homonuclear scalar coupling between elements in different chemical environments evolves as described in previous chapters. When subjected to a 180°_{y} pulse, the coupling nuclei flip and also change coupling partners. The nucleus coupling to the higher energy nucleus is now coupling to the lower energy one and vice versa. Thus they precess at the frequency of the original coupling partner. The slower precessing nucleus now possesses the frequency that the originally faster precessing one had, and the faster precessing nucleus now posesses the frequency that the originally slower precessing one had. This is illustrated in figure 26.[29]

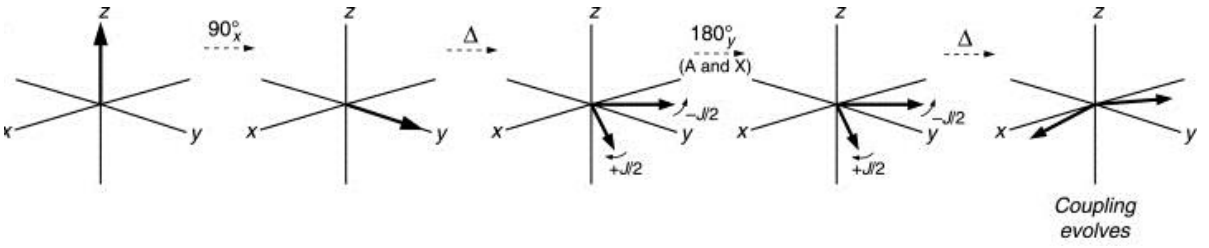

Figure 26: Illustration of how couplings continue to evolve in a homonuclear coupling scheme by use of the vector model. The same is also true for a heteronuclear system where both elements are subjected to the 180°_{y} pulse.

Heteronuclear couplings may evolve similarly to homonuclear couplings. This is done by subjecting both elements to a 180°_{y} pulse and may also be seen in figure 26. In an aliphatic compound the excited elements would then be ^{1}H and ^{13}C. If only one of the nuclei is subjected to the pulse, the coupling will refocus. This is illustrated in figure 27. To make

heteronuclear couplings evolve as homonuclear couplings, two frequencies are required, as (in a heteronuclear AX system) A and X precess at different frequencies.[29]

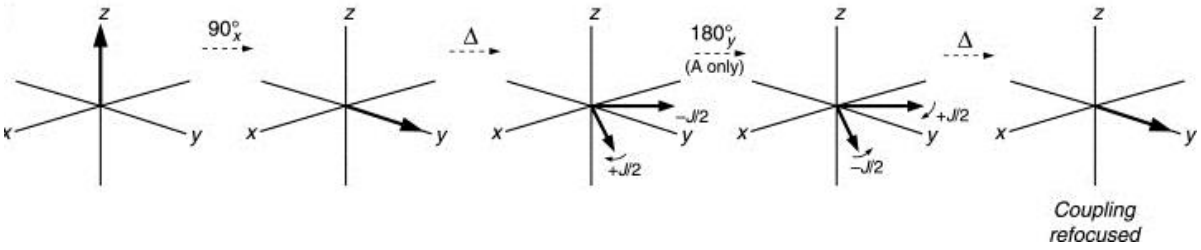

Figure 27: Illustration of how couplings can refocus by selective excitation of only one of the nuclei in the coupling scheme which leads to refocusing of the coupling.

Phase cycling

Isolation of desired signals can be achieved by carefully selected changes to phases of the pulses so that the desired signals add coherently with time averaging. The other signals cancel at the end of the cycle and are thus absent in the resulting spectrum. By alternating the phase from 90°_x to 90°_y between scans, storing the data separately and adding them coherently will produce a spectrum where the signals add together while the noise is canceled out. The separate storing of the data may be effectively done with quadrature detection (two-channel detection). This way the data is stored in phase and 90° out of phase. The same technique may be used to prevent wrapping, which is when a signal with a frequency outside the spectral width appears on the other end of the spectrum.[29]

Spin-lock and -decoupling

The refocusing of chemical shifts while couplings evolve have been exploited in numerous pulsing schemes such as Malcolm Levitt's composite-pulse decoupling (MLEV) sequences, MLEV-16,[32] -17,[33] decoupling in the presence of scalar interaction (DIPSI-2)[34] and wideband, alternating-phase, low-power technique for residual splitting (WALTZ) sequence WALTZ-16[35] to reveal entire spin systems. The spin-lock sequence makes the coupling of coupling partners propagate through a continuous chain of protonated carbons (methyl, methylene, methine) which then reveals the entire spin system. The technique is applied during the mixing time. These pulse sequences each have their advantages. The DIPSI-2 and

MLEV-17 sequence employs spin lock trim pulses to dephase inhomogeneity to prevent too rapid T_2 relaxation. The DIPSI-2 sequence also employs phase cycling.

The MLEV-16 and MLEV-17 sequences consist of numerous MLEV-4 sequences which is also termed the 'magic cycle'. The MLEV-4 sequence starts with a 90°_x pulse followed by a 180°_y pulse and ends with a 90°_x pulse and can be viewed as a series of 180°_y pulses and are separated by an infinitesimal time segment, δ. A scheme of MLEV-4 and -17 are shown in figure 28, where the MELV-17 sequence substitutes the 180°_y pulses with 270°_y pulses. [29]

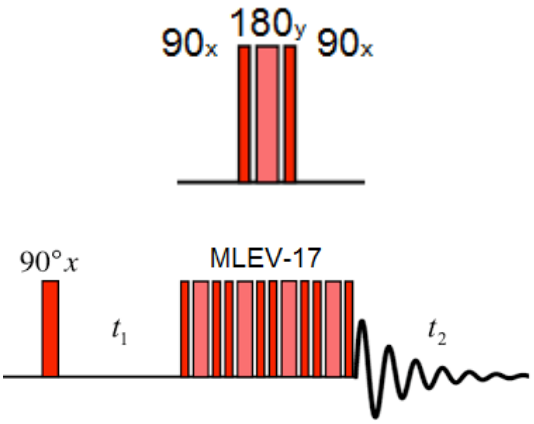

Figure 28: MLEV-4 cycle (top) is a short train of pulses consisting of the pulses: 90°_x-180°_y-90°_x. The bottom pulse sequence utilizes MLEV-17 which consists of 16 consecutive MLEV-4 cycles where the 180°_y pulse is substituted by 270°_y pulses. They are all separated by infinitely small time segments. The illustration is simplified and meant to highlight the train of pulses in the mixing-segment.

The WALTZ-sequence also employs these pulses but in the sequence 90_x-180_{-x}-270_x. When employed, to prevent error arising from an incorrectly calibrated pulse, the sequence is also repeated in reverse. This is the same principle as the Carr-Purcell-Meiboom-Gill spin-echo sequence. This means that the MLEV-16 sequence, which employs numerous standard MLEV-4 sequence (R), but must then also have it in reverse ($\bar{R}$) to account for pulse calibration errors. The MLEV-16 sequence employs the sequence: $RR\bar{R}\bar{R}\ \bar{R}RR\bar{R}\ \bar{R}\bar{R}RR\ R\bar{R}\bar{R}R$. The DIPSI-2 sequence is similar to the MLEV sequence. When the magnetization transfer is equally effective along the x-, y- and z-axes, the mixing scheme is termed 'isotropic'.[29]

When such pulsing schemes are employed during acquisition, the spin-lock is too fast for the listening coil and the spectrum appears decoupled. MLEV-16, -17, WALTZ-16 and GARP

(globally-optimised, alternating-phase, rectangular pulses)[36] are examples of decoupling techniques. There are two main categories of decoupling; broadband and selective decoupling. In broadband decoupling it is common notation to write the decoupled nucleus in braces. An experiment such as $^{13}C\{^{1}H\}$ will then decouple the protons while recording the signal from the ^{13}C nuclei during acquisition. When employing broadband decoupling it is important to achieve decoupling across the entire range of frequencies recorded. With higher magnetic fields it becomes harder to achieve decoupling over the same ppm-window since the frequency range increases with increasing strength of the magnetic field. To manage this, some decoupling schemes employ adiabatic pulses. GARP is one of these.[29]

Coherence transfer (Polarization Transfer)

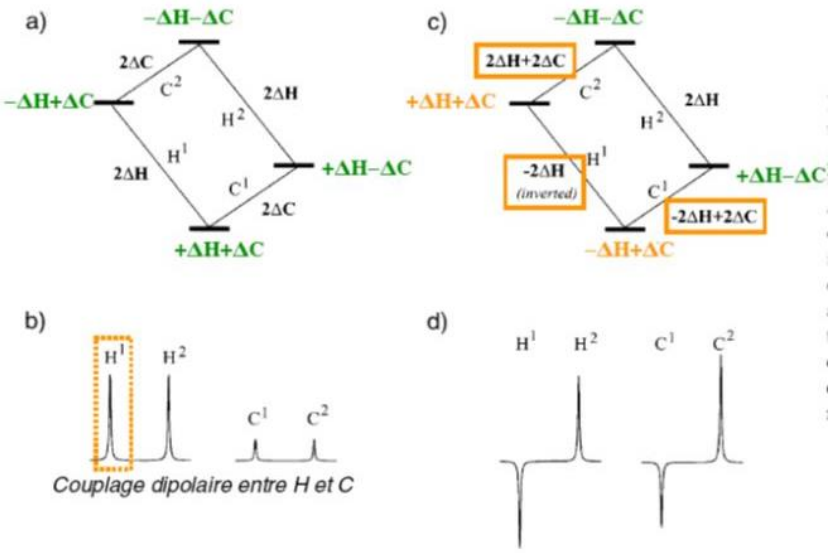

Figure 29: Transition 2ΔH is excited and the population across three transitions are altered. This is known as coherence transfer.

J-Modulated Spin-echo

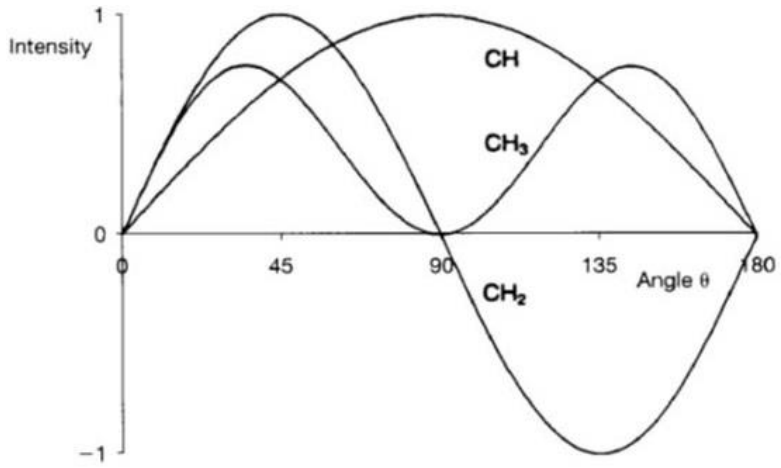

Figure 30: Timing between pulses are altered to produce phase sensitive NMR spectra. 45° gives all positive, 90° gives methine resonances only while 135° gives positive methine and methyl resonances and negative methylene resonances.[29]

Signal suppression

Most solvents employed in NMR are readily available in their deuterated form. However some samples, typically biomolecules, require a protonated solvent to observe all or most protons in the sample. Typically 5-10% of the solvent is deuterated to maintain a lock signal. There is also the added benefit avoiding deuterated solvents when the sample needs purification through liquid chromatography. Numerous techniques have been developed to meet the challenges that arises with signal-to-noise since the digital-to-analog-converter will struggle to detect the sample in the presence of an abundant water-signal. Further concerns include baseline distortion, t_1-noise in 2D experiments, radiation damping and potential spurious responses that are associated with very intense signals. The potential overlap of the solvent signal with signals from the species of interest also needs to be accounted for. The techniques considered in this project are: Excitation Sculpting (ES), Continuous Wave Presaturation (PR), Water suppression by gradient-tailored excitation (WATERGATE) and presaturated nuclear Overhauser effect spectroscopy (Presat NOESY).[29]

Presaturation: CW PR

Presaturation may be readily added to existing experiments. When utilized, it leaves resonances away from the presaturation frequency unperturbed. Signals close to this frequency will experience some loss in intensity as part of the population will become saturated. The presaturation applies a weak radio frequency irradiation to the solvent prior to the pulse program. This produces saturated solvent spins which are then unobservable. By

increasing and decreasing the intensity of the rf irradiation, both the suppressed frequency and nearby signals will experience a loss or increase in signal intensity, respectively. A notable disadvantage of presaturation is that it will lead to suppression of all protons exchanging with the solvent. This method avoids production of Bloch-Siegert shifts. A Bloch-Siegert shift may occur when an rf field, such as a decoupler frequency, is applied during acquisition. This causes the resonances near the applied rf to move away from its point of origin.[29]

Water suppression by gradient-tailored excitation: WATERGATE

WATERGATE employs a pulsed field gradient (PFG) spin-echo. The PFGs, termed G_1, are separated by an element S in the sequence G_1-S-G_1. The element S provides no net rotation of the solvent resonance, but a 180° rotation of all others. The dephasing of the non-solvent resonances is refocused by the second PFG and thereby retained. The pulsing schemes for WATERGAE and Excitation Sculpting are shown in figure 31. As seen the S-element is a shaped pulse. There are numerous profiles, but important feature of the pulse is its notch in the middle. The excitation profile can be seen in figure 32. The S-element may also be a combination of hard and soft 180° pulses. Then the soft pulses act on the water resonance to experience a 360° rotation while the rest of the sample is rotated 180° by hard pulses.[29]

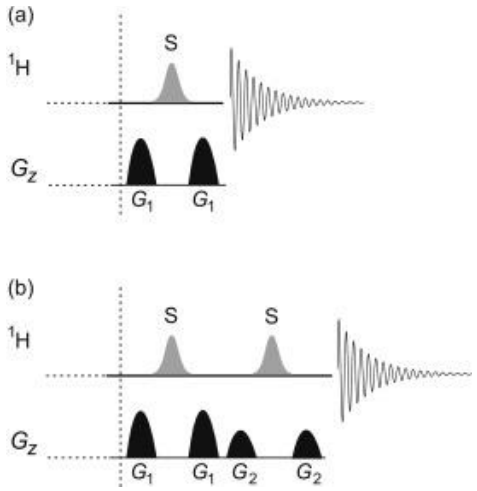

Figure 31: Pulse sequences for signal suppression techniques WATERGATE (top) and excitation sculptin (bottom) is shown. The WATERGATE sequence includes two gradient pulses G_1 and one shaped pulse S in the sequence: G_1-S-G_1. Excitation sculpint employs this scheme twice but with different sets of gradient pulses bracketing the shaped pulse S. When employing excitation sculpting, the notch in the shaped pulse is wider due to being used twice.

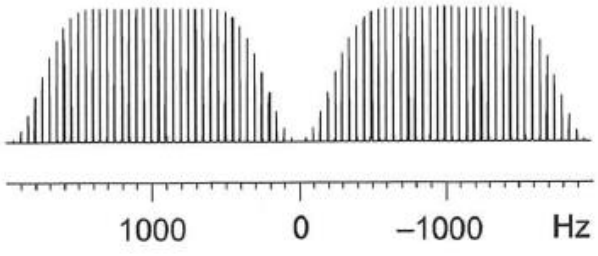

Figure 32: Illustration of an excitation profile of a shaped pulse used in WATERGATE or excitation sculpting

Excitation Sculpting: ES

This form of signal-suppression employs a double PFG spin-echo instead of one and is an improved version of WATERGATE because it refocuses the evolution of homonuclear couplings and produce spectra with less baseline distortion and improved phase properties. The S-element's notch is wider, but otherwise exactly the same. The notch is wider since it is applied twice. The general scheme for ES is shown in figure 31 (previous page). ES may also be tailored to achieve multi-site suppression, but is not explored further in this text.[29]

Presaturated NOESY

The presat NOESY has been presented and compared to other suppression techniques designed for NOE-type experiments by Guennec, Tayyari and Edison.[37] In their work, superior water suppression was achieved, though issues with "faraway water" were still present. The lack of need for gradient pulses produced cleaner spectra and the general signal intensity was kept except for resonances near the suppression frequency. The study also compared Carr–Purcell–Meiboom–Gill (CPMG) to PROJECT where PROJECT, which utilizes perfect echo, produced advantageous spectra without drawbacks such as line shape distortion caused by J-modulation not completely suppressed by CPMG. The comparison was between preset NOESY, WET[29], WATERGAE [29] and PURGE (presaturation utilizing relaxation gradients and echoes)[38].

2.1.6 1D NMR Techniques

1D Proton

The most basic variant of the 1D proton experiment is shown in figure 33. φ symbolizes the angular change of the resultant magnetic vector when exposed to the pulse. This is termed "flip angle" and is determined by the pulse strength.

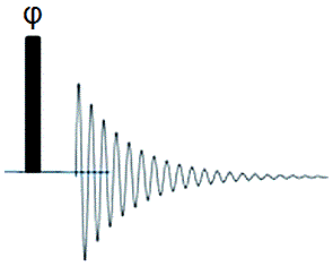

Figure 33: Basic pusling scheme for a 1D proton experiment.

Typically the Ernst angle (optimized flip angle) is not set to 90°, which would give optimal sensitivity. This is avoided because one often wants to apply signal averaging and to recover 99.3% of the longitudinal magnetization, a period of $5T_1$ is required. Instead recovery delay is done away with by adjusting the pulse conditions to maximize *steady-state* z-magnetization produced. The Ernst angle is typically set to 30° which causes the best S/N ratio.[29]

1D Carbon

The simplest experiment for carbon is analogue to the simplest 1D proton experiment. Coupling constants for ^{13}C are however quite large and it may be unambiguous which signals make up the fine structure of the signal. Due to ^{13}C being a low spin nuclide it does suffer from low sensitivity and thus low S/N. Therefore a decoupling scheme is typically applied to the frequencies of the protons. This is termed inverse-gated decoupling and removes multiplicity. If decoupling is applied to the sample before acquisition (gated decoupling), nuclear Overhauser effect (NOE) is observed and may be advantageous with low concentration samples. Heating issue may however arise if decoupling is continuously applied (power-gated decoupling). To counteract this, a lower power is applied before acquisition.[29]

The issue of experiment time and sensitivity of each scan is also an issue in 1D carbon experiments. Because of this, z-restored spin-echo pulse sequences have been experimented with. However there have been issues with baseline stability (hump, dip and roll). The z-restored spin-echo pulse sequences presented by Xia Et. Al.[39] produces a straight baseline free of these issues with a 400 µs delay between scans and only a 5% loss in sensitivity compared to a simple one-pulse pulse sequence. In our laboratory, J. Madsen, A. Wilkins and

D. Pedersen have given individual contributions to the pulse sequence to make it available for routine experiments. In our lab, the C13RESPECT experiment is not in need of a 70 µs delay between the last pulse and the acquisition.

Distortionless Enhancement by Polarization Transfer: DEPT and DEPTQ (retaining quaternary centers)

Distortionless enhancement by polarization transfer (DEPT utilizes phase cycling, polarization transfer and J-modulated spin-echo to produce a 1D carbon spectrum. The phase cycling removes what would otherwise be dispersive contributions from quaternary carbons. The polarization transfer enhances the sensitivity while the J-modulated spin-echo produces phase separation and thus distinguishability between methylene-type carbons from methyl- and methine-type carbons. From the section of J-modulated spin-echo, it is apparent the angles 45°, 90° and 135° are suited to discern between the carbon species. By incorrect placement, the experiments may exhibit some nature of spectra produced with the other angles. Sensitivity will also be impaired. The most typical error in DEPT is incorrect setting of the θ-pulse. Care should be taken to set the θ-pulse correctly. When DEPT is paired with a regular 1D carbon spectrum, determination of quaternary carbons is possible. The pulse sequence for a general DEPT experiment is shown in figure 34. Other issues may arise from quaternary carbons which exhibit unusually large multiple bond coupling constants and thus polarization transfer.[29]

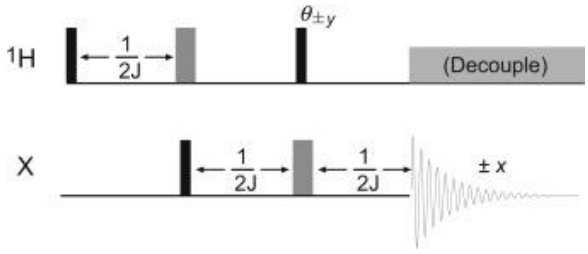

Figure 34: Pulse sequence for a general DEPT experiment.

To save instrument time, distortionless enhancement by polarization transfer with retention of quaternaries (DEPTQ) has been developed, which also utilizes polarization transfer and J-modulated spin-echo. Two DEPTQ sequences are illustrated in figure 35.

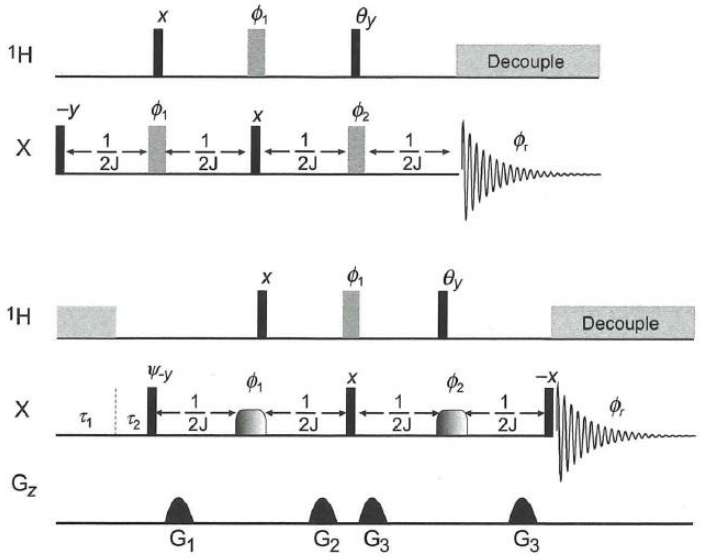

Figure 35: DEPTQ pulse sequences.

Additionally DEPTQ also incorporates a pulse segment at the beginning of the sequence to excite and manipulate the quaternary centers to appear in the same phase as methylene-type carbons. They do however not benefit from NOE nor polarization transfer since ^{1}H decoupling is gated off to allow for proton relaxation before polarization transfer. In modern versions, gradient pulses have been implemented for clearer signal selection, only protonated centers or only quaternary centers. This is equally valid at high bandwidths at high-field instruments.[29]

2.1.7 Homonuclear 2D NMR techniques

Homonuclear experiment exhibit symmetry across the diagonal (bottom left to top right). Peaks on the diagonal are termed *diagonal peaks* while off-diagonal peaks are termed *crosspeaks*. Crosspeaks arise from couplings and are signal which correlate differing shifts in the two dimensions.[29]

Correlation Spectroscopy: COSY

The COSY experiment is a 2D experiment and the general pulse sequence can be seen in figure 36.

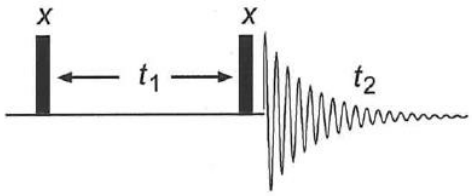

Figure 36: COSY pulsing scheme.

The crosspeaks observed are typically correlations connecting vicinal (^{2}J) and geminal (^{3}J) coupling protons. Longer correlations, 'long-range' crosspeaks, may be observed when the bonding facilitates long range couplings. Examples of this are *w*- and *u*-conformations. The typical correlation pattern provides a step-wise approach towards elucidating spin systems. Crosspeaks close to the diagonal may be hard to identify due to overlap with broad diagonal peaks, making the step-wise elucidation somewhat limited. By adjustment of the mixing pulse (less than 90°), the limitation may be circumvented since the diagonal will appear smaller. This also causes a loss in sensitivity. This variant is termed COSY-β. The fine structure is typically not well resolved. Other variants of the COSY experiment have been developed to enhance the fine structure, but at the cost of S/N.[29]

Total Correlation Spectroscopy and Decoupling In the Presence of Scalar Interactions: TOCSY and DIPSI-2

The total correlation spectroscopy (TOCSY) and DIPSI-2 sequences are similar to the COSY sequence. The most general form is shown in figure 37.

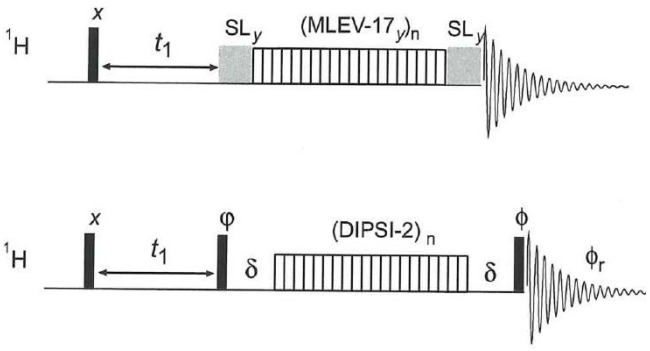

Figure 37: Pusling schemes for TOCSY (top) and DIPSI-2 (bottom) utilizing their respective spin-lock sequences.

The experiments are initiated by a 90°_{x} pulse which directs the resultant magnetic vector along the y-axis. The pulse sequences then utilizes a spin-lock sequence which refocuses the evolution of chemical shifts. This is done by the TOCSY sequence by applying the MLEV-17 spin-lock, which can be viewed as a train of consecutive 180°_{y} pulses. The chemical shift is then prevented from evolving by being kept along the y-axis. It is then said to be spin-locked. The TOCSY sequence enclaves the spin-lock sequence with soft, continuous wave, spin lock trim pulses to achieve pure-phase data. The same is achieved by the DIPSI-2 spin-lock, but utilizes hard pulses encompassing the spin lock while phase cycling.[29]

Nuclear Overhauser Effect Spectroscopy: NOESY

Nuclei may also exhibit dipolar couplings. These couplings are couplings through space and arise from forbidden transitions. zero- or double-quantum relaxation. NOESY exploits steady-state NOE. In its simplest form it's very similar to the COSY experiment.

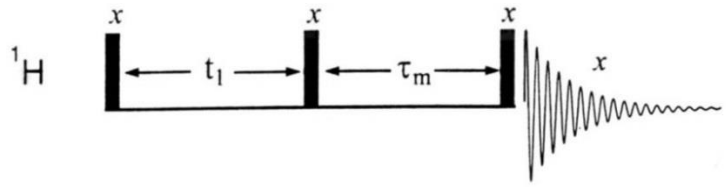

Figure 38: Simples pusling scheme for a NOESY experiment.

Rotating-Frame Nuclear Overhauser Effect Spectroscopy: ROESY

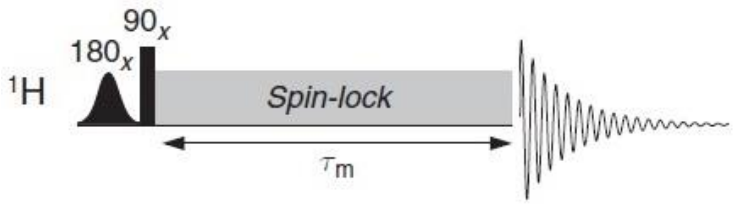

Figure 39: ROESY pusling scheme.

2.1.8 Heteronuclear NMR techniques

These techniques concentrate on couplings between different nuclides. The nuclide observed in heteronuclear experiments depend on the experiment. Most modern experiments observe

the ^{1}H-nucleus rather than other nuclei because of the high relative abundance as well as being a high-spin nucleus. ^{13}C has a relative abundance of 1.109% compared to 99.985% for ^{1}H. This segment will focus solely on ^{1}H-observing heternuclear 2D experiments.[29]

Heteronuclear Single Quantum Spectroscopy: HSQC

In heteronuclear single quantum spectroscopy (HSQC), the entities of interest are the satellites in a typical 1D proton spectrum, where the ^{1}H-nucleus is bound to a ^{13}C-nucleus. However, the primary signal in the 1D proton spectrum arises from ^{1}H-^{12}C entities and must be suppressed. The general pulse sequence for an HSQC experiment is shown in figure 40.

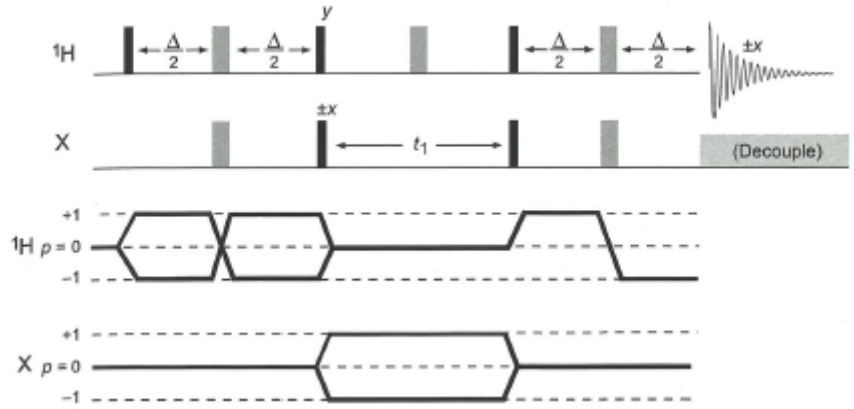

Figure 40: HSQC pulsing scheme.

The pulse sequence utilizes polarization transfer and is J-modulated so to maximize the $^{1}J_{XH}$-coupling. The coupling manipulation is performed so that the acquisition observes in-phase proton magnetization. The manipulation consists of a forward and reverse INEPT-sequence (Insensitive nuclei enhanced by polarization transfer) which utilizes polarization transfer. These are separated by t_1 where the X-nucleus magnetization evolves. This magnetization is what is transferred to the protons when the reverse-INEPT sequence is performed. Since the proton couplings are refocused, decoupling of the heteronucleus may be utilized to collapse the satellites into one signal. This decoupling sequence is termed GARP. Artefacts from ^{1}H-^{12}C couplings may still appear. They are best removed by PFGs. A pulsing scheme exploiting PFGs is shown in figure 41.

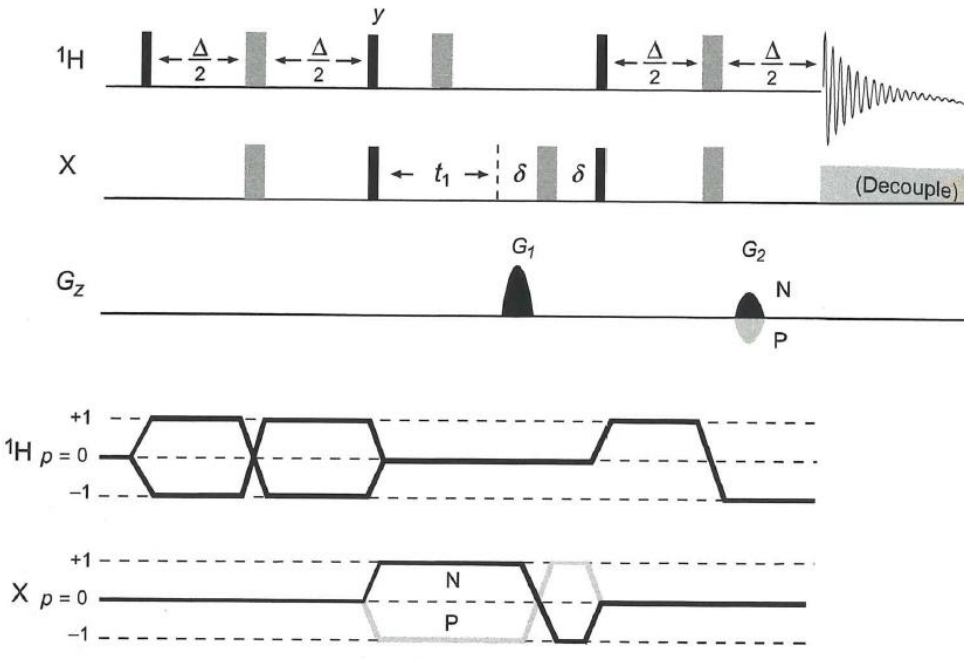

Figure 41: Phase sensitive HSQC pulsing scheme utilizing PGFs.

The HSQC spectrum provides information of which protons are connected to which carbons. By dispersing the signals of one nuclide along the dimension of the other, the distinct groups which may be overlapped in the proton spectrum are revealed, or the HSQC spectrum may then indicate which correlations in COSY are geminal which are vicinal. It is common practice to perform HSQC experiments between ^{1}H and ^{15}N on samples containing amino acids.[29]

Heteronuclear Multiple-Bond Correlation Spectroscopy: HMBC

The heteronuclear multiple-bond correlation (HMBC) experiment is similar to the HSQC experiment in that the nuclide of interest is the protons and it establishes a chemical relationship between different types of nuclei. This experiment also utilizes coherence transfer. The goal of HMBC, however, is to produce correlations across multiple bonds. Typically the experiment is ‘tuned’ to detect small couplings over two to three chemical bonds. Two pulse sequences for general HMBC experiments are given in figure 42.

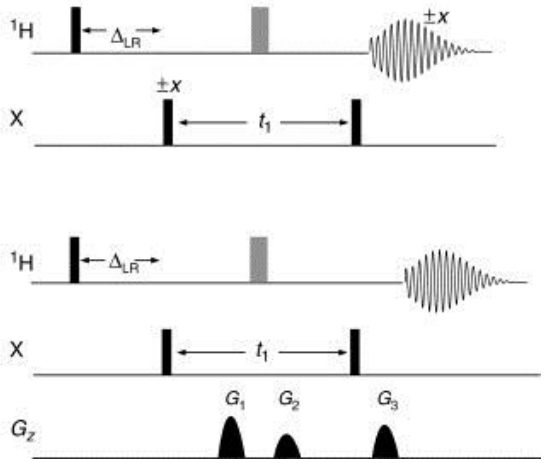

Figure 42: HMBC pulsing scheme.

The 'tuning', or selection of which couplings to detect is determined by Δ_{LR}. This time segment allows for the long-range couplings between protons and the hetero-nuclide of interest to evolve and produce anti-phase displacement. By increasing Δ_{LR}, the sample may relax before acquisition. Thus not all couplings may be selected due to relaxation losses.

By application of PGFs, the parent resonances are effectively removed and the correlations become easily discernable from noise as PGFs filter it away.[29]

Hybrid experiments: HSQC-DIPSI/TOCSY and DEPT135-HSQC

HSQC and SHSQC may be combined with DEPT135 to produce phase sensitive HSQC where methylene correlation are negative while methyl and methine correlation are positive. This type of HSQC and SHSQC is what has been utilized in this thesis. HSQC may also be combined with DIPSI-2. Pulse sequences may be combined to form HSQC-DIPSI as well as DIPSI-HSQC.[29]

2.1.9 Selective experiments

Selective homonuclear experiments: SelTOCSY, SelROESY, Homonuclear decoupling

Selective TOCSY (SelTOCSY) and Selective ROESY (SelROESY) experiments select one frequency to irradiate. This is chosen by what will produce fruitful information. Typically the

frequency is set to the uncalibrated frequency of a signal of interest. The resulting spectrum will be a 1D spectrum where nuclei interacting with excited nuclei are exclusively shown. Thus a SelTOCSY experiment will produce propagation from the irradiated proton through its spin system. This is particularly fruitful when signals overlap. In an analogue fashion, a SelROESY experiment will produce a 1D spectrum with signals from which it interacts with through dipolar couplings. Issues regarding classical ROESY experiments also apply here.[29]

Homonuclear decoupling experiments decouple a selective frequency. This results in a 1D where the decoupled signal's coupling constants are removed, resulting in a simpler multiplicity of its coupling partners. This may be a useful tool when determining coupling constants.[29]

Band-Selective Heteronuclear experiments: SHSQC and SHMBC

The pulse sequences thus far has typically utilized hard pulses to achieve excitation of the entire spectrum. When employing such techniques, the spectral window (SW) must be wide enough to record all correlations. Otherwise folding will appear. The detection method for the F1 dimension, time proportional phase incrementation (TTPI), will not be able to filter them away like in the F2 dimension, where States-detection is utilized. To achieve a smaller spectral window without folding, softer pulses are used to excite a frequency window. Furthermore PFGs are used to filter away unwanted resonances.

Band-selective HMBC and HSQC may record segments of the carbon spectrum without folded signals. This may save spectrometer time and/or provide better resolution in the F1 dimension. It is very thus a good option to resolve clusters of correlations with similar chemical shifts for ^{13}C such as amide linkages.[29]

2.1.10 NMR processing

A recorded unprocessed NMR spectrum may exhibit numerous traits which encumbers elucidation. Thus it is standard practice to mathematically alter the recorded signal to account for these encumbering factors as well as enhance the features of interest.

A freshly recorded NMR experiment, before subjected Fourier-Transform (FT), is termed the free induction decay (FID). This is the signal recorded by the listening coil and is the sum of all frequencies resulting from precession in the sample. Three examples of a FID is illustrated in figure 43.

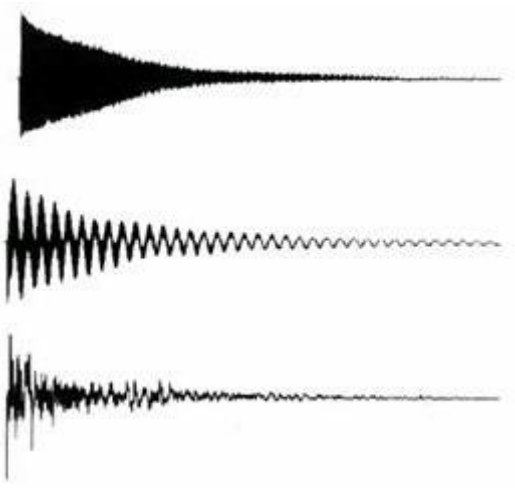

Figure 43: Three different FIDs recorded during acquisition.

Zero-Filling

If the sample does not fully relax during acquisition, the sample signals does not die off and the FID isn't pure noise by the end of acquisition. This may more prominent for slowly relaxing nuclei such as quaternary carbons. Numerous mathematical approaches may be applied to the FID with advantage. One of these is zero-filling. Zero-filling is the process of appending zeros to the end of the FID. By doing this, the digital resolution is artificially enhanced and may reveal fine structure and lineshape definition. If the acquisition time is too short and zero-filling applied, the FID is termed a truncated FID. A truncated FID produces 'sinc wiggles' in the spectrum when FT is applied. A way to manage sinc wiggles and enhance fine structure is linear prediction.[29]

Linear prediction

Linear prediction is a more sophisticated way of extending the FID. Linear prediction predicts the next data points. The next data point can be estimated by linear prediction of the immediately preceding values. It can be applied to both ends of the FID, but is typically

applied to the end of the FID. This is termed forward linear prediction. This type of FID manipulation needs a high S/N to accurately predict the linear prediction coefficients.[29]

Window functions (WDW)

Window functions (WDWs) are another way of mathematically manipulating the FID. This is typically done to enhance S/N or reveal fine structure. Window functions are mathematical weighing functions. The FID contains a lot of S/N at the start of the FID. By the end of the FID, the couplings will have had plenty of time to evolve, and this segment contains prominent fine structure. If employing a weighing function which weighs the start of the FID more heavily than the end, S/N in the resulting spectrum will be improved at the cost of fine structure. An example of this is an exponential weighing function. A weighing function that focuses on the end will in the same fashion enhance fine structure at the cost of S/N. An example of this is a Laurentz-Gauss weighing function. Additionally, this is another approach towards removing effects seen in a truncated FID. By forcing the FID to zero, the weighed FID is no longer truncated.[29]

Linebroadening is typically employed together with window functions. By applying too much of a window function, the lines in the spectrum may broaden. This may be adjusted for with linebroadening.[29]

Phase correction

After the FID has been subjected to FT, the spectrum is produced. The spectrum may need phase correction. This is caused by the receiver not being perfectly matched with the initial phase of the resultant magnetic vector. This is termed zero-order phase correction and independent of resonance frequencies. The other type of phase correction is frequency dependent and termed first-order phase correction. This arises in the pre-acquisition delay where the nuclei may precess a little before acquisition. When phasing a spectrum, ideally the phase corrected signals should be as far apart as possible to create proper phase correction for the entire spectrum.[29]

Calibration

Liquid-state NMR utilizes a deuterated solvent which contains a small amount of the proton analogue of the molecule. This produces a signal which is routinely used to calibrate the spectrum to produce the same chemical shifts when using different instruments. The chemical shift of the most common solvents sued for calibration has been tabulated by Gottlieb Et. al. (1997). The shift induced by this calibration is known as the spectrum reference frequency (SR). When acquiring numerous spectra of the same sample, it is advantageous to use the same SR for all spectra, as this will produce the same chemical shifts across spectra.[28]

Chemical shift assignment and integration

Chemical shift is the resonance frequency from which a nucleus exhibits when couplings are removed of absent. It is this resonance that is reported when documenting chemical shift, which is standard practice. Integration over each set of resonances which produces chemical shifts is a method utilized to determine the relative amount of nuclei residing at each chemical shift. The relative size of these integrals may be indicative of the nature of the species which produces the integrated peaks. E.g. if integration of all peaks in a 1D proton spectrum has been completed and one peak, A, is calibrated to 1, there are two signals, B and C, which respectively integrate to ~2 and ~3. This then indicates that there are twice and three times as many protons producing signal B and C respectively. This may then indicate that A is a methine, B is a methylene and C is a methyl, pending on the rest of the spectrum. Unless extra care is taken, integrals are fairly inaccurate and may be 10-20% off from their true values. Some signal suppression techniques such as ES may affect integrals by perturbing the baseline.[28]

3 Experimental Section

The experiments were performed at the NMR laboratory at the Department of Chemistry, University of Oslo under the supervision of Prof. Frode Rise (University of Oslo) and Prof.Em. Alistair L. Wilkins (University of Waikato). The samples were produced by Greenwater Laboratories CyanoLab (Florida, USA) by M.Sc. Amanda Foss and supplied by project owner Ph.D. Christopher O. Miles (https://www.nrc-cnrc.gc.ca/eng/about/directions/halifax.html#). Ph.D. Per Eugen Kristiansen at IBV, University of Oslo was invited to join the project as a consultant and has acted as such.

The samples were sent to the Norwegian Veterinary Institute and prepared by Ph.D. Silvio Uhlig prior to the start of the project in 3 mm NMR tubes by dilution in *d3*-MeOH. The NMR tubes used were of outer diameter 3 mm, thin wall (0.29 mm) with 7" length from Wilmad Precision NMR Sample Tubes (USA), SKU: 341-PP-7, Class A Glass material, Batch 120516A. The samples are estimated to be 200 µg each.

The solvent used (*d3*-MeOH) was bought from Sigma-Aldrich Pcode: 1002621452 343854-1G Lot # MBBC0699. The NMR tube holder used initially for the experiments were supplied by Prof. Finn Lillelund Aachmann from the Department of Biotechnology and Food Science, The Norwegian University of Science and Technology and two identical spinner were later bought from Rototec-Spintec (Laienberstr 12, 75323 Bad Wildbad, Germany): 3 mm Bruker Spinner Turbine, VT optimized for non-spinning operation -150° to +200°C, +/-13g, PEEK, 3 mm PEEK Fingers.

The NMR instrument used for the experiments was composed of an 800 MHz magnet (Ascend^{TM} 800) paired with electronics console (AVANCE III HD), sample holder (SAMPLECASE COOLED) paired with air supply unit (BCU I 40/50) and a TCI Cryogenic Probe (^{1}H, ^{13}C and ^{15}N) cooled by cooling system (CRYO PLATFORM), all supplied by Bruker Biospin Fällanden Switzerland.

The software used for interpretation and processing of spectra was Bruker TopSpin 3.5 patch level 6 and 7. The software used for conducting experiments was Bruker TopSpin 3.5 patch level 7.

All experiments were conducted at 300.8 °K which was electronically calibrated to be 25°C. All experiments except PROTON were written by Prof.Em. Alistair L. Wilkins, whom may be contacted at wilkinsalw@hotmail.com in case inquiry regarding them are needed. The experiment "PROTON" was an original experiment. The pulse programs are given (copied) in appendix and are referenced in this section.

Every time a sample was entered into the instrument, it was left to temperature equilibrate for ca 15 min. The solvent (*d3*-MeOH) using Bruker's lock made for d3-MeOH. The sample was consequently tuned and matched, before shimming. Shimming was initiated by loading of a shim file. The shim files used were made by Prof. Frode Rise and Prof.Em. Alistair. L. Wilkins. Rise's shim file, made 15.08.2018, was used till the creation of Wilkins' file was made 15.10.2018. Further shimming was conducted in the TopShim GUI window shown in figure 44.

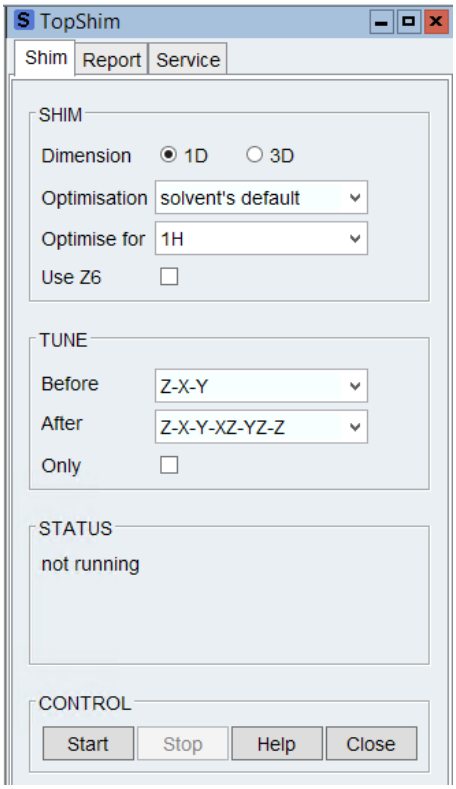

Figure 44: The graphical unit interface (GUI) in TopSpin for shimming NMR samples, TopShim.

The shimming was optimized for ^{1}H as these were the bulk of experiments run for each session. In the TUNE section "z-x-y" was selected for the "Before"-slot while "z-x-y-xz-yz-z" was selected for the "After"-slot. Shimming was conducted till the finished report showed a maximum change of shim directions (z-x-y-xz-yz-z) of two digits. All experiments were run

by use of the “zg”-command (zero go) and set in TopSpin’s spooler queue unless otherwise specified. All proton spectra and proton-dimensions were calibrated to 15.11 Hz by use of the SR input window in TopSpin. All carbon spectra and carbon-dimensions were calibrated to negative 318.04 Hz by use of the SR input window in TopSpin.

3.1 1D experiments

All relevant 1-dimensional experiments can be found in this subchapter apart from selective experiments: Selective TOCSY and selective ROESY.

3.1.1 1D Proton experiments on sample #1

Different solvent-suppression techniques were employed with different level of suppression to determine optimal conditions. Decoupling frequencies, for all experiments, were set to 3890 Hz and 2663 Hz respectively. When suppressing only one frequency, suppression at 3890 Hz was prioritized.

PROTON

A standard Bruker version proton experiment was performed on sample number 1 under the name 1. The spectrum was centered at 4940.19 Hz (O1). Acquisition and processing parameters are given in table 3. The pulse program is in Appendix A (p. 156).

Table 3: Table of acquisition and processing parameters for experiment 1.

Acquisition parameters		Processing parameters	
Type	Magnitude or selection	Type	Magnitude or selection
Spectral width [ppm]	20.0312	WDW	EM
NS	16	LB [Hz]	0.3
TD	65 536	LPBIN	0
TD0	1	NOCOEF	0
AQ [sec]	2.0447233	BC_mod	quad
rpar file	PROTON	ME_mod	no
Pulse program	zg30	SI	65 536
RG	203		

awProtonES

A proton spectrum with excitation sculpting was run on sample number 1 under the name 2. Aqcuisition and processing parameters are given in table 4. The pulse program is in Appendix A (p. 156).

Table 4: Table of acquisition and processing parameters for experiment 2.

Acquisition parameters		Processing parameters	
Type	Magnitude or selection	Type	Magnitude or selection
Spectral width [ppm]	20.0312	WDW	EM
NS	8	LB [Hz]	0.1
TD	131 072	LPBIN	0
TD0	1	NCOEF	0
AQ [sec]	4.0894465	BC_mod	quad
rpar file	awprotones	ME_mod	no
Pulse program	zgesgp	SI	131 072
RG	203		

awProtonPR

A proton spectrum with presaturation was collected on sample number 1 under the name 3. Aqcuisition and processing parameters are given in table 5. The pulse program is in Appendix A (p. 156).

Table 5: Table of acquisition and processing parameters for experiment 3.

Acquisition parameters		Processing parameters	
Type	Magnitude or selection	Type	Magnitude or selection
Spectral width [ppm]	20.0312	WDW	EM
NS	4	LB [Hz]	0.1
TD	131 072	LPBIN	0
TD0	1	NCOEF	0
AQ [sec]	4.0894465	BC_mod	quad
rpar file	awprotonpr	ME_mod	no
Pulse program	zgpr	SI	131 072
RG	16		

awProtonESPRF1PRF2

A series of proton spectra were collected with suppression at 2663 Hz and 3890 Hz using the techniques presaturation and excitation sculpting, respectively. The frequency 3890 Hz was suppressed utilizing both presaturation and excitation sculpting, while the frequency 2663 Hz was suppressed by only presaturation. Acquisition and processing parameters consistent for

the series are given in tables 6. The pulse program is in Appendix A (p. 156). The names of the experiments altered parameters are given in table 7.

Table 6: Table of acquisition and processing parameters consistent for experiments 7-13

Acquisition parameters		Processing parameters	
Type	Magnitude or selection	Type	Magnitude or selection
Spectral width [ppm]	20.0312	WDW	EM
NS	8	LB [Hz]	0.1
TD	131 072	LPBIN	0
TD0	1	NCOEF	0
AQ [sec]	4.0894465	BC_mod	quad
rpar file	awprotonesprf1prf2	ME_mod	no
Pulse program	awprotonesprf1prf2	SI	131 072
RG	203		
SPW10 [dB]	26.98		
SPNAM10	Sinc1.1000		
P40 [µs]	2000		

Table 7: Altered parameters for experiments 7-13.

Exp. Name	PLW21 [dB]
7	55
8	50
9	47
10	45.56
11	40
12	35
13	38

awProtonESPR

A proton spectrum with excitation sculpting and presaturation on the same frequency was collected under the name 4 on sample number 1 under the name 4. Acquisition and processing parameters are given in table 8. The pulse program is in Appendix A (p. 156).

Table 8: Table of acquisition and processing parameters for experiment 3.

Acquisition parameters		Processing parameters	
Type	Magnitude or selection	Type	Magnitude or selection
Spectral width [ppm]	20.0312	WDW	EM
NS	8	LB [Hz]	0.1
TD	131 072	LPBIN	0
TD0	1	NCOEF	0

AQ [sec]	4.0894465	BC_mod	quad
rpar file	awprotonespr	ME_mod	no
Pulse program	awprotonespr	SI	262 144
RG	16		

awProtonESF1PRF2

Upon completion of all aforementioned experiments in this subchapter, a series proton spectra with optimal suppression with PR and different conditions for ES were collected under the names 6007 and 7002. ES was set to suppress 3890 Hz while PR was set to suppress 2663 Hz. Acquisition and processing parameters for experiments 6007 and 7002 are given in table 9 and 10 respectively. The pulse program is the same for the remaining experiments in this segment and given in appendix A (p. 156). P40 (ES pulse time) was set to 4000 μsec, SPW10 (ES pulse "hardness") was set to 32.98 dB and PLW21 (PR "hardness") was set to 45.56 dB for both experiments.

Table 9: Table of acquisition and processing parameters for experiment 6007.

Acquisition parameters		Processing parameters	
Type	Magnitude or selection	Type	Magnitude or selection
Spectral width [ppm]	9.0140	WDW	EM
NS	8	LB [Hz]	0.3
TD	131 072	LPBIN	0
TD0	1	NCOEF	0
AQ [sec]	9.0876589	BC_mod	quad
rpar file	awprotonesprf2	ME_mod	no
Pulse program	awprotonesprf2	SI	131 072
RG	203		

Table 10: Table of acquisition and processing parameters for experiment 7002.

Acquisition parameters for 7002		Processing parameters for 7002	
Type	Magnitude or selection	Type	Magnitude or selection
Spectral width [ppm]	9.0140	WDW	EM
NS	512	LB [Hz]	0.3
TD	131 072	NCOEF	0
TD0	1	LPBIN	0
AQ [sec]	9.0876589	BC_mod	quad
rpar file	awprotonesprf2	ME_mod	no
Pulse program	awprotonesprf2	SI	131 072

RG	203		

3.1.2 1D Carbon experiments on sample #1

No special suppression techniques which aren't typically present in their respective experiments were employed. The experiments were optimized for coupling constants of 145 Hz.

awDEPT135

A carbon experiment was run on sample number 1 under the name 7062. Acquisition and processing parameters are given in table 11. The pulse program is in Appendix A (p. 156).

Table 11: Table of acquisition and processing parameters for experiment 7062.

Acquisition parameters		Processing parameters	
Type	Magnitude or selection	Type	Magnitude or selection
Spectral width [ppm]	238.9630	WDW	EM
NS	50 191	LB [Hz]	2
TD	65 536	NCOEF	0
TD0	1	LPBIN	0
AQ [sec]	0.6815744	BC_mod	quad
rpar file	awdept135sp	ME_mod	no
Pulse program	deptsp135	SI	65 536
RG	196.48		

awDEPTQ

A carbon spectrum specialized to set to only filter away all but quaternary carbons (DEPTQ) was collected on sample number 1 under the name 7063. Acquisition and processing parameters are given in table 12. The pulse program is in Appendix A (p. 156).

Table 12: Table of acquisition and processing parameters for experiment 7063.

Acquisition parameters		Processing parameters	
Type	Magnitude or selection	Type	Magnitude or selection
Spectral width [ppm]	70.0029	WDW	EM
NS	73 728	LB [Hz]	2
TD	19 110	NCOEF	32

TD0	1	LPBIN	160
AQ [sec]	0.6784050	BC_mod	quad
rpar file	awdeptq	ME_mod	no
Pulse program	deptqgpsp	SI	65 536
RG	196.48		

3.1.3 1D Proton experiments on sample #2

awProtonESF1PRF2

A trial proton experiment, 2, employing ES on 3890 Hz and PR on 2663 Hz was run. Acquisition and processing parameters are given in table 13. The pulse program is in Appendix A (p. 156).

Table 13: Table of acquisition and processing parameters for experiment 2.

Acquisition parameters		Processing parameters	
Type	Magnitude or selection	Type	Magnitude or selection
Spectral width [ppm]	9.0140	WDW	EM
NS	8	LB [Hz]	0.3
TD	131 072	NCOEF	0
TD0	1	LPBIN	0
AQ [sec]	9.0876589	BC_mod	Sfil
rpar file	awprotonesprf2	ME_mod	no
Pulse program	awprotonesprf2	SI	131 072
RG	203		

An analogue experiment, 100, was run with NS set to 256.

3.1.4 1D Carbon experiments on sample #2

No special suppression techniques, which aren't typically present in the experiment, were employed. The experiments were optimized for coupling constants of 145 Hz.

awDEPTQ

A carbon spectrum, DEPTQ, was collected on sample number 2 under the name 160. Acquisition and processing parameters are given in table 14. The pulse program is in Appendix A (p. 156).

Table 14: Table of acquisition and processing parameters for experiment 160.

Acquisition parameters		Processing parameters	
Type	Magnitude or selection	Type	Magnitude or selection
Spectral width [ppm]	190.1979	WDW	EM
NS	65 536	LB [Hz]	2
TD	65536	NCOEF	32
TD0	1	LPBIN	160
AQ [sec]	0.8563371	BC_mod	quad
rpar file	awdeptq	ME_mod	no
Pulse program	deptqgpsp	SI	65 536
RG	196.48		

3.2 2D experiments

3.2.1 Homonuclear 2D experiments on sample #1

COSY

A longer COSY experiment was run with identical suppression to experiment 7002 under the name 7010. Acquisition and processing parameters are given in table 15. The pulse program is given in the Appendix A (p. 156).

Table 15: Table of acquisition and processing parameters for experiment 7010.

Acquisition parameters		
	Magnitude or selection	
Type	F2	F1
TD	2 048	256
NS	64	
TD0	0	
TDav	0	
Spectral width [ppm]	9.0140	9.0140
AQ [sec]	0.1419947	0.0177493
RG	203	

rpar file	awcosyesprf2	
Pulse program	awcosyesprf2	
Processing parameters		
	Magnitude or selection	
Type	F2	F1
SI	32 768	2048
WDW	SINE	SINE
LB [Hz]	0.3	0.3
SSB	0	0
ME_mod	no	LPfc
NCOEF	0	64
LPBIN	0	320
BC_mod	quad	no

DIPSI-2

Two longer DIPSI-2 experiments was run with PR-suppression on both frequencies set to 45.56 dB. Experiment 7020 was collected with a shorter mixing time (0.079999998 μsec) while 7023 was run with a mixing time of 0.159999996 μsec. Acquisition and processing parameters for 7020 and 7023 are given in tables 16 and 17 respectively. The pulse program is given in the Appendix A (p. 156).

Table 16: Table of acquisition and processing parameters for experiment 7020.

Acquisition paramete		
	Magnitude or selection	
Type	F2	F1
TD	2 048	256
NS	32	
TD0	1	
TDav	0	
Spectral width [ppm]	9.0140	9.0140
AQ [sec]	0.1419947	0.0177493
RG	203	
rpar file	awdipsi2prf1prf2	
Pulse program	awdipsi2prf1prf2	
Processing parameters		
	Magnitude or selection	
Type	F2	F1
SI	2 048	2048
WDW	QSINE	QSINE
LB [Hz]	1	0.3

SSB	2	2
BC_mod	quad	no
ME_mod	no	LPfr
NCOEF	0	64
LPBIN	0	320

Table 17: Table of acquisition and processing parameters for experiment 7023.

Acquisition parameters		
	Magnitude or selection	
Type	F2	F1
TD	2 048	256
NS	64	
TD0	1	
TDav	0	
Spectral width [ppm]	9.0140	9.0140
AQ [sec]	0.1419947	0.0177493
RG	203	
rpar file	awdipsi2prf1prf2	
Pulse program	awdipsi2prf1prf2	
Processing parameters		
	Magnitude or selection	
Type	F2	F1
SI	2 048	2048
WDW	QSINE	QSINE
LB [Hz]	1	0.3
SSB	2	2
BC_mod	quad	no
ME_mod	no	LPfr
NCOEF	0	64
LPBIN	0	320

NOESY

A trial NOESY spectrum, named 190, was collected with identical suppression as experiment 7002. The acquisition and processing parameters are given in table 18. The pulse program is given in the Appendix A (p. 156).

Table 18: Table of acquisition and processing parameters for experiment 190.

Acquisition parameters	
	Magnitude or selection

Type	F2	F1
TD	2 048	256
NS	8	
TD0	1	
TDav	0	
Spectral width [ppm]	12.0187	12.0187
AQ [sec]	0.1064960	0.0133120
RG	203	
rpar file	awnoesyesprf2	
Pulse program	awnoesygpesprf2	
Processing parameters		
	Magnitude or selection	
Type	F2	F1
SI	2 048	2048
WDW	QSINE	QSINE
LB [Hz]	1	0.3
SSB	2	2
BC_mod	quad	no
ME_mod	no	no
NCOEF	0	0
LPBIN	0	0

ROESY

A ROESY experiment, named 279, was run with identical suppression as experiment 7002. The acquisition and processing parameters are given in table 19. The pulse program is given in the Appendix A (p. 156).

Table 19: Table of acquisition and processing parameters for experiment 279.

Acquisition parameters		
	Magnitude or selection	
Type	F2	F1
TD	2 048	256
NS	80	
TD0	0	
TDav	0	
Spectral width [ppm]	10.0156	10.0156
AQ [sec]	0.1277952	0.0159744
RG	203	
rpar file	awroesy2esprf2	
Pulse program	awroesyesprf2	

Processing parameters		
	Magnitude or selection	
Type	F2	F1
SI	2 048	2048
WDW	QSINE	QSINE
LB [Hz]	1	0.3
SSB	2	2
BC_mod	quad	no
ME_mod	no	no
NCOEF	0	0
LPBIN	0	0

ROESY

A ROESY spectrum, named 7072, was collected with identical ES suppression as experiment 7002, but with softened PR-suppression to PLW21 equal to 51.56 dB. The acquisition and processing parameters are given in table 20. The pulse program is given in the Appendix A (p. 156).

Table 20: Table of acquisition and processing parameters for experiment 7072.

Acquisition parameters		
	Magnitude or selection	
Type	F2	F1
TD	2 048	256
NS	128	
TD0	0	
TDav	0	
Spectral width [ppm]	9.0140	9.0140
AQ [sec]	0.1419947	0.0177493
RG	203	
rpar file	awnoesyesprf2	
Pulse program	awroesyesprf2	
Processing parameters		
	Magnitude or selection	
Type	F2	F1
SI	2 048	2048
WDW	QSINE	QSINE
LB [Hz]	1	0.3
SSB	2	2
BC_mod	quad	no
ME_mod	no	LPfr

NCOEF	0	32
LPBIN	0	320

3.2.2 Heteronuclear 2D experiments on sample #1

HSQC and SHSQC

The HSQC and SHSQC experiments were set to suppress 3890 and 3884 Hz with PR-suppression respectively. PLW9 was set equal to 45.56 dB. All experiments were optimized for 145 Hz couplings.

A HSQC experiment named 7040 was run. The acquisition and processing parameters are given in table 21. The pulse program is given in the Appendix A (p. 156).

Table 21: Table of acquisition and processing parameters for experiment 7040.

Acquisition parameters		
	Magnitude or selection	
Type	F2	F1
TD	2 048	160
NS	256	
TD0	1	
TDav	0	
Spectral width [ppm]	9.0140	179.9847
AQ [sec]	0.1419947	0.0022093
RG	203	
rpar file	awhsqcedetgpsisp2.3-135pr	
Pulse program	awhsqcedetgpsisp2.3-135pr	
Processing parameters		
	Magnitude or selection	
Type	F2	F1
SI	2 048	2048
WDW	QSINE	QSINE
LB [Hz]	1	0.3
SSB	2	2
BC_mod	quad	no
ME_mod	no	LPfr
NCOEF	0	64
LPBIN	0	320

A series of SHSQC experiments were run. Significantly varying acquisition parameters for the series is given in table 22. All processing parameters were identical and are given in the same table. All experiments were set with a spectral width of 10.0156 ppm in the F2 dimension and between 19.9997 and 20.0002 ppm in the F1 dimension. AQ(F2) = 0.127952 sec and AQ(F1) = 0.0099417 sec. Rpar file; awshsqcedetgpsisp2.3-135pr and pulse program: awshsqcedetgpsisp2.3-135pr. RG = 203, TD0 = 1, TDav = 0.

Table 22: Table of altered acquisition and consistent processing parameters for experiments 8051, 8052 and 8053.

Acquisition parameters		
Exp. Name	NS	F1O1 [ppm]
8051	144	29.000
8052	144	44.000
8053	48	16.500
Processing parameters		
	F2	F1
SI	2048	512
WDW	QSINE	QSINE
LB [Hz]	1	0.3
SSB	2	2
BC_mod	quad	no
ME_mod	no	LPfr
NCOEF	0	32
LPBIN	0	160

HMBC and SHMBC

The HMBC and SHMBC experiments were set up without suppression. All experiments were optimized for 8 Hz couplings.

A HMBC experiment named 7052 was collected. The acquisition and processing parameters are given in table 23. The pulse program is given in the Appendix A (p. 156).

Table 23: Table of acquisition and processing parameters for experiment 7052.

Acquisition parameters		
	Magnitude or selection	
Type	F1	F2
TD	2 048	128

NS	480	
TD0	1	
TDav	0	
Spectral width [ppm]	9.0140	1890.0009
AQ [sec]	0.1419947	0.0016743
RG	203	
rpar file	awhmbcgplpndqfpr	
Pulse program	awhmbcgplpndqfpr	
Processing parameters		
	Magnitude or selection	
Type	F1	F2
SI	2 048	2048
WDW	SINE	SINE
LB [Hz]	0	0
SSB	0	0
BC_mod	quad	no
ME_mod	no	LPfr
NCOEF	0	64
LPBIN	0	320

A series of SHMBC experiments were collected. Acquisition parameters in table 24 were constant for all experiments while acquisition parameters in table 25 were changed. Processing parameters were equal for all experiments in the series. The pulse program is given in the Appendix A (p. 156).

Table 24: Table of acquisition parameters consistent for experiments 8061, 8064 and 8065.

F2		F1					
SW	AQ	SW	AQ	Rpar file	RG	TD0	TDav
9.0140	0.1419947	190.0009	0.0016743	awshmbcq5	23	1	0

Table 25: Table of changed acquisition and consistent processing parameters for experiments 8061 and 8064.

Acquisition parameters		
Exp. Name	NS	F1O1 [ppm]
8061	416	29.000
8064	880	44.000
Processing parameters		
	F2	F1
SI	2048	512
WDW	QSINE	QSINE
LB [Hz]	0	0
SSB	0	0

BC_mod	quad	no
ME_mod	no	LPfr
NCOEF	0	32
LPBIN	0	160

HSQC-DIPSI

A HSQC-DIPSI experiment was conducted and stored as 7045 in the same domain as the other experiments by Prof.Em. Alistair L. Wilkins and is added as supplementary data to the thesis. The acquisition and processing parameters are given in table 26. The pulse program is given in the Appendix A (p. 156). Suppression of 3840.14 Hz was achieved by application of PR-suppression with PLW9 set to 45.56 dB.

Table 26: Table of acquisition and processing parameters for experiment 7045.

Acquisition parameters		
	Magnitude or selection	
Type	F1	F2
TD	2 048	160
NS	512	
TD0	1	
TDav	0	
Spectral width [ppm]	10.0156	164.9992
AQ [sec]	0.1277952	0.0024100
RG	203	
rpar file	awhsqcdietgpsisp	
Pulse program	hsqcdietgpsisp	
Processing parameters		
	Magnitude or selection	
Type	F1	F2
SI	2 048	2048
WDW	QSINE	QSINE
LB [Hz]	1	0.3
SSB	2	2
BC_mod	quad	no
ME_mod	no	LPfr
NCOEF	0	64
LPBIN	0	160

3.2.3 Homonuclear 2D experiments on sample #2

COSY

A COSY spectrum, named 110, was collected with identical suppression as experiment 100. The acquisition and processing parameters are given in table 27. The pulse program is given in the Appendix A (p. 156).

Table 27: Table of acquisition and processing parameters for experiment 110.

Acquisition parameters		
	Magnitude or selection	
Type	F1	F2
TD	2 048	256
NS	32	
TD0	1	
TDav	0	
Spectral width [ppm]	9.0140	9.0140
AQ [sec]	0.1419947	0.0177493
RG	203	
rpar file	awnoesyesprf2	
Pulse program	awroesyesprf2	
Processing parameters		
	Magnitude or selection	
Type	F1	F2
SI	2 048	2048
WDW	SINE	SINE
LB [Hz]	1	0.3
SSB	0	0
BC_mod	quad	no
ME_mod	no	LPfr
NCOEF	0	32
LPBIN	0	320

DIPSI-2

Two DIPSI-2 experiments was run with identical suppression as experiment 100. Experiment 120 was collected with a shorter mixing time (0.079999998 µsec) while 121 was run with a mixing time of 0.159999996 µsec. Acquisition and processing parameters for 120 and 121 are identical and given in tables 28. The pulse program is given in the Appendix A (p. 156).

Table 28: Table of acquisition and processing parameters for experiment 120 and 121.

Acquisition parameters

	Magnitude or selection	
Type	F1	F2
TD	2 048	256
NS	32	
TD0	1	
TDav	0	
Spectral width [ppm]	9.0140	9.0140
AQ [sec]	0.1419947	0.0177493
RG	203	
rpar file	awdipsi2esprf2	
Pulse program	awdipsi2esprf2	
Processing parameters		
	Magnitude or selection	
Type	F1	F2
SI	2 048	2048
WDW	QSINE	QSINE
LB [Hz]	1	0.3
SSB	2	2
BC_mod	quad	no
ME_mod	no	LPfr
NCOEF	0	32
LPBIN	0	320

ROESY2

A ROESY2 experiment, named 130, was run with identical suppression as experiment 100. The acquisition and processing parameters are given in table 29. The pulse program is given in the Appendix A (p. 156).

Table 29: Table of acquisition and processing parameters for experiment 130.

Acquisition parameters		
	Magnitude or selection	
Type	F1	F2
TD	2 048	160
NS	128	
TD0	1	
TDav	0	
Spectral width [ppm]	9.0140	9.0140
AQ [sec]	0.1419947	0.0110933
RG	203	
rpar file	awroesy2esprf2	

Pulse program	awroesy2esprf2	
Processing parameters		
	Magnitude or selection	
Type	F1	F2
SI	2 048	2048
WDW	QSINE	QSINE
LB [Hz]	1	0.3
SSB	2	2
BC_mod	quad	no
ME_mod	no	LPfr
NCOEF	0	32
LPBIN	0	320

A ROESY experiment, named 134, was run with ES-suppression set equal to experiment 100, but PR-suppression (PLW21) softened to 51.56 dB. The acquisition and processing parameters are given in table 30. The pulse program is given in the Appendix A (p. 156).

Table 30: Table of acquisition and processing parameters for experiment 134.

Acquisition parameters		
	Magnitude or selection	
Type	F1	F2
TD	2 048	256
NS	104	
TD0	0	
TDav	0	
Spectral width [ppm]	9.0140	9.0140
AQ [sec]	0.1419947	0.0177493
RG	203	
rpar file	awroesyesprf2	
Pulse program	awroesyesprf2	
Processing parameters		
	Magnitude or selection	
Type	F1	F2
SI	2 048	2048
WDW	QSINE	QSINE
LB [Hz]	1	0.3
SSB	2	2
BC_mod	quad	no
ME_mod	no	LPfr
NCOEF	0	32
LPBIN	0	320

3.2.4 Heteronuclear 2D experiments on sample #2

HSQC and SHSQC

A HSQC and two SHSCQ spectrum were collected. All experiments utilized PR-suppression with PLW9 equal to 45.56 dB and were optimized for 145 Hz. Acquisition and processing parameters the HSQC, 140, are given in table 31. The associated pulse program is given in the Appendix A (p. 156).

Table 31: Table of acquisition and processing parameters for experiment 140.

Acquisition parameters		
	Magnitude or selection	
Type	F1	F2
TD	2 048	128
NS	128	
TD0	1	
TDav	0	
Spectral width [ppm]	9.0140	9.0140
AQ [sec]	0.1419947	0.0159061
RG	203	
rpar file	awhsqcedetgpsisp2.3-135pr	
Pulse program	awhsqcedetgpsisp2.3-135pr	
Processing parameters		
	Magnitude or selection	
Type	F1	F2
SI	2 048	512
WDW	QSINE	QSINE
LB [Hz]	1	0.3
SSB	2	2
BC_mod	quad	no
ME_mod	no	LPfc
NCOEF	0	32
LPBIN	0	320

The SHSQC experiments are analogue to each other and centered on O1F1 equal to 43.000 and 20.000 ppm for experiments 141 and 142 respectively. The equal parameters for both experiments are given in table 32. The pulse program is given in the Appendix A (p. 156).

Table 32: Table of acquisition and processing parameters for experiment 141 and 142.

Acquisition parameters		
	Magnitude or selection	
Type	F1	F2
TD	2 048	128
NS	128	
TD0	1	
TDav	0	
Spectral width [ppm]	9.0140	9.0140
AQ [sec]	0.1419947	0.0159061
RG	203	
rpar file	awshsqc135pr	
Pulse program	awshsqcedetgpsisp2.3-135pr	
Processing parameters		
	Magnitude or selection	
Type	F1	F2
SI	2 048	512
WDW	QSINE	QSINE
LB [Hz]	1	0.3
SSB	2	2
BC_mod	quad	no
ME_mod	no	LPfc
NCOEF	0	32
LPBIN	0	160

HMBC and SHMBC

A HMBC and SHMBC experiment were run. No suppression techniques were utilized for the SHMBC experiment, but HMBC exploited PR-suppression with PLW9 equal to 45.56 dB. All of the experiments were optimized for 8 Hz. F1SW was set to approximately 20 ppm. Acquisition and processing parameters the HMBC, 150, are given in table 33. The associated pulse program is given in the Appendix A (p. 156).

Table 33: Table of acquisition and processing parameters for experiment 150.

Acquisition parameters		
	Magnitude or selection	
Type	F1	F2
TD	2 048	256
NS	320	
TD0	1	

TDav	0	
Spectral width [ppm]	9.0140	190.0019
AQ [sec]	0.1419947	0.0033485
RG	203	
rpar file	awhmbcgplpndqfpr	
Pulse program	awhmbcgplpndqfpr	
Processing parameters		
	Magnitude or selection	
Type	F1	F2
SI	2 048	2048
WDW	SINE	SINE
LB [Hz]	0	0
SSB	0	0
BC_mod	quad	no
ME_mod	no	LPfr
NCOEF	0	64
LPBIN	0	320

Acquisition and processing parameters for the SHMBC experiment 151 are given in table 34. The associated pulse program is given in the Appendix A (p. 156).

Table 34: Table of acquisition and processing parameters for experiment 151.

Acquisition parameters		
	Magnitude or selection	
Type	F1	F2
TD	2 048	72
NS	880	
TD0	1	
TDav	0	
Spectral width [ppm]	10.0156	19.9994
AQ [sec]	0.1277952	0.0089465
RG	203	
rpar file	awshmbcq5	
Pulse program	awhmbcgplpndqfpr	
Processing parameters		
	Magnitude or selection	
Type	F1	F2
SI	2 048	512
WDW	SINE	SINE
LB [Hz]	0	0
SSB	0	0
BC_mod	quad	no

ME_mod	no	LPfr
NCOEF	0	32
LPBIN	0	160

HSQC-DIPSI

A HSQC-DIPSI experiment was conducted and stored as 143 in the same domain as the other experiments by Prof. Frode Rise and is added as supplementary data to the thesis. The acquisition and processing parameters are given in table 35. The pulse program is given in the Appendix A. Suppression of 3840.14 Hz was achieved by application of PR-suppression with PLW9 set to 45.56 dB.

Table 35: Table of acquisition and processing parameters for experiment 143.

Acquisition parameters		
	Magnitude or selection	
Type	F1	F2
TD	2 048	160
NS	320	
TD0	1	
TDav	0	
Spectral width [ppm]	10.0156	164.9992
AQ [sec]	0.1277952	0.0024100
RG	203	
rpar file	awhsqcdietgpsisp	
Pulse program	hsqcdietgpsisp	
Processing parameters		
	Magnitude or selection	
Type	F1	F2
SI	2 048	512
WDW	SINE	SINE
LB [Hz]	0.5	0.3
SSB	2	2
BC_mod	quad	no
ME_mod	no	LPfc
NCOEF	0	64
LPBIN	0	256

3.3 Selective experiments

3.3.1 Selective TOCSY on sample #1

A series of selective TOCSY experiments, 8019-8024, 8030-8035, 8040-8044 and 12, were conducted. The rpar-file used to load the experiment was awseltocsyprf2. In all but experiment 8020, the decoupling frequency O2 was set to 3884 Hz, while for 8020, it was set to 3871 Hz. PLW9 was set to 45.56 dB for all experiments. Mixing time, D9, was set to 160 msec for all but 8043 and 8044 which were set to 80 msec. Table 36 contains all of the experiments which includes other parameters. The point of irradiation was set on an uncalibrated 1D proton spectrum by entering the signal of interest's frequency in Hz. Processing parameters are given in table 37. All experiments were set up and run by Prof.Em. Alistair L. Wilkins after consultation with the author. The pulse program is given in the Appendix A (p. 156).

Table 36: Acquisition parameters for selective TOCSY experiments run.

Exp. No	O1 [ppm]	NS	SW [ppm]	RG
8019	4.295	512	12.0187	203
8020	4.600	1024	9.0140	203
8021	4.423	512	12.0187	203
8022	4.130	512	12.0187	203
8023	0.909	512	18.0282	203
8024	1.387	512	18.0281	203
8030	7.717	1024	18.0280	203
8032	7.987	1024	18.0280	203
8033	8.176	1024	18.0280	203
8034	8.317	1024	18.0280	203
8035	8.353	1024	18.0280	203
8040	1.036	512	18.0282	203
8041	1.057	512	18.0282	203
8042	1.074	512	18.0282	203
8043	4.394	4096	12.0187	203
8044	4.417	512	12.0187	203
*12	2.840	320	10.0156	144

*Was stored under KWT#1a with exp. No. 12.

Table 37: Processing parameters for selective TOCSY experiments run.

Processing parameters

Exp. No	SI	WDW	LB [Hz]	GB	SSB	BC_mod	ME_mod	NCOEF	LPBIN
8019-8024	65 536	EM	0.50	0.3	0	quad	LPfr	64	320
8030	65 536	EM	0.50	0.3	0	quad	LPfr	64	320
8032-8044	65 536	EM	0.50	0.3	0	quad	LPfr	64	320
12*	65 536	EM	0.50	0.3	0	quad	LPfr	64	320

*Was stored under KWT#1a with exp. No. 12.

3.3.2 Selective ROESY on sample #1

A series of selective ROESY experiments, 8091-8110, were conducted. The rpar-file used to load the experiment was awselroesyprf2. The decoupling frequency O2 was set to 3890 Hz and PLW9 were set to 45.56 dB for all experiments. Mixing time, P15, was set to 250, 500 and 300 msec for all experiments. Table 38 contains all of the experiments which includes acquisition parameters altered. The point of irradiation was set on an uncalibrated 1D proton spectrum by entering the frequency in Hz. Processing parameters are given in table 39. All experiments were set up and run by Prof.Em. Alistair L. Wilkins after consultation with the author. The pulse program is given in the Appendix A (p. 156) and spectra in appendix B (p. 275).

Table 38: Acquisition parameters for selective ROESY experiments run.

Ex. No	NS	SW [ppm]	RG	Mixing time P15 [msec]	O1 [ppm]
8091	1024	16.0250	203	250	1.069
8092	2048	12.0187	144	250	5.571
8093	1024	16.0250	203	500	1.069
8094	2048	12.0188	203	500	1.713
8095	2048	13.9503	203	500	1.933
8096	2048	16.0250	203	500	1.713
8097	2048	11.0030	71.8	500	5.459
8098	2048	16.0249	203	500	8.175
8099	2048	12.0187	80.6	500	6.262
8100	2048	13.0203	161	300	2.541
8101	2048	13.0203	144	300	2.840
8103	2048	13.9503	203	300	2.138
8104	2048	13.0203	144	300	2.692
8105	2048	13.0203	144	300	2.592
8106	2048	12.0187	144	300	5.872
8107	2048	12.0187	144	300	3.366
8108	2048	13.9503	203	300	2.069
8109	2048	15.0235	144	300	4.862
8110	2048	16.0249	144	300	4.862

Table 39: Processing parameters for selective ROESY experiments run.

Processing parameters									
Exp. No	SI	WDW	LB [Hz]	GB	SSB	BC_mod	ME_mod	NCOEF	LPBIN
8091-8101	65 536	EM/GM	0.5/-1	0.3	0	quad	LPfr	32	160
8103-8110	65 536	EM/GM	0.5/-1	0.3	0	quad	LPfr	32	160

3.3.3 Selective TOCSY on sample #2

A series of selective TOCSY experiments, 211-218, 221-226, 10-15 and 21-25, were conducted. The rpar-file used to load the experiment was awseltocsyprf2. In all experiments the decoupling frequency O2 was set to 3884 Hz, while for 8020, PLW9 was set to 45.56 dB. Table 40 contains all of the experiments which includes other acquisition parameters. The point of irradiation was set on an uncalibrated 1D proton spectrum by entering the signal of interest's frequency in Hz. Processing parameters are given in table 41. All experiments were set up and run by Prof.Em. Alistair L. Wilkins after consultation with the author. The pulse program is given in the Appendix A (p. 156).

Table 40: Acquisition parameters for selective TOCSY experiments.

Acquistion parameters						
Exp. No	O1 [ppm]	NS	SW [ppm]	AQ [sec]	RG	D9 [msec]
211	3.147	4096	12.0187	1.7039360	71.8	80
212	4.394	4096	12.0187	1.7039360	203	80
213	4.355	4096	12.0187	1.7039360	71.8	80
214	4.354	4096	12.0187	1.7039360	71.8	80
215	4.295	256	12.0187	1.7039360	203	80
216	4.135	256	12.0187	1.7039360	203	80
217	4.632	512	12.0187	1.7039360	203	80
218	4.582	768	12.0187	1.7039360	203	80
221	8.331	256	18.0280	2.2719147	203	80
222	8.565	256	18.0280	2.2719147	203	80
223	8.283	256	18.0280	2.2719147	203	80
224	8.126	256	18.0280	2.2719147	203	80
225	7.925	256	18.0280	2.2719147	203	80
226	7.830	256	18.0280	2.2719147	203	80
*10	1.366	64	16.0250	2.5559039	71.8	80
*11	3.614	320	16.0250	2.5559039	128	80

*12	4.576	320	16.0250	2.5559039	128	80
*13	4.361	320	16.0250	2.5559039	128	80
*14	4.389	320	16.0250	2.5559039	128	80
*15	3.146	320	16.0250	2.5559039	128	80
*21	3.614	320	16.0250	2.5559039	128	160
*22	4.576	320	16.0250	2.5559039	128	160
*23	4.365	80	16.0250	2.5559039	128	160
*24	4.385	256	16.0250	2.5559039	128	160
*25	3.146	320	16.0250	2.5559039	128	160

*Stored under folder KWT#2a

Table 41: Processing parameters for selective TOCSY experiments run.

Processing parameters									
Exp. No	SI	WDW	LB [Hz]	GB	SSB	BC_mod	ME_mod	NCOEF	LPBIN
180-183	65 536	EM	0.50	0.3	0	quad	LPfr	64	320
211-218	32 768	EM	0.50	0.3	0	quad	LPfr	32	160
221-226	65 536	EM	0.50	0.3	0	quad	LPfr	64	320
*10-25	65 536	EM	0.50	0.3	0	quad	LPfr	32	160

3.3.4 Selective ROESY on sample #2

A series of selective ROESY experiments, 232-248, were run. The rpar-file used to load the experiment was awselroesyprf2. In all experiments the decoupling frequency O2 was set to 3890 Hz, P15 was set to 45.56 dB. Table 42 contains includes other acquisition parameters while table 43 contains the resonances of interest.. The point of irradiation was set on an uncalibrated 1D proton spectrum by entering the signal of interest's frequency in Hz. Processing parameters are given in table 44. All experiments were set up and run by Prof.Em. Alistair L. Wilkins after consultation with the author. The pulse program is given in the Appendix A (p. 156).

Table 42: Acquisition parameters for selective ROESY experiments run.

Ex. No	NS	SW [ppm]	RG
232-237	1600	16.9829	203
238	1600	12.0188	203
240-242	1600	10.0156	57
243	1600	10.0156	90.5
244	1600	10.0156	101

245	1600	10.0156	90.5
246	1600	10.0156	203
247	1600	15.0235	203
248	1600	15.0235	203

Table 43: Irradiated resonances of selective ROESY experiments run.

Ex. No	O1 [ppm]
232	8.568
233	8.337
234	8.283
235	8.120
236	7.942
237	7.833
238	1.713
240	4.131
241	4.384
242	4.295
243	4.130
244	5.878
245	5.427
246	6.264
247	1.610
248	1.531

Table 44: Processing parameters of selective ROESY experiments run.

Processing parameters									
Exp. No	SI	WDW	LB [Hz]	GB	SSB	BC_mod	ME_mod	NCOEF	LPBIN
232-238	65 536	EM/GM	0.50/-1	0.3	0	quad	LPfr	32	160
240-248	65536	EM/GM	0.50/-1	0.3	0	quad	LPfr	32	160

4 Results and discussion

The strategy applied to the elucidation may be described as the following: The COSY, DIPSI-2 and selective TOCSY spectra were utilized to determine the spin system. The order of constituents were determined by the COSY and HSQC spectra. Linking together amino acids and other spin systems was primarily done by interpreting the HMBC spectra. When the HMBC spectra were found to be inadequate, NOE-data were used instead. Where the ROESY spectra were inadequate, selective ROESY experiments were utilized to determine what the situation was likely to be. When the collected NMR data was found to be inadequate, the literature covering NMR shifts for MCs were used. When the available NMR data were inadequate, data from mass spectrometry was utilized.[40]

4.1 Sample #1

4.1.1 Spectra:

A series of different suppression techniques were utilized in short 1D proton experiments to determine the optimal combination and level of suppression. During calibration of PR-suppression, it was noted by Prof.Em. Alistair L. Wilkins that one of the overlapping resonances were being suppressed by PR-suppression. It also became clear that one signal overlaps with the satellite of the solvent at 3.35 ppm. To account for this, PR on 3890 Hz were abandoned and ES on the same frequency was softened. The spectra with suppression with ES, ESPRPR and ESPR on 3890 Hz and 2663 Hz are given in figures 45, 46 and 47 respectively.

The following spectra were used to elucidate the structure of sample #1 and will be frequently referenced throughout the thesis. Supplementary spectra are given in Appendix B (p. 275). The 1D proton, DEPT135, DEPTQ, COSY, DIPSI-2, HSQC, SHSQC, HMBC, SHMBC, ROESY2 and selective experiments used to elucidate the structure will be given in this order.

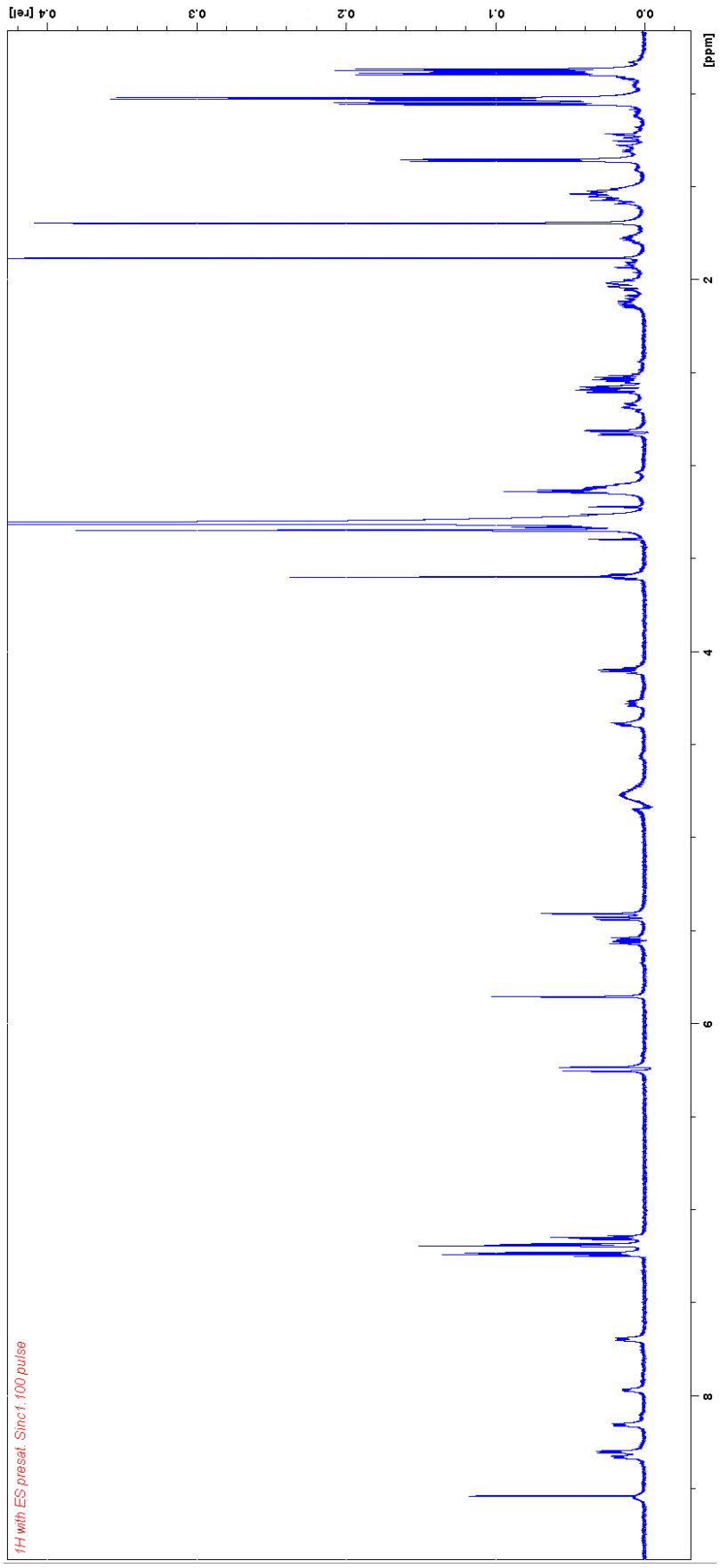

Figure 45: Experiment number 2 with ES applied to 3890 Hz. Overlapping resonances at 8.53 ppm.

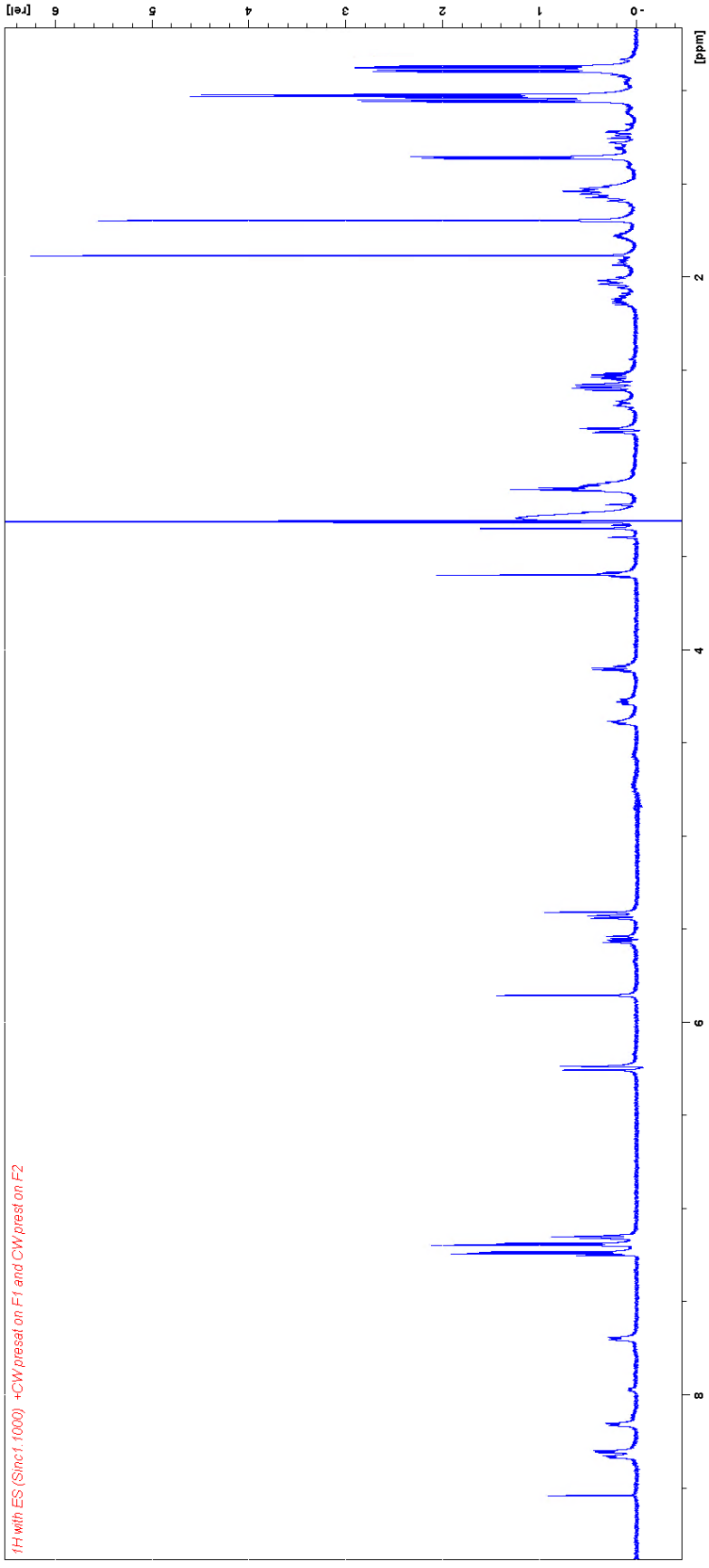

Figure 46: Experiment number 7 with ES and PR applied to 3890 Hz and PR applied to 2663 Hz. Suppressed resonance at 8.53 ppm.

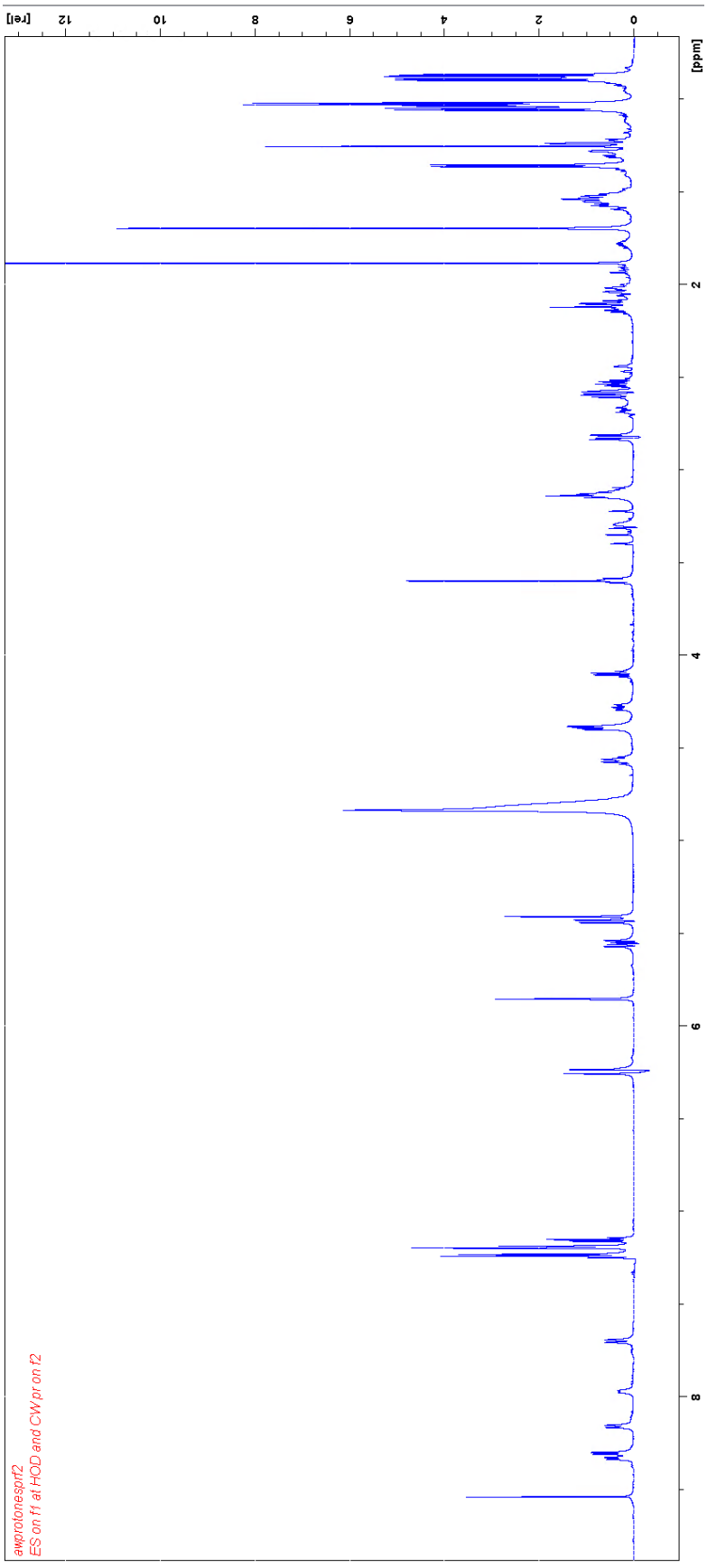

Figure 47: Experiment 7002 with softened ES on 3890 Hz and PR on 2663 Hz. Partially suppressed resonance at 8.53 ppm.

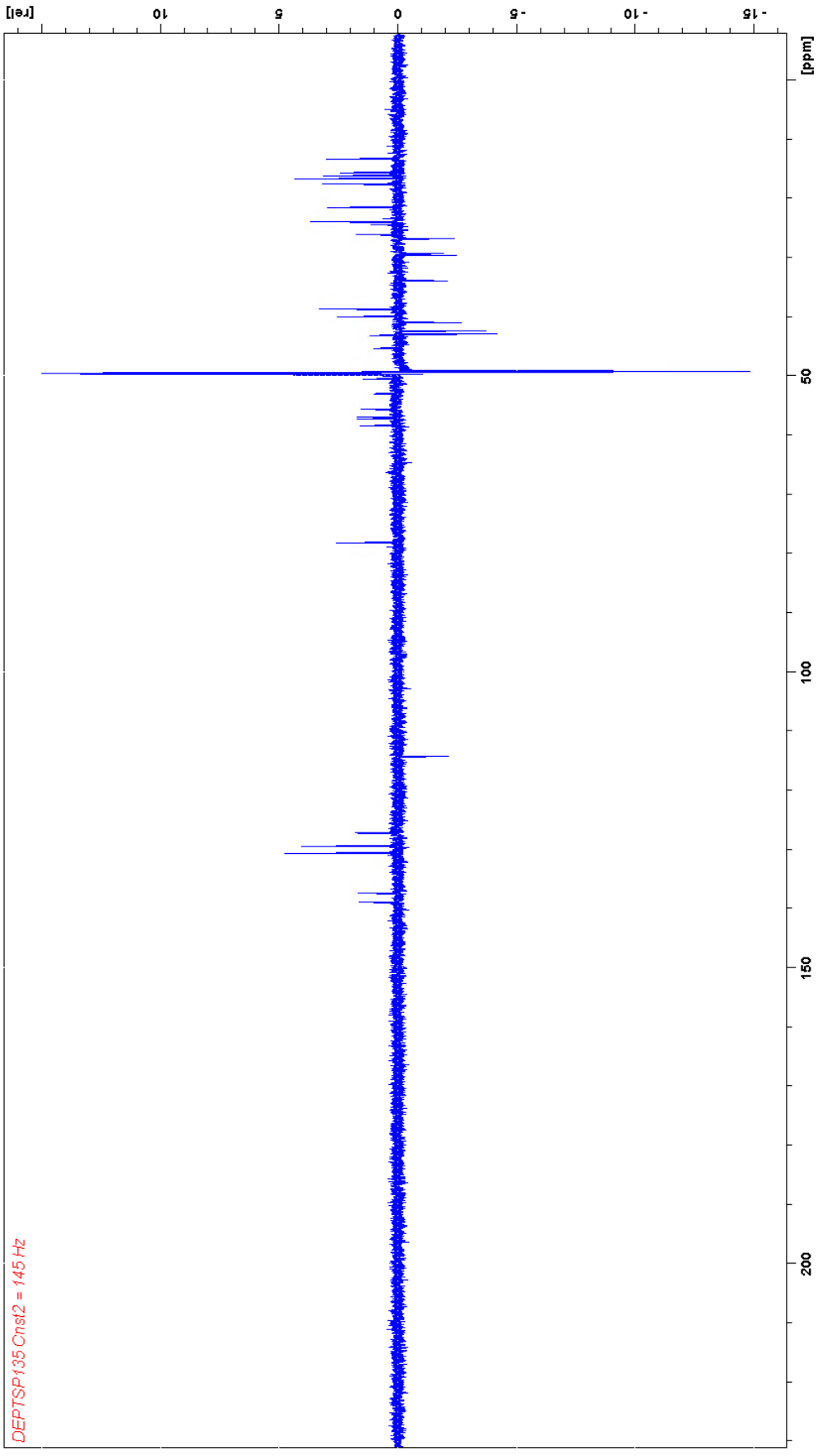

Figure 48: DEPT135 experiment 7062.

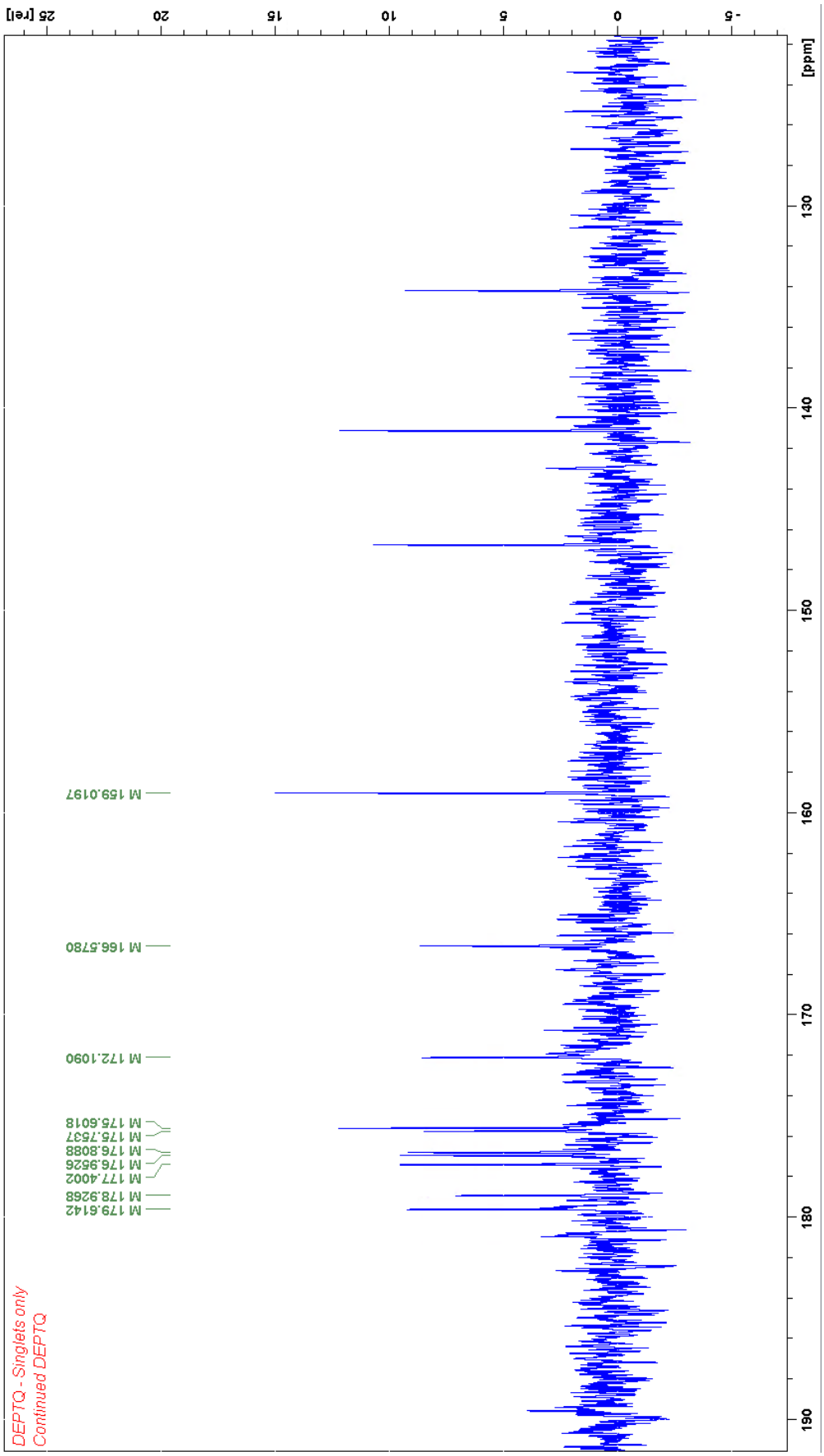

Figure 49: DEPTQ experiment 7063.

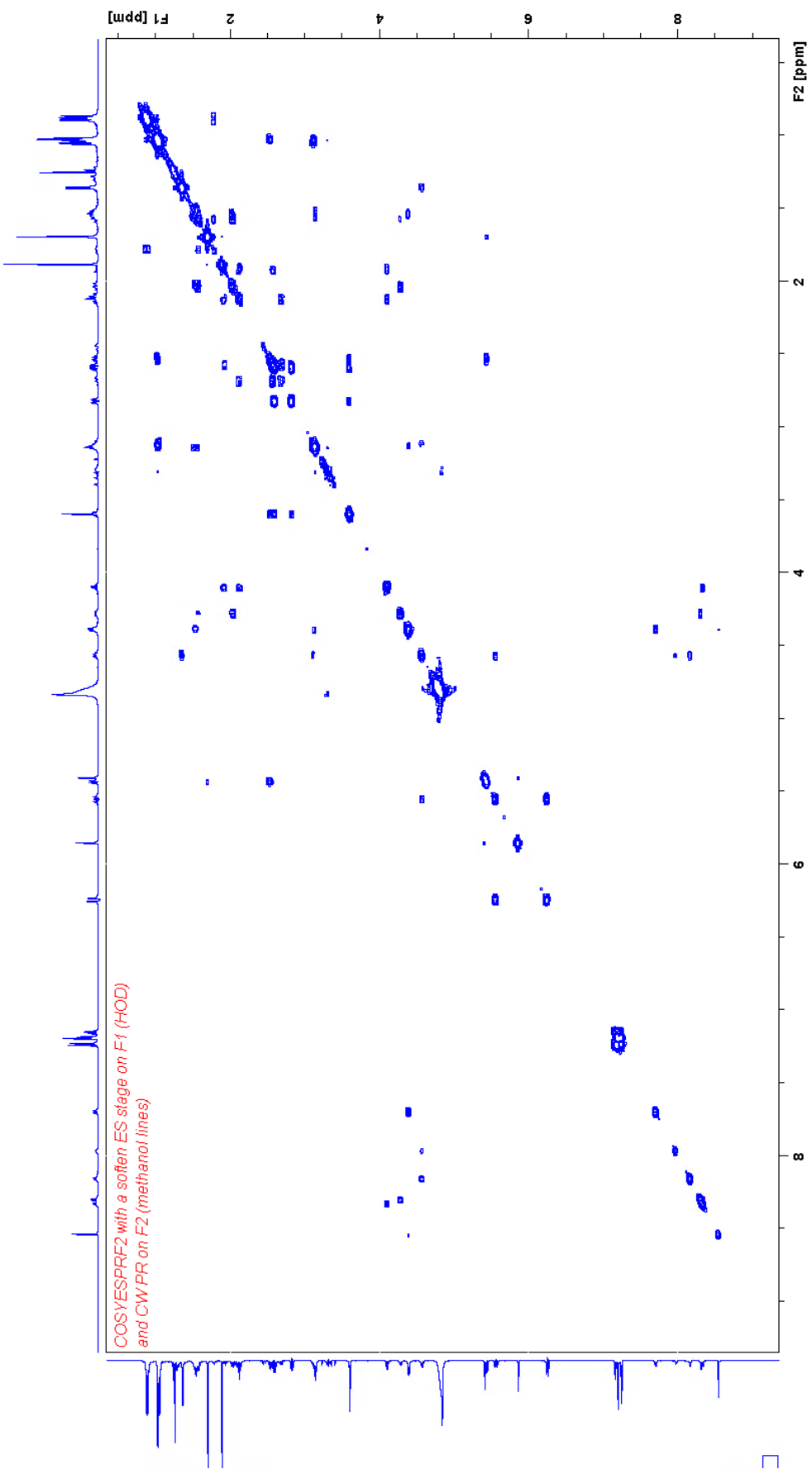

Figure 50: A COSY spectrum, experiment 7010, with ES- and PR-suppression on their respective frequencies.

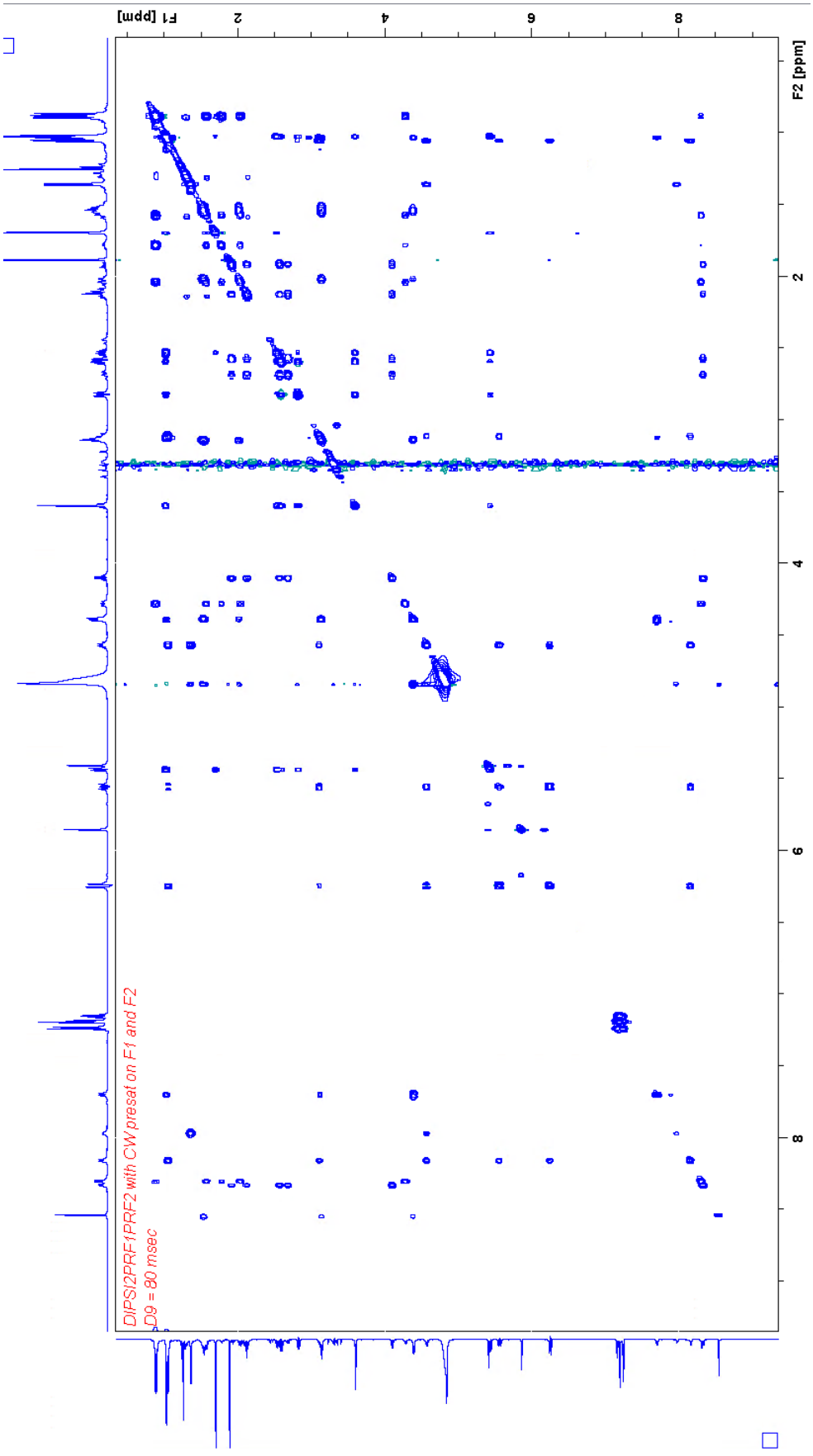

Figure 51: DIPSI-2, experiment 7020, with PR-suppression on both frequencies and a mixing time of 80 µs.

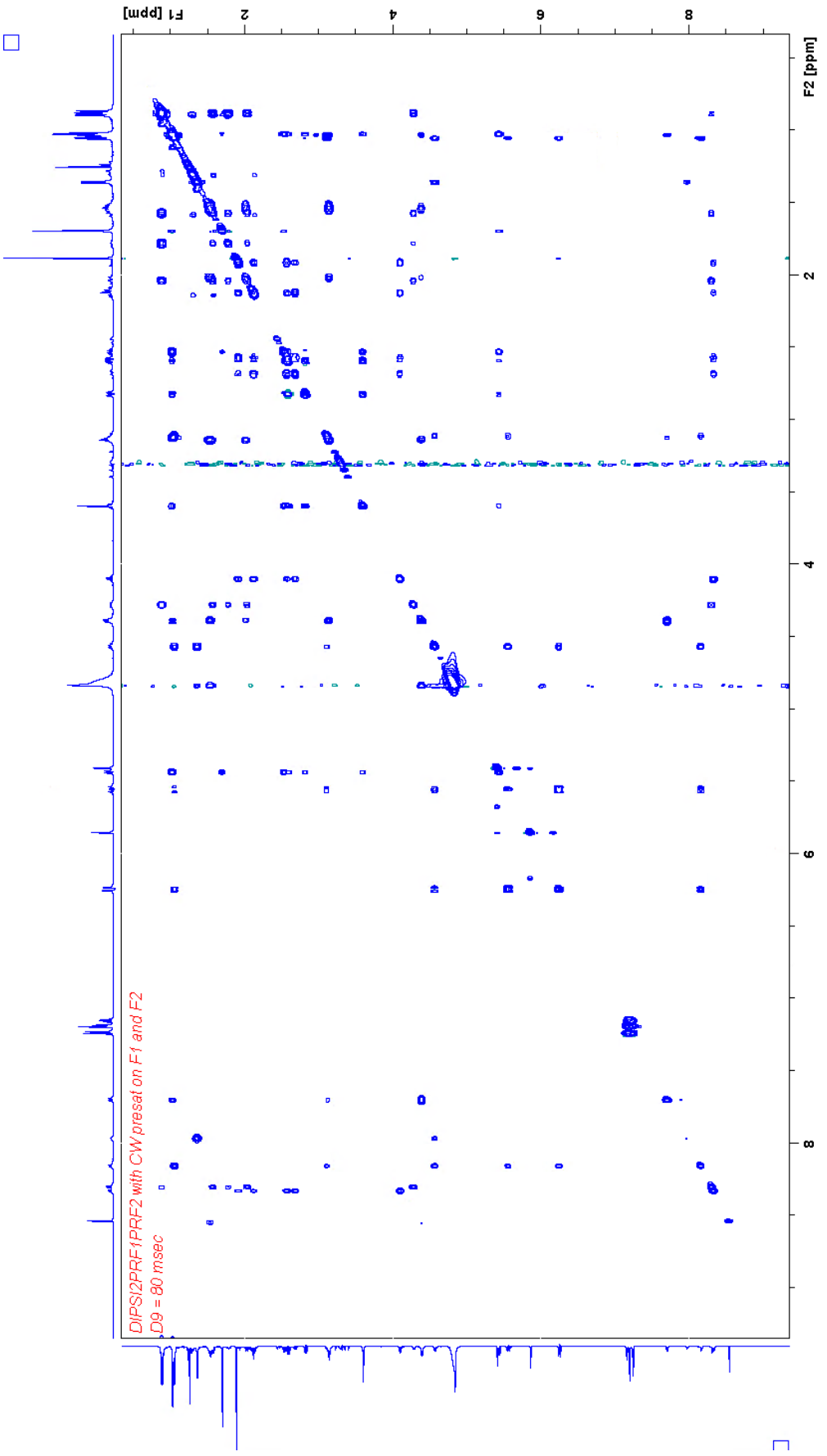

Figure 52: DIPSI-2, experiment 7023, with PR-suppression on both frequencies and a mixing time of 160 µs.

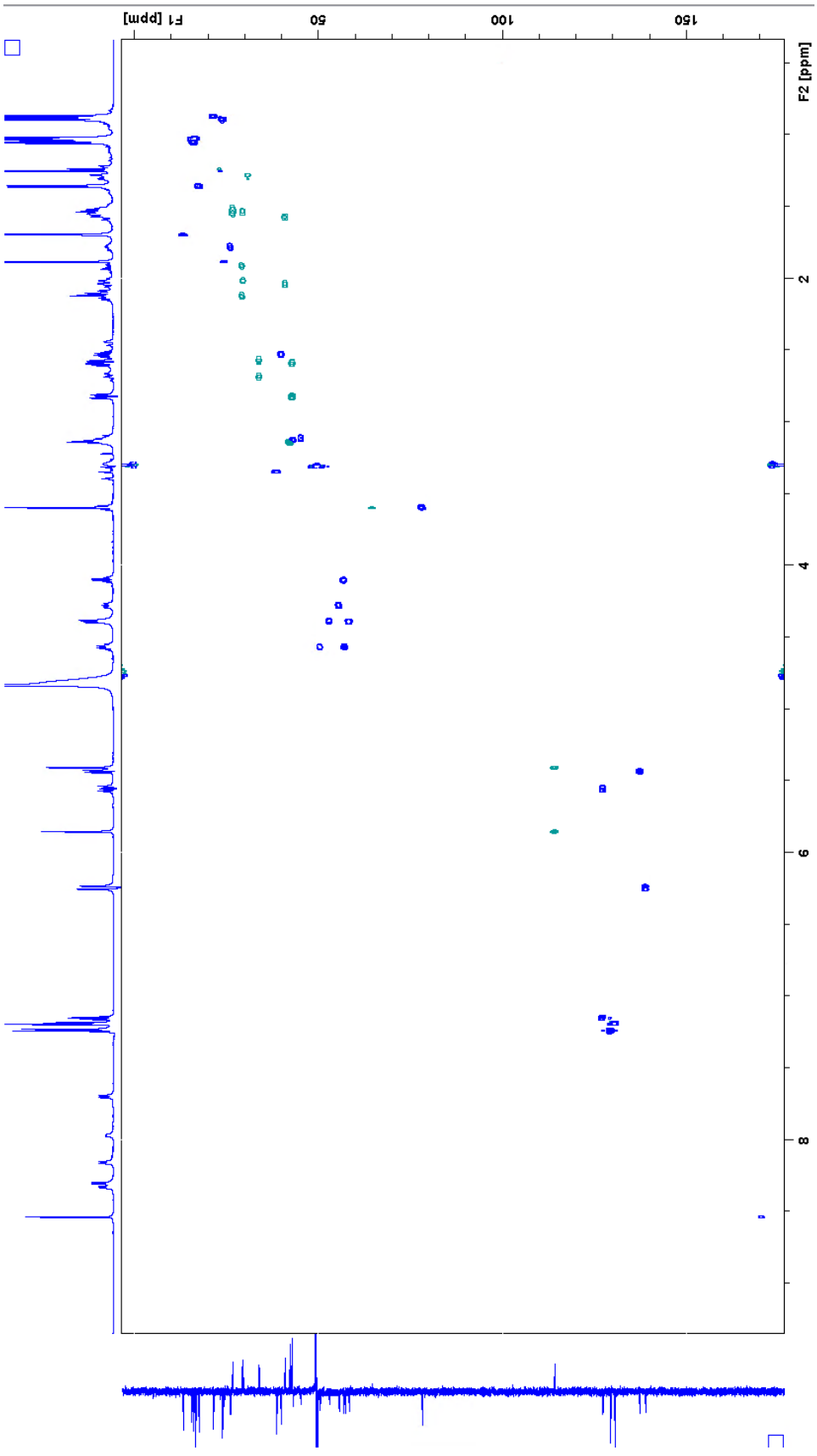

Figure 53: HSQC experiment, 7040, with PR on 3890 Hz.

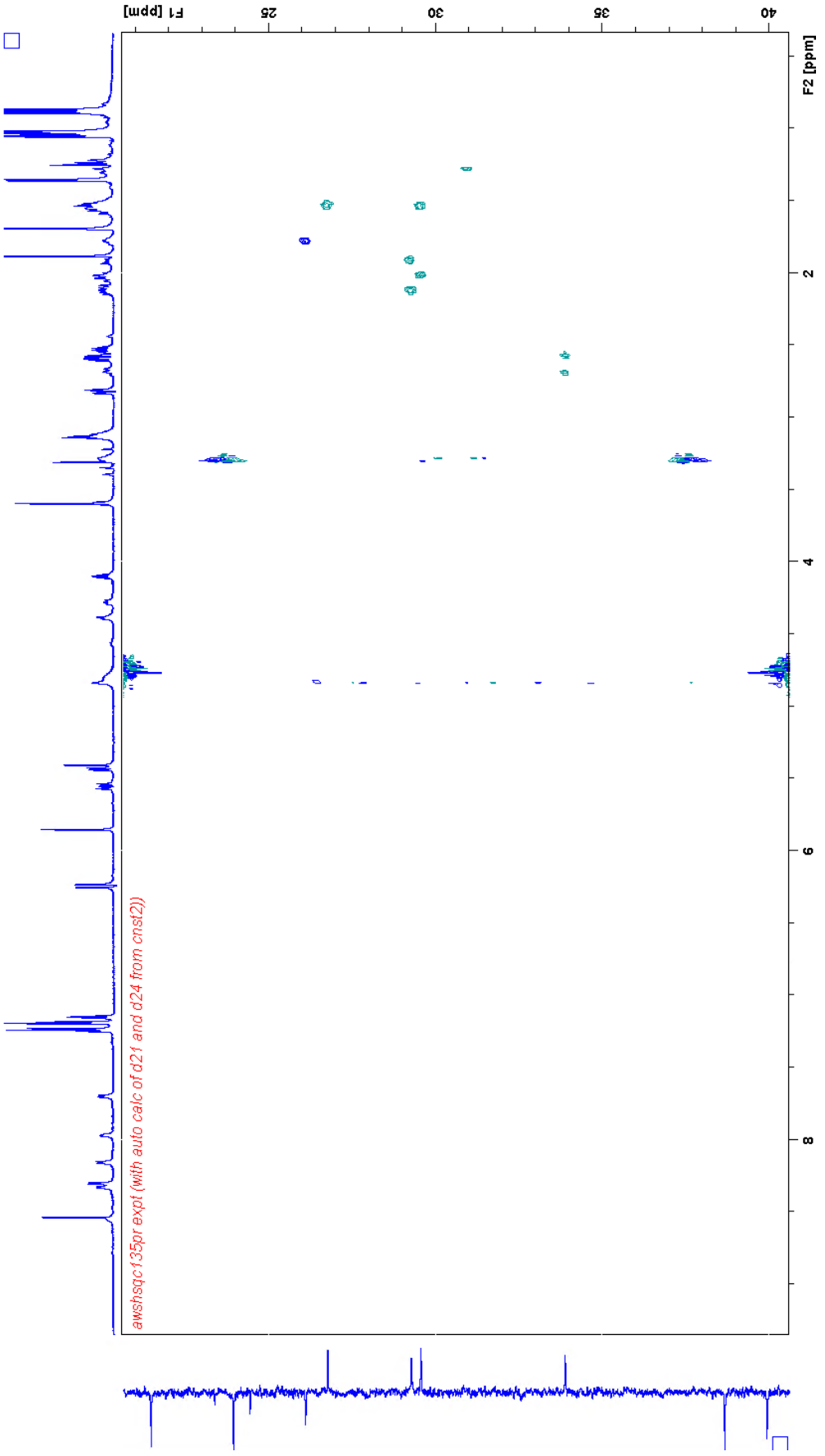

Figure 54: SHSQC experiment, 8051, centered at 29.000 ppm.

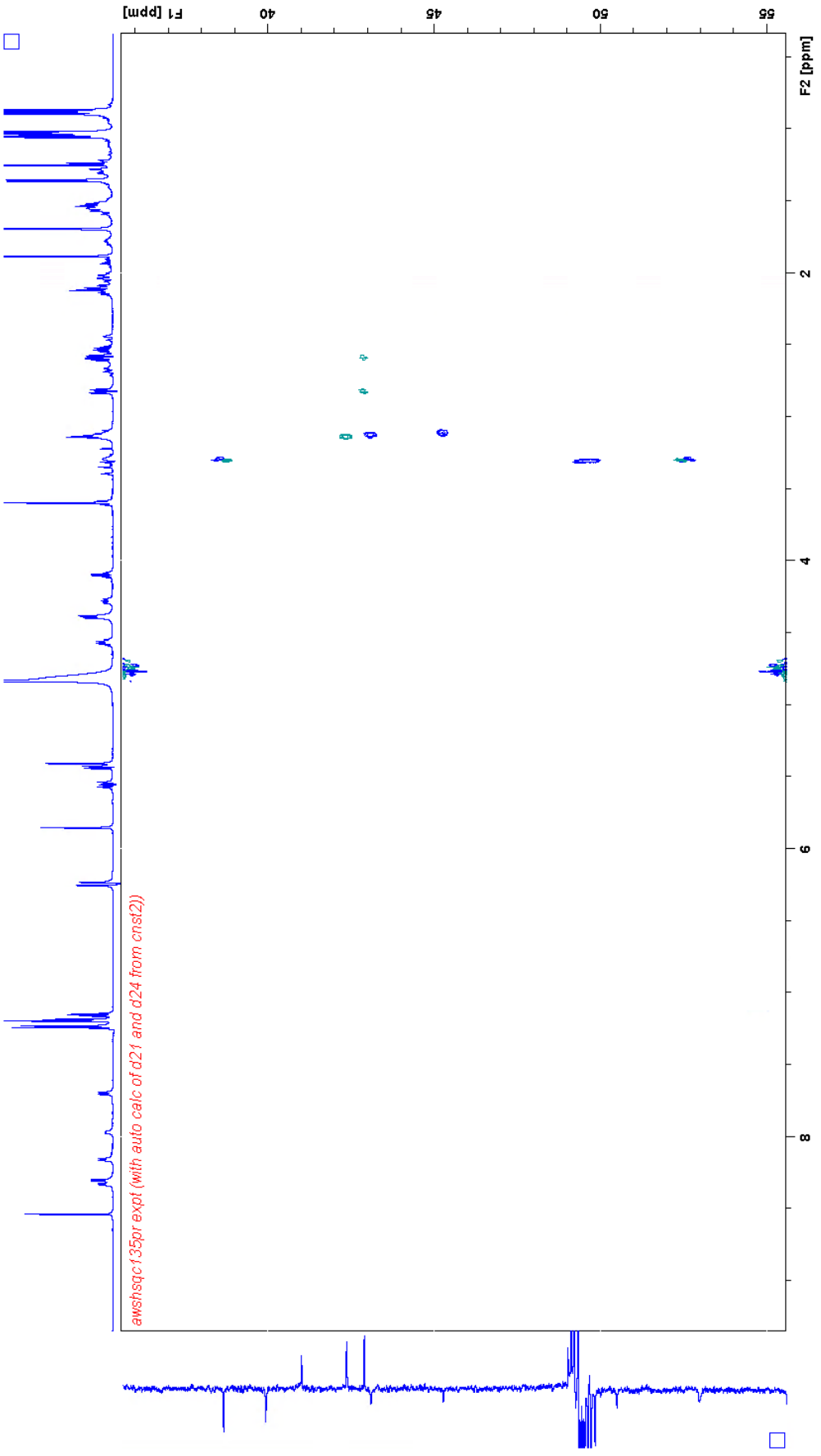

Figure 55: SHSQC experiment, 8052, centered at 44.000 ppm.

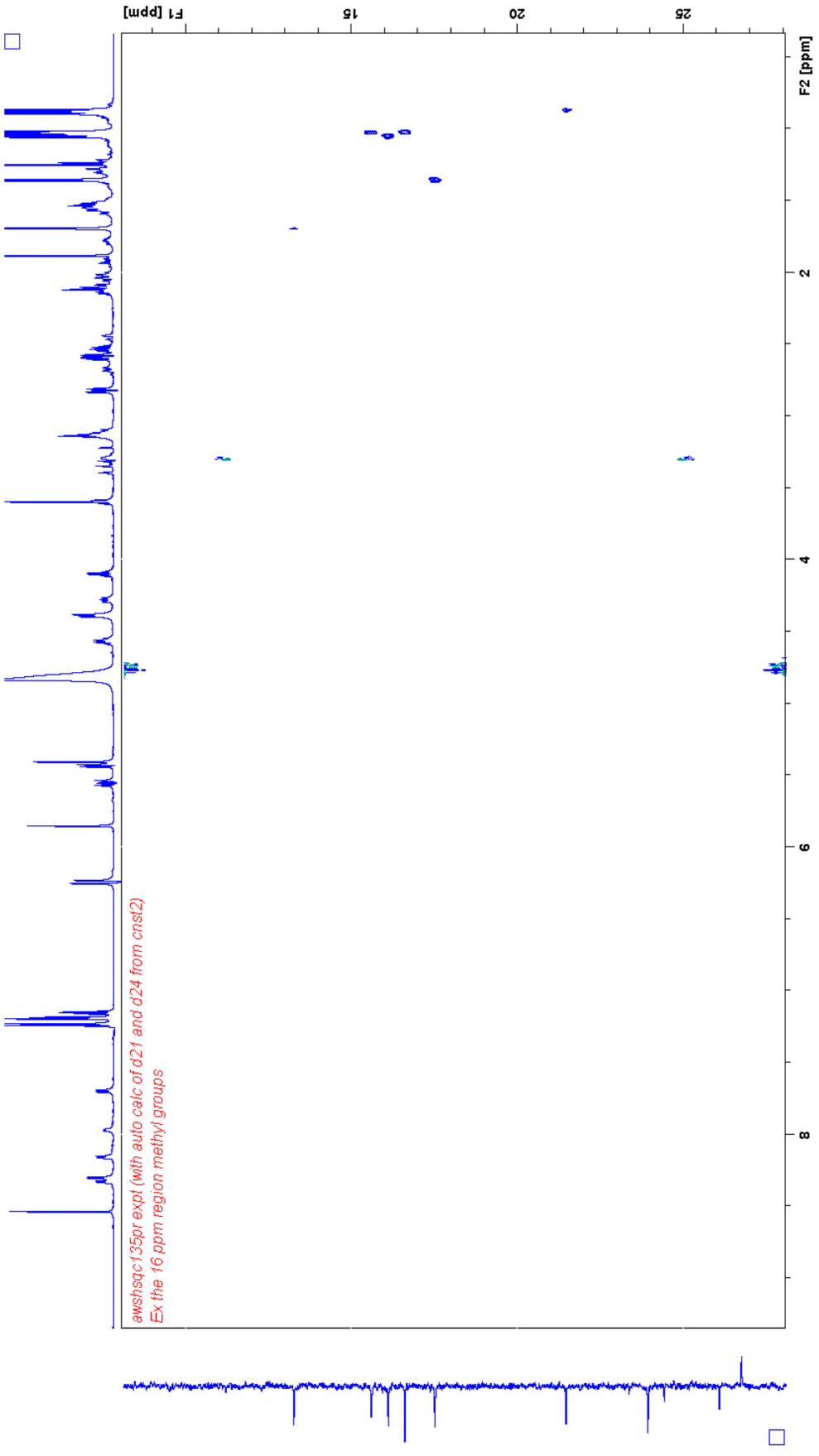

Figure 56: SHSQC, 8053, centered ppm 16.500 ppm.

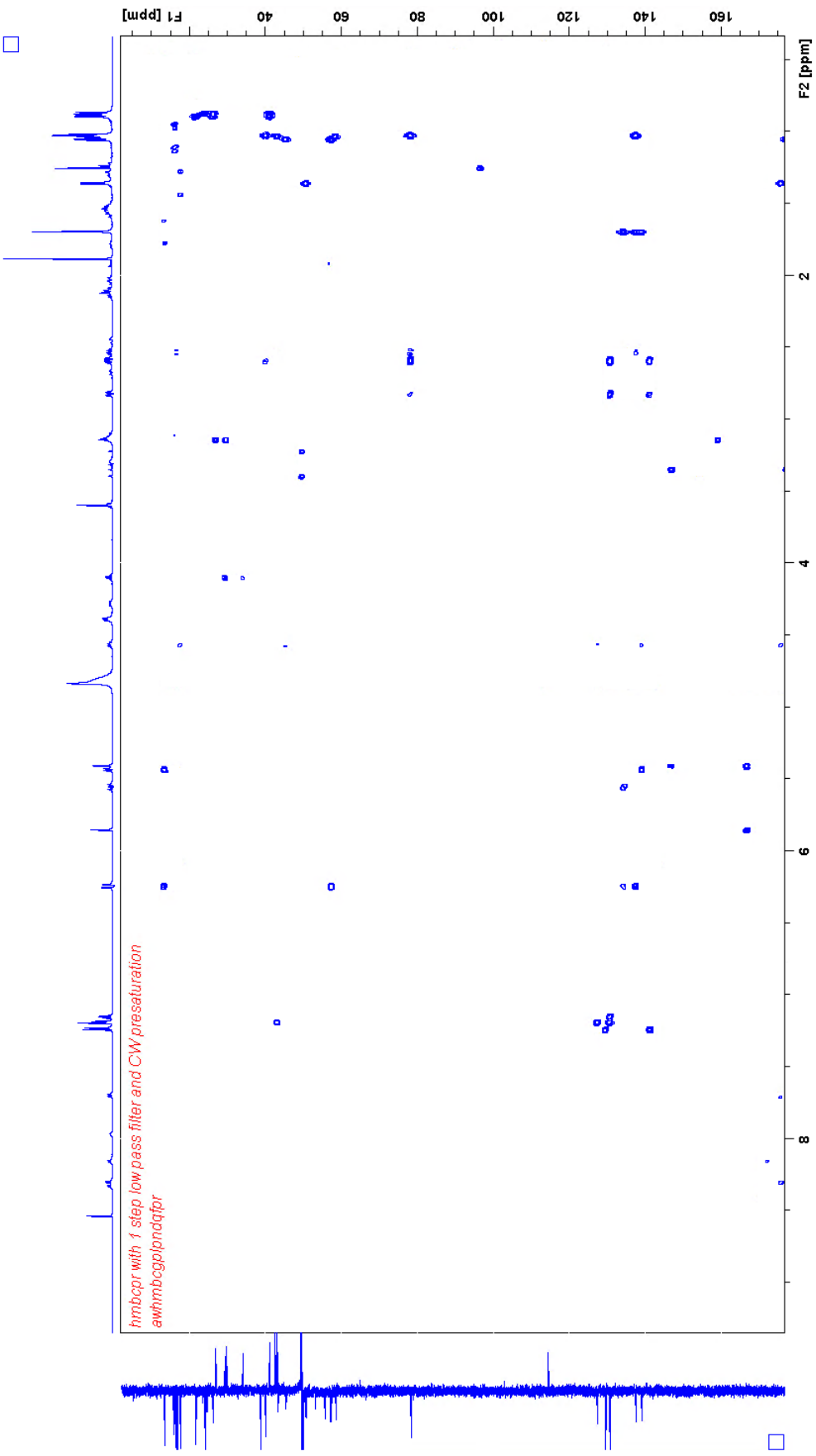

Figure 57: HMBC experiment, 7052.

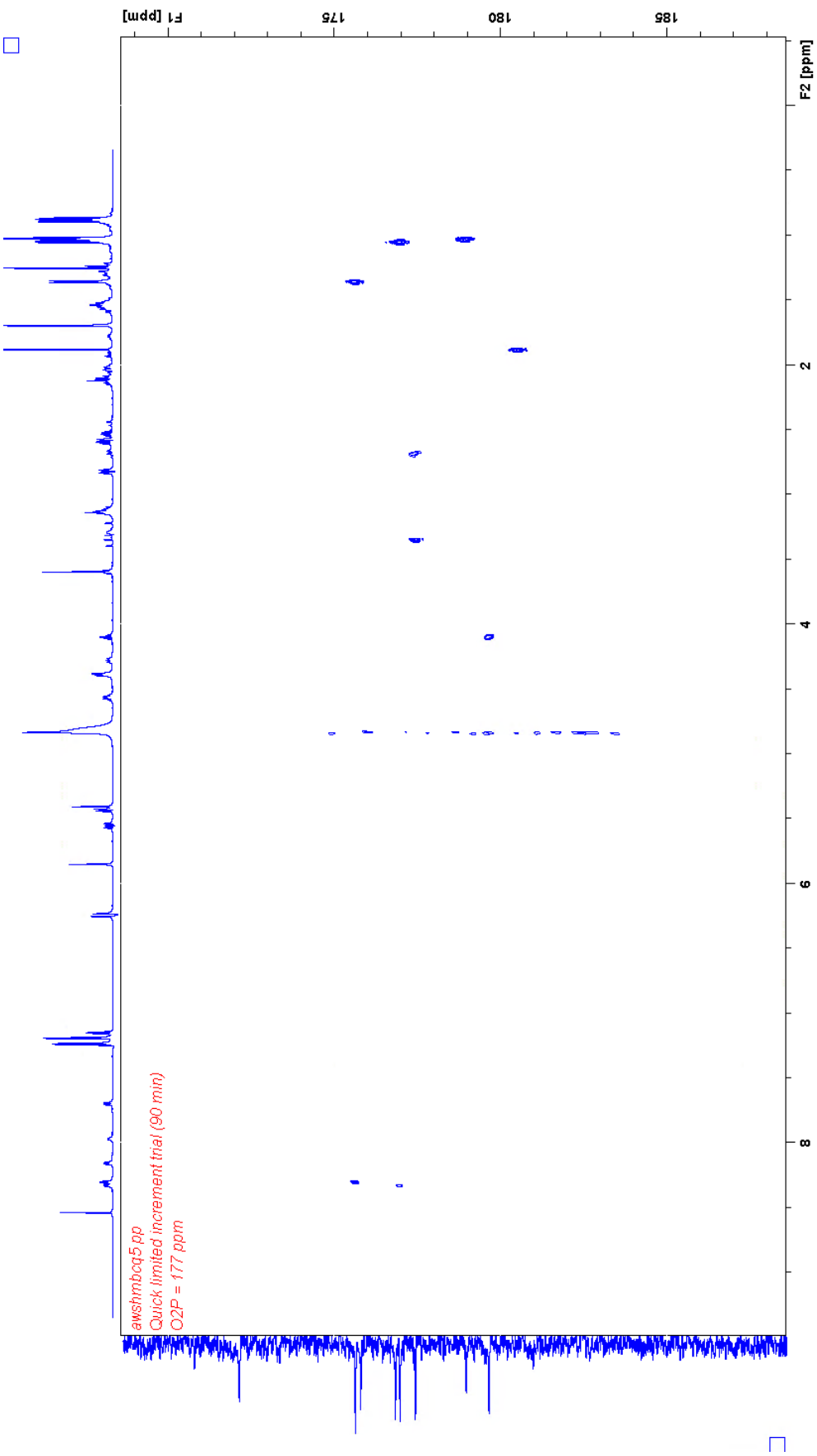

Figure 58:S HMBC experiment, 8061.

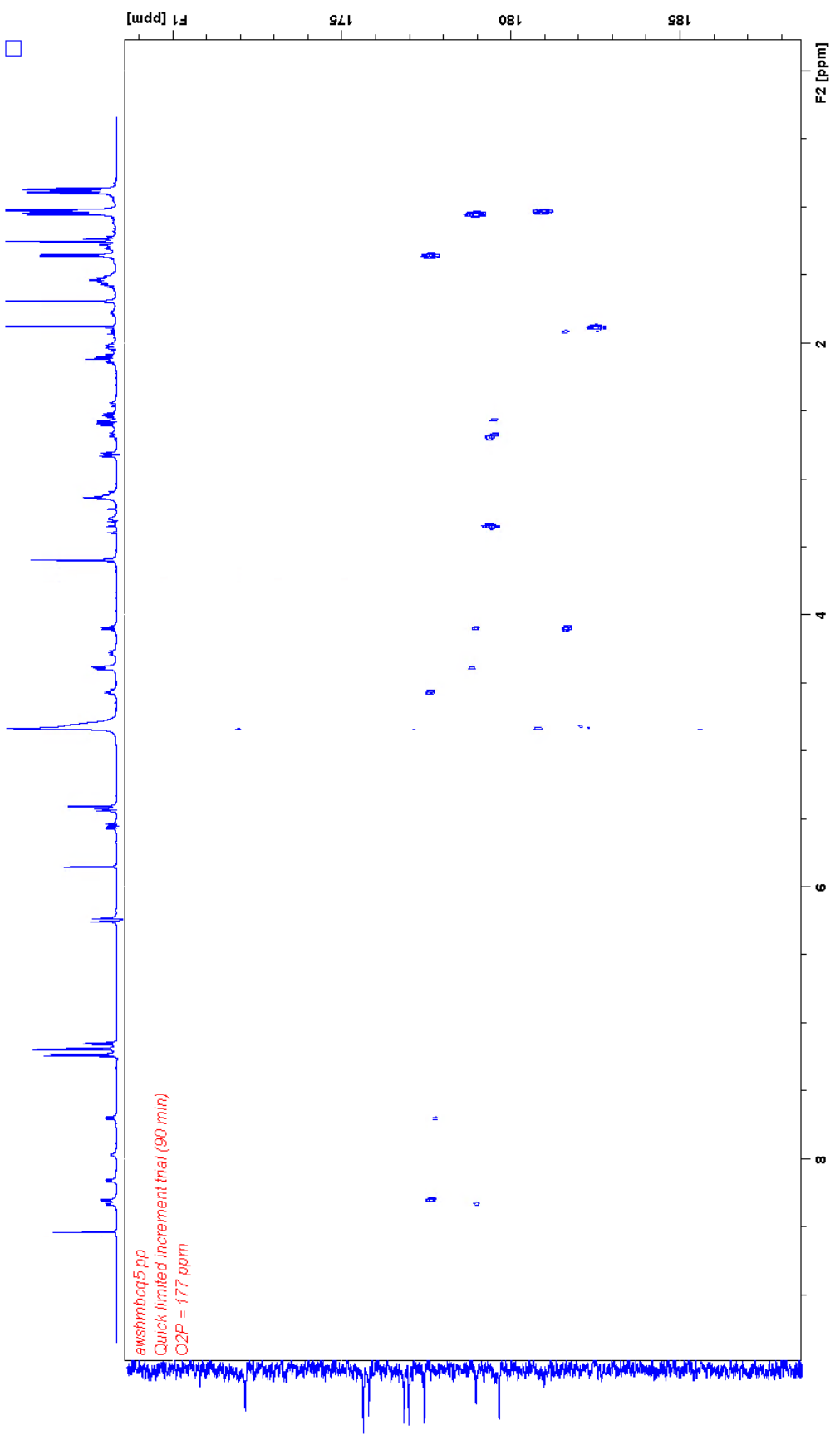

Figure 59: HMBC experiment, 8064.

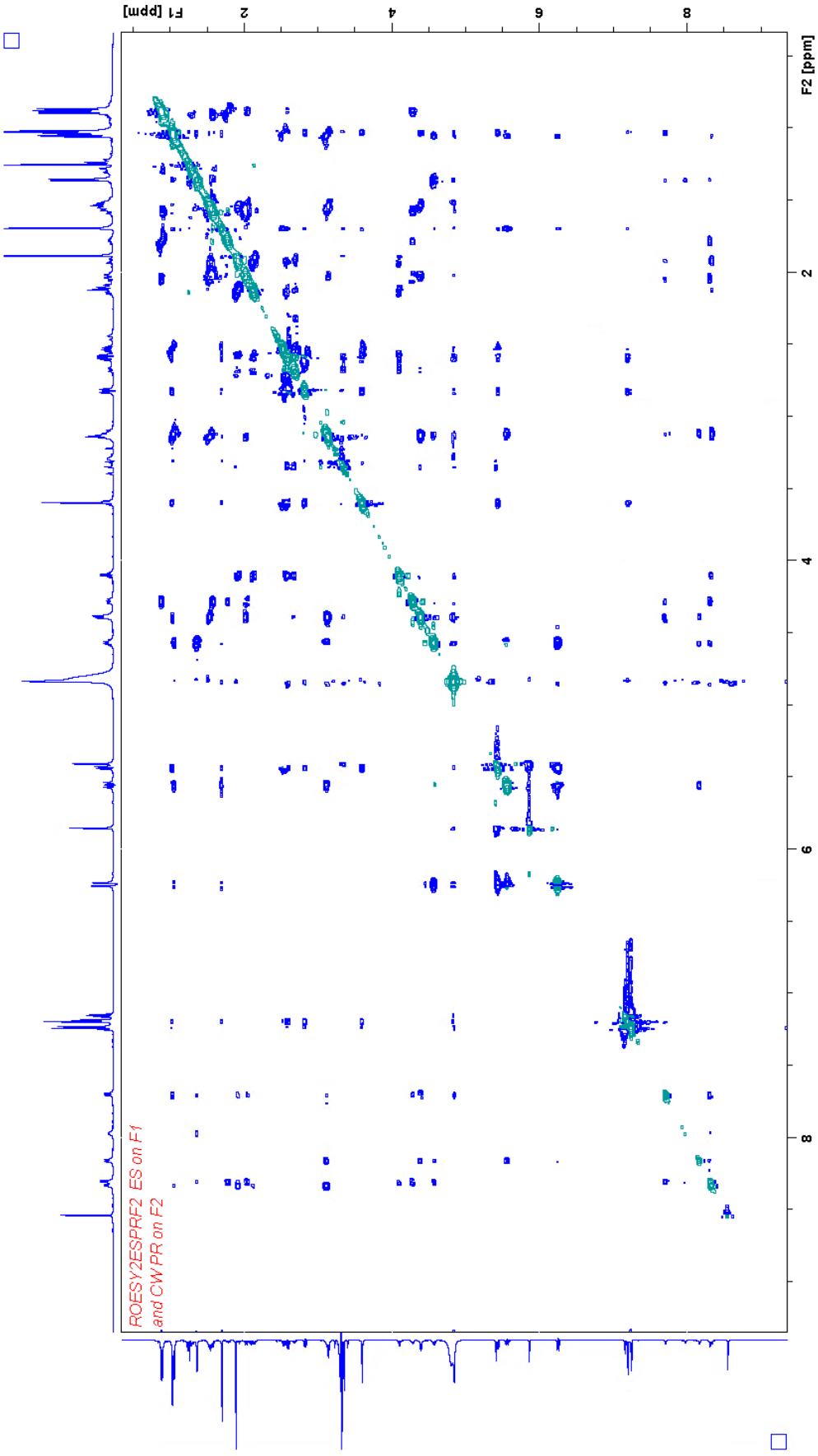

Figure 60: Experiment 7072 with softened ES on 3890 Hz and softened PR on 2663 Hz.

4.1.2 Elucidation of atom sequence:

N-methyl dehydroalanine: Mdha

By superficial inspection of the 1D proton spectrum (p. 72), there appears to be many overlapping signals downfield. The α-proton region (4-5 ppm) shows four signals and the peptide region (7.5-9 ppm) shows six signals.[29] By closer inspection of the α-proton region, the fine structure of the signal at 4.57 ppm indicate that there may be overlapping signals there. HSQC confirms that there are indeed two overlapping signals at 4.57 ppm in addition to revealing that there are two overlapping signals at 4.39 ppm. In total there are six α-protons and six peptide-protons, which is in accordance with the literature for MCs. The lack of a 7th peptide- and α-proton may be explained by the presence of N-methyl dehydroalanine (Mdha) which is shown in figure 61. Mdha is so called since the peptide-bonded nitrogen is methylated and there is a double bond between the 2- and 3-position, making the R-group a methylene.

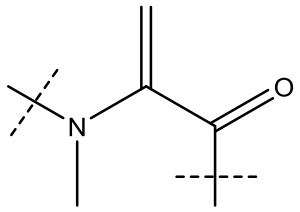

Figure 61: Mdha doubly peptide bonded at the N- and C-terminus. Complete peptide bonds not shown.

The alkene region of the spectrum has few and isolated signals. All signals which display multiplicity in this region have coupling constants which are too large to be Mdha and may be part of vicinal couplings in an sp^2-hybridized system. Geminal alkene couplings are typically very small where electronegative and electropositive substituents respectively contribute negatively and positively to the coupling constant. This leaves the two singlets (5.85 and 5.41 ppm). The two singlets are seen to connect to the same carbon (114.23 ppm) in HSQC spectrum (p. 78). The HMBC spectrum (p. 82) shows a ^{3}J-coupling to another carbon in the sp^2-hybridized region at 146.69 ppm. Both carbons correlate to a singlet (3.35 ppm) in HMBC, indicating that it is indeed Mdha. The two aforementioned protons (5.85 and 5.41 ppm) also correlate to another carbon (166.57 ppm) in the HMBC spectrum (p. 82) which is absent in the HSQC spectrum (p. 78) and its chemical shift is consistent with an amide,

providing ample evidence for the presence of Mdha and is depicted with numbering, assigned signals and correlations in figure 62.

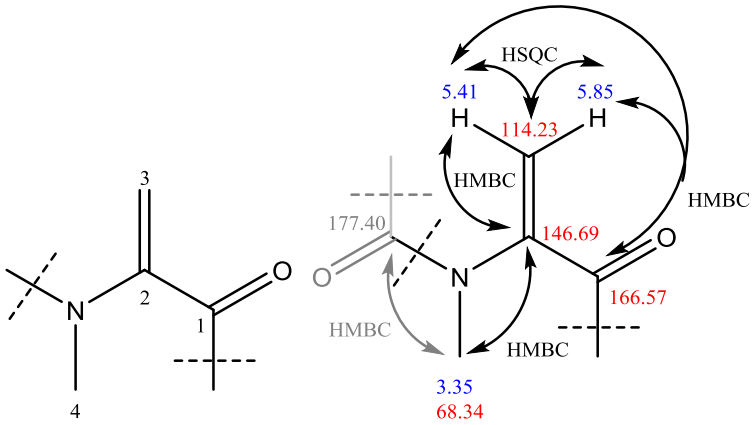

Figure 62: Mdha with number assignments (left) shown in its doubly peptide bonded form. Complete peptide bonds not shown. Mdha with HSQC and HMBC correlations is shown (right). Correlations are elucidated from spectrums in figure 53 and 57 at pages 78 and 82.

The methyl signal at 3.35 ppm found to correlate in the HMBC spectrum (p. 82) at 146.69 ppm, further correlates to a carbon consistent with a carbonyl-type entity (177.40 ppm), making it an amide.

Glutamic acid: Glu

The external coupling to the amide carbon from the previous segment (177.40 ppm highlighted in gray in figure 62) further correlates to a proton at 2.68 ppm in the HMBCspectrum (p. 82). Analysis of the DIPSI-2 spectrums (80 ms at p. 76 and 160 msat p. 77) reveals the spin system to consist of the chemical shifts; 1.91, 2.12, 2.57, 4.10 and 8.33 ppm. Pairing these shifts with carbons in the HSQC spectrum (p. 78) reveals 2.57 and 2.68 ppm to belong to the same carbon (33.84 ppm) as a CH_2. Further, 2.12 and 1.91 ppm also belong to the same carbon (29.23 ppm) as a CH_2 constituent. 8.33 ppm is absent in the ^{1}H-^{13}C HSQC spectrum (p. 78) and is thus assumed to be bonded to a nitrogen. This makes the constituents of the spin system; CH_2, CH_2, CH and NH. The COSY spectrum (p. 75) shows that the sequence of constituents is CH_2-CH_2-CH-NH where all neighboring and geminal protons couple apart from 2.57 and 2.12 ppm as well as 2.68 and 1.91 ppm. The homonuclear coupling pattern is shown in figure 63 and the elucidation thus far in figure 64.

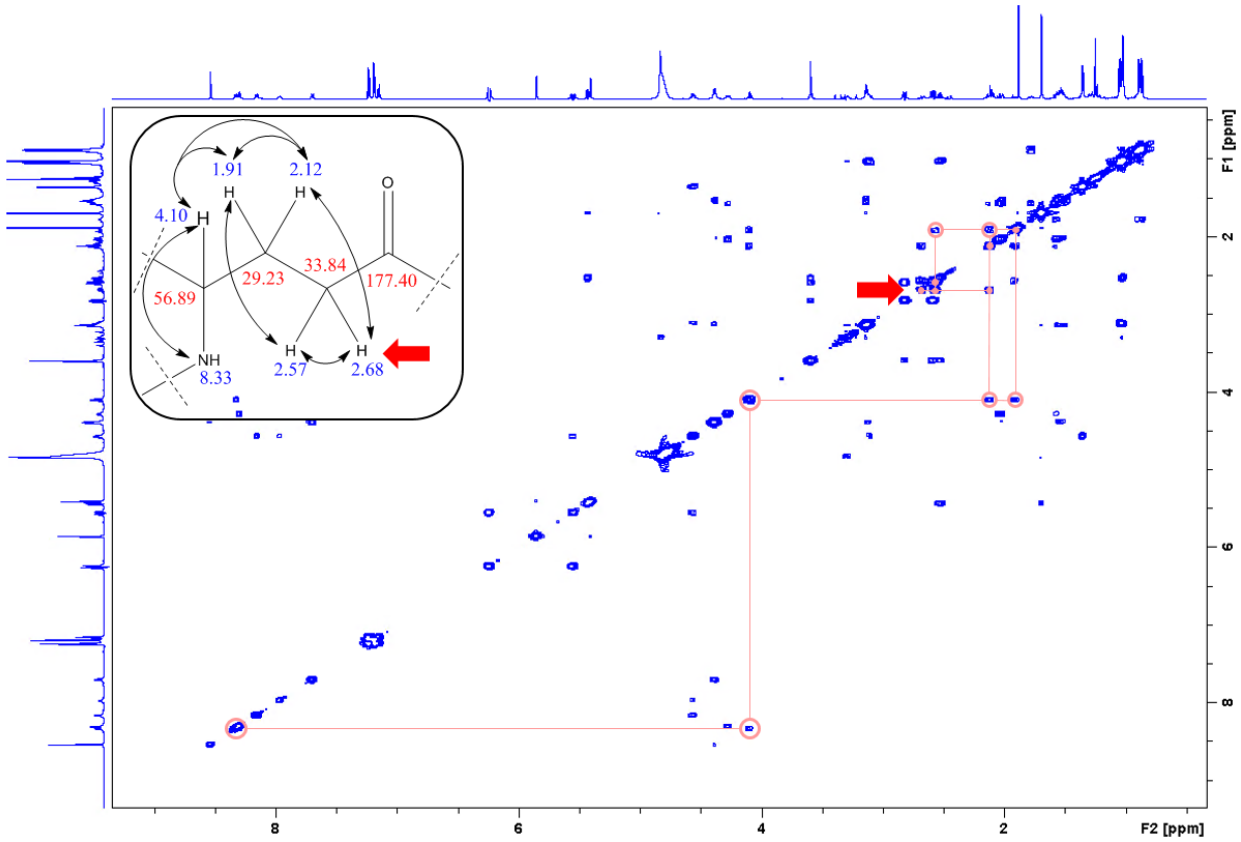

Figure 63: COSY spectrum, 7010, with correlation pattern for protons consistent with Glu. The red arrow notes the start of elucidation and indicates which diagonal peak belongs to which proton in the structure.

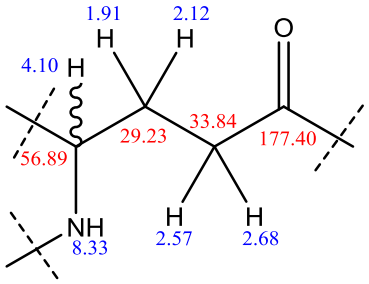

Figure 64: Elucidation of aliphatic chain consistent with Glu.

HMBC correlations (p. 82) are consistent with the structure elucidation thus far. Other HMBC correlations (p. 82) reveal the last neighbor of the CH-proton (4.10 ppm) to be a carbonyl-carbon (197.62 ppm). The NH correlates to 179.96 ppm which is consistent with an amide carbonyl. The HMBC correlations mentioned are illustrated in figure 65.

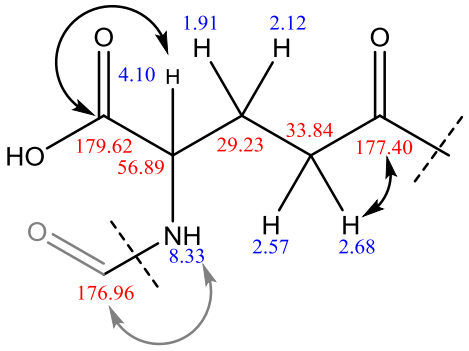

Figure 65: HMBC correlations from aliphatic chain in figure 61. The glutamic acid shows Glu to form an iospeptide bond.

The elucidation is consistent with the literature describing glutamic acid in MCs. Glutamic acid is shown in figure 64.

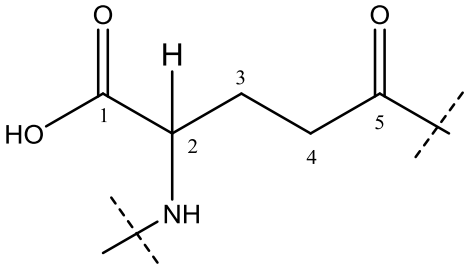

Figure 66:Glutamic acid bound with an isopeptide bond.

O-Demethyl 3-amino-9-methoxy-2,6,8-trimethyl-10-phenyl-deca-4,6-dienoic acid: DMAdda

Starting from the external carbonyl found through interpretation of HMBC, the carbon shift correlates to a proton signal at 1.05 ppm. Analysis of a DIPSI-2 spectrum reveals the spin system, however it is ambiguous which correlations belong to the spin system at ~3.14 ppm and 4.57 ppm. By selective TOCSY, irradiating 1.05 ppm, the spin system; 1.05, 3.11. 4.57, 5.55, 6.25 and 8.16 ppm is excited. The spectrum can be seen in figure 67.

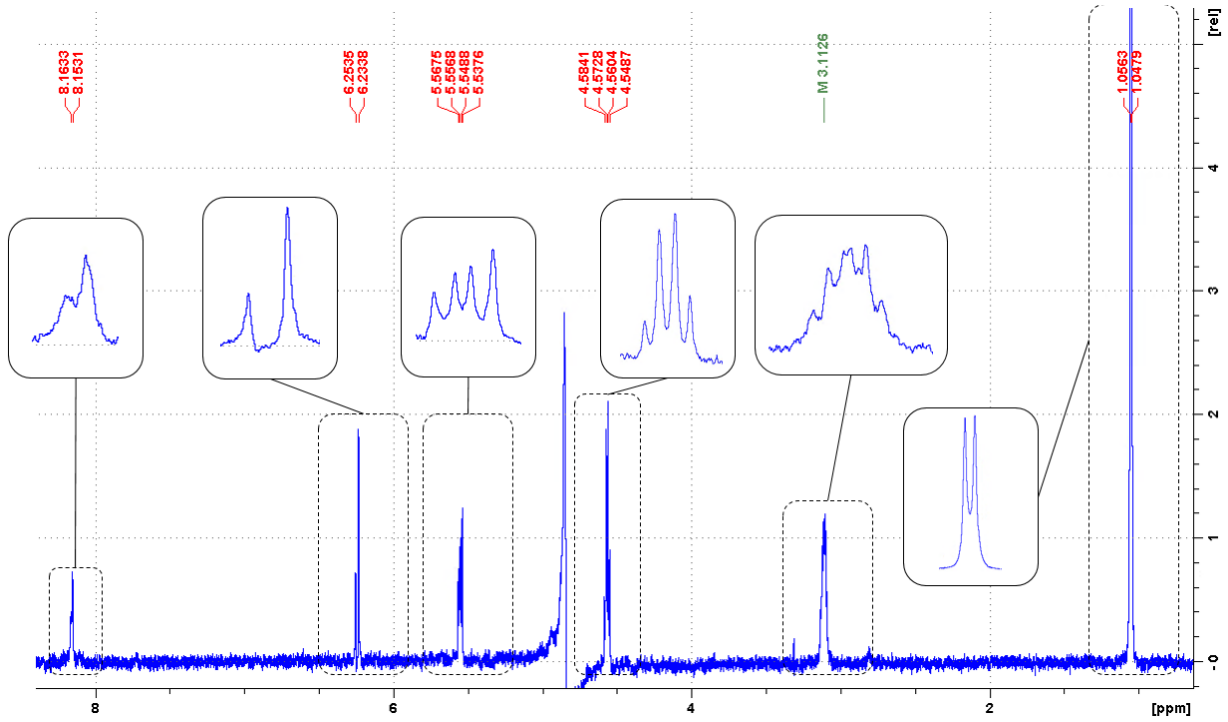

Figure 67: Selective TOCSY experiment (Appendix B) where the resonance at 1.05 ppm was selectively irradiated to show its spin system. Processing parameters for the big spectrum: SI = 262 144, ME-mod = LPfr NOCOEF = 64, LPBIN = 320, WDW = EM, LB = 0.50 Hz. Changed processing parameters for expanded region: WDW = GM, GB = 0.2 and LB = -3 Hz. All expanded regions exceot 1.05 ppm are displayed without height manipulation.

The HSQC spectrum (p. 78) reveals them all, apart from 8.16 ppm, to be CH/CH_3. 8.16 ppm is absent and assumed to be bound to nitrogen. The signals' respective carbon shifts, found in HSQC (p. 78), are; 16.08, 45.24, 57.22, 127.38 and 138.88 ppm. The COSY spectrum (p. 75) incorporates a correlation pattern with sequence; 1.05-3.11-4.57 ppm which forks into two branches; 8.16 ppm (NH) and 5.55-6.25 ppm as shown in figure 68.

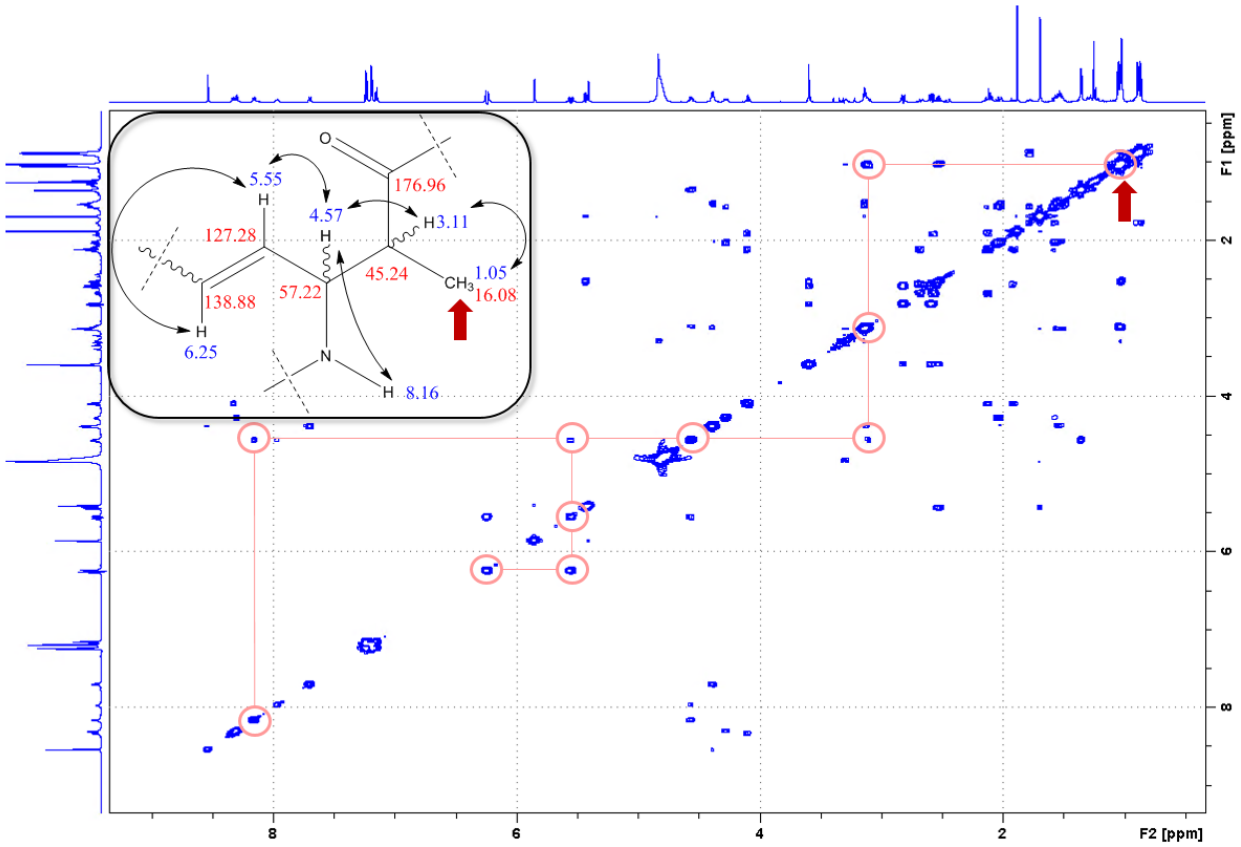

Figure 68: COSY correlation pattern (experiment 7010) for the spin system revealed in figure 65 with assigned carbons from HSQC spectrum (figure 51 on page76). The red arrow notes the start of elucidation and indicates which diagonal peak belongs to which proton in the structure.

A peak at 5.55 ppm in the HMBC spectrum (p. 82) correlates through a ^{3}J-coupling to 134.18 ppm which is absent in the HSQC spectrum (p. 78). A HMBC from 6.25 ppm correlates to 13.24 ppm. The shift, 13.24 ppm, correlates positively with 1.69 ppm in the HSQC spectrum (p. 78) and is thus of a CH/CH_3 nature. 13.24 and 1.69 ppm respectively only correlate further to shifts; 5.43 and 137.32 ppm which correlates with each other in the HSQC spectrum (p. 78). The correlation between 1.69 and 13.24 ppm suggests that there are no other electron donating or withdrawing groups. Its integral (not shown) and multiplicity (figure 72) indicates it's a CH_3. The HMBC correlations are illustrated in figure 69 (on p. 92).

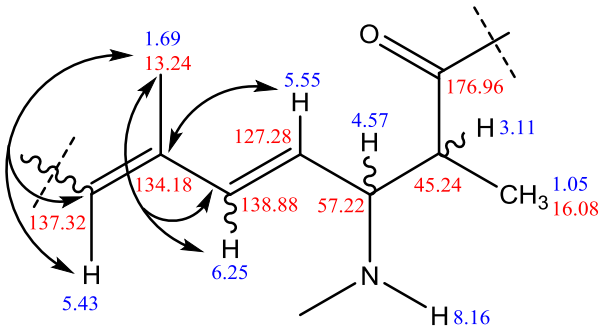

Figure 69: HMBC correlations for further elucidation is shown.

In the DIPSI-2 spectrum (p. 76 and 77) the 5.43 ppm correlation reveals its spin system to consist of the signals; 1.02, 1.69, 2.53, 2.59, 2.82, 3.60 and 5.43 ppm. However, the other members of the list do not correlate to 1.69 ppm. Comparison of proton and carbon shifts in the HSQC spectrum (p. 78) determines the heteronuclear bonds of the new shifts to be between the following: 1.02 (H) with 15.56 ppm (C), 2.53 (H) with 39.89 ppm (C), 2.59 (H) and 2.82 (H) with 42.86 ppm (C), and 3.60 (H) with 78.16 ppm (C). Further elucidation in the COSY spectrum (p. 75) arranges the constituents from 134.18 ppm: 5.43-2.53 ppm which forks into 1.02 ppm and 3.60-2.59 and 2.82 ppm (figure 54). The multiplicity of 5.43 (doublet), 1.02 (doublet), 6.92 (doublet) ppm suggests that the signal at 2.53 ppm is a CH while the integral of overlapping signals at ~1 ppm in addition to the complex splitting of the signal at 2.53 ppm (ddq) suggests that 1.02 ppm signal represents a CH_3. The signal at 3.60 ppm overlaps with another signal, making the multiplicity ambiguous.

The elucidation done in the COSY spectrum (p. 75) suggests the shift to couple distinctly with CH_2 protons 2.82 and 2.59 ppm as well as 2.53 ppm, meaning the correlating signal has a complex coupling pattern and cannot be a singlet. The total integral of the overlapping signals (mot shown) is not enough to satisfy a hypothesis that it may be a CH_3, which is unlikely given the number of coupling partners. It is thus concluded to be a CH. The high chemical shift suggests the presence of a neighboring heteroatom. The chemical shift is in the typical range of an oxygen. The HMBC spectrum (p. 82) does not show any correlation between 3.60 ppm and any new signals. Nor does its corresponding carbon (78.16 ppm). Thus it is assumed to be an alcohol which is exchanging with the solvent and therefore not present in any spectrum. The structure is shown in figure 71 and the COSY elucidation is shown in figure 72 on the next page.

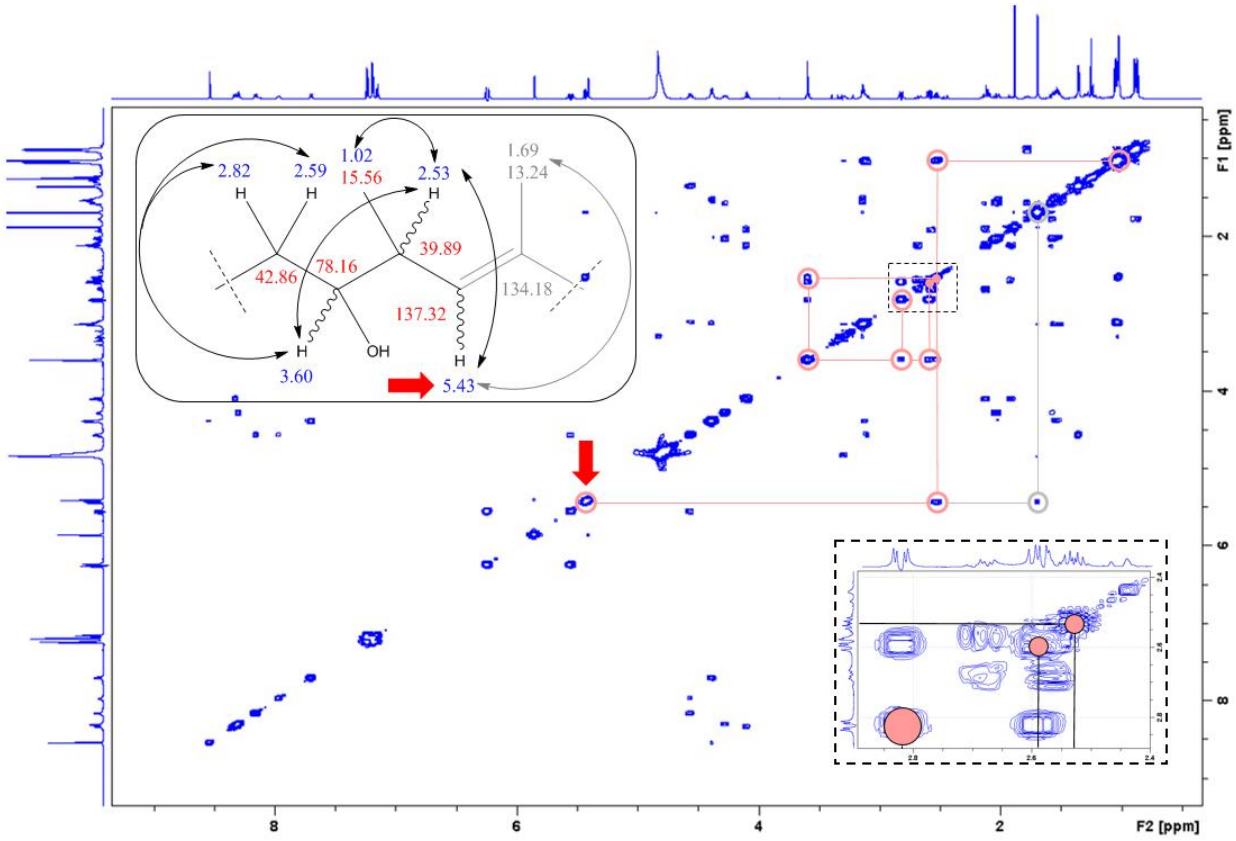

Figure 70: COSY correlation pattern (experiment 7010) showing further correlations from figure 52. Correlations going back through the molecule are shown in gray. The region with tightly packed correlations has been expended in the lower right corner. The red arrow notes the start of elucidation and indicates which diagonal peak belongs to which proton in the structure.

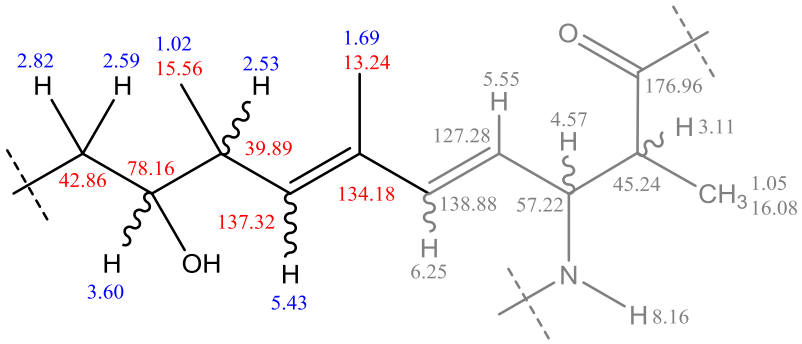

Figure 71: Further elucidation from figure 53. Previously elucidated structure is shown in gray.

In the HMBC spectrum (p. 82), the ^{13}C resonance at 42.86 ppm can be seen to correlate to 7.19 ppm. In this region signals; 7.24, 7.19 and 7.15 ppm can be found, which is typical for aromatic species. The shifts integrate with a relationship of 2:2:1. Their respective carbon shifts, found by investigation of the HSQC spectrum (p. 78), also has an intensity relationship of 2:2:1 (129.37, 130.62, 127.16 ppm). These signals are consistent with the protonated members of a phenyl ring. The multiplicity of these peaks suggests that chemical shift 7.19 ppm (doublet) arises from the coupling to one neighbor, revealing this shift to be the *ortho-*

position. The relative intensity of the two triplets (7.24 and 7.15 ppm) suggests that 7.24 ppm is the *meta*-position, while 7.15 ppm is the *para*-position.

HMBC correlations from the hydrogens in the phenyl ring appear to be mostly ^{3}J-couplings. What is assumed to be the *ortho*-position correlates further to the other *ortho*-position and neighboring *para*-position. The assumed *meta*-position correlates to the other *meta*-position, the neighboring positions (*ortho* and *para*) through a ^{2}J as well as 141.11 ppm. This chemical shift is very similar to the chemical shift of a quaternary carbon in an aromatic ring.[15, 41] The hydrogens of the CH_2 substituent (2.82 and 2.59 ppm) also correlates to this 141.11 ppm correlation, which is then assumed to be a quaternary carbon, where the CH_2-hydrogens correlate through a ^{2}J-coupling and the *meta*-position correlates through a ^{3}J-coupling. The *para*-position correlates to 131.10 ppm, the *ortho*-position through a ^{3}J-coupling. This elucidation concludes that this amino acid is DMAdda, though the conformation (including stereogenic centers) remains to be determined. The HMBC correlations of the benzyl species of DMAdda is illustrated in figure 72.

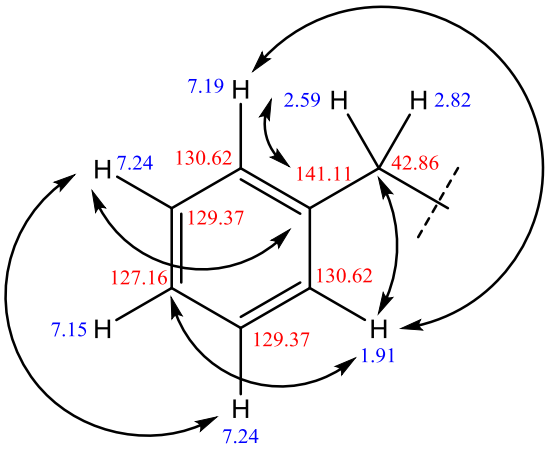

Figure 72: HMBC correlations in a benzyl species. Further elucidation from figure 55.

The elucidation is consistent with the literature describing DMAdda in MCs.[15, 42, 43] The elucidation of DMAdda thus far is shown in figure 73. DMAdda is shown in figure 74.

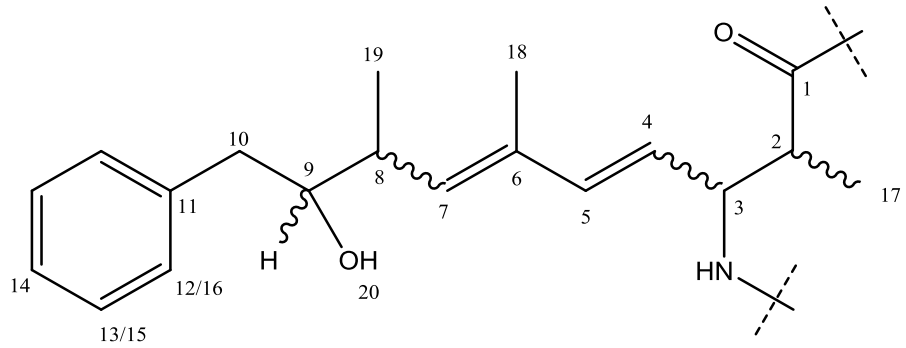

Figure 73: Structure elucidated of atom sequence consistent with DMAdda. The numbering presented is consistent with DMAdda.

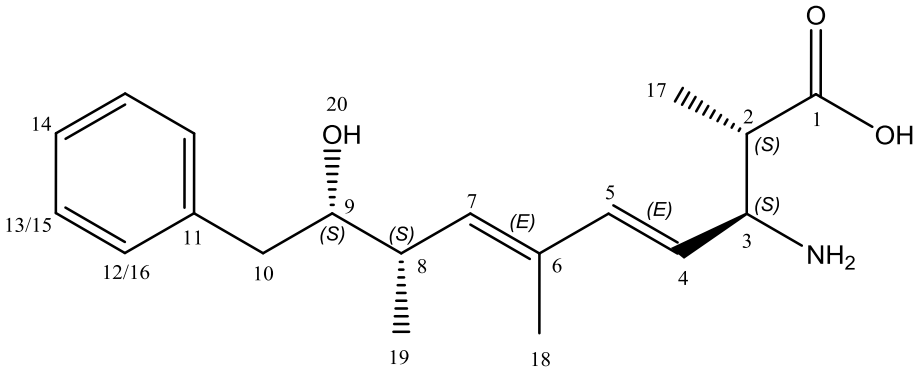

Figure 74: DMAdda with stereogenic centers shown.

Alanine: Ala

In the HMBC spectrum (p. 82) there is a correlation from 8.16 ppm to 172.11 ppm. In the ROESY2 spectrum (p.85) the shift 8.16 ppm correlates with 4.39, 4.57 and 5.55 ppm, suggesting that the peptide bond consists of the shifts from HMBC and the α-proton is 4.39 ppm. Correlation from 172.11 to 4.39 ppm is absent in the HMBC spectrum (p. 82). The signals at 4.39 ppm were discovered to arise from two different carbons during the introductory analysis, making further elucidation difficult. 4.57 ppm was also discovered to arise from two overlapping species. One of them has been determined to be the 3-position of DMAdda. Selective TOCSY with irradiation of 4.57 ppm reveals the spin system of DMAdda as well as the spin system of the overlapping species. The only non-DMAdda signals produced are 7.97 ppm as well as 1.36 ppm (Appendix B p. 275). Selective TOCSY on 1.36 produces a spectrum (p. 96) of the unknown spin system isolated from the known and can be seen in figure 75.

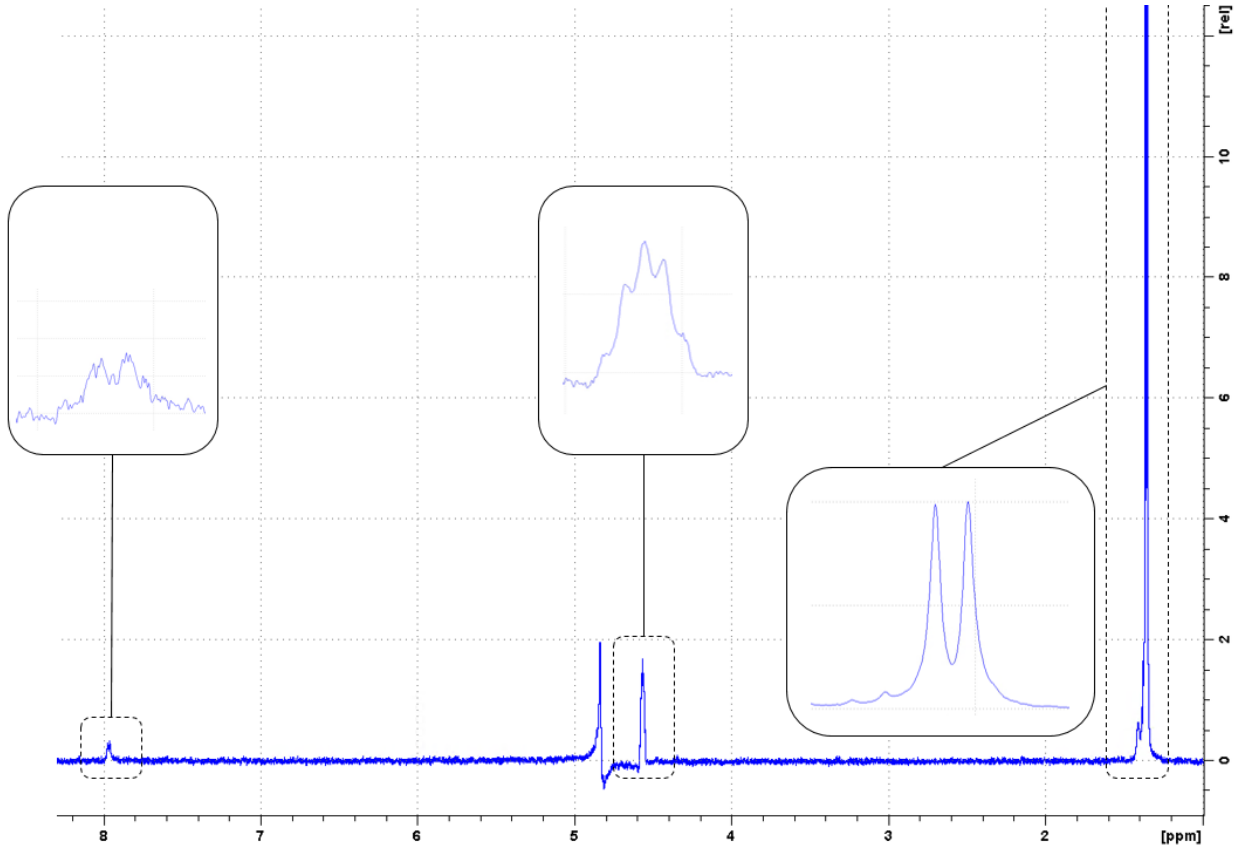

Figure 75: Selective TOCSY experiment where the resonance at 1.36 ppm was selectively irradiated to show its spin system. Processing parameters for the big spectrum: SI = 65 536, ME-mod = LPfr NOCOEF = 64, LPBIN = 320, WDW = EM, LB = 0.50 Hz. Changed processing parameters for expanded region: WDW = GM, GB = 0.1 and LB = -3 Hz. All expanded regions except 1.36 ppm are displayed without height manipulation.

The HSQC spectrum (p.78) combines the new 4.57 ppm (H) shift with the carbon at 50.47 ppm (C), 1.36 ppm (H) with 17.49 ppm (C) while the signal 7.97 ppm from the selective TOCSY is absent and assumed to be bonded to nitrogen. Both carbon species are found to be CH/CH_3 where the multiplicity of 1.36 reveals 4.57 ppm to be a CH. Selective TOCSY on 1.36 ppm (figure 75) reveals the multiplicity of 4.57 ppm to be a quintet and confirming that 1.36 ppm is a methyl.

In the SHMBC spectra (p. 83-84) the signals 1.36 and 4.57 ppm correlates with 175.60 ppm which correlates further to 8.30 ppm. The COSY spectrum (p. 75) shows the sequence of constituents to be: CH_3-CH which branches into C=O and NH. The COSY elucidation can be seen in figure 77. The HMBC correlations are illustrated in figure 76 with the spectra on page (p. 82-84).

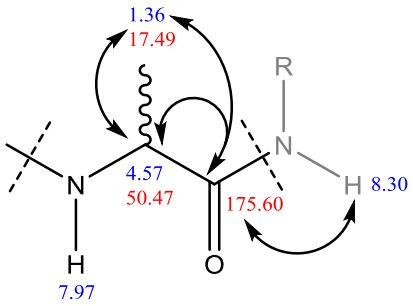

Figure 76: HMBC correlations for Ala.

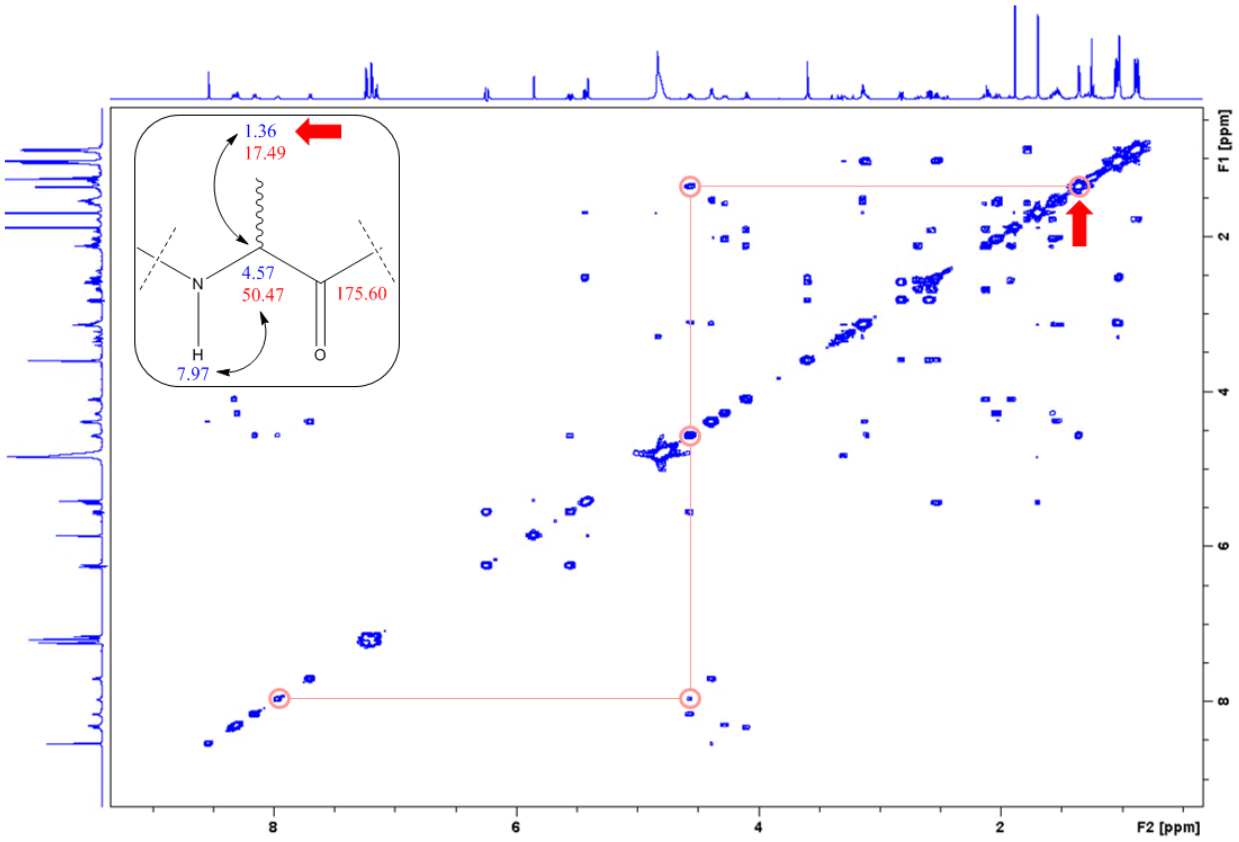

Figure 77: COSY correlation sequence for Ala (experiment 7010). The red arrow notes the start of elucidation and indicates which diagonal peak belongs to which proton in the structure.

Leucine: Leu

Further elucidation in the DIPSI-2 spectrum (p. 76 and 77) reveals the spin system of the signal at 8.30 ppm in the F2 dimension of the HMBC spectrum (p. 82) to consist of; 8.30, 4.28, 2.04, 1.78, 1.57, 0.89 and 0.87 ppm. Connecting the shifts with their respective carbons in the HSQC spectrum (p. 78) produces the constituents: 4.28 (H) with 55.59 ppm (C), 2.04 (H) and 1.57 ppm (H) with 40.97 ppm (C), 1.78 (H) with 26.06 ppm (C), 0.89 (H) with 23.90 ppm (C) and 0.87 ppm (H) with 21.43 ppm (C). 8.30 ppm is absent in the HSQC spectrum (p.

78) and assumed to be connected to nitrogen. Excitation of the signals at 8.30 ppm in a selective TOCSY experiment (Appendix B p. 275) confirmed the spin system but did not produce a spectrum with readable multiplicity. It is suspected that the heteroatom disrupts the propagation through the spin system. Excitation of the signal at 0.89 ppm in a selective TOCSY did however produce a spectrum with interpretable multiplicity and can be seen in figure 78.

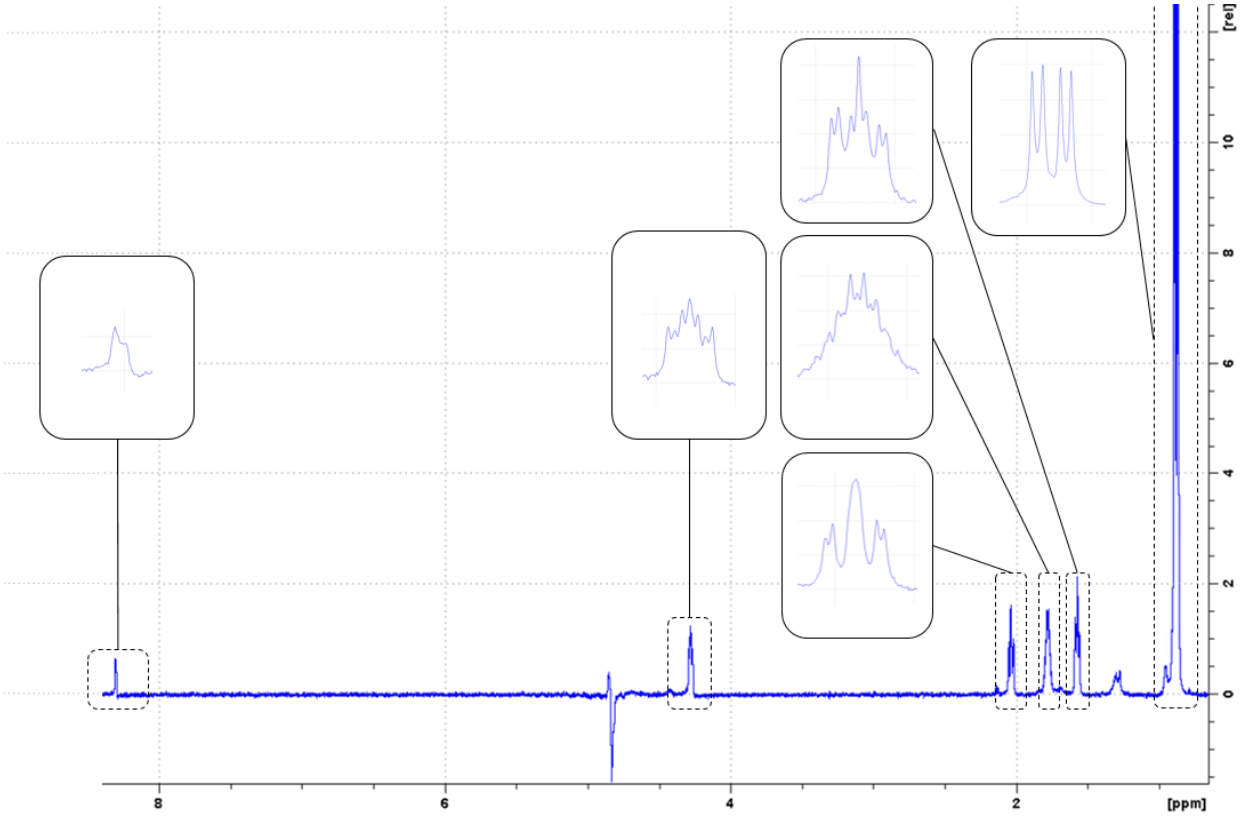

Figure 78: Selective TOCSY experiment where the resonance at 0.89 ppm was selectively irradiated to show its spin system. Processing parameters for the big spectrum: SI = 65 536, ME-mod = LPfr NOCOEF = 64, LPBIN = 320, WDW = EM, LB = 0.50 Hz. Changed processing parameters for expanded region: WDW = GM, GB = 0.25 and LB = -3 Hz. All expanded regions except 1.36 ppm are displayed without height manipulation.

The excitation appears to have produced additional signals in the spectrum. It is assumed to be an impurity due to its absence in the other selective TOCSY experiment and has been emphasized in figure 79 (next page).

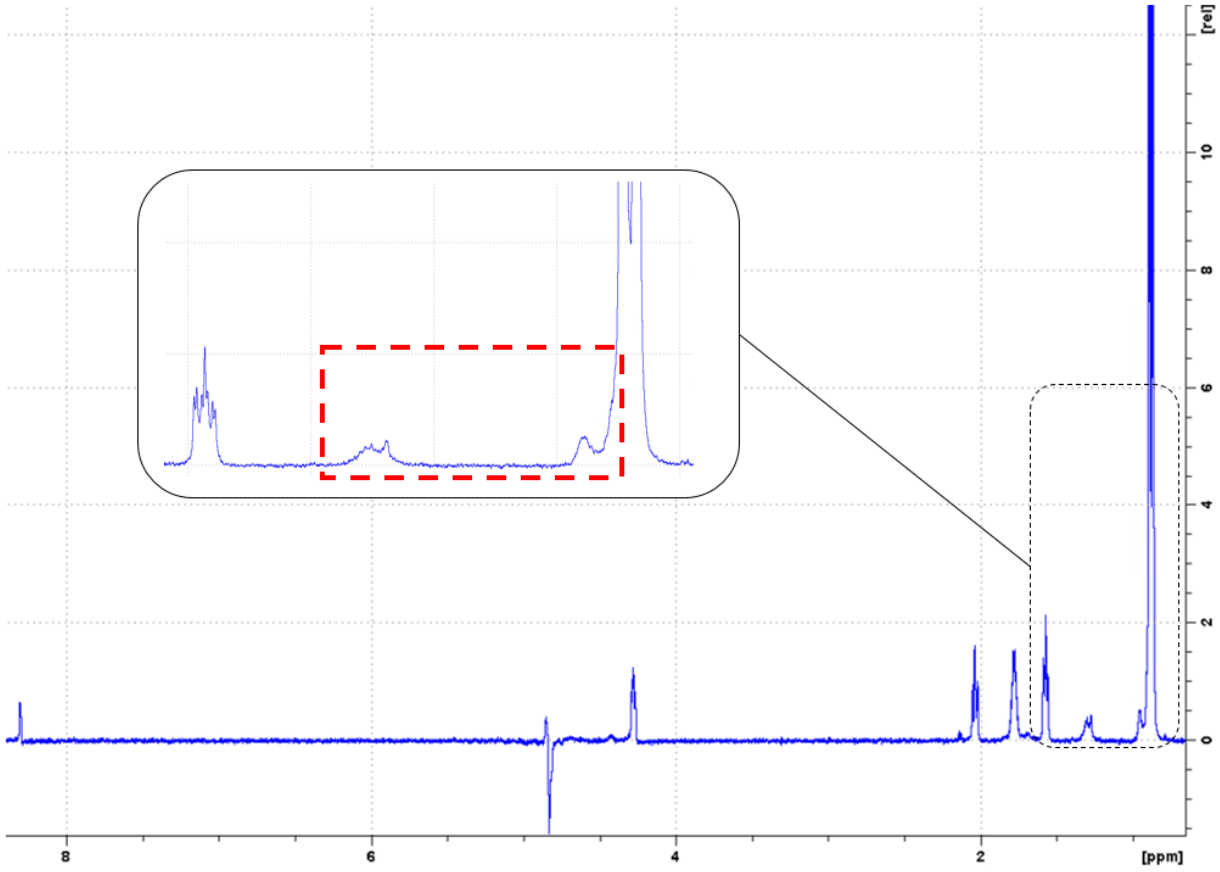

Figure 79: Additional signals excited from irradiation of the resonance at 0.89 ppm. The zoomed in window highlights the extra signals with a dashed red box. SI = 65 536, ME-mod = LPfr NOCOEF = 64, LPBIN = 320, WDW = EM, LB = 0.50 Hz

Elucidation in the COSY spectrum (p. 75) from 8.30 ppm determines the sequence of constituents of the spin system to be: 8.30-4.28-2.02 and 1.57-1.78-0.89 and 0.87 ppm. The elucidation is shown in figure 80.

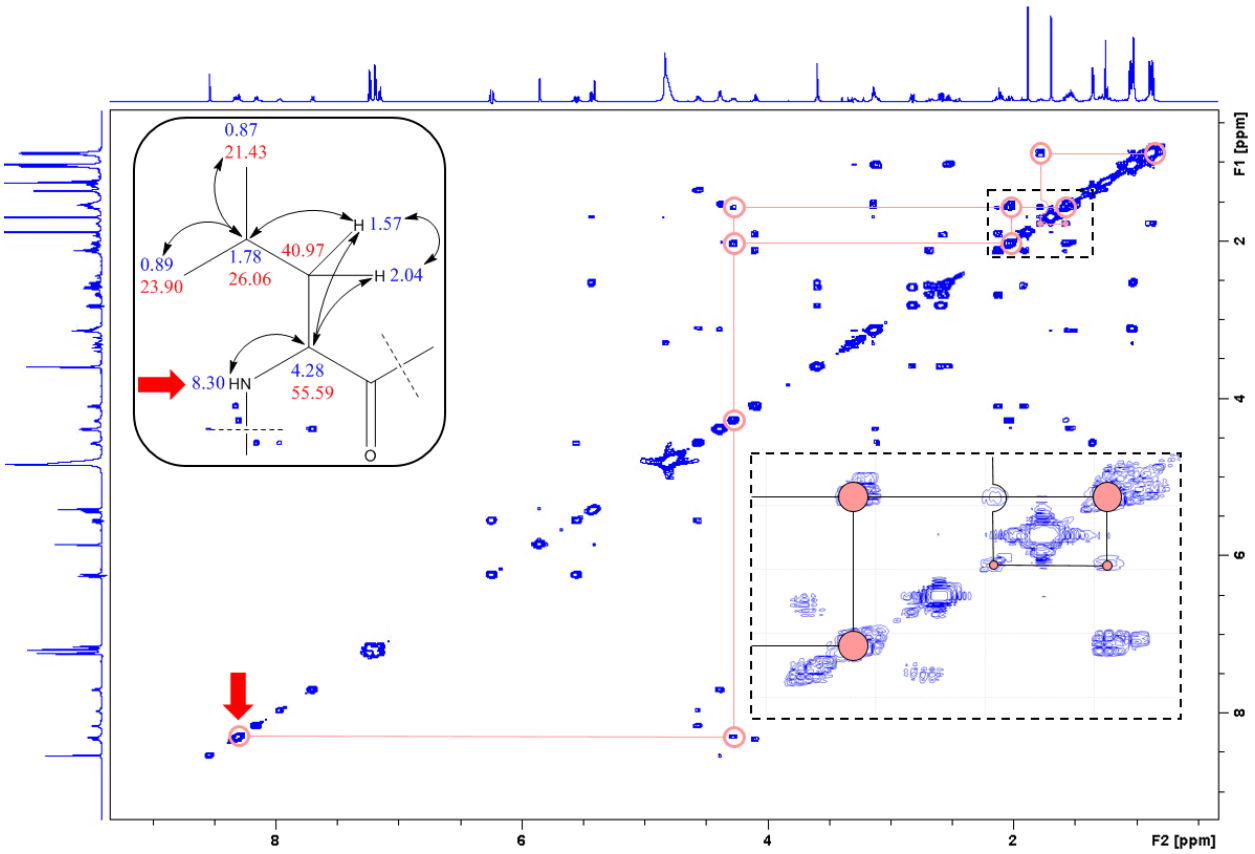

Figure 80: COSY correlation sequence for Leu (experiment 7010). The red arrow notes the start of elucidation and indicates which diagonal peak belongs to which proton in the structure.

Combining the sequence of constituents produced by and determined in the selective TOCSY (Appendix B p. 275) and COSY (p. 75) experiments, the multiplicity of 8.30 ppm (doublet) suggests that 4.28 ppm is a CH. For the same reason, the multiplicity of 0.89 (doublet) and 0.87 ppm (doublet) suggest that 1.78 ppm (multiplet) is a CH. The neighboring protons, which consists of four individual chemical shifts, may produce a doublet of doublets of quartets of quartets which may result in some of the multiplicity being imbedded in the noise. Correlations from the HMBC spectrum (p. 82) are consistent with the elucidation and are depicted in figure 81.

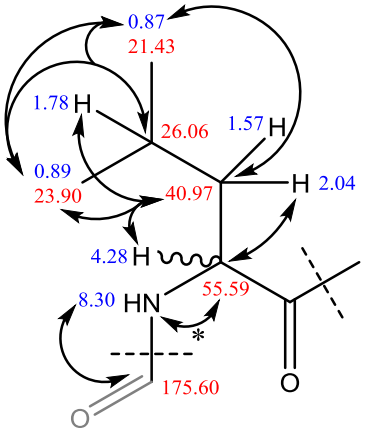

*^{2}J HSQC

Figure 81: HMBC correlations for Leu. The correlation for the starred arrow is found in HSQC spectrum displayed in figure 66.

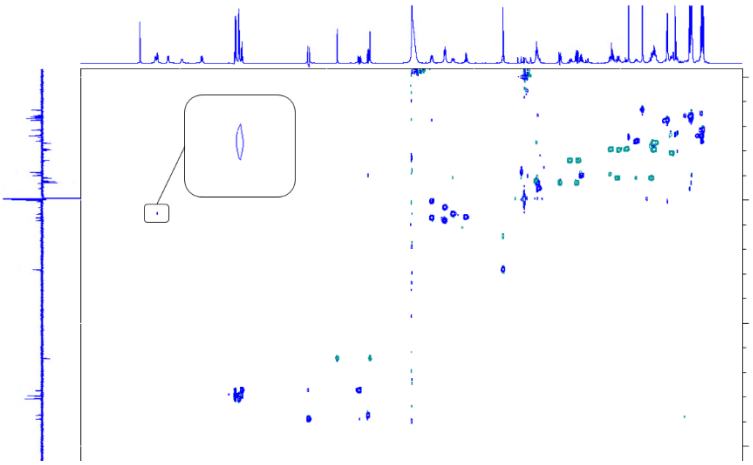

Figure 82: Highlighted is a ^{2}J correlation between 8.30 (H) and 55.59 (C) ppm. The experiment is 7040.

The elucidation is consistent with the literature for Leucine. Figure 83 show the elucidation and leucine respectively.

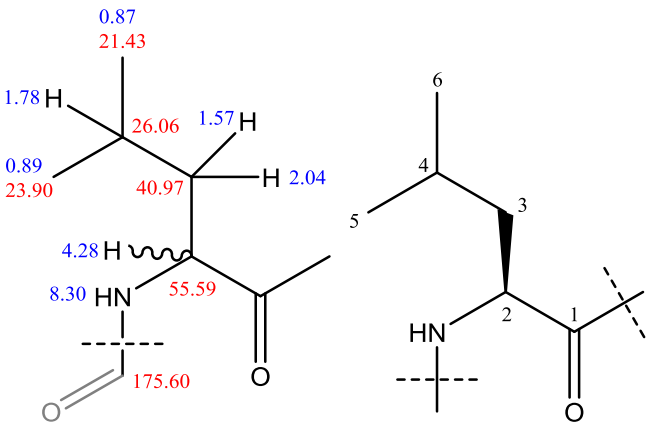

Figure 83: Elucidation of atom sequence for Leu (left) is consistent with structure for L-Leu (right).

From 4.28 ppm, there is a correlation to 175.75 ppm in the SHMBC (Appendix B p. 275) spectrum which further correlates to 7.70 ppm.

D-erytro-β-methyloaspartic acid: Masp

The DIPSI-2 (p. 76 and 77) and COSY (p. 75) spectra respectively show ambiguity at correlations from 7.70 to 4.39 ppm and ~3.14 ppm as well as the correlation between 7.70 and 4.39 ppm. A selective TOCSY (Appendix B p. 275) where 7.70 ppm is excited produces a spin system consisting of: 7.70 (d), 4.39 (dd), 3.12 (m) and 1.03 ppm (d) seen in figure 84.

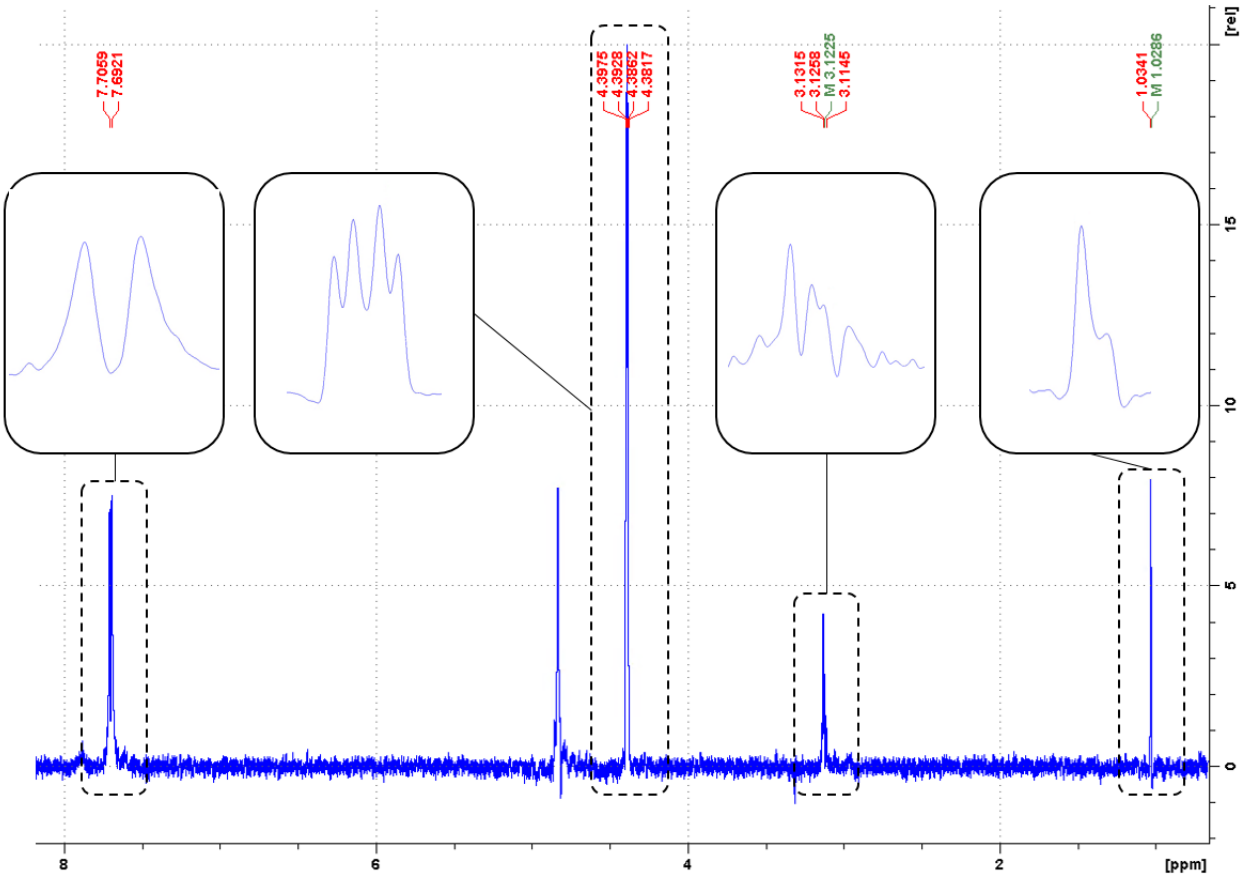

Figure 84: Selective TOCSY experiment where the resonance at 7.70 ppm was selectively irradiated to show its spin system. Processing parameters for the big spectrum: SI = 65 536, ME-mod = LPfr, NOCOEF = 64, LPBIN = 320, WDW = EM, LB = 0.50 Hz. Changed processing parameters for expanded region: WDW = GM, GB = 0.3 and LB = -3 Hz. All expanded regions except 4.39 ppm are displayed without height manipulation.

The multiplicity of the signal at 7.70 ppm indicates that the resonance at 4.39 ppm is a methine. Likewise, the signal at 4.39 ppm reveals that the signal at 3.12 ppm is a methine. The multiplicity of the resonance at 1.03 ppm suggests that the signal at 3.12 ppm is a methine, while the complex multiplicity of the signal at 3.12 ppm indicates that the signal at 1.03 ppm is a methyl. The integral of the overlapping signals at ~1.03 ppm supports the indication of a methyl signal at 1.03 ppm. The elucidation is illustrated in figure 85.

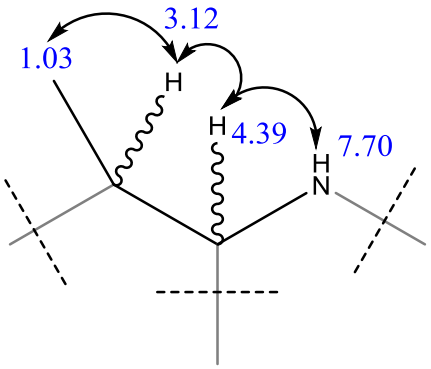

Figure 85: COSY correlation pattern for Masp.

Combining these protons to carbons in the HSQC spectrum (p. 78) produces the constituent; 1.03-15.57 ppm (H-C) but can't resolve the ambiguity of the corresponding carbon shifts of 3.12 or 4.39 ppm. The proton signal at 1.03 ppm correlates in the HMBC spectrum (p. 82) to 58.33 and 43.06 ppm. By overlaying the HSQC and HMBC spectra (not shown) it becomes clear that the corresponding carbons to proton shifts; 4.39 and 3.12 ppm are respectively 58.33 and 43.06 ppm. The methine nature of the signals at 3.12 and 4.39 ppm leaves one substituent bound to both constituents. In the SHMBC spectra (83, 84 and Appendix B p. 275), at 1.03 ppm in the F2 dimension there is a correlation with 178.93 ppm. The signal at 7.70 ppm does not correlate to any new carbons.

By close inspection of the SHMBC spectrum (p. 83, 84 and Appendix B p. 275) there are two correlations for both the proton shifts 4.39 and 3.12 ppm in the carbonyl region. One of the correlations at 3.12 ppm has already been determined to be the 1-position of DMAdda and does not have room for any more constituents. The other also correlates with the signal at 178.93 ppm.

At 4.39 ppm there are two overlapping constituents which was noted at the start of elucidation (p. 100). It was also noted that this is within the typical region where α-proton appear. With the two correlations to the signal at 176.94 ppm it is suspected that both are α-protons and correlate to the same carbonyl. With signal at 3.12 ppm and one of the two constituents at 4.39 ppm correlating to both carbonyls, it is thus far impossible to determine if this amino acid is peptide bonded in the typical fashion or the iso-variant. 1.03 ppm correlates to 176.94 ppm, making the isopeptidebonded orientation the only possible option. The other carbonyl (178.93 ppm) is assumed to be a carboxylic acid since there are no more amide protons left when addressing what was just assumed to be the last amino acid and there is no correlation

to suggest that it is a ketone or an aldehyde. The HMBC correlations is illustrated in figure 86.

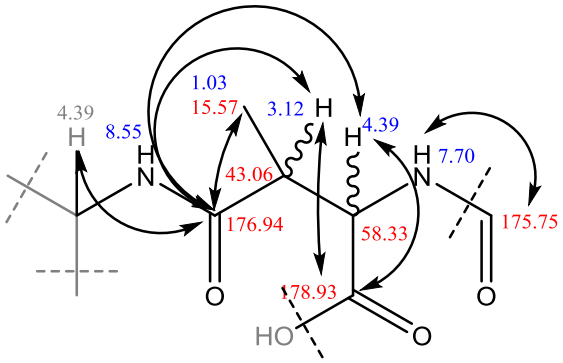

Figure 86: HMBC correlations present in Masp.

This structure is consistent with the structure for Masp, seen in figure 87.

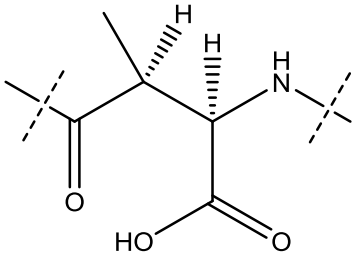

Figure 87: Masp shown doubly peptide bonded. One of them isopeptide bonded.

Arginine: Arg

The last α-proton and its associated AA is up next. By eliminating the correlations, arising from the known AAs, in the COSY spectrum (p. 75) one may then continue the elucidation in the sequence followed thus far. From the chemical shift at 4.39 ppm in the COSY spectrum (p. 75), one can deduce that constituents with proton shifts of 8.53 and 1.53 ppm neighbor it. Investigation in the HSQC spectrum (p. 78) to find their respective carbon shifts and nature produces a 3rd proton shift; 2.02 ppm which is bound to the same carbon as 1.53 ppm; 29.5 ppm. The chemical shift in the peptide region, 8.53 ppm, is absent and assumed to be bound to nitrogen while the chemical shift of this AA's α proton, 4.39 ppm, is bound to a carbon with chemical shift; 52.9 ppm. A weak, but confirming, correlation is seen between the α-proton and the chemical shift at 2.02 ppm. The further correlation partner from "2.02 ppm" is found at 1.54 ppm, which is ambiguous whether correlates to 1.53 ppm due to their close proximity. It is assumed that they do since COSY is designed to show produce correlations

between neighboring protons and the diagonal peak is fat relative to the rest of the diagonal. The diagonal peak at 1.54 ppm further correlates to 3.14 ppm. In the HSQC spectrum (p. 78), correlations between 1.54 and 26.7 ppm are found as well as 3.14 and 42.3 ppm. The SHSQC spectrum (p. 78) shows complete separation between the cluster at 3.14 ppm and confirms the pairing of 3.14 and 42.3 ppm and that it is a methylene. The DIPSI-2 spectra (76 an 77) shows no further correlations from any of the constituents and it is thus assumed to be the entire spin system, which indicates that the remaining constituent is likely to be proton-less. The HMBC spectrum (82) provides correlations in accordance with the elucidation so far and is illustrated in figure 88.

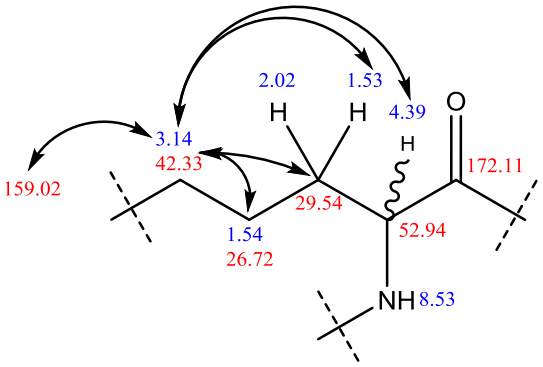

Figure 88: HMBC correlations for the remaining substituent, consistent with Arg.

There is a peculiar correlation from the proton shift 3.14 to carbon shift 159.0 ppm. It is significantly lower than the shifts for carboxylic acids and amides and thus unlikely to be of such a nature. It is too long to be Glu or Gln. Arginine is however reported to produce a carbon shift at close to 160 ppm.[44, 45] For MCs in d3-MeOH, the NH separating the isolated caron from the rest of the R-group has however not been detected[46] and is assumed to be exchanging with the solvent.

Arg-DMAdda

From the structure elucidation of DMAdda it was assumed to be peptide bonded with a carbonyl with a chemical shift of 172.1 ppm. ROESY-data (p. 85) was used to determine that one of the α-protons at 4.39 ppm were close enough to bind to this carbonyl. Arg's α proton needs a substituent and has the correct chemical shift and is thus assumed to be bonded to the carbonyl at 172.1 ppm.

In the ROESY2 spectrum (p. 85), a correlation between 4.39 ppm and DMAdda-NH was found. By using Mdha's terminal alkene protons as a reference, the distance between DMAdda-NH and the proton of 4.39 ppm was determined to be 338 pm:

Sum of angles in a triangle: 180°. The bond angle in alkene: 120° which when the sum of angles is 180°, makes the other two become 30° each since the bonds are of similar length. The sum of angles then become: 30+30+120 = 180. The distance between protons in terminal alkene is r_{ref} in the following formula (sinus sentence): $r_{ref} = \frac{108 \sin 120}{\sin 30} = 187\ pm$. The formula to use on all proton distances which are not the terminal alkene protons can then be calculated by the following:

$$r_{ij} = r_{ref}(\frac{a_{ref}}{a_{ij}})^{-6}$$

This distance is acceptable to allow the proton signal at 4.39 ppm to be bound to the carbon signal at 172.11 ppm and forming a peptide backbone to the molecule.

The NH-proton of Ala (7.97 ppm) is a doublet with an integral similar to the other peptide protons. It is unlikely to be charged and must therefore be bound to a proton-less species. There are no HMBC correlations from Mdha and the HSQC (p. 78) reveals there to be no ^{1}J-correlation at the carbon shift; 166.6 ppm. There are several ROESY correlations (p. 85) between non-neighboring AAs, which suggests that the polypeptide may be cyclic.

Mdha-Ala

In MS-data supplied by Ph.D. Christopher Miles from the same batch, fragment ions consistent with Mdha-Ala-Leu-Masp as well as Mdha-Ala were identified. An excerpt from the data is given in appendix C (p. 321). Coordinates 10, 25 and 10,12 are of particular interest. Further more, the crystal structure of MC-LR bound to a catalytic subunit of protein serine/threonine phosphatase-1.[47]

Supplementary spectra

Selective TOCSY spectra of each α and amide proton (apart from Arg-NH) is given in appendix B (p. 275) together with a supplementary HSQC-TOCSY spectra and SHMBC.

4.1.3 Final structure of amino acids

Ala:

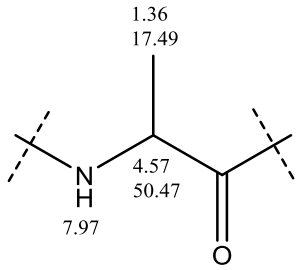

Figure 89: Alanine

Table 45: A Summary of chemical shifts and correlations consistent with Ala.

Entry	δH	δC	Atom type	COSY	DIPSI-2 (80μs)	DIPSI-2 (160 μs)	HMBC & SHMBC
Ala							
1		175.60	-C(O)-N				Leu-NH, Ala-2, 3
2	4.57, q	50.47	>CH-	Ala-3, NH	Ala-3, NH	Ala-3, NH	Ala-1, 3
3	1.36, d	17.49	-CH3	Ala-2	Ala-2, NH	Ala-2, NH	Ala-1, 2
NH	7.97, d		NH	Ala-2	Ala-2, 3	Ala-2, 3	N.D.

Table 46: NOE-data collected but not utilized in the elucidation.

ROESY2 (internal)	ROESY2 (external)
D-Ala	
N.D	N.D
Ala-2, NH (w)	Masp-5 (s)
Ala-2 (w), Ala-3 (m)	Leu-NH (w)

Leu:

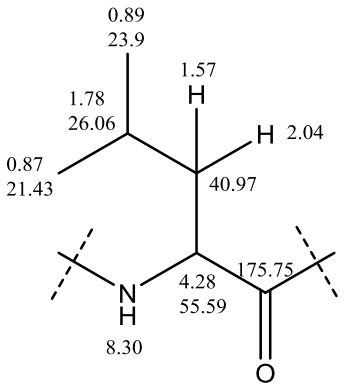

Figure 90: Leucine

Table 47: A Summary of chemical shifts and correlations consistent with Leu.

Entry	δH	δC	Atom type	COSY	DIPSI-2 (80µs)	DIPSI-2 (160 µs)	HMBC & SHMBC
Leu							
1		175.75	-C(O)N-				
2	4.28, ddd	55.59	>CH-	Leu-3A, 3B	Leu-3A, 3B, 4, 5, 6, NH	Leu-3A, 3B, 4, 5, 6, NH	Leu-1
3A	2.04			Leu-2, 3B	Leu-2, 3B, 4, 5, 6, NH	Leu-2, 3B, 4, 5, 6, NH	Leu-2
3B	1.57	40.97	-CH2-	Leu-2, 3A, 4	Leu-2, 3A, 4, 5, 6, NH	Leu-2, 3A, 4, 5, 6, NH	N.D.
4	1.78	26.06	-CH<	Leu-3B, 5, 6	Leu-2, 3A, 3B, 5, 6, NH	Leu-2, 3A, 3B, 5, 6, NH	N.D.
5	0.89, d	23.90	-CH3	Leu-4	Leu-2, 3A, 3B, 4, 6, NH	Leu-2, 3A, 3B, 4, 6, NH	Leu-3, 4, 6
6	0.87, d	21.43	-CH3	Leu-4	Leu-2, 3A, 3B, 4, 5, NH	Leu-2, 3A, 3B, 4, 5, NH	Leu-3, 4, 5
NH	8.30, d			Leu-2	Leu-2, 3A, 3B, 4, 5, 6	Leu-2, 3A, 3B, 4, 5, 6	Ala-2

Table 48: NOE-data collected but not utilized in the elucidation.

ROESY2 (internal)	ROESY2 (external)
L-Leu	
Leu-2 (m), 3A (m), 3B (s), 4 (m), 5 (s), 6 (s)	Masp-2 (w)
Leu-2 (m), 3B (s), 5 (s), 6 (s), NH (s)	Masp-2 (m/s), NH (w)
Leu-2 (s), 5 (s), 6 (s)	
Leu-2 (m), NH (m), 5 (s), 6 (s)	Mdha-N-CH3 (w)
Leu-2 (s), 3A (s), 3B, 4 (s)	
Leu-2 (s), 3A (s), 3B, 4 (s)	
Leu-2 (s), 3A (s), 4 (m)	Masp-NH (s), Ala-2 (s), 3 (w)

Masp (L-threo-3-Methylaspartate):

Table 49: A Summary of chemical shifts and correlations consistent with Masp.

Entry	δH	δC	Atom type	COSY	DIPSI-2 (80µs)	DIPSI-2 (160 µs)	HMBC & SHMBC
Masp							
1		178.93	-COOH				
2	4.39, d	58.33	>CH-	Masp-3, NH	Masp-3, 5, NH	Masp-3, 5, NH	Masp-1, 3, 4
3	3.12, m	43.06	-CH<	Masp-3, 5	Masp-2, 5, NH	Masp-2, 5, NH	Masp-4
4		176.94	-C(O)N-				Masp-2, 3, 5, Arg-2
5	1.03, d	15.57	-CH3	Masp-3	Masp-2, 3, NH	Masp-2, 3, NH	Masp-1, 2, 3, 4
NH	7.70, d		NH	Masp-2	Masp-2, 3, 5	Masp-2, 3, 5	Leu-1

Table 50: NOE-data collected but not utilized in the elucidation.

ROESY2 (internal)	ROESY2 (external)
Masp	
Masp-3 (s), 5, NH (s)	DMAdda-3 (m), Arg-2 (s), 3B (s), 5 (s), Mdha-N-CH3 (m), Glu-4A (w)
Masp-2 (s), 3 (s), 5, NH (s)	Ala-3 (s), Glu-3A (m)
Masp-2 (w), 3(s), 5(s)	Leu-NH (s), Leu-2 (s), 3A (m), Arg-2 (s), Glu-3A (w), Ala-2 (w)

Arg:

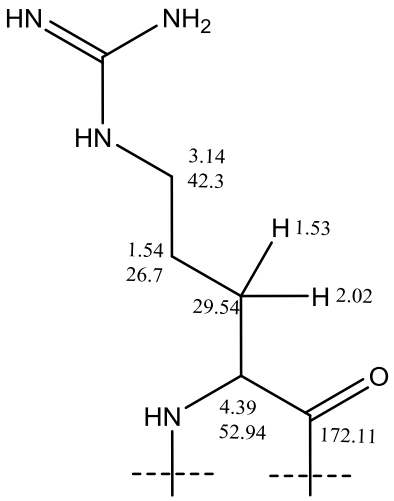

Figure 91: Arginine

Table 51: A Summary of chemical shifts and correlations consistent with Arg.

Entry	δH	δC	Atom type	COSY	DIPSI-2 (80µs)	DIPSI-2 (160 µs)	HMBC & SHMBC
Arg							
1		172.11	-C(O)-N				Adda-3, NH
2	4.39, dd	52.94	CH	Arg-3A, 3B, NH	Arg-3A, 3B, 4, 5, NH	Arg-3A, 3B, 4, 5, NH	Masp-5
3A	1.53			Arg-2, 3B, 4	Arg-2, 3B, 4, 5, NH	Arg-2, 3B, 4, 5, NH	Masp-5
3B	2.02	29.5	CH2	Arg-2, 3A, 4	Arg-2, 3A, 4, 5, NH	Arg-2, 3A, 4, 5, NH	N.D.
4	1.54	26.7	CH2	Arg-3A, 3B, 5	Arg-2, 3A, 3B, 5, NH	Arg-2, 3A, 3B, 5, NH	Masp-5
5	3.14	42.3	CH2	Arg-4	Arg-2, 3A, 3B, 4, NH	Arg-2, 3A, 3B, 4, NH	Arg-3, 4, 6
6		159.02	H2N-C(NH)-NH				Arg-5
	8.55, d		NH	Arg-2			N.D.

Table 52: NOE-data collected but not utilized in the elucidation.

ROESY2 (internal)	ROESY2 (external)
Arg	
Arg-3A (s), 3B (s), 5 (s)	DMAdda-3 (m), NH (m), Masp-3, 5 (s), NH (s), Mdha-N-CH3 (m), Glu-4A (w)
Arg-2 (s), 3B (s), 5 (s)	
Arg-2 (s), 3B (s), 4 (s), 5 (s)	
Arg-2 (s), 3B (s), 5 (s)	
Arg-2 (s), 3B (s), 5 (s)	
Arg-3B (s), 3A (s), 3B (s), 4 (s)	Adda-17 (s)
Arg-5 (w)*	

DMAdda:

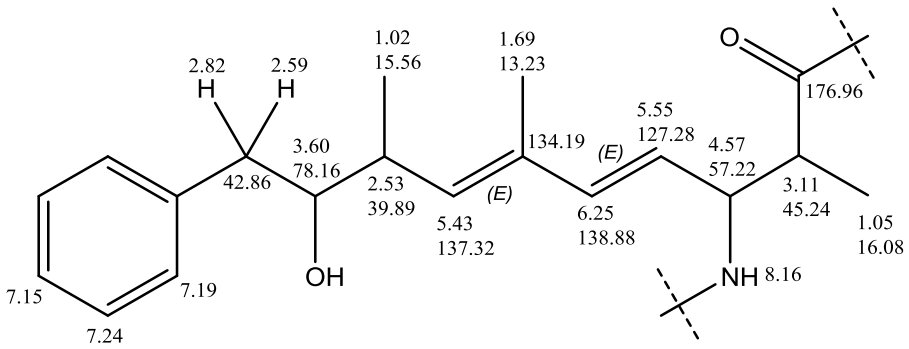

Figure 92: DMAdda

Table 53: A Summary of chemical shifts and correlations consistent with DMAdda.

# in the molecule	δH (J in Hz)	δC	Atom type	COSY	DIPSI-2 (80µs)	DIPSI-2 (160 µs)	HMBC & SHMBC
DMAdda							
14	7.15, t	127.16	Ar	Adda-13/15, 14			DMAdda-12/16
12/16	7.19, d	130.62	Ar	Adda-12/16, 4			DMAdda-10, 12/16, 14
13/15	7.24, t	129.37	Ar	Adda-12/16, 13/15			
11		141.11	Ar				DMAdda-10A, 10B, 13/15
10A	2.82, dd		CH	Adda-9, 10B		DMAdda-7, 8, 9, 10B, 19	
10B	2.59, dd	42.86	CH	Adda-9, 10A		DMAdda-7, 8, 9, 10A, 19	
9	3.60, ddd	78.16	CH	Adda-10A, 10B, 8		DMAdda-7, 8, 10A, 10B, 19	DMAdda-19
8	2.53, ddq	39.89	CH	Adda-7, 9, 19	DMAdda-7, 9, 10A, 10B, 18, 19	DMAdda-7, 9, 10A, 10B, 18, 19	DMAdda-6, 7, 9, 19
7	5.43, d	137.31	-CH=	Adda-8, 18	DMAdda-8, 9, 10A, 10B, 18, 19	DMAdda-8, 9, 10A, 10B, 18, 19	DMAdda-5, 8, 9, 18
6		134.18	=C<				DMAdda-4, 5, 8, 18
19	1.02, d	16.57	CH3	Adda-8			DMAdda-7, 8, 9
18	1.69, d	13.23	CH3	Adda-7			DMAdda-5, 6, 7, 19
5	6.25, d	138.88	-CH=	Adda-4			DMAdda-3, 6, 7, 18
4	5.55, dd	127.28	-CH=	Adda-3, 5			DMAdda-6
3	4.57, q	57.22	CH	Adda-2, NH			DMAdda-3, 4, 5, 17
2	3.11, dd	45.24	CH	Adda-3, 17			DMAdda-1, 2, 17
17	1.05, d	16.08	CH3	Adda-2			
NH	8.16, d		NH	Adda-3			Arg-1
1		176.96	-C(O)-N				Glu-2, NH, DMAdda-2, 17

Table 54: NOE-data collected but not utilized in the elucidation.

Entry	δH	δC	ROESY2 (internal)	ROESY2 (external)
DMAdda				
14	7.15, t	127.16	DMAdda-12/16, 13/15	
12/16	7.19, d	130.62	DMAdda-9 (m), 10A (m), 10B (m) 13/15, 14, 18 (m), 19 (m)	
13/15	7.24, t	129.37	DMAdda-12/16, 14	
11		141.11		
10A	2.82, dd	42.86	DMAdda-8 (s), 10B (s), 18 (m), 19 (m)	Leu-5 (w), 6 (w), Glu-4A (m)
10B	2.59, dd		DMAdda-7 (m), 9 (s), 10A (s), 12/16 (m), 13/15 (w), 18 (m), 19 (m)	
9	3.60, ddd	78.16	DMAdda-7 (s), 10A (s), 10B (s), 12/16 (m), 13/15 (w), 18(w), 19 (s)	
8	2.53, ddq	39.89	DMAdda-7 (s), 9 (s), 10A (s), 12/16 (w), 18 (s), 19 (m)	
7	5.43, d	137.31	DMAdda-5 (s), 8 (s), 9 (s), 10A (s), 10B (m), 18 (m), 19 (s)	
6		134.18		
19	1.02, d	16.57	DMAdda-7 (s), 8 (s), 9 (s), 10A (s), 18 (m)	Mdha-N-CH3 (w), Arg-5 (s)
18	1.69, d	13.23	DMAdda-3 (w), 4 (s), 5 (m), 7 (m), 8 (s), 9 (m), 10A (m), 10B (m), 12/16 (w), 12/16 (m), 19 (m)	Mdha-N-CH3, Arg-5 (w)
5	6.25, d	138.88	DMAdda-3 (s), 4 (s), 7 (s), 17 (m), 18 (m)	
4	5.55, dd	127.28	DMAdda-3.12, 5 (s), 17 (m), 18 (s)	
3	4.57, q	57.22	DMAdda-2 (s), 4 (m), 5 (s), 17 (s), 18 (w), NH	
2	3.11, dd	45.24		
17	1.05, d	16.08	DMAdda-2 (s), 3 (s), 4 (m), 5 (m), 18 (m)	Glu-NH (w)
NH	8.16, d		DMAdda-2 (m), 3 (m), 4 (m),	Arg-2 (m)
1		176.96		

Glu:

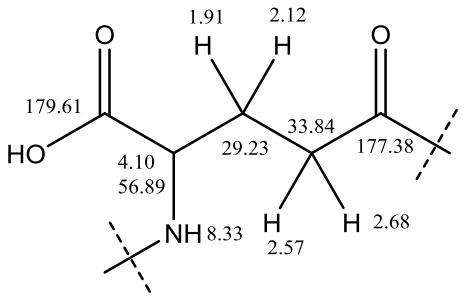

Figure 93: Glutamic acid

Table 55: A Summary of chemical shifts and correlations consistent with Glu.

Entry	δH	δC	Atom type	COSY	DIPSI-2 (80µs)	DIPSI-2 (160 µs)	HMBC & SHMBC
Glutamic acid							
1		179.61	-COOH				
2	4.10, q	56.89	CH	Glu-3A, 3B, NH	Glu-3A, 3B, 4A, 4B, NH	Glu-3A, 3B, 4A, 4B, NH	Glu-1, 3, 4, Adda-1
3A	1.91, ddd	29.23	CH2	Glu-2, 3B, 4A, 4B	Glu-2, 3B, 4A, 4B, NH	Glu-2, 3B, 4A, 4B, NH	Glu-1, 2, 4
3B	2.12, ddd			Glu-2, 3A, 4A, 4B	Glu-2, 3A, 4A, 4B, NH	Glu-2, 3A, 4A, 4B, NH	N.D.
4A	2.68, ddd	33.84	CH2	Glu-3A, 3B, 4B	Glu-2, 3A, 3B, 4B, NH	Glu-2, 3A, 3B, 4B, NH	Glu-3, 5
4B	2.57, ddd			Glu-3A, 3B, 4A	Glu-2, 3A, 3B, 4A, NH	Glu-2, 3A, 3B, 4A, NH	Glu-5
5		177.40	-C(O)-N				Glu-4A, 4B
NH	8.33, d		NH		Glu-2, 3A, 3B, 4A, 4B	Glu-2, 3A, 3B, 4A, 4B	Glu-5

Table 56: NOE-data collected but not utilized in the elucidation.

ROESY2 (internal)	ROESY2 (external)
Glutamic acid	
Glu-3A (m/s), 3B (s), 4A (m), 4B (s), NH (s)	N.D.
Glu-2 (m), 3B, (vs), 4A (m), 4B (s), NH (m)	Masp-NH (w), Arg-3A/4 (m)
Glu-NH (w), 2 (s), 3A (s), 4A (m), 4B (m)	N. D.
Glu-2 (m), 3A (m), 3B (m)	Mdha-N-CH3 (m)
Glu-2 (s), 3A (s), 3B (m)	Mdha-N-CH3 (m)

Mdha:

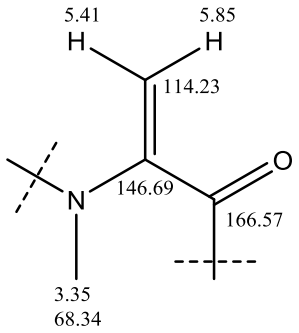

Figure 94: Mdha

Table 57: A Summary of chemical shifts and correlations consistent with Mdha.

Entry	δH	δC	Atom type	COSY	DIPSI-2 (80µs)	DIPSI-2 (160 µs)	HMBC & SHMBC
Mdha							
1		166.57	-C(O)-N				Mdha-3A, 3B
2		146.69	>C=				Mdha-3A, 3B, N-CH3
3A	5.41, s	114.23		Mdha- 3B	Mdha- 3B	Mdha- 3B	Mdha-1, 2
3B	5.85, s	114.23	=CH2	Mdha- 3A	Mdha- 3A	Mdha- 3A	Mdha-1
N-CH3	3.35, s	38.63	N-CH3				Mdha-2, Glu-5

Table 58: NOE-data collected but not utilized in the elucidation.

ROESY2 (internal)	ROESY2 (external)
Mdha	
Mdha-N-CH3 (s), 3B	
Mdha-3A	
Mdha-3A (s)	Masp/Arg-2 (m), Glu-4A (m), 4B (m), Leu-4 (w)

4.1.4 Complete atom sequence: [DMAdda^5]MC-LR

By elucidation where data in the previous subchapters (4.1.1-3) were utilized the atom sequence is known. Due to time constraints, the remaining collected data (NOE-data) was not utilized in the elucidation. The atom sequence for sample 1 is shown in figure 95.

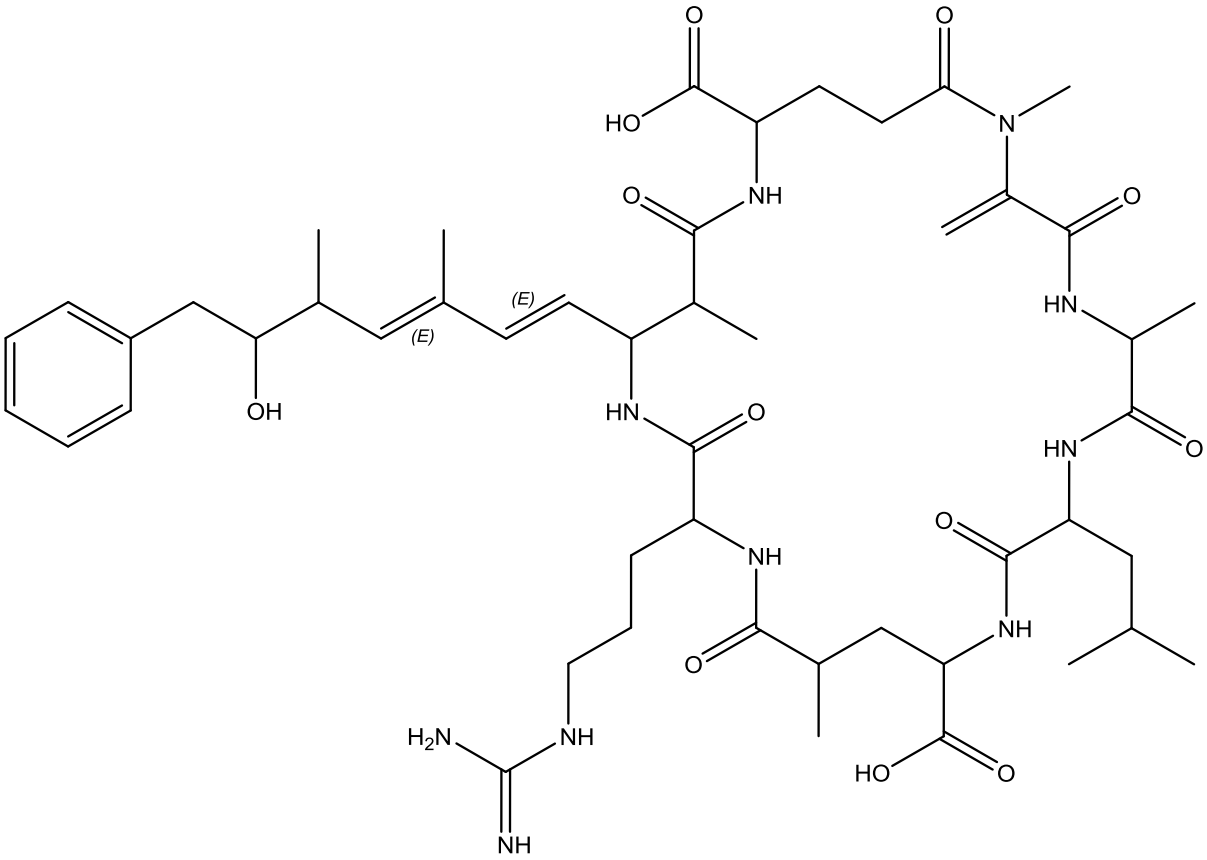

Figure 95:The elucidation of the atom sequence for sample 1. By ignoring stereogenic centra, the molecule is [DMAdda^5]MC-LR.

4.1.5 Impurities

There is no correlation to the signals: 8.55, 3.60, 1.88 and the interval 1.22-1.25 ppm. The shifts are compared to chemical shift values provided by Gottlieb Et. al. (1997). The shift at 3.60 ppm aligns with the reported chemical shift for ethylene glycol (3.59 ppm). The cluster at 1.22-1.25 ppm may be from long-chain, linear aliphatic hydrocarbons ("grease"). To be "grease", there must also be signals near 0.88 ppm. When 0.89 ppm (d) was irradiated by selective TOCSY (Appendix B p. 275), signals arose at 1.29 and 0.96 ppm and were assumed to be an impurity. This is deemed sufficient to determine that the cluster at 1.22-1.25 and 0.96 ppm to be "grease". 8.55 ppm shows no correlation to anything in homonuclear experiments. It does however correlate in the HSQC spectrum (p.78) to a carbon shift of: It is thus assumed to be formate.

4.2 Sample #2

4.2.1 Spectra:

The following spectra were used to elucidate the structure of sample #1 and will be frequently referenced throughout the thesis. Supplementary spectra are given in Appendix B (p. 275). The 1D proton, DEPTQ, COSY, DIPSI-2, HSQC, SHSQC, HMBC, SHMBC, ROESY and selective experiments used to elucidate the structure will be given in this order.

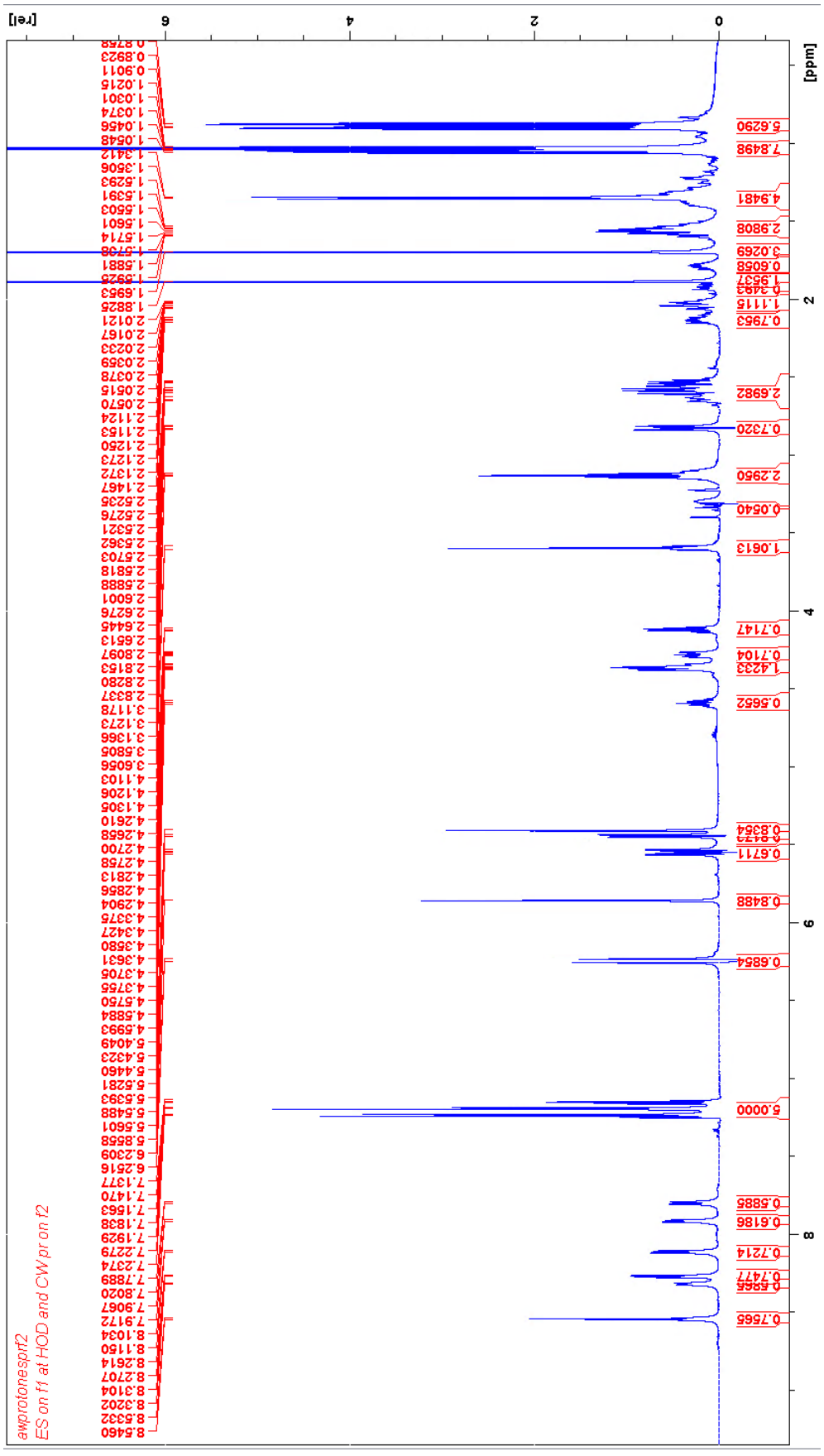

Figure 96: A 1D proton spectrum with softened ES on 3890 Hz and PR on 2663 Hz. The experiment is named 100.

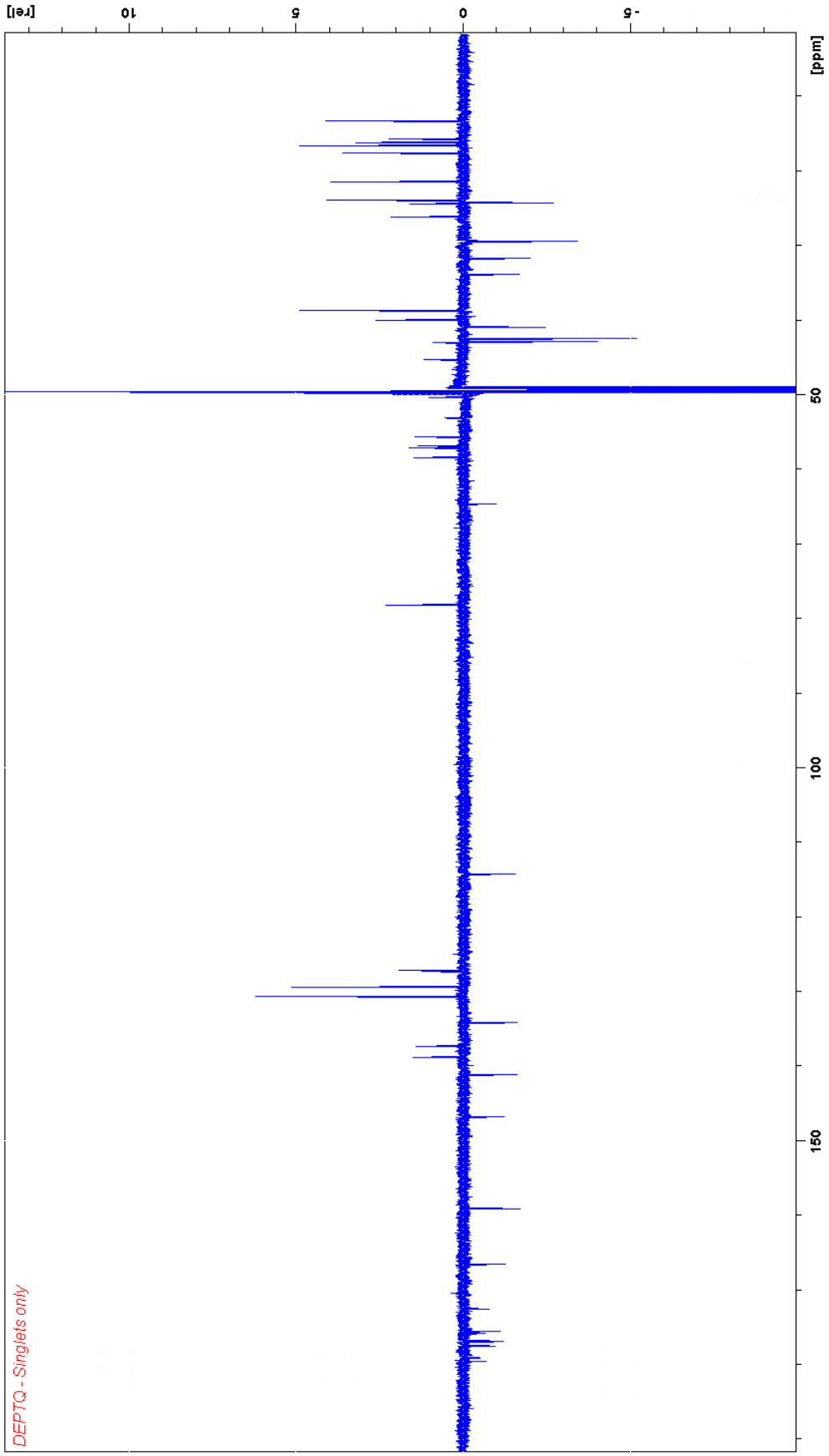

Figure 97: DEPTQ experiment optimized for coupling constant; 145 Hz. The experiment is named 160.

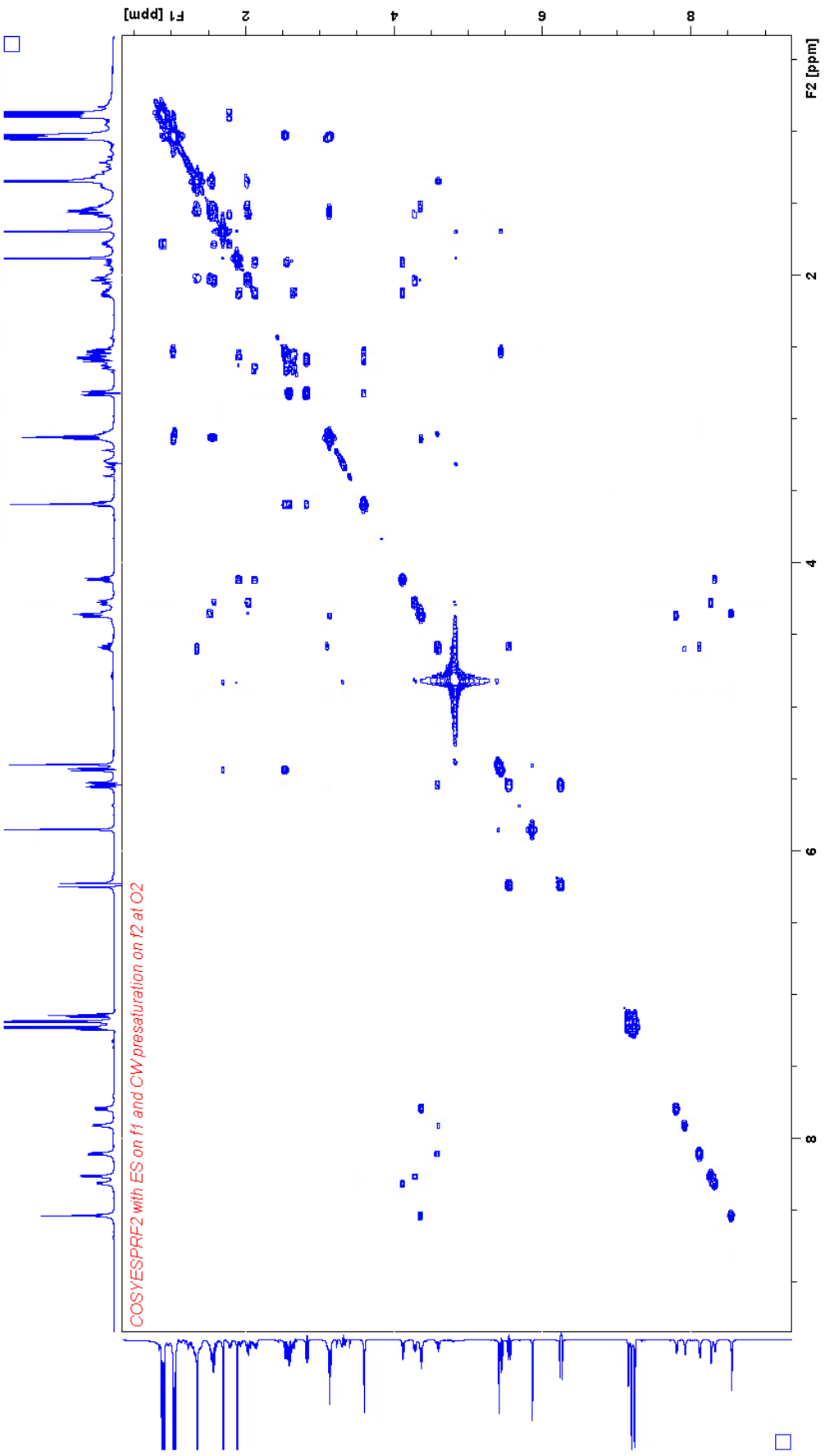

Figure 98: A COSY spectrum, experiment 110, with ES- and PR-suppression on their respective frequencies.

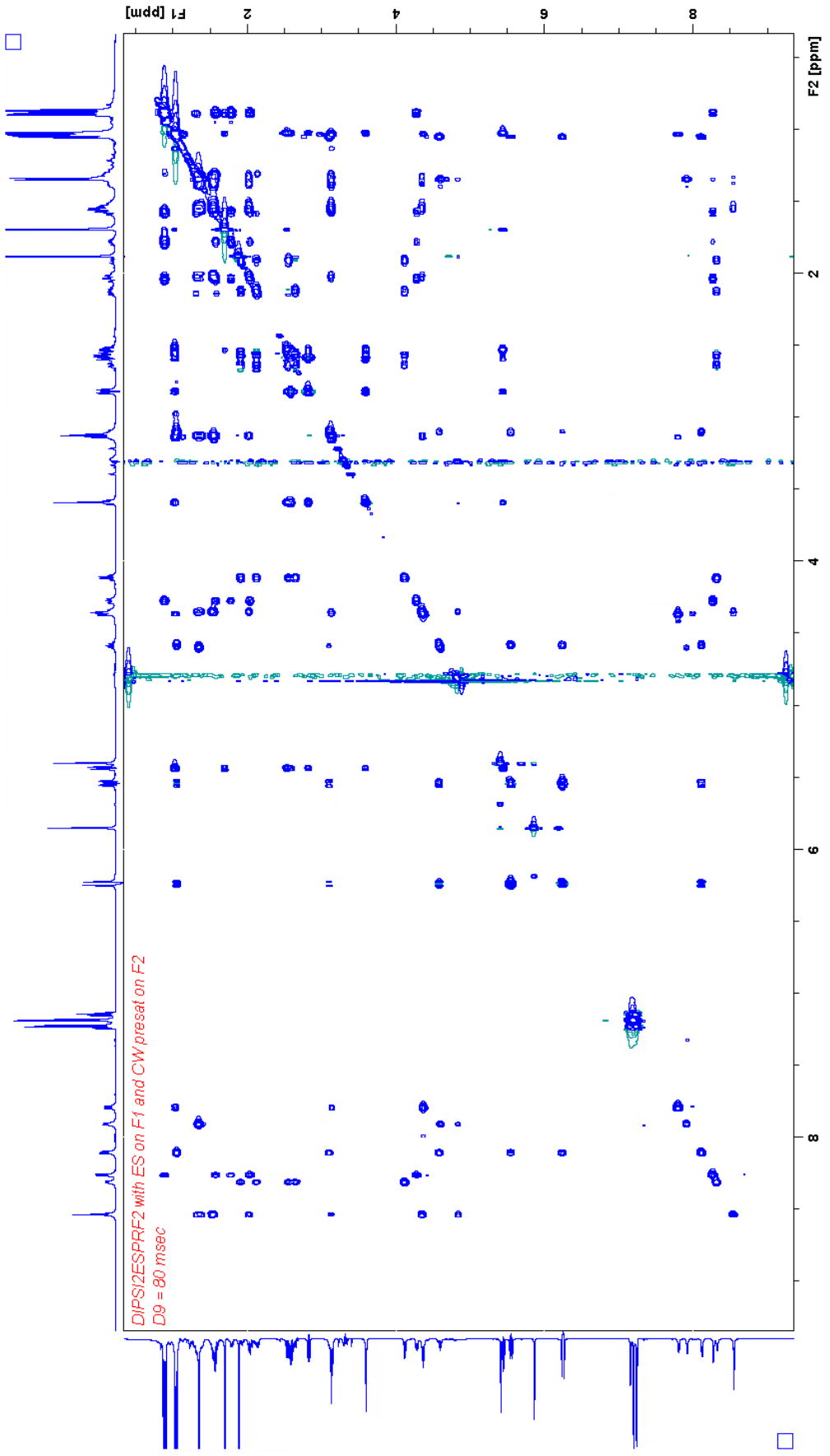

Figure 99: DIPSI-2, experiment 120, with PR-suppression on both frequencies and a mixing time of 80 µs.

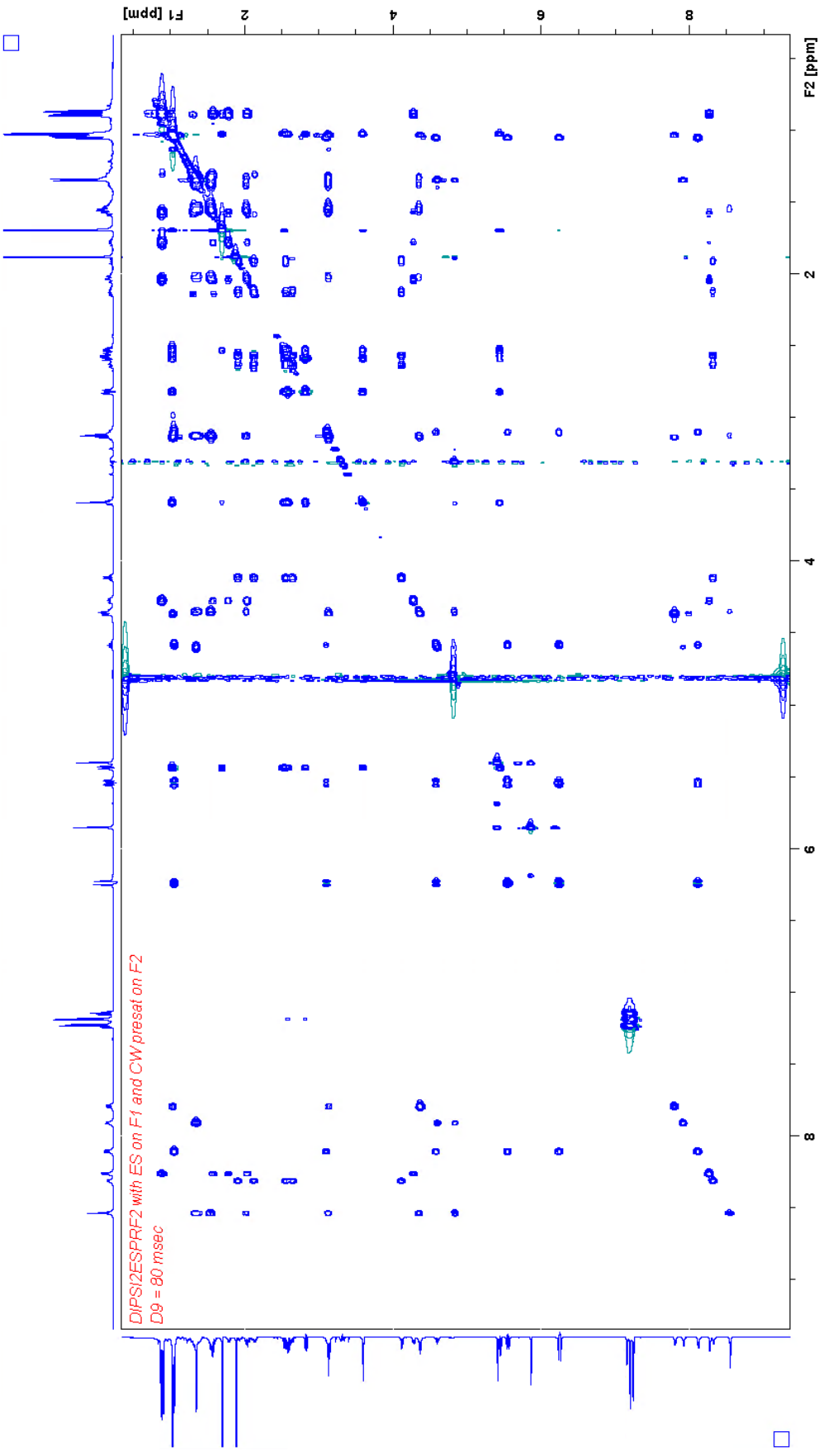

Figure 100: DIPSI-2, experiment 121, with PR-suppression on both frequencies and a mixing time of 160 µs.

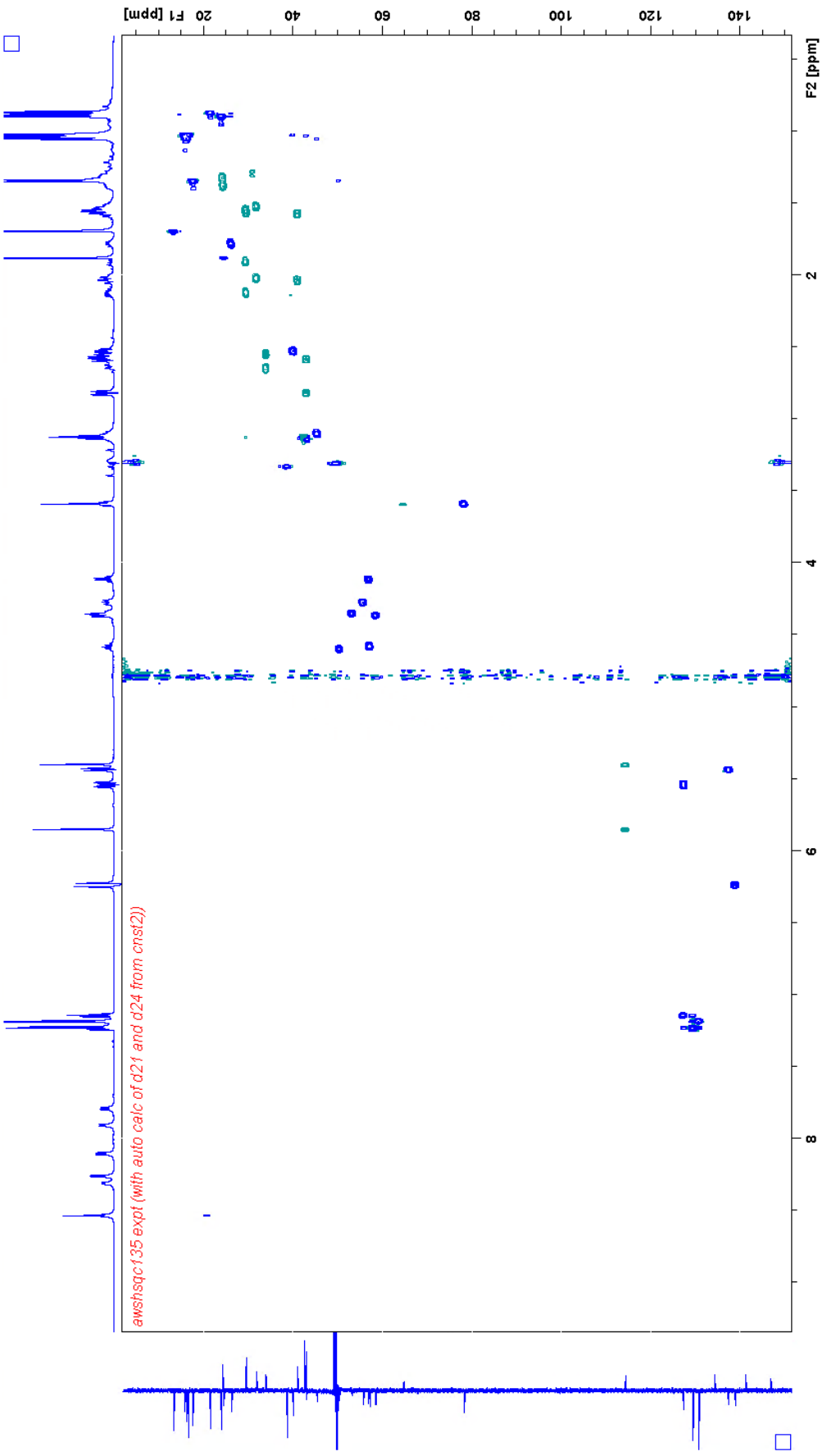

Figure 101: HSQC experiment, 140, with PR on 3890 Hz.

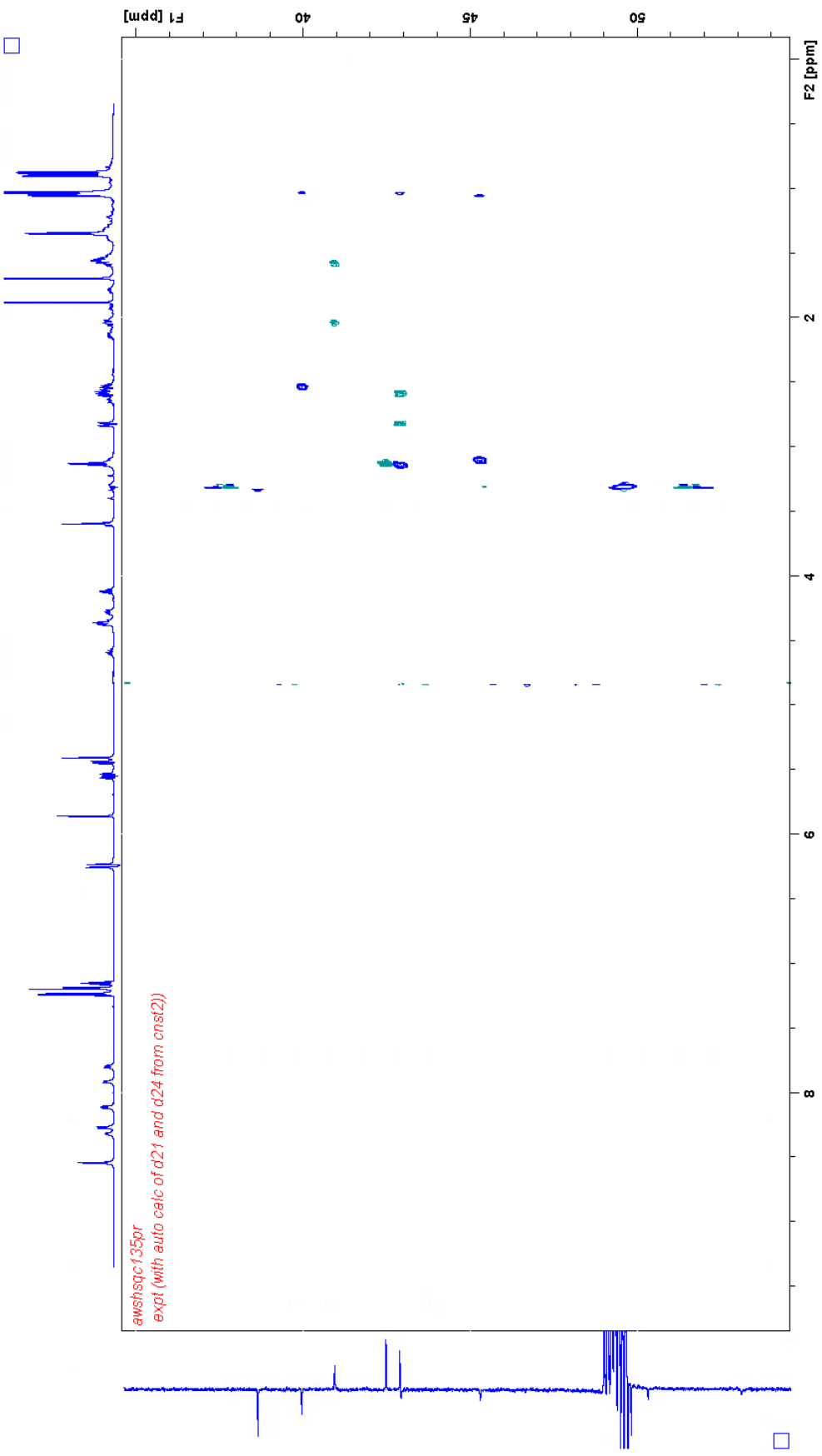

Figure 102: SHSQC experiment, 141, centered at 43.000 ppm.

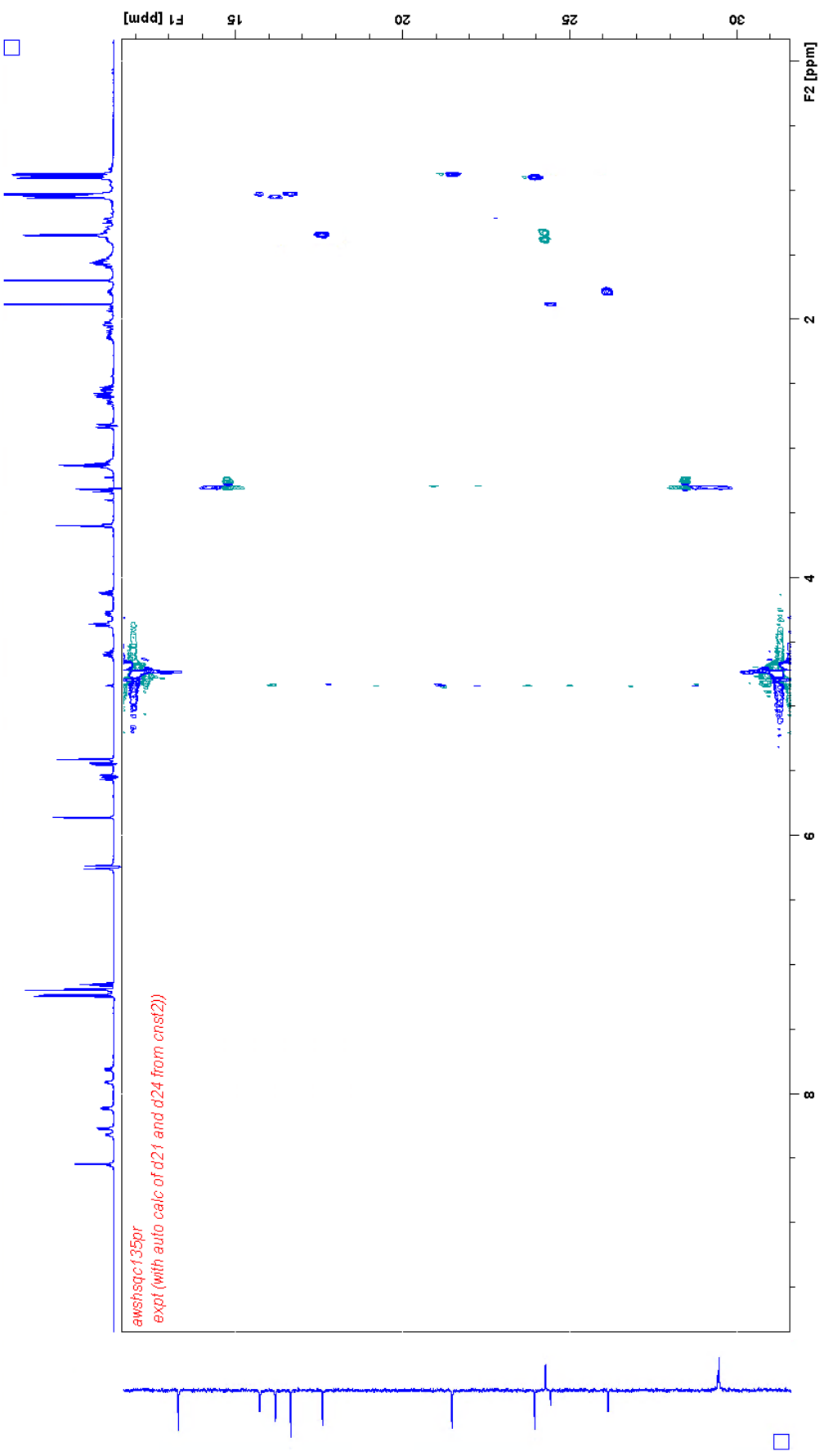

Figure 103: SHSQC experiment, 142, centered at 20.000 ppm.

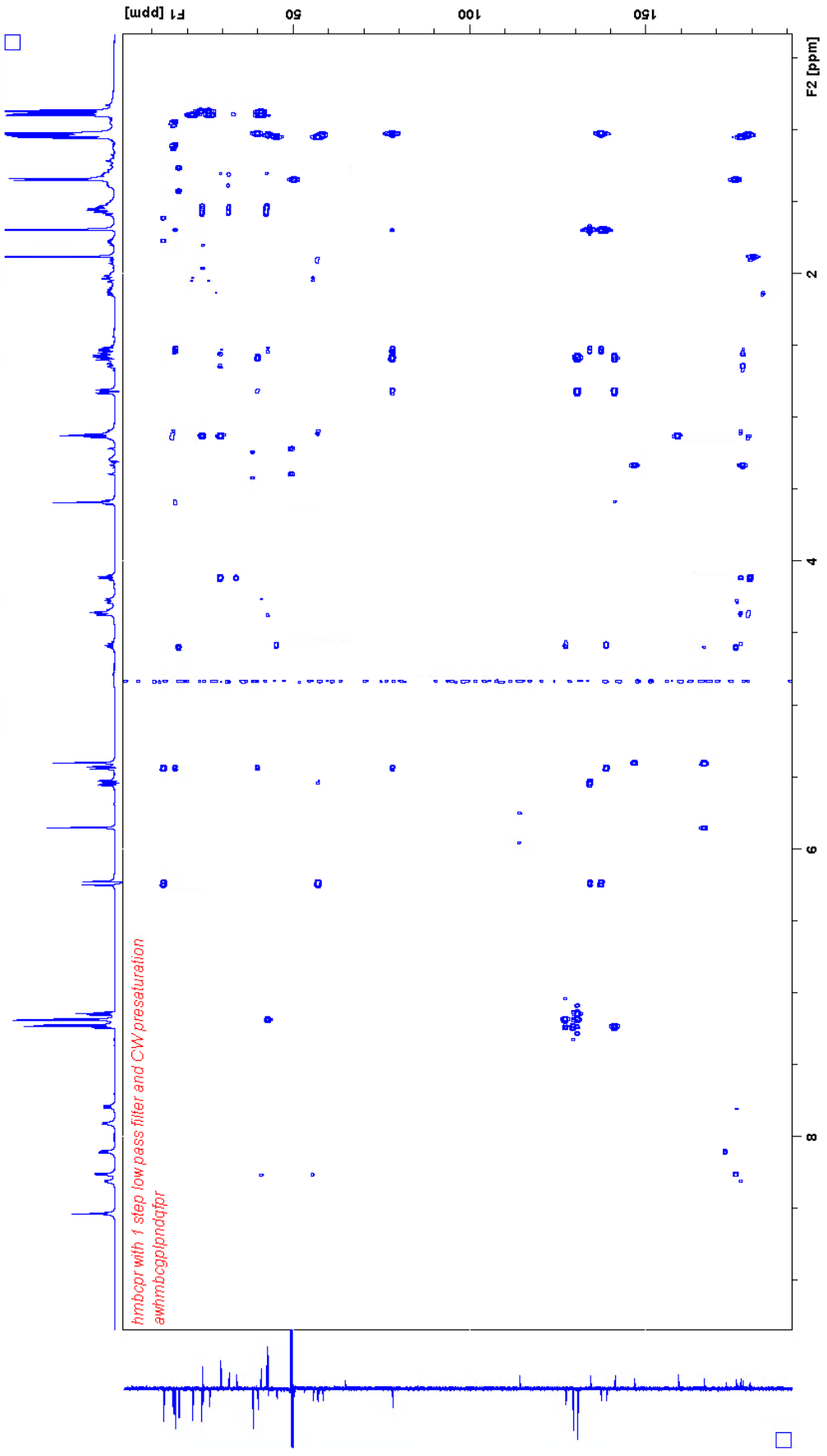

Figure 104: HMBC experiment, 150.

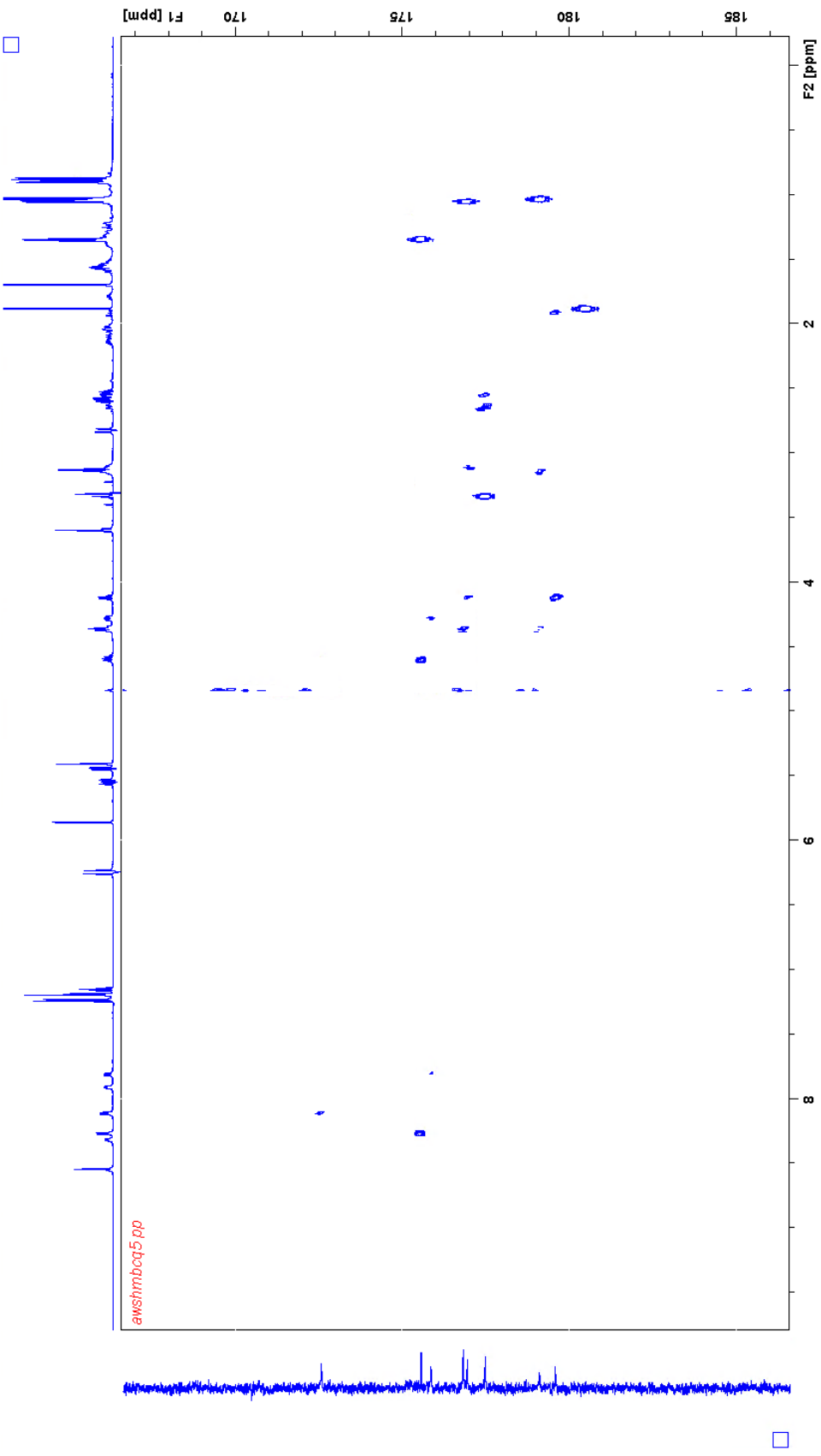

Figure 105: SHMBC experiment, 151 centered at 175.000 ppm.

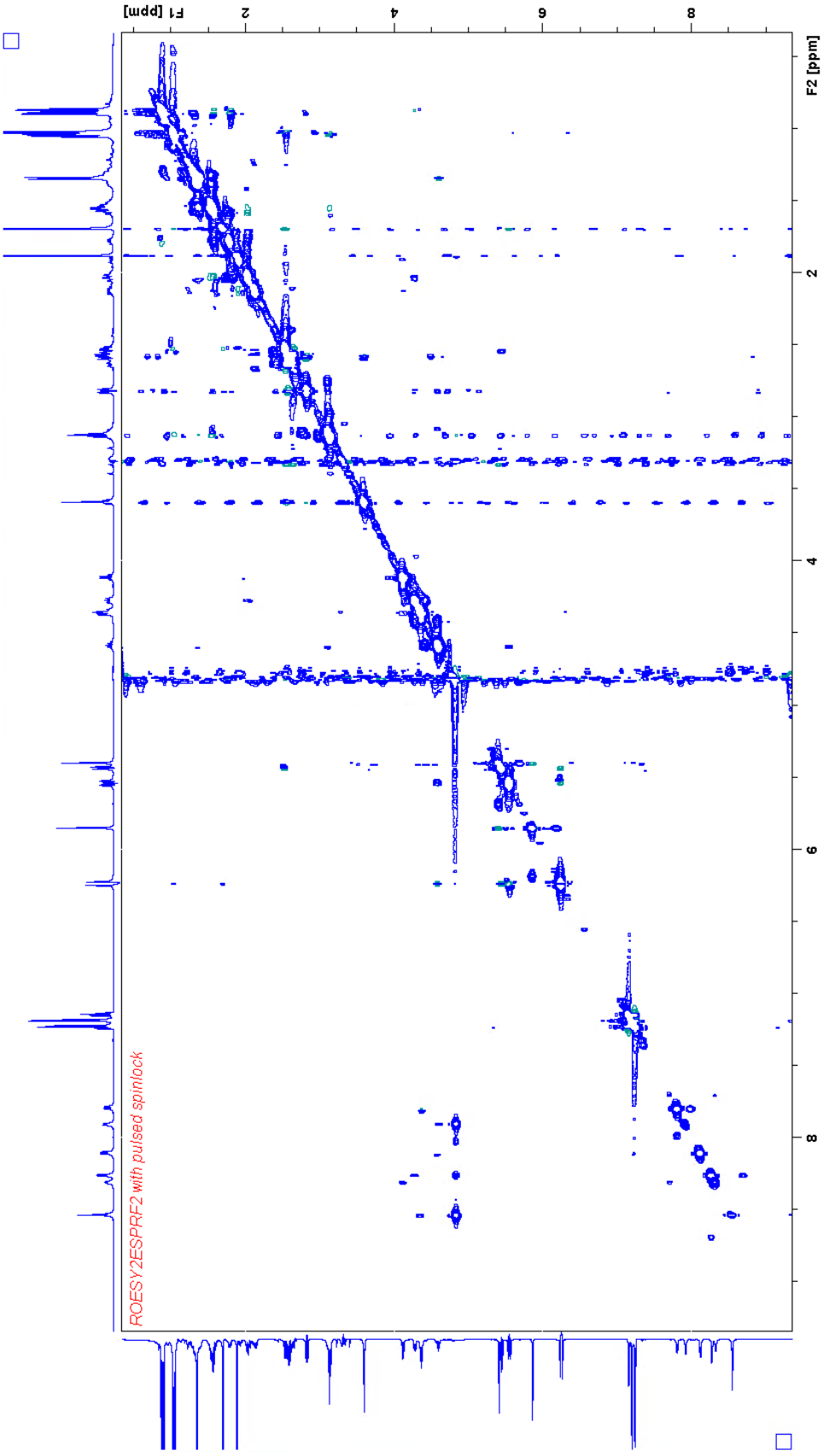

Figure 106: ROESY experiment 130.

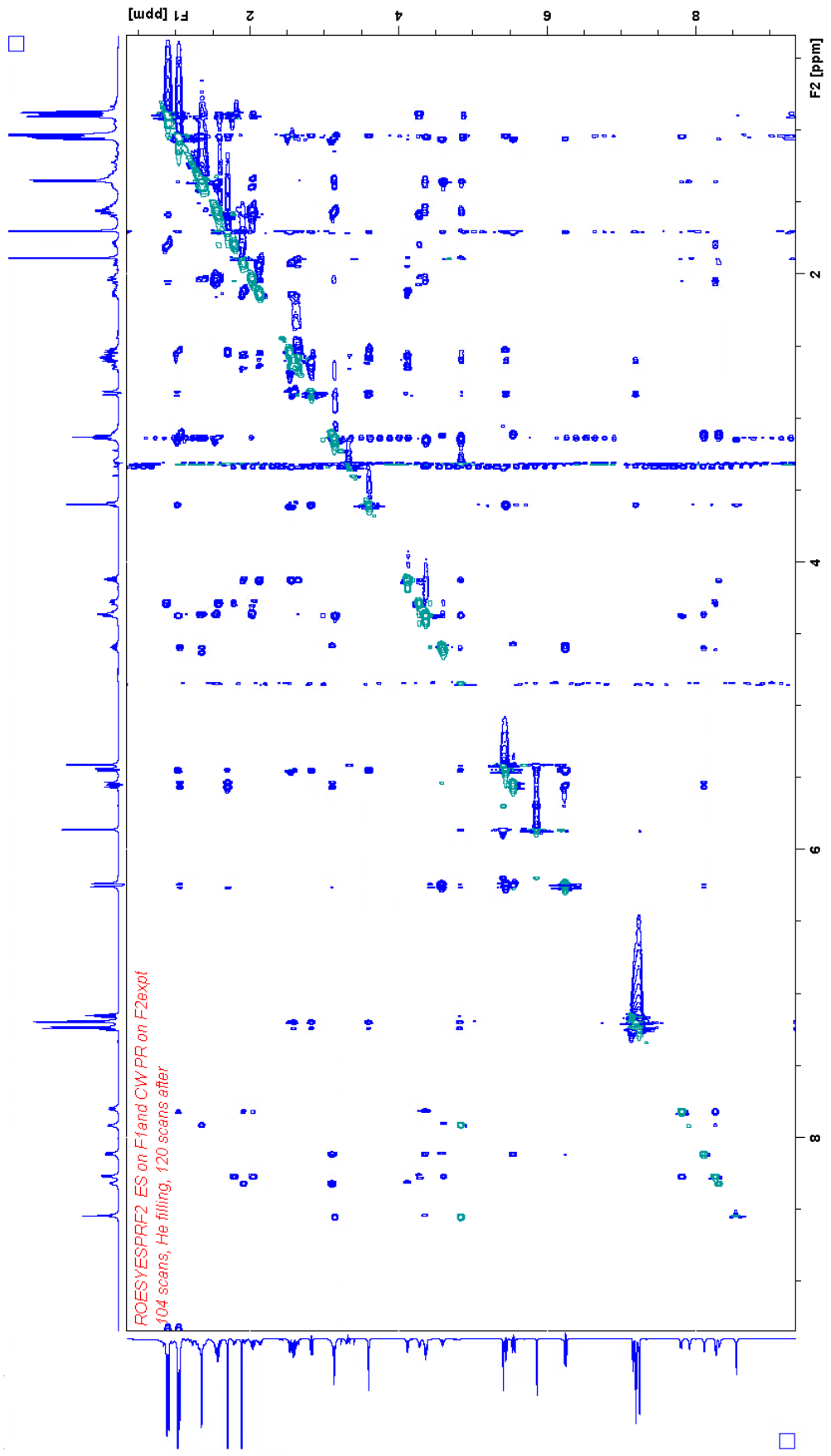

Figure 107: ROESY experiment 134.

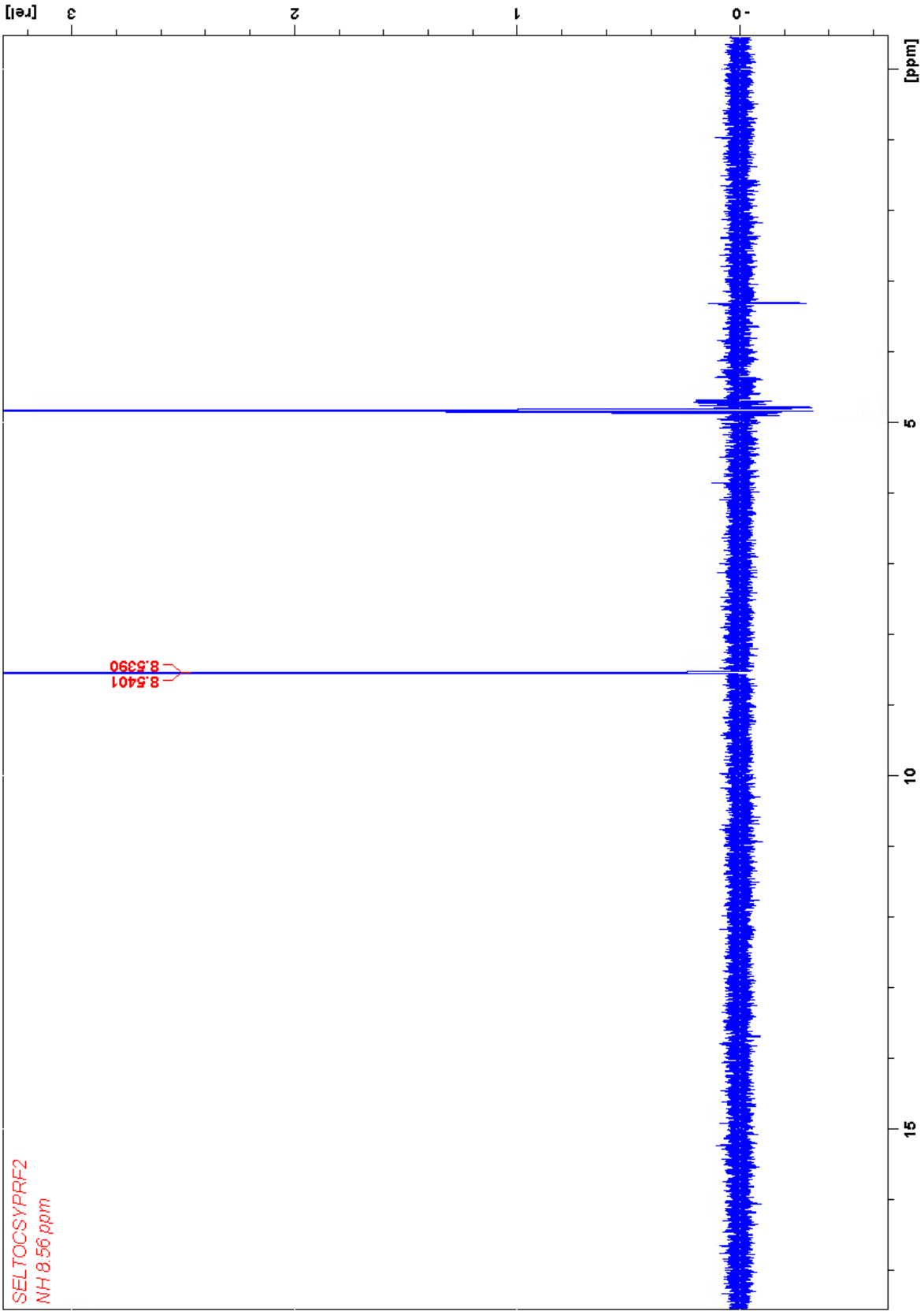

Figure 108: SelTOCSY experiment 222 with irradiation at the resonance at 8.54 ppm.

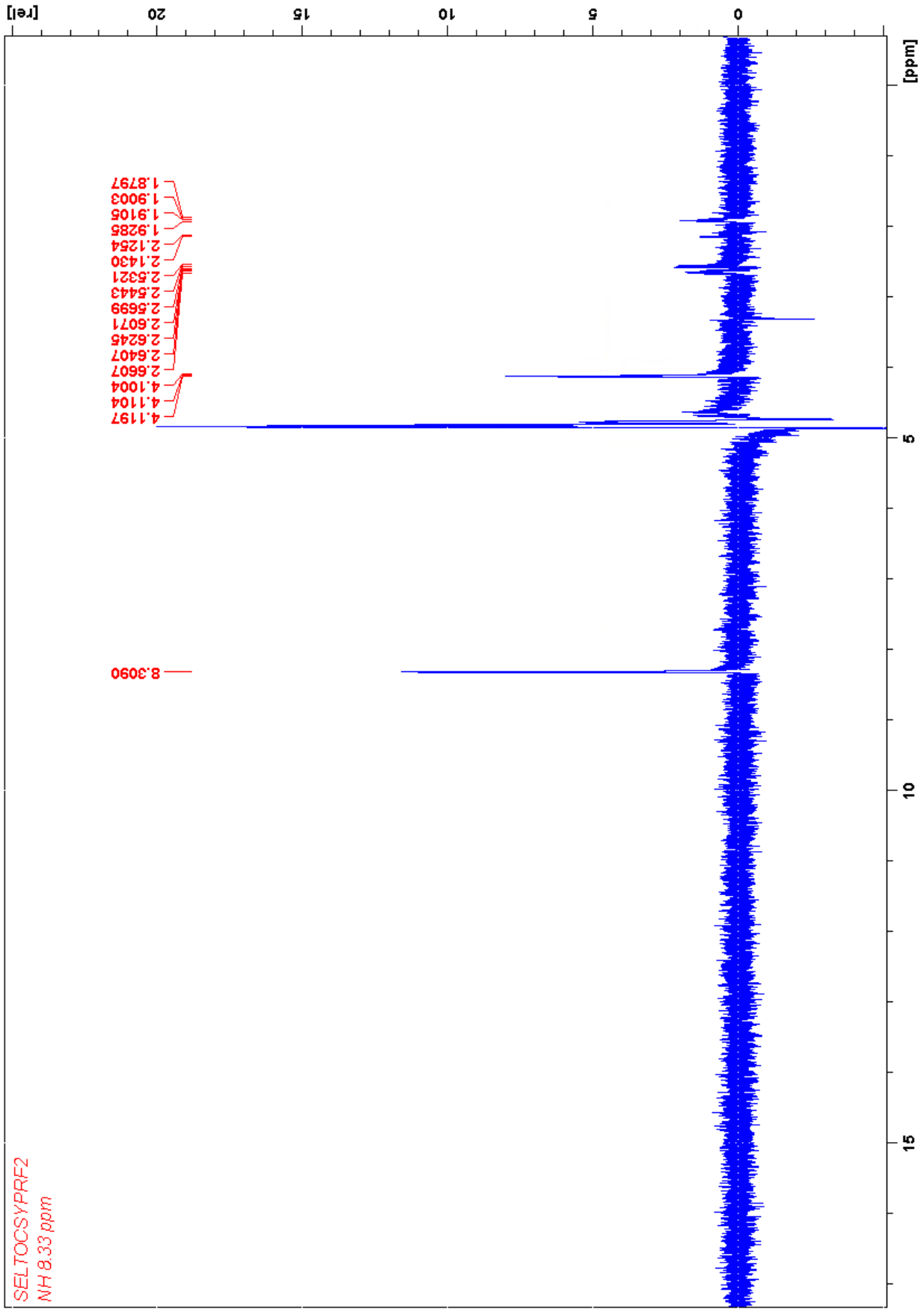

Figure 109: SelTOCSY experiment 221 with irradiation at the resonance at 8.31 ppm.

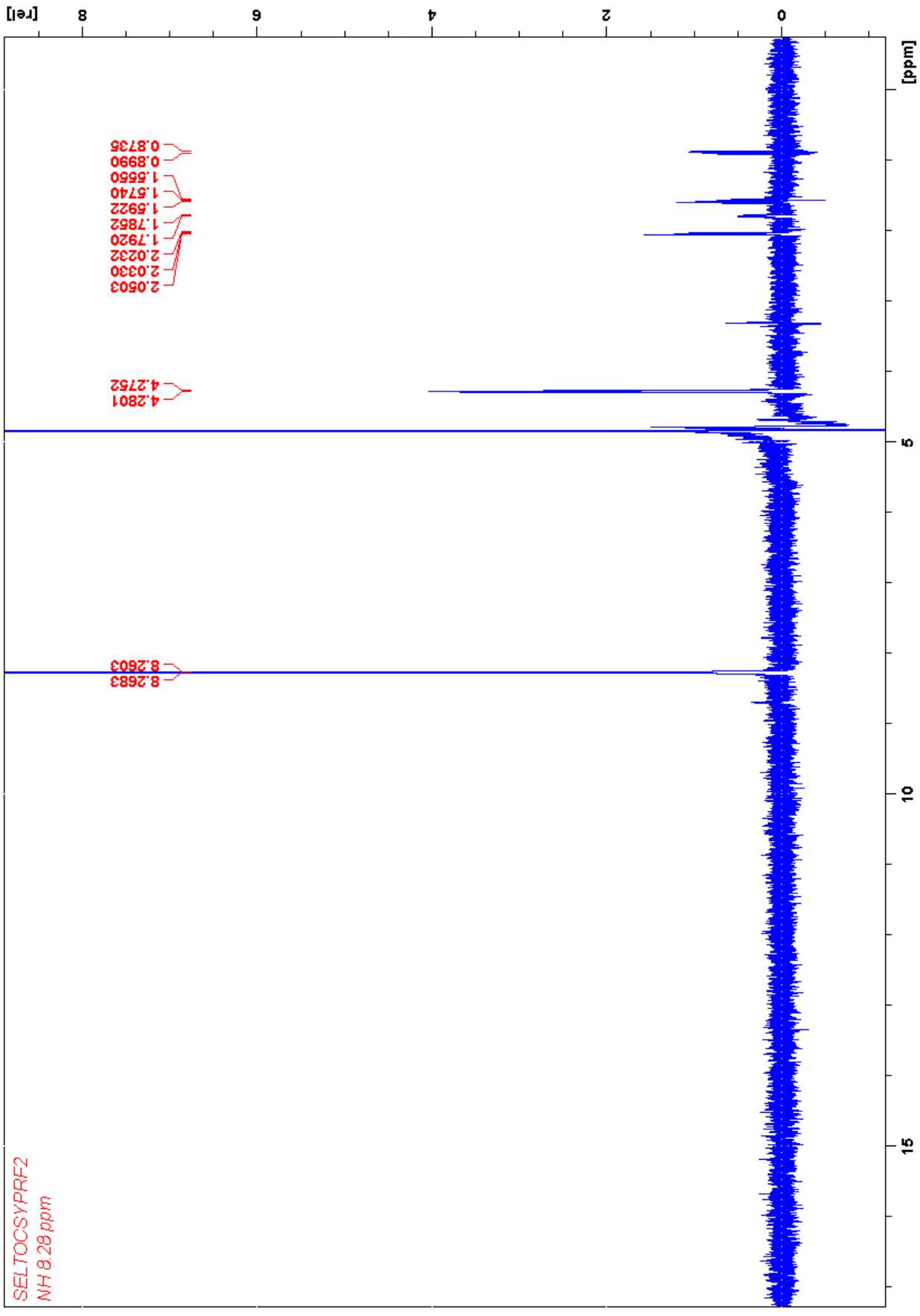

Figure 110: SelTOCSY experiment 223 with irradiation at the resonance at 8.31.

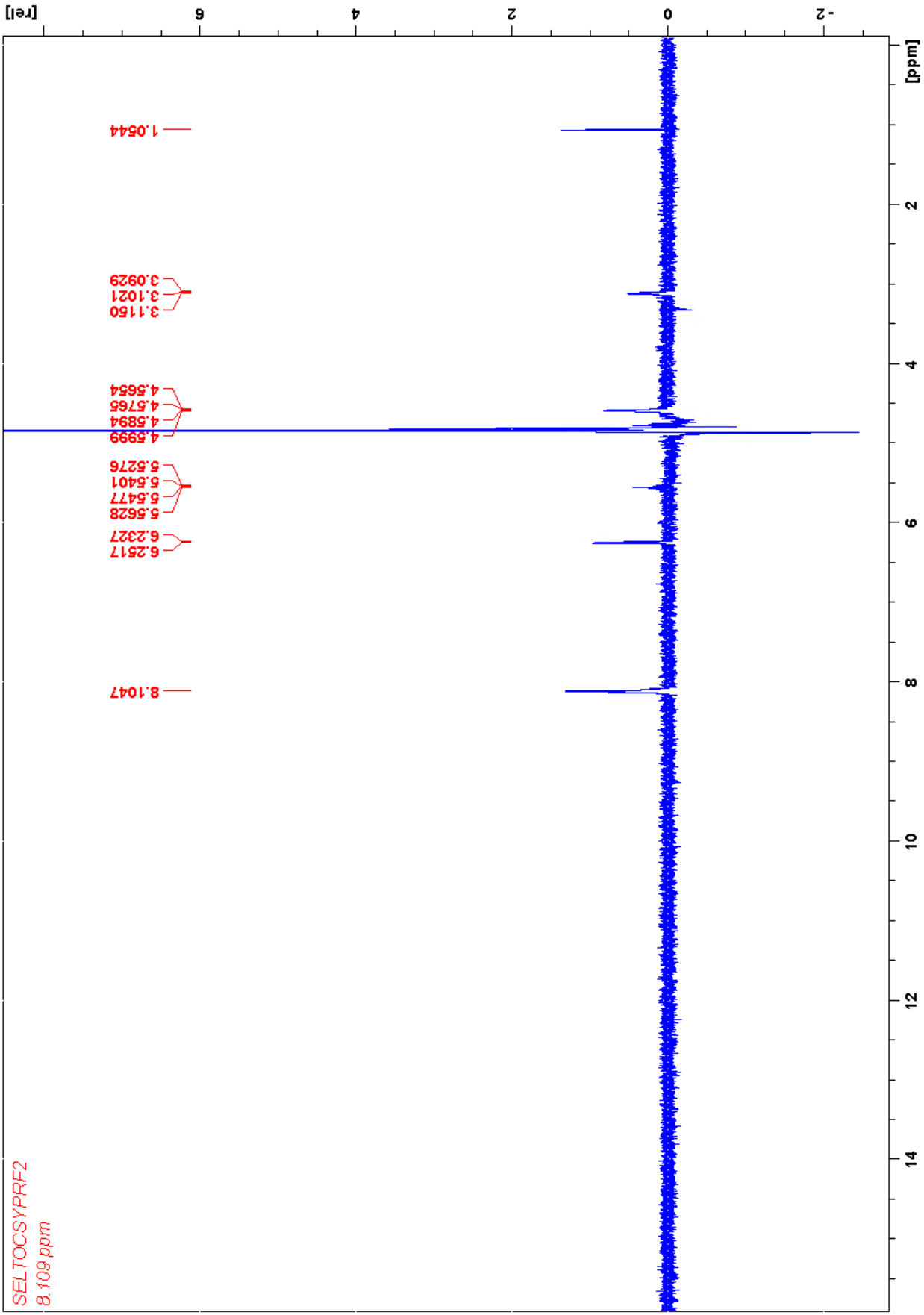

Figure 111: SelTOCSY experiment 173 with irradiation at the resonance at 8.11 ppm.

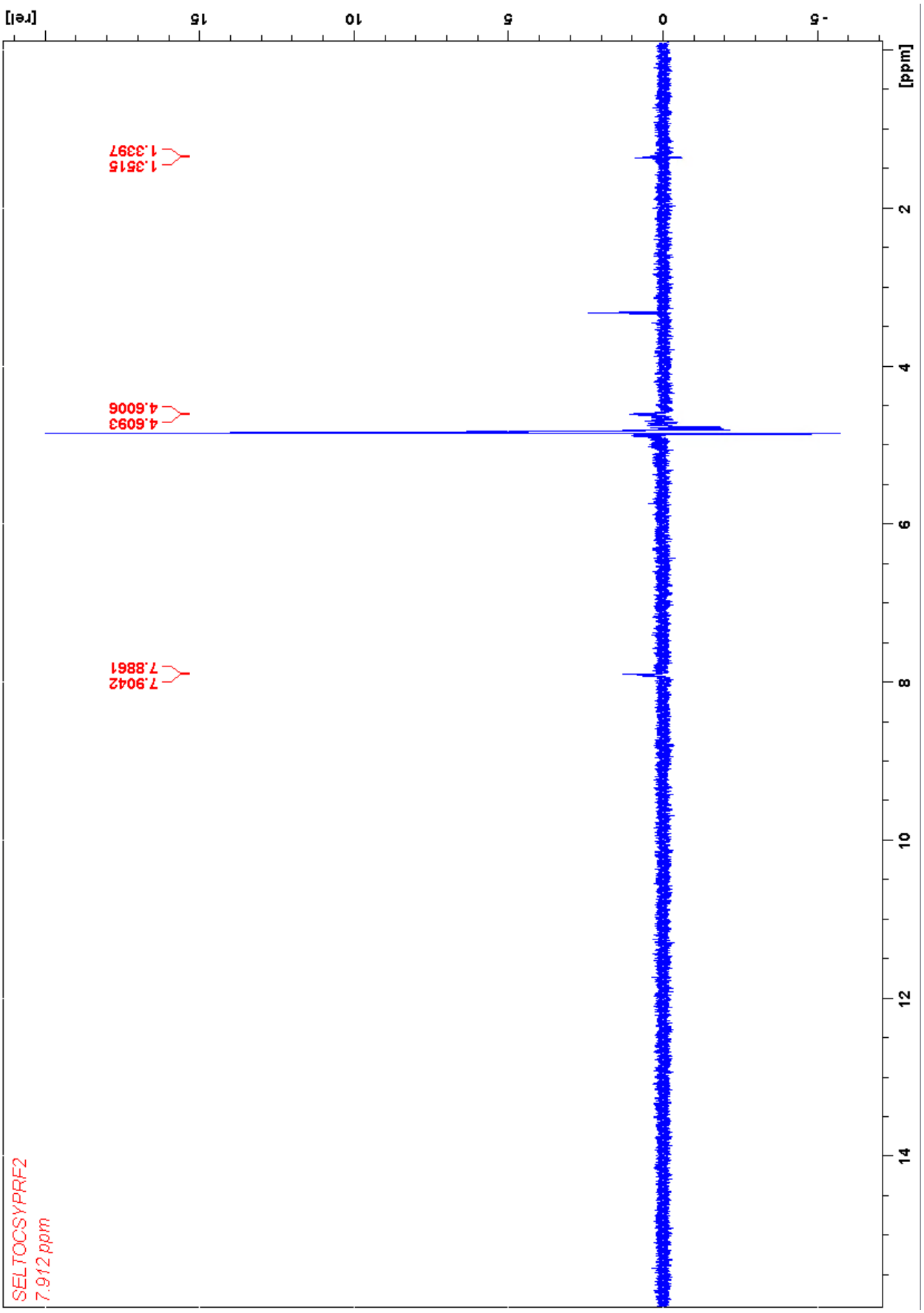

Figure 112: SelTOCSY experiment 174 with irradiation at the resonance at 7.91 ppm.

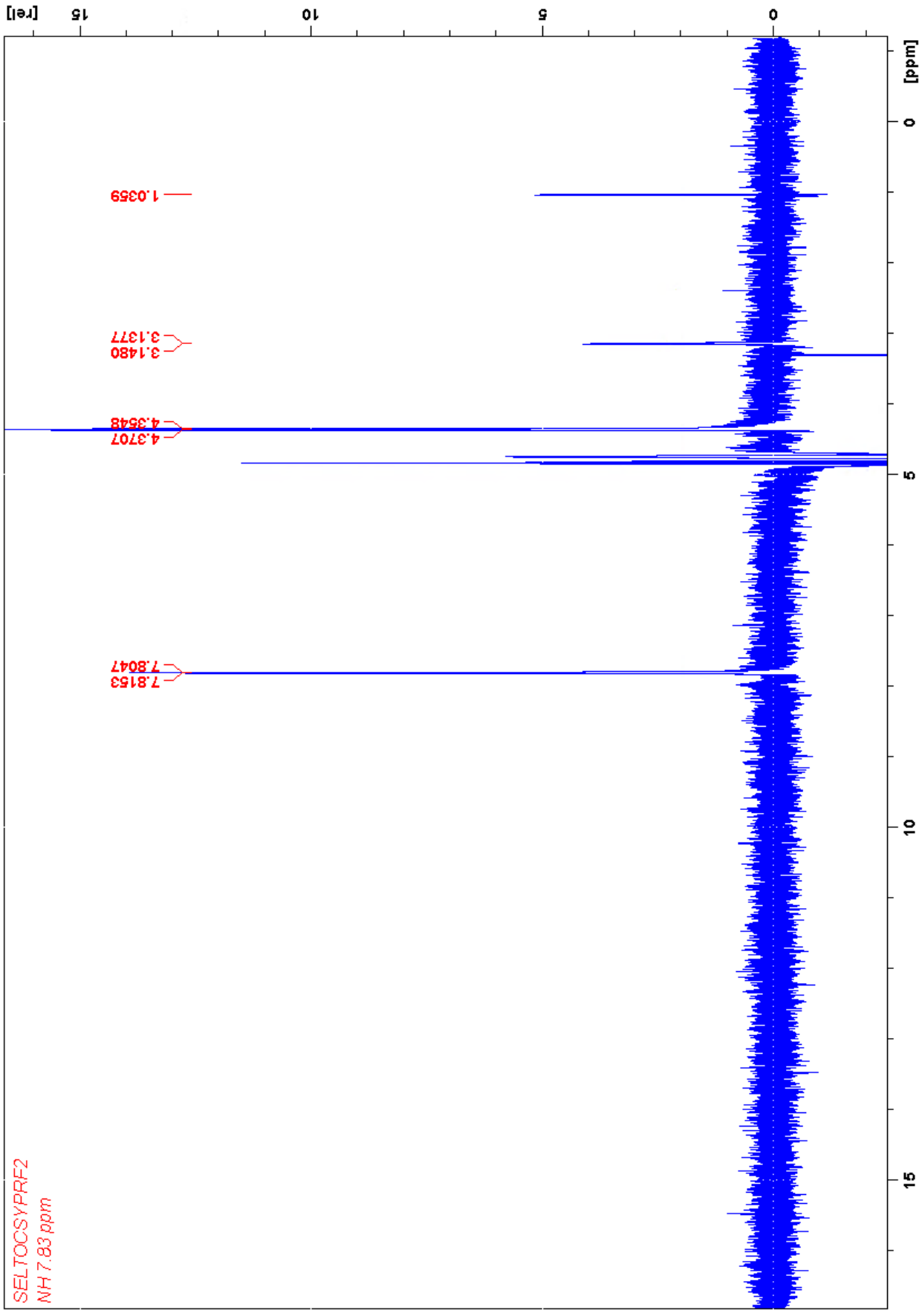

Figure 113: SelTOCSY experiment 226 with irradiation at the resonance at 7.80 ppm.

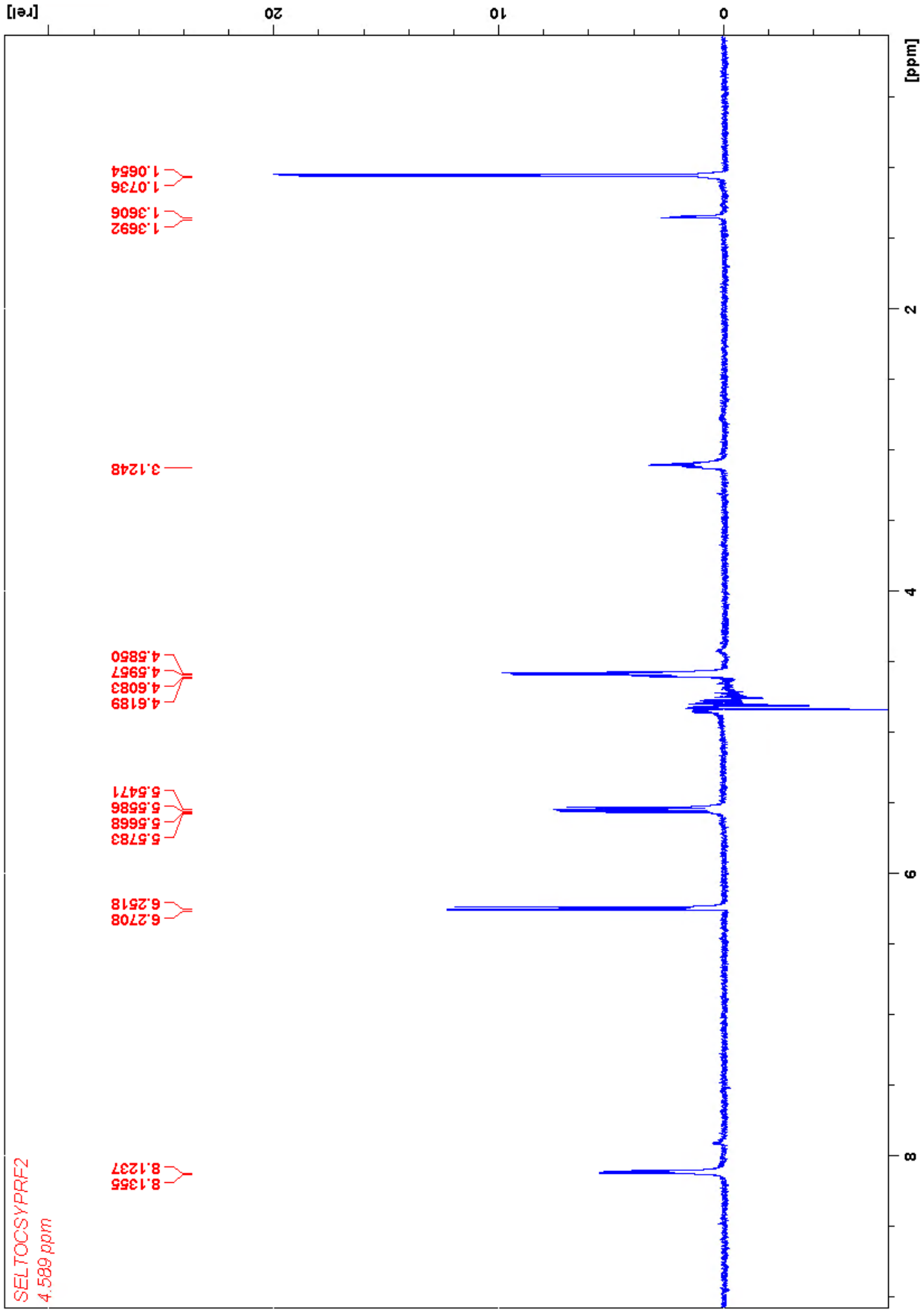

Figure 114: SelTOCSY experiment 180 with irradiation at the resonance at 4.60 ppm.

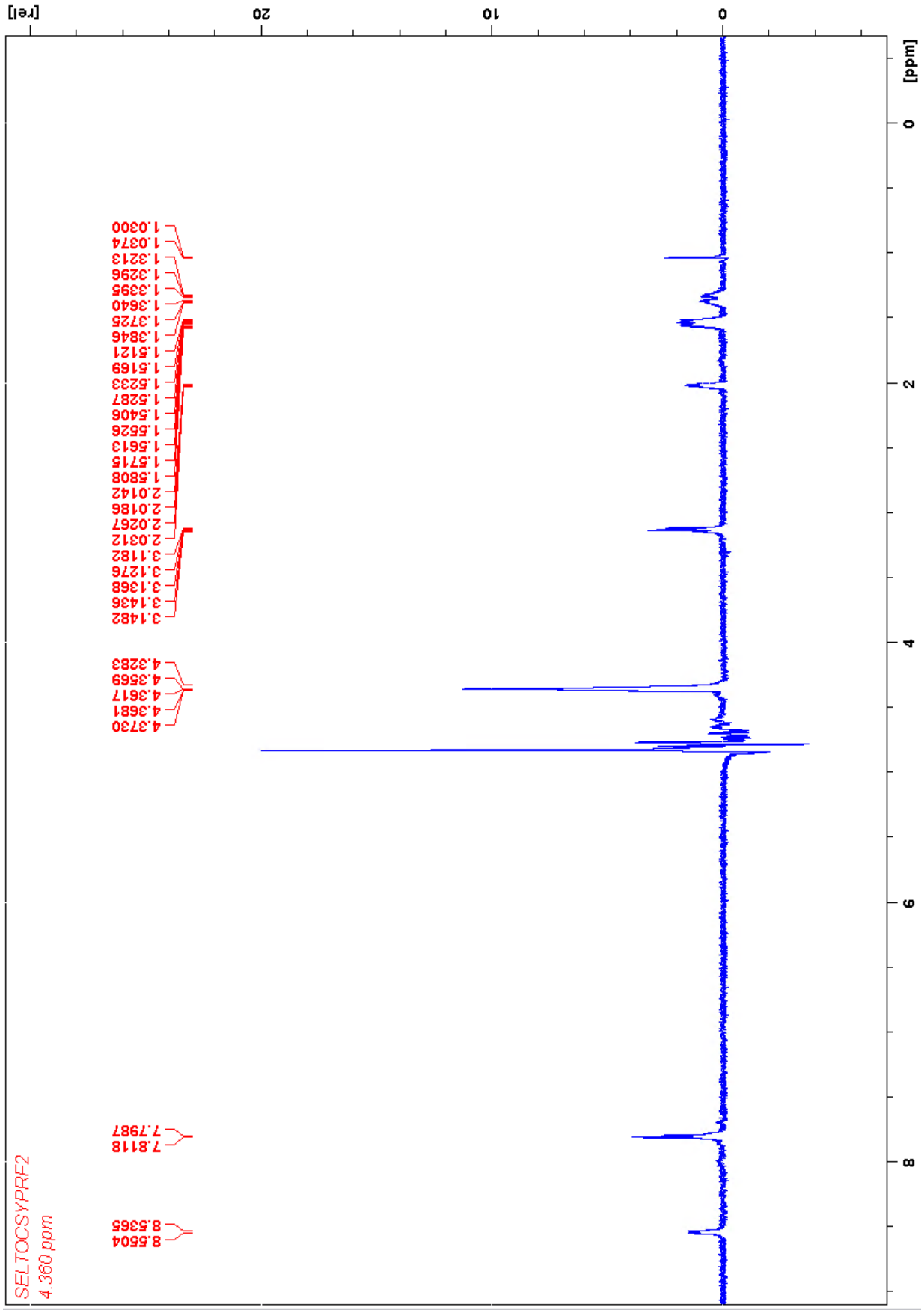

Figure 115: SelTOCSY experiment 181 with irradiation at the resonance at 4.38 ppm.

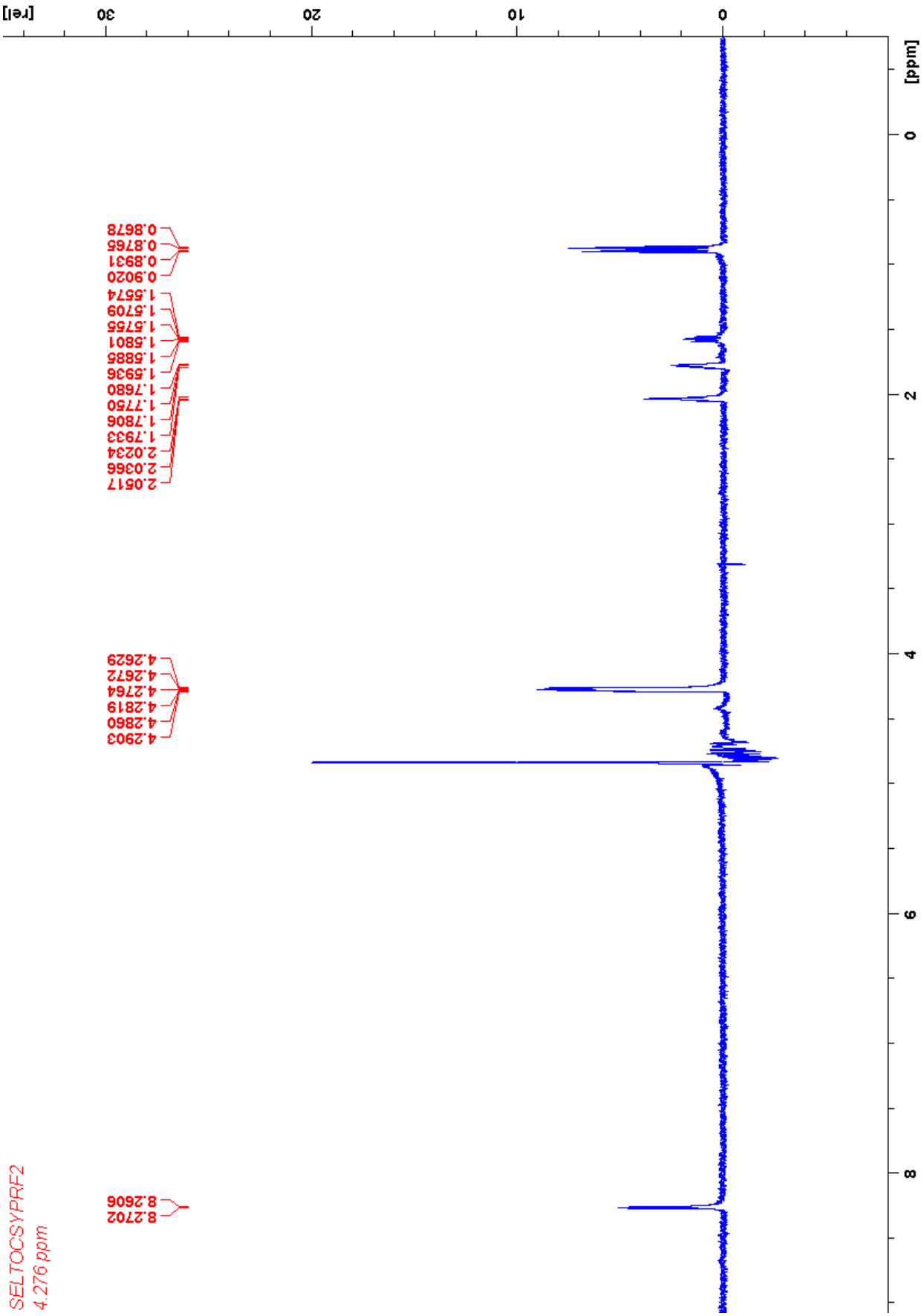

Figure 116: SelTOCSY experiment 182 with irradiation at the resonance at 8.27 ppm.

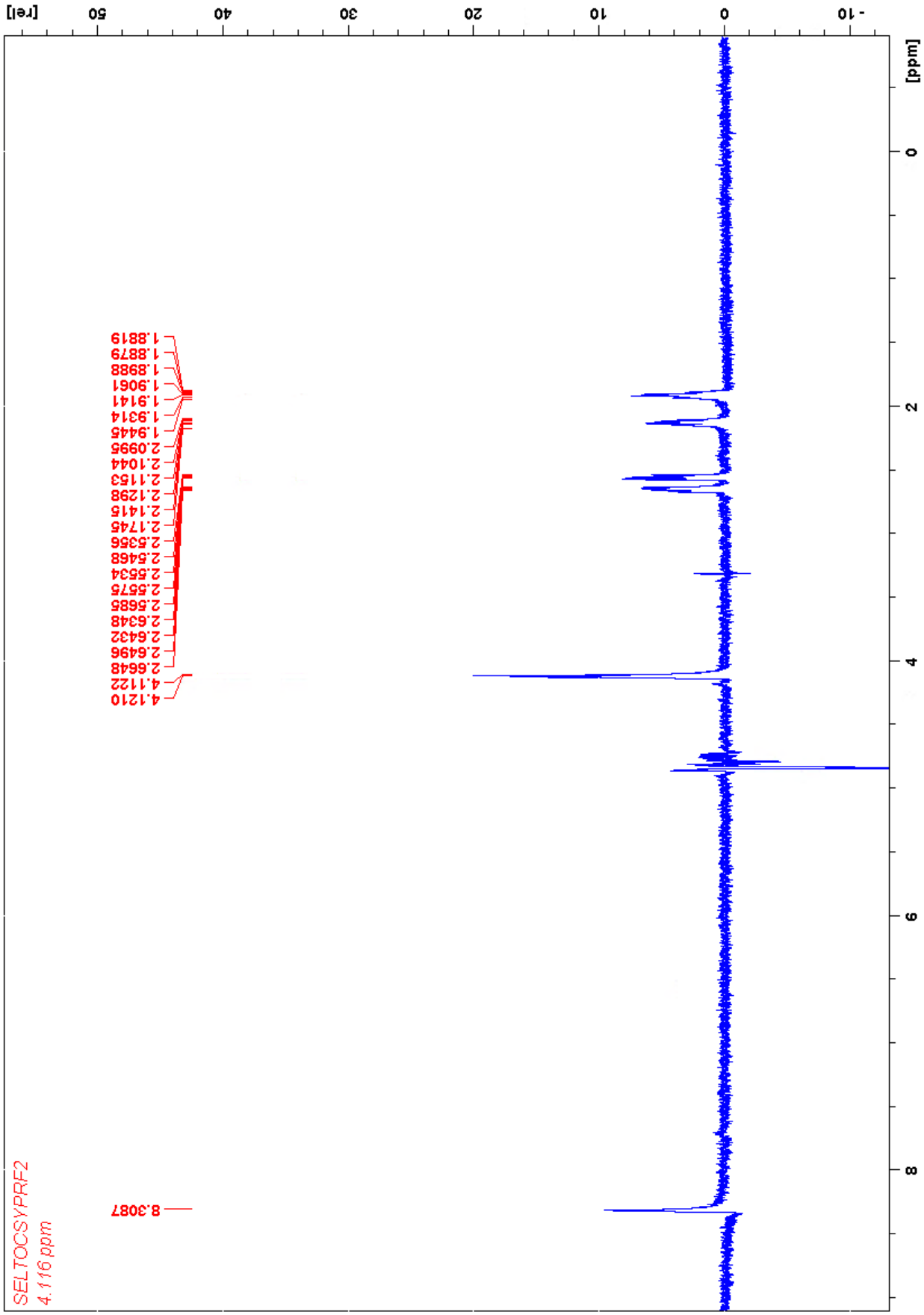

Figure 117: SelTOCSY experiment 183 with irradiation at the resonance at 4.11 ppm.

4.2.2 Elucidation of atom sequence

In the same manner as with molecule #1, the elucidation is initiated by superficial inspection of the 1D proton spectrum. Also here there appears to be many overlapping signals downfield. The α-proton region shows four signals and the peptide region shows six signals. By closer inspection of the α-proton region, the fine structure of 4.36 ppm indicates that there are may be overlapping signals at this frequency. HSQC confirms that there are indeed two overlapping signals at 4.36 ppm in addition to also revealing that there are two overlapping signals at 4.59 ppm. In total there are six α-protons and six peptide protons, as with the other MC and is consistent with the literature. The lack of a 7th peptide- and α-proton may be explained by the presence of Mdha.

By comparing COSY from molecule #1 and #2, there appears to be a high degree of overlap which indicates that there is a lot of similarity between the samples. The spectra are overlapped in figure 118.

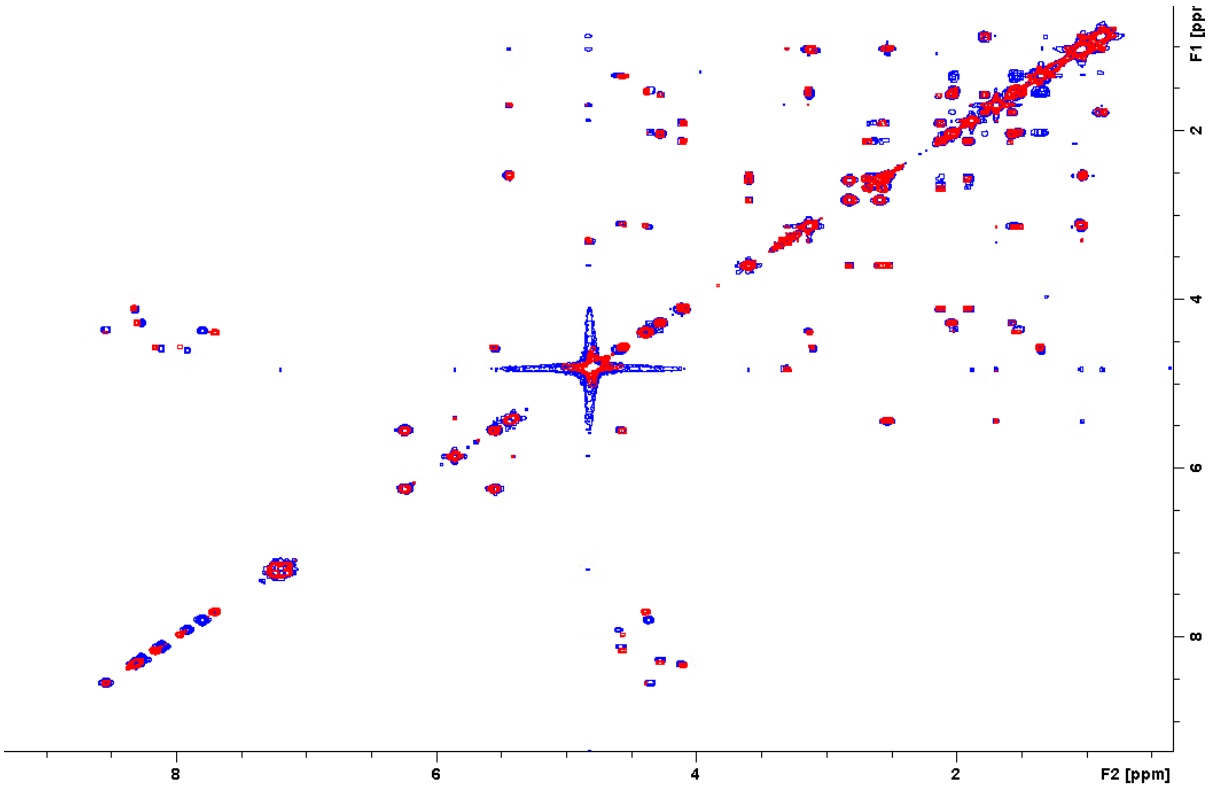

Figure 118: COSY spectra 7010 (red) and 110 (blue) are overlapped.

By comparison of HSQC spectra from both molecules, it becomes apparent that only the correlations from Arginine are different, with sample #2 containing one extra CH_2 in the molecule. Overlapped HSQC spectra are shown in figure 119:

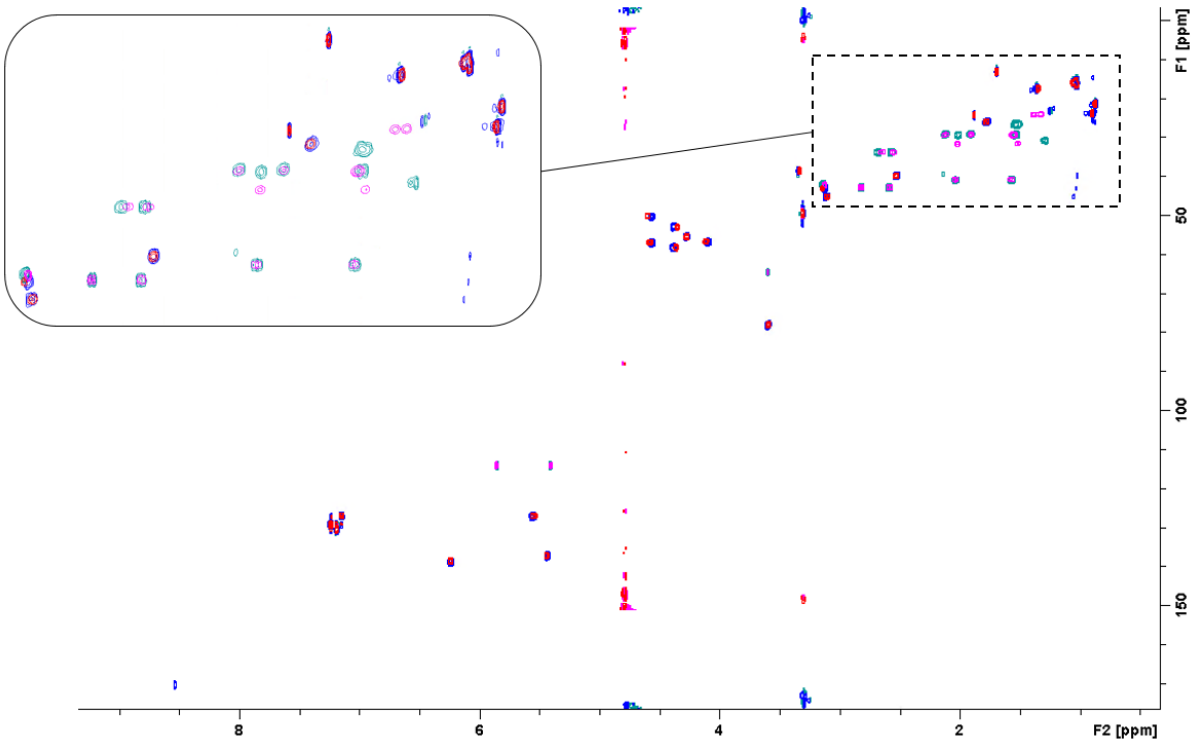

Figure 119: HSQC spectra 7040 (blue/green) and 140 (red/purple) are overlapped.

Due to the high degree of similarity, the description is kept short in this thesis for the positions in the molecule which contain the same amino acid as in molecule #1. The analysis applied to sample #2 is of the same nature as for sample #1.

There are two singlets in the 1D proton spectrum (5.86 and 5.40 ppm). HSQC and HMBC confirms the presence of Mdha. Continuing from the methyl protons on the N-end of Mdha, Mdha is found to be bound to a carbonyl through an HMBC correlation. Further HMBC correlations specify protons which are used to determine the sequence of constituents in COSY. HSQC connects the protons to their respective carbons. Ambiguity at 29.4 ppm was solved by different processing parameters. The result may be seen in figure 120.

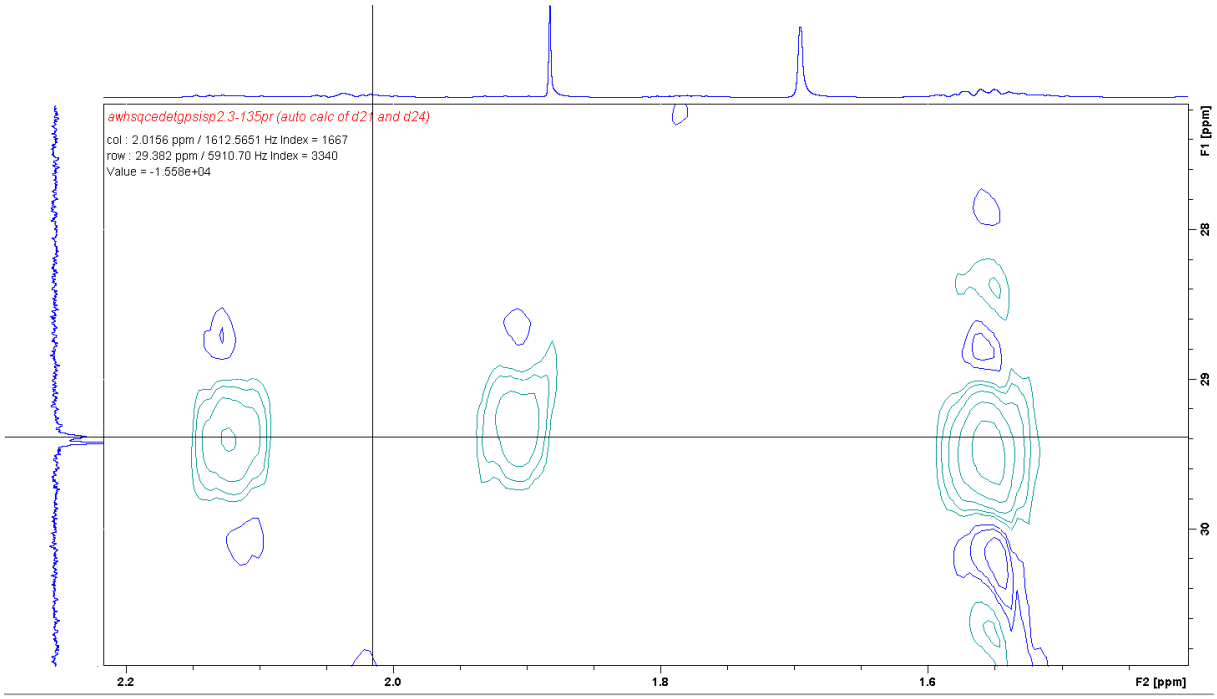

Figure 120: F2-processing: SI = 2048, WDW = QSINE, LB = 1 Hz, SSB = 2, Me_mod = no, NOCOEF = 0, LPBIN = 0. F1-prosessing: SI = 4096, WDW = EM, LB = 2 Hz, Me_mod = LPfc, NOCOEF = 32, LPBIN = 320.

HMBCs from the end of the spin system are found to correlate with two carbonyls, where peptide-proton indicates which is part of a peptide bond and which one isn't. The chemical shifts for protons and carbons are consistent with the literature for Glutamine. Further HMBC from the peptide-carbonyl gives protons which are used to determine the nature of their spin system of the 3rd amino acid. COSY combined with HSQC form the sequence of constituents in the spin system. DIPSI-2 clarifies ambiguity at ~3.13 and ~4.59 ppm. This spin system seems to be part of DMAdda or one of its analogues. HMBC from 6.25 ppm a singlet CH_3 (1.69 ppm H-shift and 13.22 ppm C-shift) and further HMBC correlations from this methyl to methine (5.43 ppm H-shift and 127.27 ppm C-shift) which consists of another spin system of many constituents. All are consistent with the literature for DMAdda.[48] The coupling constants for the trisubstituted diene to be of a *cis*-type conformation and are concluded to be *trans* to each other. Elucidation of COSY combined with HSQC determines the spin system which through HMBC further correlates to a terminal spin system. The 3.59 ppm resonance with a fine structure of ddd, doesn't correlate in COSY or HMBC with any other constituents than those described for the analogue 3.60 ppm shift from molecule #1. Thus the same conclusion is reached, that its carbon is bound to an alcohol which exchanges enough with the solvent to be absent in all spectra obtained and concludes that the amino acid is indeed

DMAdda (excluding the nature of the stereogenic centra). The elucidation thus far has covered Mdha, Glu and DMAdda and are given in figure 95.

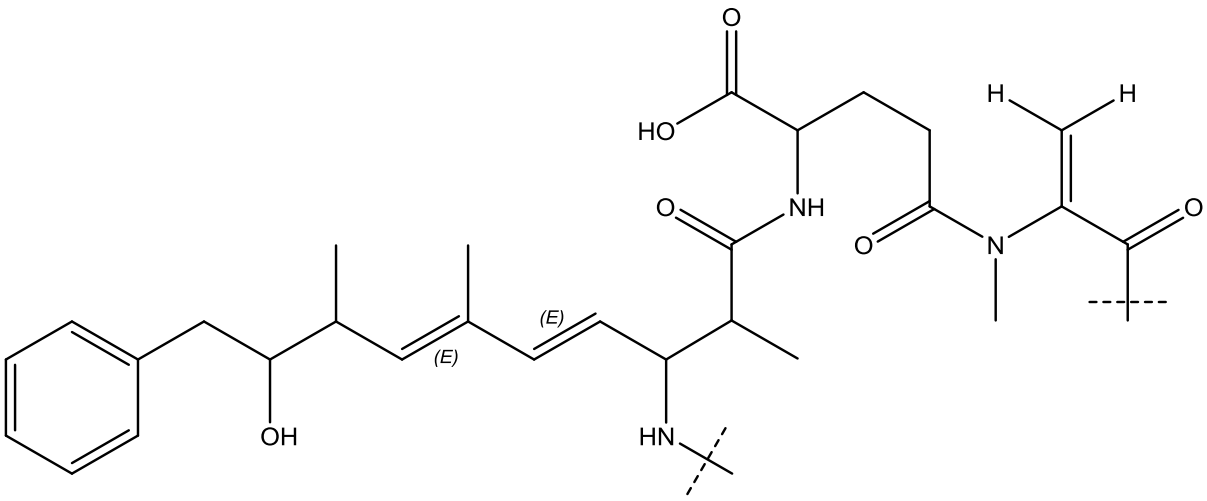

Figure 121: DMAdda-Glu-Mdha (disregarding the stereogenic centra).

DMAdda-NH shows a HMBC correlation to 172.5 ppm, this resonance show no more correlations. Thus the elucidation, just as with sample #1, jumps to the other correlation to at 4.60 ppm (H-shift).

SelTOCSY on 4.60 ppm reveal additional resonances to DMAdda. The resonances are consistent with Ala, as with sample #1. Investigation of the DIPSI-2 spectrum, where 4.60 correlates to 7.91 ppm, shows that the spin system of the 7.91 ppm is consistent with Ala. HMBCs and elucidating in the COSY-spectrum confirms. There is almost complete overlap between the different Ala-species in the overlapped HSQC spectrum. It is concluded that this AA is Ala. Ala-2 shows a HMBC over to Mdha-1. Elucidating further from Ala's C-terminus, a HMBC to 8.27 ppm is found. COSY and DIPSI-2 spectra reveals the spin system and sequence of protons. Investigation of the HSQC spectrum form the constituents and the resonance at 4.28 ppm shows an HMBC to 175.8 ppm. The AA is determined to be Leu. The resonance at 1775.8 ppm further HMBCs to a proton resonance at 7.80 ppm. The DIPSI-2 spectrum reveals the spin system and the COSY spectrum paired with the HSQCs reveal the sequence and constituents of the spin system. Numerous constituents in the spin system show correlations to two carbonyl-type resonances; 176.8 and 179 ppm. This indicates that the AA is Masp. The overlapping resonance at 4.35 ppm correlates in HMBC to 179. The resonance at 4.35 correlates to 8.54 ppm in the COSY spectrum. Investigation of the DIPSI-2 spectrum produces the spin system and investigation of the HSQC spectrum jointly order the

constituents. There are six protonated constituents, one of which is absent in the HSQC spectrum and assumed to be bound to nitrogen. The proton resonance at the end of the spin system, 3.13 ppm, shows a HMBC to 159.0 ppm, which indicates a CN_3-type species like Arg. There are no HMBC correlations between this part of the molecule and 172.5 ppm which is suspected to be a carbonyl-species peptide bonded to DMAdda. A ROESY-correlation between DMAdda-9 and Arg-NH puts them to be in close proximity. The chemical shift of 4.35 ppm suggests that the constituent has something more electron withdrawing than just one peptide bond. The resonance fits perfectly with the carbonyl correlation which is peptide bonded to DMAdda. These factors lead to the conclusion that the spin system of the resonance at 4.35 ppm is Har.

4.2.3 Final structure of amino acids

Ala:

Table 59: A Summary of chemical shifts and correlations consistent with Ala.

Entry	δH	δC	Atom type	COSY	DIPSI-2 (80µs)	DIPSI-2 (160 µs)	HMBC
Ala							
1		175.5	CON				Leu-NH
2	4.60, q	50.3	CH	Ala-3, NH	Ala-3, NH	Ala-3, NH	Ala-3, Mdha-1
3	1.35, d	17.5	CH3	Ala-2	Ala-2, NH	Ala-2, NH	Ala-1, 2
NH	7.91, d		NH		Ala-2, 3	Ala-2, 3	N.D.

Table 60: NOE-data collected but not utilized in the elucidation.

ROESY (internal)	ROESY (external)
Ala	
Ala-3	N.D.
Ala-2, NH	Masp-NH, Leu-NH
Ala-2	Har-3B, 5

Leu:

Table 61: A Summary of chemical shifts and correlations consistent with Leu.

Entry	δH	δC	Atom type	COSY	DIPSI-2 (80µs)	DIPSI-2 (160 µs)	HMBC

Leu							
1		175.8					Leu-2, 3A/3B, Masp-NH
2	4.28	55.6	CH	Leu-3A, 3B, NH	Leu-3A, 3B, 4, 5, 6, NH	Leu-3A, 3B, 4, 5, 6, NH	Leu-1, 3A/3B
3A	2.04			Leu-2, 3B, 4	Leu-2, 3B, 4, 5, 6, NH	Leu-2, 3B, 4, 5, 6, NH	Leu-1, 2, 4, 6
3B	1.57	40.9	CH2	Leu-2, 3A, 4	Leu-2, 3A, 4, 5, 6, NH	Leu-2, 3A, 4, 5, 6, NH	Leu-5
4	1.78	26.1	CH	Leu-3A, 3B, 5, 6	Leu-2, 3A, 3B, 5, 6, NH	Leu-2, 3A, 4, 5, 6, NH	Leu-6
5	0.90	23.9	CH3	Leu- 4	Leu-2, 3A, 3B, 4, 6, NH	Leu-2, 3A, 3B, 4, 6, NH	Leu-3A/3B, 4 ,6
6	0.87	21.4	CH3	Leu- 4	Leu-2, 3A, 3B, 4, 5, NH	Leu-2, 3A, 3B, 4, 5, NH	Leu-3A/3B, 4, 5
NH	8.27, d			Leu-2	Leu-2, 3A, 3B, 4, 5, 6	Leu-2, 3A, 3B, 4, 5, 6	Ala-1

Table 62: NOE-data collected but not utilized in the elucidation.

ROESY (internal)	ROESY (external)
Leu	
Leu-3A, 3B	N.D.
Leu-2, 3B, NH	Masp-2, Har-2, 3A, 5
Leu-2, 3A, 4, 5, 6	
Leu-2, 5, 6, NH	
Leu-3A, 3B, 4	Har-4A
Leu-2, 3A, 3B, 4	Har-4B
Leu-2, 3A, 4	Masp-NH, Ala-2

Masp:

Table 63: A Summary of chemical shifts and correlations consistent with Masp.

Entry	δH	δC	Atom type	COSY	DIPSI-2 (80µs)	DIPSI-2 (160 µs)	HMBC
Masp							
1		176.8					Masp-2
2	4.38	58.4	CH	Masp-3, NH	Masp-2, 3, NH	Masp-2, 3, NH	Masp-1, 3, 4
3	3.14	42.9	CH	Masp-2, 4	Masp-2, 5, NH	Masp-2, 5, NH	Masp-4
4		179.0	CON				Masp-2, 3, 5, Har-2
5	1.03	15.7	CH3	Masp-3	Masp-2, 3, NH	Masp-2, 3, NH	Masp-2, 3, 4
NH	7.80, d			Masp-2	Masp-2, 3, 5	Masp-2, 3, 5	Leu-1

Table 64: NOE-data collected but not utilized in the elucidation.

ROESY (internal)	ROESY (external)
Masp	
Masp-3, 5, NH	
Masp-2	DMAdda-19
Masp-2, 3, NH	DMAdda-8
Masp-2, 5	Leu-NH

Har:

Table 65: A Summary of chemical shifts and correlations consistent with Har.

Entry	δH	δC	Atom type	COSY	DIPSI-2 (80µs)	DIPSI-2 (160 µs)	HMBC
Homoarginine Har							
1		172.5	CON				DMAdda-3
2	4.35, d	53.1	CH	Har-3A, 3B, NH	Har-3A, 3B, 4A, 4B, 5, 6, NH	Har-3A, 3B, 4A, 4B, 5, 6, NH	Masp-2
3A	2.02	31.7	CH2	Har-2, 3B, 4A, 4B	Har-2, 3B, 4A, 4B, 5, 6, NH	Har-2, 3B, 4A, 4B, 5, 6, NH	N.D.
3B	1.52			Har-2, 3A, 4A, 4B	Har-2, 3A, 4A, 4B, 5, 6, NH	Har-2, 3A, 4A, 4B, 5, 6, NH	Har-4A/4B, 6
4A	1.32	24.2	CH2	Har- 3A, 3B, 4B, 5	Har-2, 3A, 3B, 4B, 5, 6, NH	Har-2, 3A, 3B, 4B, 5, 6, NH	Har-3A/3B, 5, 6
4B	1.37			Har- 3A, 3B, 4A, 5	Har-2, 3A, 3B, 4B, 5, 6, NH	Har-2, 3A, 3B, 4A, 5, 6, NH	Har-3A/3B
5	1.54	29.38	CH2	Har-4A, 4B, 6	Har-2, 3A, 3B, 4A, 4B, 6, NH	Har-2, 3A, 3B, 4A, 4B, 6, NH	Har-3A/3B, 4A/4B, 6
6	3.13	42.4	CH2	Har-5	Har-2, 3A, 3B, 4A, 4B, 5, NH	Har-2, 3A, 3B, 4A, 4B, 5, NH	Har- 4A/4B, 5, 7
7		159.0	CN3				Har-6
NH	8.54, d			Har-2	Har-2, 3A, 3B, 4A, 4B, 5, 6	Har-2, 3A, 3B, 4A, 4B, 5, 6	N.D.

Table 66: NOE-data collected but mostly not utilized in the elucidation.

ROESY (internal)	ROESY (external)
Homoarginine Har	
Har-3A, 3B, 4A, 5	
Har-2, 3B, 4A, 4B, 5	
Har-2	Leu-3A
Har-3A, 3B, 4A, 5, 6	
Har-3A, 3B, 5, 6	
Har-2, 4B, 6	Leu-2, 3A

Har-3B, 5	Masp-5
Har-2, 6	DMAdda-9

DMAdda:

Table 67: A Summary of chemical shifts and correlations consistent with DMAdda.

Entry	δH	δC	Atom type	COSY	DIPSI-2 (80µs)	DIPSI-2 (160 µs)	HMBC
DMAdda							
13/15	7.24, t	129.4	Ar	Adda-12/16, 14	DMAdda-12/16, 14	DMAdda-12/16, 14	DMAdda-11, 12/16, 13/15, 14
12/16	7.19, d	130.6	Ar	Adda-13/15, 14	DMAdda- 13/15, 14	DMAdda- 13/15, 14	DMAdda-10A/10B, 12/16, 14
14	7.15, t	127.2	Ar	Adda-12/16, 13/15	DMAdda-12/16, 13/15	DMAdda-12/16, 13/15	DMAdda-12/16, 13/15
11		141.1	Ar				DMAdda-10A, 10B, 14
10A	2.82, dd	42.9	CH	Adda-9, 10B	DMAdda-7, 8, 9, 10B, 19	DMAdda-7, 8, 9, 10B, 19	DMAdda-8, 9, 11, 12/16
10B	2.59, dd		CH	Adda-9, 10A	DMAdda-7, 8, 9, 10A, 19	DMAdda-7, 8, 9, 10A, 19	DMAdda-8, 9, 11, 12/16
9	3.60, ddd	78.2	CH	Adda-10A, 10B, 8	DMAdda-7, 8, 10A, 10B, 19	DMAdda-7, 8, 10A, 10B, 19	DMAdda-11, 19
8	2.53, ddd	39.9	CH	Adda-7, 9, 19	DMAdda-7, 9, 10A, 10B, 18, 19	DMAdda-7, 9, 10A, 10B, 18, 19	DMAdda-6, 7, 9, 10A/10B, 19
7	5.44, d	137.3	-CH=	Adda-8, 18	DMAdda-8, 9, 10A, 10B, 18, 19	DMAdda-8, 9, 10A, 10B, 18, 19	DMAdda-5, 8, 9, 18, 19
6		134.1	=C<				DMAdda-4, 5, 8, 19
19	1.02, d	16.6	CH3	Adda-8	DMAdda-7, 8, 9, 10A, 10B, 18	DMAdda-7, 8, 9, 10A, 10B, 18	DMAdda-7, 8, 9
18	1.70, d	13.2	CH3	Adda-7	DMAdda-7, 8, 19	DMAdda-7, 8, 9, 19	DMAdda-5, 6, 7, 8, 9, 19
5	6.24, d	138.7	-CH=	Adda-4	DMAdda-2, 3, 4, 17, NH	DMAdda-2, 3, 4, 17, NH	DMAdda-3, 4, 6, 7, 18
4	5.54, dd	127.3	-CH=	Adda-3, 5	DMAdda-2, 3, 5, 17, NH	DMAdda-2, 3, 5, 17, NH	DMAdda-2, 3, 6
3	4.58, dd	57.1	CH	Adda-2, NH	DMAdda-3, 4, 5, 17, NH	DMAdda-3, 4, 5, 17, NH	DMAdda-1, 2, 4, 5
2	3.10, dd	45.3	CH	Adda-3, 17	DMAdda-3, 4, 5, 17, NH	DMAdda-3, 4, 5, 17, NH	DMAdda-1, 3
17	1.05, d	16.1	CH3	Adda-2	DMAdda-2, 3, 4, 5, NH	DMAdda-2, 3, 4, 5, NH	DMAdda-1, 2, 3
1		176.9	-C(O)-N				DMAdda-2, 3, 17, Glu-2, NH

NH	8.11, d		NH	Adda-3	DMAdda-2, 3, 4, 5, 17	DMAdda-2, 3, 4, 5, 17	Har-1

Table 68: NOE-data collected but not utilized in the elucidation.

ROESY (internal)	ROESY (external)
Adda	
DMAdda-9, 10A, 10B	
DMAdda-7, 9, 10B, 12/16, 19	
DMAdda-8, 9, 10B	
DMAdda-7, 10A, 10B, 12/16, 17	Har-NH
DMAdda-7, 9, 17, 18, 19	Glu-3A, 3B, Masp-5
DMAdda-5, 9, 10A, 10B, 18	
DMAdda-2, 7, 9, 10A	Masp-3, Glu-4B
DMAdda-3, 5, 6, 7, 8, 9, 10A, 10B, 19	
DMAdda-3, 4, 7, 18	
DMAdda-2, 5, 18, NH	
DMAdda-2, 4, 5, 17, NH	N.D.
DMAdda-3, 4, 17, NH	Glu-NH
DMAdda-2, 3, 4, 5,	
DMAdda-2, 3, 4	Har-2

Glu:

Table 69: A Summary of chemical shifts and correlations consistent with Glu.

Entry	δH	δC	Atom type	COSY	DIPSI-2 (80µs)	DIPSI-2 (160 µs)	HMBC
Glutamic acid							
1		179.6	-COOH				Glu-2, 3A
2	4.11, q	58.8	CH	Glu-3A, 3B, NH	Glu-3A, 3B, 4A, 4B, NH	Glu-3A, 3B, 4A, 4B, NH	Glu-1, 3A/3B, 4A/4B, DMAdda-1
3A	1.91,	29.42	CH2	Glu-2, 3B, 4A, 4B	Glu-2, 3A, 3B, 4B, NH	Glu-2, 3A, 3B, 4B, NH	Glu-1
3B	2.12,			Glu-2, 3A, 4B, 4A	Glu-2, 3A, 3B, 4A, NH	Glu-2, 3A, 3B, 4A, NH	N.D.
4A	2.65,	33.8	CH2	Glu-3A, 3B, 4B	Glu-2, 3A, 3B, 4B, NH	Glu-2, 3A, 3B, 4B, NH	Glu-3A/3B, 5

4B	2.55,			Glu-3A, 3B, 4A	Glu-2, 3A, 3B, 4A, NH	Glu-2, 3A, 3B, 4A, NH	Glu-3A/3B, 5
5		177.5	-C(O)-N				Glu-4A/4B, Mdha-N-CH3
NH	8.31, d		NH	Glu-2	Glu-2, 3A, 3B, 4A, 4B	Glu-2, 3A, 3B, 4A, 4B	DMAdda-1

Table 70: NOE-data collected but not utilized in the elucidation.

Glutamic acid	
Glu-3A, 3B, 4A, 4B	N.D.
Glu-3B, 4A, 4B, NH	
Glu-2, 3A, 4A, 4B	
Glu-2, 3A, 3B, 4B	
Glu-2, 3A, 3B, 4A	
Glu-2, 3A	DMAdda-2

Mdha:

Table 71: A Summary of chemical shifts and correlations consistent with Mdha.

Entry	δH	δC	Atom type	COSY	DIPSI-2 (80µs)	DIPSI-2 (160 µs)	HMBC
Mdha							
1		166.5	CON				Mdha-3A, 3B, Ala-2
2		146.8	>C=				Mdha-3A, N-CH3
3A	5.41, s	114.2	CH2	3B	3B	3B	Mdha-1, 2
3B	5.86, s	114.2		3A	3A	3A	Mdha-1
N-CH3	3.33, s	38.6	CH3		N.D.	N.D.	Mdha-2, Glu-5

Table 72: NOE-data collected but not utilized in the elucidation.

ROESY (internal)	ROESY (external)
Mdha	
Mdha-3B, N-CH3	
Mdha-3A	
Mdha-3A	

4.2.4 Complete atom sequence: [DMAdda^{5}]MC-LHar

By elucidation where data in the previous subchapters (4.2.1-3) were utilized the atom sequence is known. Due to time constraints, the remaining collected data (NOE-data) was not utilized in the elucidation. The atom sequence for sample 2 is shown in figure 122. The elucidation suggests that the structure is [DMAdda^{5}]MC-LHar, which for MS-data has been reported.[49]

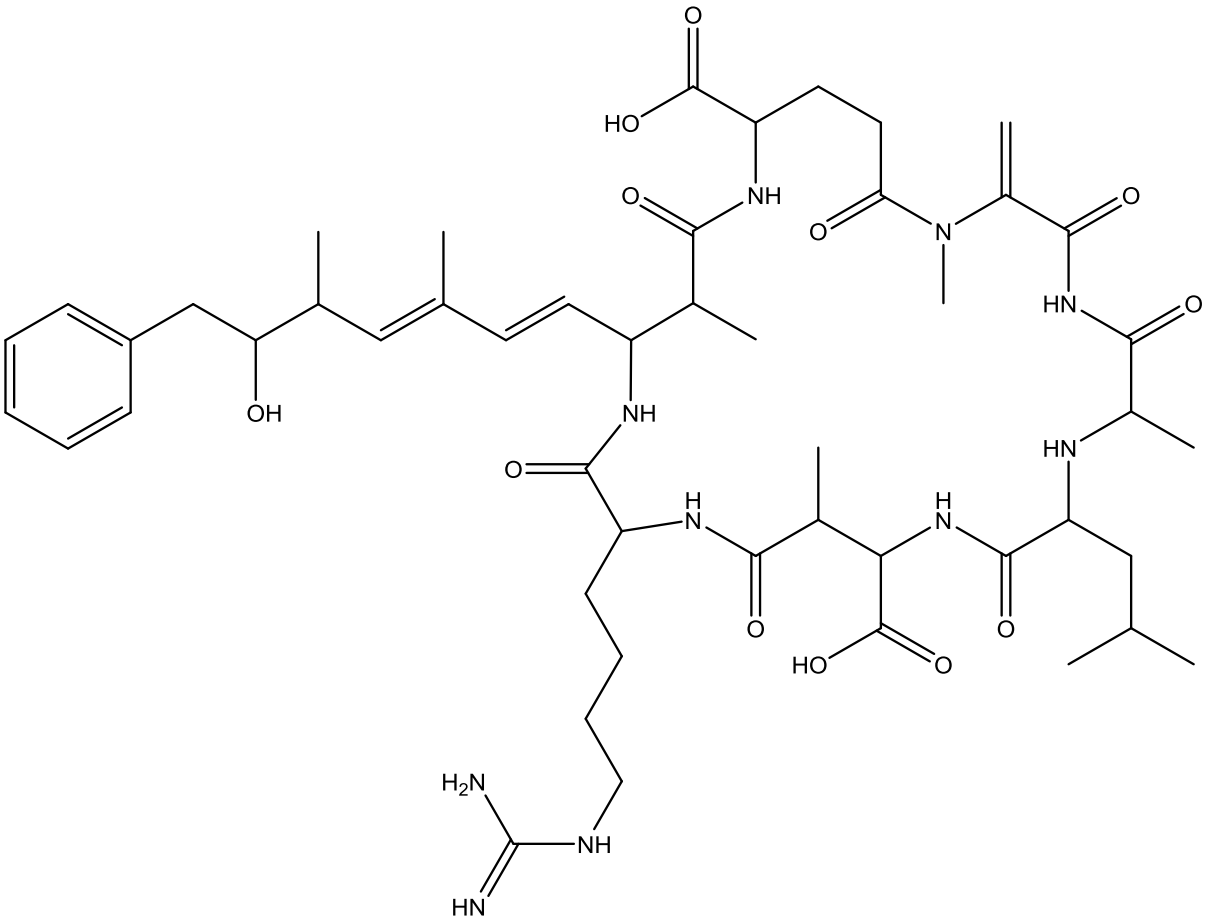

Figure 122: The elucidation of the atom sequence for sample 2. By ignoring stereogenic centra, the molecule is [DMAdda^{5}]MC-LHar.

5 Conclusion and future work

5.1 Sample #1

The NMR-data utilized in elucidation as well as MS-data supplied by Miles is consistent with the structure in the literature for [DMAdda^5]MC-LR.[48] The collected NOE-data in tables 46, 48, 50, 52, 54, 56 and 58 remain to be interpreted to determine the stereogenic centra's relative orientation and the molecule's overall conformation.

5.2 Sample #2

The elucidation suggests that the structure is [DMAdda^5]MC-LHar, which for MS-data has been reported.[49] Therefore it is important to determine the complete structure of the molecule, to provide ample evidence of its structure, to aid the cause of determining the toxicity of all MCs. NOE-data in tables 60, 62, 64, 66, 68, 70 and 72 may be utilized for this purpose.

References

1. Pelley, J. *Nitrogen Triggers Extra-Toxic Algal Blooms In Lake Erie*. 2016 [cited 2016 13.01.2016]; Available from: https://cen.acs.org/articles/94/web/2016/01/Nitrogen-Triggers-Extra-Toxic-Algal.html.
2. Pelley, J. *Scientists debate the best way to tame toxic algal blooms*. 2016 [cited 2018 07.07.2018]; Available from: https://cen.acs.org/articles/94/i12/Scientists-debate-best-way-tame.html.
3. Webb, S. *Detecting Toxins from Freshwater Algae*. 09.06.2011 [cited 2018 06.07.2018]; Available from: https://cen.acs.org/articles/89/web/2011/06/Detecting-Toxins-Freshwater-Algae.html.
4. Wilson, E.K. *Danger From Microcystins In Toledo Water Unclear*. [News] 2014 August 8, 2014 [cited 2014 11.08.2014]; Available from: https://cen.acs.org/articles/92/i32/Danger-Microcystins-Toledo-Water-Unclear.html.
5. Werner J. Fischer, I.G., Christopher O. Miles, Kathryn M. Ross, James B. Aggen, A. Richard Chamberlin, Neal R. Towers, Daniel R. Dietrich, *Congener-Independent Immunoassay.* Environ. Sci. Technol, 2001. **35**(24): p. 4849-4856.
6. Poste, A.E., R.E. Hecky, and S.J. Guildford, *Evaluating microcystin exposure risk through fish consumption.* Environ Sci Technol, 2011. **45**(13): p. 5806-11.
7. Diehnelt, C.W.D., N. R.; Peterman, S. M.; Budde, W. L., *Identification of Microcystin Toxins from a Strain of Microcystis aeruginosa by Liquid Chromatography Introduction into a Hybrid Linear Ion Trap-Fourier Transform Ion Cyclotron Resonance Mass.* Anal. Chem, 2006. **78**: p. 501-512.
8. Samdal, I.A., et al., *Multihapten approach leading to a sensitive ELISA with broad cross-reactivity to microcystins and nodularin.* Environ Sci Technol, 2014. **48**(14): p. 8035-43.
9. Jones, G.J., *Persistence of Cyclic Peptide Toxins in Dried Microcystis aeruginosa Crusts from Lake Mokoan, Australia.* John Wiley & Sons, 1995. **10**: p. 19-24.
10. Schindler, D.W., *Eutrophication and Recovery in Experimental Lakes: Implications for Lake Management.* American Association for the Advancement of Science, 1974. **184**(4139): p. 897-899.
11. Marion, J.W., et al., *In vivo phycocyanin flourometry as a potential rapid screening tool for predicting elevated microcystin concentrations at eutrophic lakes.* Environ Sci Technol, 2012. **46**(8): p. 4523-31.
12. Miles, C.O., et al., *LC-MS analysis with thiol derivatization to differentiate [Dhb(7)]-from [Mdha(7)]-microcystins: analysis of cyanobacterial blooms, Planktothrix cultures and European crayfish from Lake Steinsfjorden, Norway.* Environ Sci Technol, 2013. **47**(9): p. 4080-7.
13. Chorus, I.B., J., *Toxic Cyanobacteria in Water. A guide to their public health consequences monitoring and management.* WHO: London, 1999: p. 400.
14. Miles, C.O., J.E. Melanson, and A. Ballot, *Sulfide oxidations for LC-MS analysis of methionine-containing microcystins in Dolichospermum flos-aquae NIVA-CYA 656.* Environ Sci Technol, 2014. **48**(22): p. 13307-15.
15. Miles, C.O., et al., *Thiol derivatization for LC-MS identification of microcystins in complex matrices.* Environ Sci Technol, 2012. **46**(16): p. 8937-44.
16. Puddick, J., et al., *Structural characterization of new microcystins containing tryptophan and oxidized tryptophan residues.* Mar Drugs, 2013. **11**(8): p. 3025-45.

17. Nonga, H.E., et al., *Possible involvement of microcystins in the unexplained mass mortalities of Lesser Flamingo (Phoeniconaias minor Geoffroy) at Lake Manyara in Tanzania.* Hydrobiologia, 2011. **678**(1): p. 167-178.
18. Fellet, M. *Algal Toxins Accumulate In Fish*. Chemical & Engineering 2011 05.08.2011 [cited 2018 06.07.2018]; Available from: https://cen.acs.org/articles/89/web/2011/08/Algal-Toxins-Accumulate-Fish.html.
19. Pelley, J. *Toxic Algae May Add To Estrogen Pollution*. 2011 [cited 2018 06.07.2018]; Available from: https://cen.acs.org/articles/89/i7/Toxic-Algae-Add-Estrogen-Pollution.html.
20. Miles, C.O., et al., *Conjugation of Microcystins with Thiols Is Reversible: Base-Catalyzed Deconjugation for Chemical Analysis.* Chem Res Toxicol, 2016. **29**(5): p. 860-70.
21. Mayumi, T.K., H.; Imanishi, S.; Kawasaki, Y.; Hasegawa, M.; Harada, K.-I., *Structural Characterization of Microcystins by LC/MS/MS under Ion Trap Conditions.* J. Antibiot., 2006. **59**: p. 710-719.
22. JENNIFER L. GRAHAM, K.A.L., MICHAEL T. MEYER, ANDREW C. ZIEGLER, *Cyanotoxin Mixtures and Taste-and-Odor Compounds in Cyanobacterial Blooms from the Midwestern United States.* Environ. Sci. Technol, 2010. **44**(19): p. 7361-7368.
23. Cotruvo, J.A., *Water Danger Overstated*. 2014, Chemical & Engineering.
24. Cathrine, L.S.a.A., *Handbook of Cyanobacterial Monitoring and Cyanotoxin Analysis, First edition*. 2017: John Wiley & Sons Ltd.
25. Susana R. Pereira, V.M.V.a.A.A., *Computational study of the covalent bonding of microcystins to cysteine residues – a reaction involved in the inhibition of the PPP family of protein phosphatases.* FEBS J, 2011. **280**: p. 674-680.
26. Pelley, J. *Sniffing Out Toxic Bacteria Blooms*. 2010 [cited 2018 06.07.2018]; Available from: https://cen.acs.org/articles/88/web/2010/09/Sniffing-Toxic-Bacteria-Blooms.html.
27. Peter Atkins, J.d.P., *Magnetic Resonance*, in ***Atinks' Physical chemistry 10th ed***, O.U. Press, Editor. 2014, Oxford University Press. p. 560-592.
28. Donald L. Pavia, G.S.L., George S. Kirz, James R. Vyvyan, ***Nuclear Magnetic Resonance Spectroscopy 4th ed***, in *Introduction to Spectroscopy*

2009, Brooks/Cole, Cengage Learning: Australia, Brazil, Japan, Korea, Mexico, Singapore, Spain, United Kingdom. p. 105-361.
29. Claridge, T.D.W., *High-Resolution NMR Techniques in Organic Chemistry 3rd ed*. 2016: Elsevier.
30. Dirac, P., *The Principles of Quantum Mechanics (International Series of Monographs on Physics) 4th Edition*. 1930: Oxford University Press.
31. Pauli, W., *Über den Zusammenhang des Abschlusses der Elektronengruppen im Atom mit der Komplexstruktur der Spektren.* ZS. f. Phys., 1925. **31**(1): p. 765-783.
32. *NMR Building Blocks The MLEV Block*. 2018 [cited 2018 15.12.2018]; Available from: http://triton.iqfr.csic.es/guide/eNMR/eNMRblock/toblock.html.
33. Ad Bax, D.G.D., *MLEV-17-based two-dimensional homonuclear magnetization transfer spectroscopy.* J. Magn. Reson., 1969. **65**(2): p. 355-360.
34. *Composite Sequences DIPSI Schemes*. Available from: http://triton.iqfr.csic.es/guide/eNMR/eNMRcomp/dipsi.html.
35. A. J Shaka, J.K., Tom, Frenkiel, RayFreeman, *An improved sequence for broadband decoupling: WALTZ-16.* J. Magn. Reson., 1969. **52**(2): p. 335-338.

36. A. J. Shaka, P.B.B., Ray Freeman, *Computer-optimized decoupling scheme for wideband applications and low-level operation.* J. Magn. Reson., 1969. **64**(3): p. 547-552.
37. Adrien Le Guennec, F.T., Arthur S. Edison, *Alternatives to Nuclear Overhauser Enhancement Spectroscopy Presat and Carr-Purcell-Meiboom-Gill Presat for NMR-Based Metabolomics.* Anal. Chem., 2017. **89**: p. 8582-8588.
38. Simpson A. J, B.S.A., *Purge NMR: effective and easy solvent suppression.* J. Magn. Reson., 2005. **175**(2): p. 340-346.
39. Xia, M.S., Nikonowicz EP, Gao X., *Z-restored spin-echo 13C 1D spectrum of straight baseline free of hump, dip and roll.* Magn Reson Chem, 2008. **46**(5): p. 432-435.
40. Wilkins, A.L., *NMR limitations*, F.R. Kristian W. Trovik, Chris O. Miles, Editor. 2018.
41. Robin Panisch, M.B., and, and Thomas Müller, *Hydrogen- and Fluorine-Bridged Disilyl Cations and Their Use in Catalytic C−F Activation.* J Am Chem Soc, 2006. **128**(30): p. 9676-9682.
42. Ilona Oksanen, J.J., David P. Fewer, Matti Wahlsten, Jouko Rikkinen, and Kaarina Sivonen, *Discovery of Rare and Highly Toxic Microcystins from Lichen-Associated Cyanobacterium Nostoc sp. Strain IO-102-I.* PMC, 2004. **70**(10): p. 5756-5763.
43. David P.Fewer, M., JuliaÖsterholm, JouniJokela, LeoRouhiainen, UllaKaasalainen, JoukoRikkinen, KaarinaSivonen, *The Genetic Basis for O-Acetylation of the Microcystin Toxin in Cyanobacteria.* Chem. Biol., 2013. **20**(7): p. 861-869.
44. Bank, B.M.R.D. *L-Arginine (C6 H14 N4 O2).* [cited 2018 11.12.2018]; Available from: http://bmrb.wisc.edu/metabolomics/mol_summary/show_data.php?id=bmse000711.
45. Book, C. *L-Arginine 13CNMR.* [cited 2018 11.12.2018]; Available from: https://www.chemicalbook.com/SpectrumEN_74-79-3_13CNMR.htm.
46. Jan Schripsema, D.D., *Complete assignment of the NMR spectra of [D-Leu1]-microcystin-LR and analysis of its solution structure.* Magn. Reson. Chem., 2002. **40**: p. 614-617.
47. Jonathan Goldberg, H.-b.H., Young-guen Kwon, Paul Greengard, Angus C. Nairn & John Kuriyan, *Three-dimensional structure of the catalytic subunit of protein serine/threonine phosphatase-1.* Nature, 1995. **376**: p. 745-753.
48. Michio Namikoshi, K.L.R., Ryuichi Sakai, Richard R. Stotts, Andrew M. Dahlem, Val R. Beasley, Wayne W. Carmichael, and William R. Evan, *Identification of 12 Hepatotoxins from a Homer Lake Bloom of the Cyanobacteria Microcystis aeruginosa, Microcystis viridis, and Microcystis wesenbergii: Nine New Microcystins.* J. Org. Chem., 1992. **57**: p. 866-872.
49. David P Fewer, L.R., Jouni Jokela, Matti Wahlsten, Kati Laakso, Hao Wang and Kaarina Sivonen, *Recurrent adenylation domain replacement in the microcystin synthetase gene cluster.* BCM Evol Biol, 2007. **7**(183): p. **1-11**.

Appendix A – Pulse programs

PROTON

```
;zg30

;avance-version (12/01/11)

;1D sequence

;using 30 degree flip angle

;

;$CLASS=HighRes

;$DIM=1D

;$TYPE=

;$SUBTYPE=

;$COMMENT=

;$RECOMMEND=y




#include <Avance.incl>




"acqt0=-p1*0.66/3.1416"
```

```
1 ze

2 30m

  d1

  p1*0.33 ph1

  go=2 ph31

  30m mc #0 to 2 F0(zd)

exit




ph1=0 2 2 0 1 3 3 1

ph31=0 2 2 0 1 3 3 1




;pl1 : f1 channel - power level for pulse (default)

;p1 : f1 channel -  90 degree high power pulse

;d1 : relaxation delay; 1-5 * T1

;ns: 1 * n, total number of scans: NS * TD0
```

;$Id: zg30,v 1.12 2012/01/31 17:49:31 ber Exp $

Zgesgp

;zgesgp

;avance-version (12/01/11)

;1D sequence

;water suppression using excitation sculpting with gradients

;T.-L. Hwang & A.J. Shaka, J. Magn. Reson.,

; Series A 112 275-279 (1995)

;

;$CLASS=HighRes

;$DIM=1D

;$TYPE=

;$SUBTYPE=

;$COMMENT=

prosol relations=<triple>

#include <Avance.incl>

#include <Grad.incl>

```
#include <Delay.incl>



"p2=p1*2"

"d12=20u"



"TAU=de+p1*2/3.1416+50u"



"acqt0=0"

baseopt_echo



1 ze

2 30m

  d12 pl1:f1 BLKGRAD

  d1

  p1 ph1


  50u UNBLKGRAD
```

p16:gp1

d16 pl0:f1

(p12:sp1 ph2:r):f1

4u

d12 pl1:f1

p2 ph3

4u

p16:gp1

d16

TAU

p16:gp2

d16 pl0:f1

(p12:sp1 ph4:r):f1

4u

d12 pl1:f1

p2 ph5

4u

```
  p16:gp2
  d16

  go=2 ph31
  30m mc #0 to 2 F0(zd)
  4u BLKGRAD
exit


ph1=0
ph2=0 1
ph3=2 3
ph4=0 0 1 1
ph5=2 2 3 3
ph31=0 2 2 0


;pl0 : 0W
;pl1 : f1 channel - power level for pulse (default)
;sp1 : f1 channel - shaped pulse 180 degree
;p1 : f1 channel -  90 degree high power pulse
```

;p2 : f1 channel - 180 degree high power pulse

;p12: f1 channel - 180 degree shaped pulse (Squa100.1000) [2 msec]

;p16: homospoil/gradient pulse

;d1 : relaxation delay; 1-5 * T1

;d12: delay for power switching [20 usec]

;d16: delay for homospoil/gradient recovery

;ns: 8 * n, total number of scans: NS * TD0

;ds: 4

;use gradient ratio: gp 1 : gp 2

; 31 : 11

;for z-only gradients:

;gpz1: 31%

;gpz2: 11%

;use gradient files:

;gpnam1: SMSQ10.100

;gpnam2: SMSQ10.100

;$Id: zgesgp,v 1.9 2012/01/31 17:49:32 ber Exp $

Awprotonpr

;zgpr

;avance-version (12/01/11)

;1D sequence with f1 presaturation

;

;$CLASS=HighRes

;$DIM=1D

;$TYPE=

;$SUBTYPE=

;$COMMENT=

#include <Avance.incl>

"d12=20u"

```
"acqt0=-p1*2/3.1416"



1 ze

2 30m

  d12 pl9:f1

  d1 cw:f1 ph29

  4u do:f1

  d12 pl1:f1

  p1 ph1

  go=2 ph31

  30m mc #0 to 2 F0(zd)

exit



ph1=0 2 2 0 1 3 3 1

ph29=0

ph31=0 2 2 0 1 3 3 1



;pl1 : f1 channel - power level for pulse (default)
```

;pl9 : f1 channel - power level for presaturation

;p1 : f1 channel - 90 degree high power pulse

;d1 : relaxation delay; 1-5 * T1

;d12: delay for power switching [20 usec]

;ns: 1 * n, total number of scans: NS * TD0

;$Id: zgpr,v 1.11 2012/01/31 17:49:32 ber Exp $

awprotonesprf1prf2

;awprotonesprf1prf2

;avance-version (12/01/11)

;1D sequence

;water suppression using excitation sculpting with gradients

;T.-L. Hwang & A.J. Shaka, J. Magn. Reson.,

; Series A 112 275-279 (1995)

;

;$CLASS=HighRes

;$DIM=1D

;$TYPE=

;$SUBTYPE=

;$COMMENT=

prosol relations=<default>

#include <Avance.incl>

#include <Grad.incl>

#include <Delay.incl>

"p2=p1*2"

"d12=20u"

"TAU=de+p1*2/3.1416+50u"

"acqt0=0"

baseopt_echo

1 ze

2 30m

d12 pl9:f1 pl21:f2

d1 cw:f1 ph29 cw:f2 ph29

4u do:f1 do:f2

d12 pl1:f1 BLKGRAD

p1 ph1

50u UNBLKGRAD

p16:gp1

d16 pl0:f1

(p40:sp10 ph2:r):f1

4u

d12 pl1:f1

p2 ph3

4u

p16:gp1

d16

TAU

p16:gp2

d16 pl0:f1

(p40:sp10 ph4:r):f1

4u

d12 pl1:f1

p2 ph5

4u

p16:gp2

d16

go=2 ph31

30m mc #0 to 2 F0(zd)

4u BLKGRAD

exit

ph1=0

ph2=0 1

ph3=2 3

ph4=0 0 1 1

ph5=2 2 3 3

ph31=0 2 2 0

ph29=0

;pl0 : 0W

;pl1 : f1 channel - power level for pulse (default)

;pl9: f2 channel CW presat power level

;sp1 : f1 channel - shaped pulse 180 degree

;p1 : f1 channel - 90 degree high power pulse

;p2 : f1 channel - 180 degree high power pulse

;p12: f1 channel - 180 degree shaped pulse (Squa100.1000)   [2 msec]

;p16: homospoil/gradient pulse

;d1 : relaxation delay; 1-5 * T1

;d12: delay for power switching [20 usec]

;d16: delay for homospoil/gradient recovery

;ns: 8 * n, total number of scans: NS * TD0

;ds: 4

;use gradient ratio: gp 1 : gp 2

; 31 : 11

;for z-only gradients:

;gpz1: 31%

;gpz2: 11%

;use gradient files:

;gpnam1: SMSQ10.100

;gpnam2: SMSQ10.100

;$Id: zgesgp,v 1.9 2012/01/31 17:49:32 ber Exp $

awprotonespr

170

```
;awprotonespr

;avance-version (12/01/11)

;1D sequence with CW presaturation on f1 plus
;water suppression using excitation sculpting with gradients
;T.-L. Hwang & A.J. Shaka, J. Magn. Reson.,
;   Series A 112 275-279 (1995)
;
;$CLASS=HighRes
;$DIM=1D
;$TYPE=
;$SUBTYPE=
;$COMMENT=


prosol relations=<triple>


#include <Avance.incl>
#include <Grad.incl>
```

```
#include <Delay.incl>



"p2=p1*2"

"d12=20u"



"TAU=de+p1*2/3.1416+50u"



"acqt0=0"

baseopt_echo



1 ze


2 30m

  d12 pl9:f1

  d1 cw:f1 ph29

  4u do:f1

  d12 pl1:f1 BLKGRAD
```

p1 ph1

50u UNBLKGRAD

p16:gp1

d16 pl0:f1

(p12:sp1 ph2:r):f1

4u

d12 pl1:f1

p2 ph3

4u

p16:gp1

d16

TAU

p16:gp2

d16 pl0:f1

(p12:sp1 ph4:r):f1

4u

d12 pl1:f1

```
  p2 ph5


  4u

  p16:gp2

  d16


  go=2 ph31

  30m mc #0 to 2 F0(zd)

  4u BLKGRAD

exit



ph1=0

ph2=0 1

ph3=2 3

ph4=0 0 1 1

ph5=2 2 3 3

ph29=0

ph31=0 2 2 0
```

;pl0 : 0W

;pl1 : f1 channel - power level for pulse (default)

;pl9 : f1 Channel - CW presaturation power

;sp1 : f1 channel - shaped pulse 180 degree

;p1 : f1 channel - 90 degree high power pulse

;p2 : f1 channel - 180 degree high power pulse

;p12: f1 channel - 180 degree shaped pulse (Squa100.1000)   [2 msec]

;p16: homospoil/gradient pulse

;d1 : relaxation delay; 1-5 * T1

;d12: delay for power switching   [20 usec]

;d16: delay for homospoil/gradient recovery

;ns: 8 * n, total number of scans: NS * TD0

;ds: 4

;use gradient ratio: gp 1 : gp 2

;   31 :   11

;for z-only gradients:

;gpz1: 31%

;gpz2: 11%

;use gradient files:

;gpnam1: SMSQ10.100

;gpnam2: SMSQ10.100

;$Id: zgesgp,v 1.9 2012/01/31 17:49:32 ber Exp $

deptsp135

;deptsp135

;avance-version (14/10/09)

;dept polarization transfer

;with decoupling during acquisition

;using shaped pulse for 180degree pulse on f1 - channel

;with 135 degree read pulse to give XH, XH3 positive and XH2 negative

;

;$CLASS=HighRes

;$DIM=1D

;$TYPE=

;$SUBTYPE=

;$COMMENT=

```
;$RECOMMEND=y



#include <Avance.incl>

#include <Delay.incl>



"p4=p3*2"

"d2=1s/(cnst2*2)"

"d12=20u"



"DELTA=p1*4/PI"



"acqt0=-p1*2/PI"



1 ze

2 30m do:f2

  d1
```

d12 pl1:f1 pl2:f2

(p3 ph1):f2

d2

(p4 ph2):f2

(p1 ph4):f1

d2 pl0:f1

(p3*1.5 ph3):f2 (p13:sp5 ph5):f1

d2

DELTA pl12:f2

go=2 ph31 cpd2:f2

30m do:f2 mc #0 to 2 F0(zd)

exit

ph1=0

ph2=0 2 1 3

ph3=1 1 1 1 3 3 3 3

ph4=0 0 0 0 0 0 0 0 1 1 1 1 1 1 1 1

2 2 2 2 2 2 2 2 3 3 3 3 3 3 3 3

ph5=0 2 0 2 0 2 0 2 1 3 1 3 1 3 1 3

ph31=1 1 3 3 3 3 1 1 2 2 0 0 0 0 2 2

3 3 1 1 1 1 3 3 0 0 2 2 2 2 0 0

;pl0 : 0W

;pl1 : f1 channel - power level for pulse (default)

;pl2 : f2 channel - power level for pulse (default)

;pl12: f2 channel - power level for CPD/BB decoupling

;sp5: f1 channel - shaped pulse (180degree)

;spnam5: Crp60comp.4

;p1 : f1 channel - 90 degree high power pulse

;p3 : f2 channel - 90 degree high power pulse

;p4 : f2 channel - 180 degree high power pulse

;p13: f1 channel - 180 degree shaped pulse

; = 2msec for Crp60comp.4

;d1 : relaxation delay; 1-5 * T1

;d2 : 1/(2J(XH))

;d12: delay for power switching [20 usec]

;cnst2: = J(XH)

;ns: 4 * n, total number of scans: NS * TD0

;ds: 8

;cpd2: decoupling according to sequence defined by cpdprg2

;pcpd2: f2 channel - 90 degree pulse for decoupling sequence

;DELTA: delay to compensate for chemical shift evolution during

; RF pulse in order to give same phase correction as

; for reference 1D spectrum

;$Id: deptsp135,v 1.13.2.1 2014/10/10 09:21:10 ber Exp $

deptqgpsp

;deptqgpsp

;avance-version (14/10/09)

;DEPTQ

;dept polarization transfer

;with decoupling during acquisition

;using shaped pulse for 180degree pulse on f1 - channel

;

;R. Burger & P. Bigler, J. Magn. Reson. 135, 529-534 (1998)

;

;$CLASS=HighRes

```
;$DIM=1D
;$TYPE=
;$SUBTYPE=
;$COMMENT=


#include <Avance.incl>
#include <Delay.incl>
#include <Grad.incl>


"p4=p3*2"
"d2=1s/(cnst2*2)"
"d12=20u"


"p0=p3*cnst12"


"DELTA=p1*4/PI-4u"
"DELTA1=d2+p1+p4-p16-d16"
```

"DELTA2=d2+p1-p16-d16"

"DELTA3=d2-p16-d16"

"acqt0=-p1*2/PI"

1 ze

2 30m do:f2

d1

d12 pl1:f1 pl2:f2

50u UNBLKGRAD

(p1 ph2):f1

p16:gp1

d16

DELTA1

(ralign (p13:sp5 ph3):f1 (p3 ph1):f2)

DELTA2

p16:gp2

d16 pl1:f1

(p4 ph3):f2

(p1 ph1):f1

p16:gp3

d16

DELTA3 pl0:f1

(p13:sp5 ph5):f1 (p0 ph4):f2

DELTA3

p16:gp3

d16

DELTA pl12:f2

4u BLKGRAD

go=2 ph31 cpd2:f2

30m do:f2 mc #0 to 2 F0(zd)

exit

ph1=0

ph2=3

ph3=0 2 1 3

ph4=1

ph5=0 2

ph31=1 1 3 3

;pl0 : 0W

;pl1 : f1 channel - power level for pulse (default)

;pl2 : f2 channel - power level for pulse (default)

;pl12: f2 channel - power level for CPD/BB decoupling

;sp5: f1 channel - shaped pulse (180degree)

;spnam5: Crp60comp.4

;p0 : f2 channel : p3 * cnst12

;p1 : f1 channel - 90 degree high power pulse

;p3 : f2 channel - 90 degree high power pulse

;p4 : f2 channel - 180 degree high power pulse

;p13: f1 channel - 180 degree shaped pulse

;   = 2msec for Crp60comp.4

;p16: homospoil/gradient pulse

;d1 : relaxation delay; 1-5 * T1

;d2 : 1/(2J(XH))

;d12: delay for power switching   [20 usec]

;d16: delay for homospoil/gradient recovery

;cnst2: = J(XH)

;cnst12: for multiplicity selection

; 0.5 (45 degree pulse) - all positive

; 1.0 (90 degree pulse) - XH only

; 1.5 (135 degree pulse) - XH, XH3 positive, XH2 negative

;ns: 4 * n, total number of scans: NS * TD0

;ds: 8

;cpd2: decoupling according to sequence defined by cpdprg2

;pcpd2: f2 channel - 90 degree pulse for decoupling sequence

;use gradient ratio: gp 1 : gp 2 : gp 3

; 31 : 31 : 31 for all C

; 0 : 31 : 31 for CHn only

; 31 : 31 : 11 for Cquat only

;for z-only gradients:

;gpz1: 31%(all/Cq) or 0%(CHn)

;gpz2: 31%

;gpz3: 31%(all/CHn) or 11%(Cq)

;use gradient files:

;gpnam1: SMSQ10.100

;gpnam2: SMSQ10.100

;gpnam3: SMSQ10.100

;DELTA: delay to compensate for chemical shift evolution during

; RF pulse in order to give same phase correction as

; for reference 1D spectrum

;$Id: deptqgpsp,v 1.5.2.1 2014/10/10 09:21:10 ber Exp $

awcosyesprf2

;awcosyesprf2

;Derived from avance-version (12/01/11)

;2D homonuclear shift correlation

;magnitude COSY spectrum with excitation sculpting (ES) on F1

;and CW PR on F2

```
;pp is  prosol compatibile with TS3.5


;JCM 2016-03-31 + ALW modifications
;
;T.-L. Hwang & A.J. Shaka, J. Magn. Reson.,
;   Series A 112 275-279 (1995)
;
;$CLASS=HighRes
;$DIM=2D
;$TYPE=
;$SUBTYPE=
;$COMMENT=



prosol relations=<default>



#include <Avance.incl>
#include <Grad.incl>
#include <Delay.incl>
```

"p2=p1*2"

"d11=30m"

"d12=20u"

"in0=inf1"

"d0=in0/2-p1*4/3.1416"

"TAU=de+p1*2/3.1416+54u"

"acqt0=0"

baseopt_echo

1 ze

2 d11

3 d12 pl21:f2

d1 cw:f2 ph29

4u do:f2

d12 pl1:f1

p1 ph1

d0

50u UNBLKGRAD

p16:gp1

d16

p0 ph2

50u UNBLKGRAD

p16:gp2

d16 pl0:f1

(p40:sp10 ph4:r):f1

4u

d12 pl1:f1

p2 ph5

4u

p16:gp3

d16

TAU

```
  p16:gp4
  d16 pl0:f1
  (p40:sp10 ph6:r):f1
  4u
  d12 pl1:f1

  p2 ph7

  4u
  p16:gp4
  d16
  4u BLKGRAD

  go=2 ph31
  d11 mc #0 to 2 F1QF(caldel(d0, +in0))
exit

ph1=0 2
ph2=0 0 2 2
ph4=0
ph5=2 2 2 2 3 3 3 3
ph6=0
ph7=2
```

```
ph29=0

ph31=0 2 0 2 2 0 2 0


;pl0 : 0W

;pl1 : f1 channel - power level for pulse (default)

;pl21: f2 channel - power level for presaturation

;sp10: f1 channel - shaped pulse 180 degree (Sinc1.000 with TS3.5)

;p0: f1 channel COSY tip angle (can be any angle up to 90 degrees)

;p1 : f1 channel -  90 degree high power pulse

;p2 : f1 channel - 180 degree high power pulse

;p40: f1 channel - 180 degree shaped pulse (Sinc1.1000)   [2 msec]

;p16: homospoil/gradient pulse

;p17: f1 channel - trim pulse                    [2.5 msec]

;d0 : incremented delay (2D)

;d1 : relaxation delay; 1-5 * T1

;d11: delay for disk I/O                         [30 msec]

;d12: delay for power switching                  [20 usec]

;d16: delay for homospoil/gradient recovery

;inf1: 1/SW = 2 * DW

;in0: 1/(1 * SW) = 2 * DW

;nd0: 1

;ns: 1 * n

;ds: 16
```

;td1: number of experiments

;FnMODE: QF

;for z-only gradients:

;gpz1: 10%

;gpz2: 41% (gpz1 + gpz3)

;gpz3: 31%

;gpz4: 11%

;use gradient files:

;gpnam1: SMSQ10.100

;gpnam2: SMSQ10.100

;gpnam3: SMSQ10.100

;gpnam4: SMSQ10.100

;set pl9 to 0W when presaturation on F1 is not required

; use pl1 + 75 to 80dB to reduce radiation damping

;Processing

;PHC0(F1): 90

;PHC1(F1): -180

;FCOR(F1): 1

;$Id: cosydfesgpphpp,v 1.7 2012/01/31 17:49:22 ber Exp $

awdipsi2prf1prf2

;awdipsi2prf1prf2

;with CW presaturation on f1 at O1 and f2 at O2

;avance-version (12/01/11)

;homonuclear Hartman-Hahn transfer using DIPSI2 sequence

; for mixing, phase sensitive

;

;$CLASS=HighRes

;$DIM=2D

;$TYPE=

;$SUBTYPE=

;$COMMENT=

#include <Avance.incl>

#include <Delay.incl>

"d11=30m"

"d12=20u"

"d13=4u"

"d20=2m"

"d21=3m"

"in0=inf1"

"d0=in0/2-p1*4/3.1416"

"FACTOR1=(d9/(p6*115.112))/2"

"l1=FACTOR1*2"

1 ze

2 d11

3 d12 pl9:f1 pl21:f2

d1 cw:f1 ph29 cw:f2 ph29

d13 do:f1 do:f2

d12 pl1:f1

p1 ph1

d0

p1 ph2

d20 pl10:f1

;begin DIPSI2

4 p6*3.556 ph23

p6*4.556 ph25

p6*3.222 ph23

p6*3.167 ph25

p6*0.333 ph23

p6*2.722 ph25

p6*4.167 ph23

p6*2.944 ph25

p6*4.111 ph23

p6*3.556 ph25

p6*4.556 ph23

p6*3.222 ph25

p6*3.167 ph23

p6*0.333 ph25

p6*2.722 ph23

p6*4.167 ph25

p6*2.944 ph23

p6*4.111 ph25

p6*3.556 ph25

p6*4.556 ph23

p6*3.222 ph25

p6*3.167 ph23

p6*0.333 ph25

p6*2.722 ph23

p6*4.167 ph25

p6*2.944 ph23

p6*4.111 ph25

p6*3.556 ph23

p6*4.556 ph25

p6*3.222 ph23

p6*3.167 ph25

p6*0.333 ph23

p6*2.722 ph25

p6*4.167 ph23

p6*2.944 ph25

p6*4.111 ph23

lo to 4 times l1

;end DIPSI2

d21 pl1:f1

p1 ph3

go=2 ph31

d11 mc #0 to 2 F1PH(calph(ph1, +90) & calph(ph29, +90), caldel(d0, +in0))

exit

ph1=0 2

ph2=0 0 0 0 2 2 2 2

ph3=0 0 2 2

ph23=3

ph25=1

ph29=0

ph31=0 2 2 0 2 0 0 2

;pl1 : f1 channel - power level for pulse (default)

;pl9 : f1 channel - power level for presaturation at O1

;pl21: f2 channel - power level for presaturation at O2

;pl10: f1 channel - power level for TOCSY-spinlock

;p1 : f1 channel - 90 degree high power pulse

;p6 : f1 channel - 90 degree low power pulse

;d0 : incremented delay (2D)

;d1 : relaxation delay; 1-5 * T1

;d9 : TOCSY mixing time

;d11: delay for disk I/O [30 msec]

;d12: delay for power switching [20 usec]

;d13: short delay [4 usec]

;d20: first z-filter delay [2 msec]

;d21: second z-filter delay [3 msec]

;l1: loop for DIPSI cycle: ((p6*115.112) * l1) = mixing time

;inf1: 1/SW = 2 * DW

;in0: 1/(1 * SW) = 2 * DW

;nd0: 1

;ns: 8 * n

;ds: 16

;td1: number of experiments

;FnMODE: States-TPPI, TPPI, States or QSEQ

;Processing

;PHC0(F1): 90

;PHC1(F1): -180

;FCOR(F1): 1

;$Id: dipsi2phpr,v 1.11 2012/01/31 17:49:23 ber Exp $

awnoesygpesprf2

;awnoesygpesprf2 with ES on f1 and CW presaturation on f2

;avance-version (07/10/04)

;2D homonuclear correlation via dipolar coupling

;dipolar coupling may be due to noe or chemical exchange.

;phase sensitive

;water suppression using excitation sculpting with gradients

;

;T.-L. Hwang & A.J. Shaka, J. Magn. Reson.,

;   Series A 112 275-279 (1995)

;

;$CLASS=HighRes

;$DIM=2D

;$TYPE=

;$SUBTYPE=

;$COMMENT=

prosol relations=<default>

```
#include <Avance.incl>

#include <Grad.incl>

#include <Delay.incl>




"p2=p1*2"

"d11=30m"

"d12=20u"

"d13=4u"




"in0=inf1"



"d0=in0/2-p1*4/3.1416"




"TAU=de+p1*2/3.1416+54u"



1 ze
```

2 d11

3 d12 pl21:f2

d1 cw:f2 ph29

d13 do:f2

d12 pl1:f1

p1 ph1

d0

p1 ph2

d8

p1 ph3

50u UNBLKGRAD

p16:gp1

d16 pl0:f1

(p40:sp10 ph4:r):f1

4u

d12 pl1:f1

p2 ph5

```
  4u
  p16:gp1
  d16
  TAU
  p16:gp2
  d16 pl0:f1
  (p40:sp10 ph6:r):f1
  4u
  d12 pl1:f1

  p2 ph7

  4u
  p16:gp2
  d16
  4u BLKGRAD

  go=2 ph31
  d11 mc #0 to 2 F1PH(ip1, id0)
exit
```

ph1= 0 0 2 2

ph2= 0

ph3= 0 0 0 0 2 2 2 2 1 1 1 1 3 3 3 3

ph4= 0 0 0 0 1 1 1 1

ph5= 2 2 2 2 3 3 3 3

ph6= 2 3

ph7= 0 1

ph31=0 2 2 0 0 2 2 0 1 3 3 1 1 3 3 1

ph29=0

;pl0 : 120dB

;pl1 : f1 channel - power level for pulse (default)

;pl21 :f2 channel - power level for presat at O2

;sp10 : f1 channel - shaped pulse 180 degree

;p1 : f1 channel - 90 degree high power pulse

;p2 : f1 channel - 180 degree high power pulse

;p30: f1 channel - 180 degree shaped pulse (Squa100.1000)   [2 msec]

;p16: homospoil/gradient pulse

;d0 : incremented delay (2D)

;d1 : relaxation delay; 1-5 * T1

;d8 : mixing time

;d12: delay for power switching [20 usec]

;d16: delay for homospoil/gradient recovery

;inf1: 1/SW = 2 * DW

;in0: 1/(1 * SW) = 2 * DW

;nd0: 1

;NS: 8 * n

;DS: 16

;td1: number of experiments

;FnMODE: States-TPPI, TPPI, States or QSEQ

;use gradient ratio: gp 1 : gp 2

; 31 : 11

;for z-only gradients:

;gpz1: 31%

;gpz2: 11%

;use gradient files:

;gpnam1: SINE.100

;gpnam2: SINE.100

;Processing

;PHC0(F1): 90

;PHC1(F1): -180

;FCOR(F1): 1

;$Id: noesyesgpph,v 1.8.2.1 2007/10/04 16:52:07 ber Exp $

awroesyesprf2

;awroesyesprf2 with CW presat on O2 and ES presat on O1

;avance-version (07/12/14)

;2D ROESY with cw spinlock for mixing

;phase sensitive

;

;A. Bax & D.G. Davis, J. Magn. Reson 63, 207-213 (1985)

;T.-L. Hwang & A.J. Shaka, J. Magn. Reson.,

; Series A 112 275-279 (1995)

;

;$CLASS=HighRes

;$DIM=2D

;$TYPE=

;$SUBTYPE=

;$COMMENT=

prosol relations=<default>

#include <Avance.incl>

#include <Grad.incl>

#include <Delay.incl>

"p2=p1*2"

"d12=20u"

"d11=30m"

"d13=4u"

"in0=inf1"

"d0=in0/2-p1*2/3.1416-4u"

"TAU=de+p1*2/3.1416+54u"

1 ze

2 d11

d12 pl21:f2

d1 cw:f2 ph29

d13 do:f2

3 d12 pl1:f1

p1 ph1

d0

4u pl11:f1

p15 ph2

50u UNBLKGRAD

p16:gp1

d16 pl0:f1

(p40:sp10 ph3:r):f1

4u

d12 pl1:f1

p2 ph4

4u

p16:gp1

d16

TAU

p16:gp2

d16 pl0:f1

(p40:sp10 ph5:r):f1

4u

d12 pl1:f1

p2 ph6

4u

p16:gp2

d16

4u BLKGRAD

go=2 ph31

d11 mc #0 to 2 F1PH(ip1, id0)

exit

ph1=0 2

ph2=0

ph3=0 0 1 1

ph4=2 2 3 3

ph5=0 0 0 0 1 1 1 1

ph6=2 2 2 2 3 3 3 3

ph29=0

ph31=0 2 2 0 2 0 0 2

;pl0 : 120dB

;pl1 : f1 channel - power level for pulse (default)

;pl11: f1 channel - power level for ROESY-spinlock

;pl21: f2 channel power level for CW presat at O2

;sp10: f1 channel - shaped pulse 180 degree

;p1 : f1 channel - 90 degree high power pulse

;p2 : f1 channel - 180 degree high power pulse

;p15: f1 channel - pulse for ROESY spinlock

;p16: homospoil/gradient pulse

;p40: f1 channel - 180 degree shaped pulse (Squa100.1000)   [2 msec]

;d0 : incremented delay (2D)

;d1 : relaxation delay; 1-5 * T1

;d12: delay for power switching   [20 usec]

;d16: delay for homospoil/gradient recovery

;inf1: 1/SW = 2 * DW

;in0: 1/(1 * SW) = 2 * DW

;nd0: 1

;NS: 8 * n

;DS: 16

;td1: number of experiments

;FnMODE: States-TPPI, TPPI, States or QSEQ

;use gradient ratio: gp 1 : gp 2

; 31 : 11

;for z-only gradients:

;gpz1: 31%

;gpz2: 11%

;use gradient files:

;gpnam1: SINE.100

;gpnam2: SINE.100

;Processing

;PHC0(F1): 180

;PHC1(F1): -180

;FCOR(F1): 1

;$Id: roesyesgpph,v 1.9.2.2 2007/12/14 16:06:46 ber Exp $

awhsqcedetgpsisp2.3-135pr

;awhsqcedetgpsisp2.3-135pr

;avance-version (12/01/11)

;aw modification with auto calc of d21 and d24 from cnst2 (1J coupling)

;2D H-1/X correlation via double inept transfer

; using sensitivity improvement

;phase sensitive using Echo/Antiecho-TPPI gradient selection

;with decoupling during acquisition

;using trim pulses in inept transfer

;with multiplicity editing during selection step

;using shaped pulses for all 180degree pulses on f2 - channel

;for matched sweep adiabatic pulses

;with gradients in back-inept

;

;A.G. Palmer III, J. Cavanagh, P.E. Wright & M. Rance, J. Magn.

; Reson. 93, 151-170 (1991)

;L.E. Kay, P. Keifer & T. Saarinen, J. Am. Chem. Soc. 114,

; 10663-5 (1992)

;J. Schleucher, M. Schwendinger, M. Sattler, P. Schmidt, O. Schedletzky,

; S.J. Glaser, O.W. Sorensen & C. Griesinger, J. Biomol. NMR 4,

; 301-306 (1994)

;W. Willker, D. Leibfritz, R. Kerssebaum & W. Bermel, Magn. Reson.

; Chem. 31, 287-292 (1993)

;C. Zwahlen, P. Legault, S.J.F. Vincent, J. Greenblatt, R. Konrat &

; L.E. Kay, J. Am. Chem. Soc. 119 6711-6721 (1997)

;(R.D. Boyer, R. Johnson & K. Krishnamurthy,

; J. Magn. Reson. 165, 253-259 (2003))

;

;$CLASS=HighRes

;$DIM=2D

;$TYPE=

;$SUBTYPE=

;$COMMENT=

;$RECOMMEND=y

```
#include <Avance.incl>

#include <Grad.incl>

#include <Delay.incl>



"p2=p1*2"

"d4=1s/(cnst2*4)"

"d11=30m"


"d21=1s/(cnst2*2)"

"d24=1s/(cnst2*8)"



"d0=3u"


"in0=inf1/2"



"DELTA=d21-p16-d16-p2-d0*2-p3*2/PI"

"DELTA1=p16+d16-p1*0.78+de+8u"
```

"DELTA2=d4-larger(p2,p14)/2"

"DELTA3=d24-cnst17*p24/2-p19-d16"

"DELTA4=d4-larger(p2,p14)/2-p16-d16"

"DELTA5=d21-p2+p3*2/PI"

"acqt0=0"

baseopt_echo

1 ze

d11 pl12:f2

2 30m

d11 do:f2

20u pl9:f1

d1 cw:f1 ph29

4u do:f1

d11 pl1:f1

3 (p1 ph1)

DELTA2 pl0:f2

216

4u

(center (p2 ph1) (p14:sp3 ph6):f2)

4u

DELTA2 pl2:f2 UNBLKGRAD

p28 ph1

4u

(p1 ph2) (p3 ph3):f2

d0

(p2 ph7)

d0

p16:gp1*EA

d16

DELTA

(p31:sp18 ph1):f2

(p2 ph1)

DELTA5

4u

(p31:sp18 ph1):f2

2u

2u pl2:f2

(center (p1 ph1) (p3 ph4):f2)

p19:gp3

d16

DELTA3

(center (p2 ph1) (p24:sp7 ph1):f2)

DELTA3

p19:gp3

d16 pl2:f2

(center (p1 ph2) (p3 ph5):f2)

p16:gp4

d16

DELTA4 pl0:f2

(center (p2 ph1) (p14:sp3 ph1):f2)

DELTA4

p16:gp4

d16

(p1 ph1)

DELTA1

(p2 ph1)

4u

p16:gp2

d16 pl12:f2

```
  4u BLKGRAD
  go=2 ph31 cpd2:f2
  30m do:f2 mc #0 to 2
    F1EA(calgrad(EA) & calph(ph5, +180), caldel(d0, +in0) & calph(ph3, +180) & calph(ph6, +180) & calph(ph31, +180))
exit


ph1=0
ph2=1
ph3=0 2
ph4=0 0 2 2
ph5=3 3 1 1
ph6=0
ph7=0 0 2 2
ph31=2 0 0 2
ph29=0

;pl0 : 0W
;pl1 : f1 channel - power level for pulse (default)
;pl2 : f2 channel - power level for pulse (default)
;pl12: f2 channel - power level for CPD/BB decoupling
```

;sp3: f2 channel - shaped pulse (180degree inversion)

;spnam3: Crp60,0.5,20.1

;sp7: f2 channel - shaped pulse (180degree refocussing)

;spnam7: Crp60comp.4

;sp18: f2 channel - shaped pulse 180 degree (adiabatic matched sweep)

;spnam18: Crp60_xfilt.2

;p1 : f1 channel - 90 degree high power pulse

;p2 : f1 channel - 180 degree high power pulse

;p3 : f2 channel - 90 degree high power pulse

;p14: f2 channel - 180 degree shaped pulse for inversion

;   = 500usec for Crp60,0.5,20.1

;p16: homospoil/gradient pulse

;p19: gradient pulse 2   [500 usec]

;p24: f2 channel - 180 degree shaped pulse for refocussing

;   = 2msec for Crp60comp.4

;p28: f1 channel - trim pulse

;p31: f2 channel - 180 degree shaped pulse for adiabatic matched sweep

;   1730 us at 600.13 MHz, otherwise: 1730*sqrt(600/x)

;d0 : incremented delay (2D)   [3 usec]

;d1 : relaxation delay; 1-5 * T1

;d4 : 1/(4J)XH

;d11: delay for disk I/O [30 msec]

;d16: delay for homospoil/gradient recovery

;d21: set d21 according to multiplicity selection

; 1/(2J(XH)) XH, XH3 positive, XH2 negative

;d24: 1/(8J)XH for all multiplicities

; 1/(4J)XH for XH

;cnst2: = J(XH)

;cnst17: = -0.5 for Crp60comp.4

;inf1: 1/SW(X) = 2 * DW(X)

;in0: 1/(2 * SW(X)) = DW(X)

;nd0: 2

;ns: 1 * n

;ds: >= 16

;td1: number of experiments

;FnMODE: echo-antiecho

;cpd2: decoupling according to sequence defined by cpdprg2

;pcpd2: f2 channel - 90 degree pulse for decoupling sequence

;use gradient ratio: gp 1 : gp 2 : gp 3 : gp 4

; 80 : 20.1 : 11 : -5 for C-13

; 80 : 8.1 : 11 : -5 for N-15

;for z-only gradients:

;gpz1: 80%

;gpz2: 20.1% for C-13, 8.1% for N-15

;gpz3: 11%

;gpz4: -5%

;use gradient files:

;gpnam1: SMSQ10.100

;gpnam2: SMSQ10.100

;gpnam3: SMSQ10.100

;gpnam4: SMSQ10.100

;cnst17: Factor to compensate for coupling evolution during a pulse

; (usually +1). A positive factor indicates that coupling

; evolution continues during the pulse, whereas a negative

; factor is necessary if the coupling is (partially) refocussed.

;$Id: hsqcedetgpsisp2.3,v 1.11 2012/01/31 17:49:26 ber Exp $

awshsqcedetgpsisp2.3-135pr

;awshsqcedetgpsisp2.3-135pr

;avance-version (12/01/11)

;aw modification with auto calc of d21 and d24 from cnst2 (1J coupling)

;2D H-1/X correlation via double inept transfer

; using sensitivity improvement

;phase sensitive using Echo/Antiecho-TPPI gradient selection

;with decoupling during acquisition

;using trim pulses in inept transfer

;with multiplicity editing during selection step

;using shaped pulses for all 180degree pulses on f2 - channel

;for matched sweep adiabatic pulses

;with gradients in back-inept

;

;A.G. Palmer III, J. Cavanagh, P.E. Wright & M. Rance, J. Magn.

; Reson. 93, 151-170 (1991)

;L.E. Kay, P. Keifer & T. Saarinen, J. Am. Chem. Soc. 114,

; 10663-5 (1992)

;J. Schleucher, M. Schwendinger, M. Sattler, P. Schmidt, O. Schedletzky,

; S.J. Glaser, O.W. Sorensen & C. Griesinger, J. Biomol. NMR 4,

; 301-306 (1994)

;W. Willker, D. Leibfritz, R. Kerssebaum & W. Bermel, Magn. Reson.

; Chem. 31, 287-292 (1993)

;C. Zwahlen, P. Legault, S.J.F. Vincent, J. Greenblatt, R. Konrat &

; L.E. Kay, J. Am. Chem. Soc. 119 6711-6721 (1997)

;(R.D. Boyer, R. Johnson & K. Krishnamurthy,

; J. Magn. Reson. 165, 253-259 (2003))

;

;$CLASS=HighRes

;$DIM=2D

;$TYPE=

;$SUBTYPE=

;$COMMENT=

;$RECOMMEND=y

#include <Avance.incl>

#include <Grad.incl>

```
#include <Delay.incl>



"p2=p1*2"

"d4=1s/(cnst2*4)"

"d11=30m"


"d21=1s/(cnst2*2)"

"d24=1s/(cnst2*8)"



"d0=3u"


"in0=inf1/2"



"DELTA=d21-p16-d16-p2-d0*2-p3*2/PI"

"DELTA1=p16+d16-p1*0.78+de+8u"

"DELTA2=d4-larger(p2,p14)/2"

"DELTA3=d24-cnst17*p24/2-p19-d16"

"DELTA4=d4-larger(p2,p14)/2-p16-d16"
```

"DELTA5=d21-p2+p3*2/PI"

"acqt0=0"

1 ze

d11 pl12:f2

2 30m

4u do:f2

20u pl9:f1

d1 cw:f1 ph29

4u do:f1

20u pl1:f1

3 (p1 ph1)

DELTA2 pl0:f2

4u

(center (p2 ph1) (p14:sp3 ph6):f2)

4u

DELTA2 pl2:f2 UNBLKGRAD

p28 ph1

4u

(p1 ph2) (p3 ph3):f2

d0

(p2 ph7)

d0

p16:gp1*EA

d16

DELTA

(p31:sp18 ph1):f2

(p2 ph1)

DELTA5

4u

(p31:sp18 ph1):f2

2u

2u pl2:f2

(center (p1 ph1) (p3 ph4):f2)

p19:gp3

d16

DELTA3

(center (p2 ph1) (p43:sp32 ph1):f2)

DELTA3

p19:gp3

d16 pl2:f2

(center (p1 ph2) (p3 ph5):f2)

p16:gp4

d16

DELTA4 ;pl0:f2

(center (p2 ph1) (p43:sp32 ph1):f2)

DELTA4

p16:gp4

d16

(p1 ph1)

DELTA1

(p2 ph1)

4u

p16:gp2

d16 pl12:f2

4u BLKGRAD

go=2 ph31 cpd2:f2

30m do:f2 mc #0 to 2

F1EA(calgrad(EA) & calph(ph5, +180), caldel(d0, +in0) & calph(ph3, +180) & calph(ph6, +180) & calph(ph31, +180))

exit

ph1=0

ph2=1

ph3=0 2

ph4=0 0 2 2

ph5=3 3 1 1

ph6=0

ph7=0 0 2 2

ph31=2 0 0 2

ph29=0

;pl0 : 0W

;pl1 : f1 channel - power level for pulse (default)

;pl2 : f2 channel - power level for pulse (default)

;pl12: f2 channel - power level for CPD/BB decoupling

;sp3: f2 channel - shaped pulse (180degree inversion)

;spnam3: Crp60,0.5,20.1

;sp7: f2 channel - shaped pulse (180degree refocussing)

;spnam7: Crp60comp.4

;sp18: f2 channel - shaped pulse 180 degree (adiabatic matched sweep)

;spnam18: Crp60_xfilt.2

;p1 : f1 channel - 90 degree high power pulse

;p2 : f1 channel - 180 degree high power pulse

;p3 : f2 channel - 90 degree high power pulse

;p14: f2 channel - 180 degree shaped pulse for inversion

;   = 500usec for Crp60,0.5,20.1

;p16: homospoil/gradient pulse

;p19: gradient pulse 2   [500 usec]

;p24: f2 channel - 180 degree shaped pulse for refocussing

;   = 2msec for Crp60comp.4

;p28: f1 channel - trim pulse

;p31: f2 channel - 180 degree shaped pulse for adiabatic matched sweep

;   1730 us at 600.13 MHz, otherwise: 1730*sqrt(600/x)

;d0 : incremented delay (2D)   [3 usec]

;d1 : relaxation delay; 1-5 * T1

;d4 : 1/(4J)XH

;d11: delay for disk I/O   [30 msec]

;d16: delay for homospoil/gradient recovery

;d21: set d21 according to multiplicity selection

; 1/(2J(XH)) XH, XH3 positive, XH2 negative

;d24: 1/(8J)XH for all multiplicities

; 1/(4J)XH for XH

;cnst2: = J(XH)

;cnst17: = -0.5 for Crp60comp.4

;inf1: 1/SW(X) = 2 * DW(X)

;in0: 1/(2 * SW(X)) = DW(X)

;nd0: 2

;ns: 1 * n

;ds: >= 16

;td1: number of experiments

;FnMODE: echo-antiecho

;cpd2: decoupling according to sequence defined by cpdprg2

;pcpd2: f2 channel - 90 degree pulse for decoupling sequence

;use gradient ratio: gp 1 : gp 2 : gp 3 : gp 4

; 80 : 20.1 : 11 : -5 for C-13

; 80 : 8.1 : 11 : -5 for N-15

;for z-only gradients:

;gpz1: 80%

;gpz2: 20.1% for C-13, 8.1% for N-15

;gpz3: 11%

;gpz4: -5%

;use gradient files:

;gpnam1: SMSQ10.100

;gpnam2: SMSQ10.100

;gpnam3: SMSQ10.100

;gpnam4: SMSQ10.100

;cnst17: Factor to compensate for coupling evolution during a pulse

; (usually +1). A positive factor indicates that coupling

; evolution continues during the pulse, whereas a negative

; factor is necessary if the coupling is (partially) refocussed.

;$Id: hsqcedetgpsisp2.3,v 1.11 2012/01/31 17:49:26 ber Exp $

awhmbcgplpndqfpr

```
;hmbcgplpndqf

;avance-version (12/01/11)

;HMBC

;2D H-1/X correlation via heteronuclear zero and double quantum

;   coherence

;optimized on long range couplings

;with low-pass J-filter to suppress one-bond correlations

;no decoupling during acquisition

;using gradient pulses for selection

;

;$CLASS=HighRes

;$DIM=2D

;$TYPE=

;$SUBTYPE=

;$COMMENT=

;$RECOMMEND=y



#include <Avance.incl>

#include <Grad.incl>
```

"p2=p1*2"

"d2=1s/(cnst2*2)"

"d6=1s/(cnst13*2)"

"d0=3u"

"in0=inf1/2"

1 ze

2 30m

  20u pl9:f1

        d1 cw:f1 ph29

  4u do:f1

  20u pl1:f1

3 p1 ph1

234

```
  d2
  p3:f2 ph3
  d6
  p3:f2 ph4
  d0
  50u UNBLKGRAD
  p16:gp1
  d16
  p2 ph2
  50u
  p16:gp2
  d16
  d0
  p3:f2 ph5
  4u
  p16:gp3
  d16
  4u BLKGRAD
  go=2 ph31
  30m mc #0 to 2 F1QF(caldel(d0, +in0))
exit
```

ph1=0

ph2=0 0 0 0 2 2 2 2

ph3=0 0 2 2

ph4=0 2

ph5=0 0 0 0 0 0 0 0 2 2 2 2 2 2 2 2

ph29=0

ph31=0 2 0 2 0 2 0 2 2 0 2 0 2 0 2 0

;pl1 : f1 channel - power level for pulse (default)

;pl2 : f2 channel - power level for pulse (default)

;pl9 : f1 channel - presaturation power

;p1 : f1 channel - 90 degree high power pulse

;p2 : f1 channel - 180 degree high power pulse

;p3 : f2 channel - 90 degree high power pulse

;p16: homospoil/gradient pulse

;d0 : incremented delay (2D) [3 usec]

;d1 : relaxation delay; 1-5 * T1

;d2 : 1/(2J)XH

;d6 : delay for evolution of long range couplings

;d16: delay for homospoil/gradient recovery

;cnst2: = J(XH)

;cnst13: = J(XH) long range

;inf1: 1/SW(X) = 2 * DW(X)

;in0: 1/(2 * SW(X)) = DW(X)

;nd0: 2

;ns: 2 * n

;ds: 16

;td1: number of experiments

;FnMODE: QF

;use gradient ratio: gp 1 : gp 2 : gp 3

; 50 : 30 : 40.1 for C-13

; 70 : 30 : 50.1 for N-15

;for z-only gradients:

;gpz1: 50% for C-13, 70% for N-15

;gpz2: 30%

;gpz3: 40.1% for C-13, 50.1% for N-15

;use gradient files:

;gpnam1: SMSQ10.100

;gpnam2: SMSQ10.100

;gpnam3: SMSQ10.100

;$Id: hmbcgplpndqf,v 1.7 2012/01/31 17:49:23 ber Exp $

awshmbcq5

;awshmbcq5

;with 2 x 90 degree Q5 pulses

;avance-version (12/01/11)

;HMBC

;2D H-1/X correlation via heteronuclear zero and double quantum

; coherence

;optimized on long range couplings

;with low-pass J-filter to suppress one-bond correlations

;no decoupling during acquisition

;using gradient pulses for selection

;

;$CLASS=HighRes

;$DIM=2D

;$TYPE=

;$SUBTYPE=

;$COMMENT=

;$RECOMMEND=y

prosol relations=<triple2>

#include <Avance.incl>

#include <Grad.incl>

"p2=p1*2"

"d2=1s/(cnst2*2)"

"d6=1s/(cnst13*2)"

"d0=3u"

"in0=inf1/2"

1 ze

2 d1

3 p1 ph1

d2

(p3 ph3):f2

d6

(p35:sp27 ph4):f2

d0

50u UNBLKGRAD

p16:gp1

d16

p2 ph2

50u

p16:gp2

240

```
  d16
  d0
  (p35:sp27 ph5):f2
  4u
  p16:gp3
  d16
  4u BLKGRAD
  go=2 ph31
  d1 mc #0 to 2 F1QF(caldel(d0, +in0))
exit


ph1=0
ph2=0 0 0 0 2 2 2 2
ph3=0 0 2 2
ph4=0 2
ph5=0 0 0 0 0 0 0 0 2 2 2 2 2 2 2 2
ph31=0 2 0 2 0 2 0 2 2 0 2 0 2 0 2 0


;pl1 : f1 channel - power level for pulse (default)
```

;pl2 : f2 channel - power level for pulse (default)

;p1 : f1 channel - 90 degree high power pulse

;p2 : f1 channel - 180 degree high power pulse

;p3 : f2 channel - 90 degree high power pulse

;p16: homospoil/gradient pulse

;d0 : incremented delay (2D) [3 usec]

;d1 : relaxation delay; 1-5 * T1

;d2 : 1/(2J)XH

;d6 : delay for evolution of long range couplings

;d16: delay for homospoil/gradient recovery

;cnst2: = J(XH)

;cnst13: = J(XH) long range

;inf1: 1/SW(X) = 2 * DW(X)

;in0: 1/(2 * SW(X)) = DW(X)

;nd0: 2

;ns: 2 * n

;ds: 16

;td1: number of experiments

;FnMODE: QF

;use gradient ratio: gp 1 : gp 2 : gp 3

; 50 : 30 : 40.1 for C-13

; 70 : 30 : 50.1 for N-15

;for z-only gradients:

;gpz1: 50% for C-13, 70% for N-15

;gpz2: 30%

;gpz3: 40.1% for C-13, 50.1% for N-15

;use gradient files:

;gpnam1: SMSQ10.100

;gpnam2: SMSQ10.100

;gpnam3: SMSQ10.100

;$Id: hmbcgplpndqf,v 1.7 2012/01/31 17:49:23 ber Exp $

awshmbcctetgpl2nd.m

;awshmbcctetgpl2nd.m

;

;using harder semiselective pulses for a wider band width

; ex JCM 2016-03-04

;

;avance-version (12/01/11)

;bandselective CT-HMBC

;2D H-1/X correlation via heteronuclear zero and double quantum

;   coherence

;phase sensitive using Echo/Antiecho gradient selection

;with two-fold low-pass J-filter to suppress one-bond correlations

;no decoupling during acquisition

;constant time version

;

;T.D.W. Claridge & I.Perez-Victoria,

;   Org. Biomol. Chem. 1, 3632-3534 (2003)

;D.O. Cicero, G. Barbato & R. Bazzo, J. Magn. Reson. 148,

;   209-213 (2001)

;

;$CLASS=HighRes

;$DIM=2D

;$TYPE=

;$SUBTYPE=

;$COMMENT=

```
#include <Avance.incl>

#include <Grad.incl>

#include <Delay.incl>


prosol relations=<triple2>


"cnst30=(1-sfo2/sfo1)/(1+sfo2/sfo1)"


define list<gradient> EA1 = { 1.000 -cnst30}

define list<gradient> EA2 = { -cnst30 1.000}




"p2=p1*2"

"d6=1s/(cnst13*2)"




"in0=inf1/2"


"in20=in0/2"
```

"d0=3u"

"d20=in20*td1/2+4u"

"DELTA1=1s/(2 * cnst6)-p16-d16"

"DELTA2=1s/(2 * cnst7)-p16-d16"

"DELTA3=d6-p16-d16-4u"

"DELTA4=p2+d0*2"

1 ze

2 d1

3 (p1 ph1)

DELTA1 UNBLKGRAD

p16:gp3

d16 pl2:f2

(p3 ph3):f2

DELTA2

p16:gp4

d16

(p3 ph3):f2

4u

p16:gp5

d16

DELTA3

d20

4u

(p14:sp3 ph1):f2

d20

4u pl2:f2

(p3 ph4):f2

d0

(p2 ph2)

d0

p16:gp1*EA1

d16

(p33:sp23 ph5):f2

DELTA4

p16:gp1*EA2

d16 pl2:f2

(p3 ph5):f2

```
  d20
  (p14:sp3 ph1):f2
  d20
  4u BLKGRAD
  go=2 ph31
  d1 mc #0 to 2
    F1EA(calgrad(EA1) & calgrad(EA2), caldel(d0, +in0) & caldel(d20, -in20) & calph(ph4, +180) & calph(ph31, +180))
exit


ph1=0
ph2=0 0 0 0 2 2 2 2
ph3=0 0 2 2
ph4=0 2
ph5=0 0 0 0 0 0 0 0 2 2 2 2 2 2 2 2
ph31=0 2 0 2 0 2 0 2 2 0 2 0 2 0 2 0


;pl1 : f1 channel - power level for pulse (default)
;pl2 : f2 channel - power level for pulse (default)
;sp3 : f2 channel - shaped pulse (180degree inversion)
```

;spnam3 : Crp60,0.5,20.1

;sp32: f2 channel - shaped pulse (180degree refocussing)

;spnam32: Q3.1000 (bandselective pulse)

;p1 : f1 channel - 90 degree high power pulse

;p2 : f1 channel - 180 degree high power pulse

;p3 : f2 channel - 90 degree high power pulse

;p14: f2 channel - 180 degree shaped pulse for inversion

;   = 500usec for Crp60,0.5,20.1

;p16: homospoil/gradient pulse   [1 msec]

;p43: f2 channel - 180 degree shaped pulse for refocussing (bandselective)

;d0 : incremented delay (2D)   [3 usec]

;d1 : relaxation delay; 1-5 * T1

;d6 : delay for evolution of long range couplings (1/2Jlr)

;d16: delay for homospoil/gradient recovery

;d20: decremented delay (2D) = in20*td1/2+4u

;cnst6: = 1J(XH)min

;cnst7: = 1J(XH)max

;cnst13: = J(XH) long range

;inf1: 1/SW(X) = 2 * DW(X)

;in0: 1/(2 * SW(X)) = DW(X)

;nd0: 2

;in20: = in0/2

;ns: 2 * n

;ds: 16

;td1: number of experiments

;FnMODE: echo-antiecho

;use gradient ratio: gp 1 : gp 3 : gp 4 : gp 5

; 80 : 15 : -10 : -5

;for z-only gradients:

;gpz1: 80%

;gpz3: 15%

;gpz4: -10%

;gpz5: -5%

;use gradient files:

;gpnam1: SMSQ10.100

;gpnam3: SMSQ10.100

;gpnam4: SMSQ10.100

;gpnam5: SMSQ10.100

;Processing

;PH_mod(F1): pk (or no)

;use xfb and xf2m

;$Id: shmbcctetgpl2nd,v 1.2 2012/01/31 17:49:28 ber Exp $

hsqcdietgpsisp

;hsqcdietgpsisp

;avance-version (12/01/11)

;HSQC-TOCSY

;2D H-1/X correlation via double inept transfer

; using sensitivity improvement and DIPSI2

; for homonuclear Hartman-Hahn mixing

;phase sensitive using Echo/Antiecho-TPPI gradient selection

;with decoupling during acquisition - using f2 (and f3)

```
;using trim pulses in inept transfer
;
;$CLASS=HighRes
;$DIM=2D
;$TYPE=
;$SUBTYPE=
;$COMMENT=



#include <Avance.incl>
#include <Grad.incl>
#include <Delay.incl>



"p2=p1*2"
"p4=p3*2"
"d11=30m"
"d4=1s/(cnst2*4)"

#   ifdef LABEL_CN
"p22=p21*2"
```

```
#   else
#   endif /*LABEL_CN*/



"d0=3u"


"in0=inf1/2"



"FACTOR1=(d9/(p6*115.112))/2"
"l1=FACTOR1*2"



"DELTA1=p16+d16-p1*0.78+de+8u"
"DELTA2=d4-p14/2"

#   ifdef LABEL_CN
"DELTA=p16+d16+larger(p2,p22)+d0*2"
#   else
"DELTA=p16+d16+p2+d0*2"
#   endif /*LABEL_CN*/
```

"acqt0=0"

baseopt_echo

1 ze

ifdef LABEL_CN

  d11 pl12:f2 pl16:f3

2 d1 do:f2 do:f3

  10u pl0:f2 pl3:f3

else

  d11 pl12:f2

2 d1 do:f2

  10u pl0:f2

endif /*LABEL_CN*/

3 (p1 ph1)

  DELTA2

  4u

254

```
  (center (p2 ph1) (p14:sp3 ph6):f2 )
  4u
  DELTA2 pl2:f2 UNBLKGRAD
  p28 ph1
  4u
  (p1 ph2) (p3 ph3):f2
  d0

#   ifdef LABEL_CN
  (center (p2 ph7) (p22 ph1):f3 )
#   else
  (p2 ph7)
#   endif /*LABEL_CN*/

  d0
  p16:gp1*EA
  d16
  (p4 ph4):f2
  DELTA
  (center (p1 ph1) (p3 ph4):f2 )
  d24
```

(center (p2 ph1) (p4 ph1):f2)

d24

(center (p1 ph2) (p3 ph5):f2)

DELTA2 pl0:f2

(center (p2 ph1) (p14:sp3 ph1):f2)

DELTA2 pl10:f1

;begin DIPSI2

4 p6*3.556 ph22

p6*4.556 ph24

p6*3.222 ph22

p6*3.167 ph24

p6*0.333 ph22

p6*2.722 ph24

p6*4.167 ph22

p6*2.944 ph24

p6*4.111 ph22

p6*3.556 ph24

p6*4.556 ph22

p6*3.222 ph24

p6*3.167 ph22

p6*0.333 ph24

p6*2.722 ph22

p6*4.167 ph24

p6*2.944 ph22

p6*4.111 ph24

p6*3.556 ph24

p6*4.556 ph22

p6*3.222 ph24

p6*3.167 ph22

p6*0.333 ph24

p6*2.722 ph22

p6*4.167 ph24

p6*2.944 ph22

p6*4.111 ph24

p6*3.556 ph22

p6*4.556 ph24

p6*3.222 ph22

p6*3.167 ph24

p6*0.333 ph22

p6*2.722 ph24

p6*4.167 ph22

p6*2.944 ph24

p6*4.111 ph22

lo to 4 times l1

;end DIPSI2

4u pl1:f1

(p1 ph1)

DELTA1

(p2 ph1)

4u

p16:gp2

ifdef LABEL_CN

d16 pl12:f2 pl16:f3

4u BLKGRAD

go=2 ph31 cpd2:f2 cpd3:f3

d1 do:f2 do:f3 mc #0 to 2

else

```
  d16 pl12:f2
  4u BLKGRAD
  go=2 ph31 cpd2:f2
  d1 do:f2 mc #0 to 2
#   endif /*LABEL_CN*/

    F1EA(calgrad(EA) & calph(ph5, +180), caldel(d0, +in0) & calph(ph3, +180) & calph(ph6, +180) & calph(ph31, +180))
exit

ph1=0
ph2=1
ph3=0 2
ph4=0 0 2 2
ph5=1 1 3 3
ph6=0
ph7=0 0 2 2
ph22=3
ph24=1
ph31=0 2 2 0
```

;pl0 : 0W

;pl1 : f1 channel - power level for pulse (default)

;pl2 : f2 channel - power level for pulse (default)

;pl3 : f3 channel - power level for pulse (default)

;pl10: f1 channel - power level for TOCSY-spinlock

;pl12: f2 channel - power level for CPD/BB decoupling

;pl16: f3 channel - power level for CPD/BB decoupling

;sp3: f2 channel - shaped pulse 180 degree

;p1 : f1 channel - 90 degree high power pulse

;p2 : f1 channel - 180 degree high power pulse

;p3 : f2 channel - 90 degree high power pulse

;p4 : f2 channel - 180 degree high power pulse

;p6 : f1 channel - 90 degree low power pulse

;p14: f2 channel - 180 degree shaped pulse for inversion

;p16: homospoil/gradient pulse [1 msec]

;p22: f3 channel - 180 degree high power pulse

;p28: f1 channel - trim pulse [1 msec]

;d0 : incremented delay (2D) [3 usec]

;d1 : relaxation delay; 1-5 * T1

;d4 : 1/(4J(XH))

;d9 : TOCSY mixing time

;d11: delay for disk I/O [30 msec]

;d16: delay for homospoil/gradient recovery

;d24: 1/(8J)XH for all multiplicities

; 1/(4J)XH for XH

;cnst2: = J(XH)

;l1: loop for DIPSI cycle: ((p6*115.112) * l1) = mixing time

;inf1: 1/SW(X) = 2 * DW(X)

;in0: 1/(2 * SW(X)) = DW(X)

;nd0: 2

;ns: 1 * n

;ds: >= 16

;td1: number of experiments

;FnMODE: echo-antiecho

;cpd2: decoupling according to sequence defined by cpdprg2

;cpd3: decoupling according to sequence defined by cpdprg3

;pcpd2: f2 channel - 90 degree pulse for decoupling sequence

;pcpd3: f3 channel - 90 degree pulse for decoupling sequence

;use gradient ratio: gp 1 : gp 2

; 80 : 20.1 for C-13

; 80 : 8.1 for N-15

;for z-only gradients:

;gpz1: 80%

;gpz2: 20.1% for C-13, 8.1% for N-15

;use gradient files:

;gpnam1: SMSQ10.100

;gpnam2: SMSQ10.100

;preprocessor-flags-start

;LABEL_CN: for C-13 and N-15 labeled samples start experiment with

; option -DLABEL_CN (eda: ZGOPTNS)

;preprocessor-flags-end

;$Id: hsqcdietgpsisp,v 1.10 2012/01/31 17:49:26 ber Exp $

awseltocsyprf2

;awseltocsyprf2

; With CW presaturation on f2

;avance-version (12/01/11)

;1D homonuclear Hartman-Hahn transfer using

;   MLEV17 sequence for mixing

;   using selective refocussing with a shaped pulse

;

;H. Kessler, H. Oschkinat, C. Griesinger & W. Bermel,

;   J. Magn. Reson. 70, 106 (1986)

;J. Stonehouse, P. Adell, J. Keeler & A.J. Shaka, J. Am. Chem. Soc 116,

;   6037 (1994)

;K. Stott, J. Stonehouse, J. Keeler, T.L. Hwang & A.J. Shaka,

;   J. Am. Chem. Soc 117, 4199-4200 (1995)

;A. Bax & D.G. Davis, J. Magn. Reson. 65, 355-360 (1985)

;

;$CLASS=HighRes

;$DIM=1D

;$TYPE=

;$SUBTYPE=

```
;$COMMENT=



#include <Avance.incl>

#include <Grad.incl>

#include <Delay.incl>



"p5=p6*.667"

"p7=p6*2"



"SCALEF=p7*2/p5"

"FACTOR1=((d9-p17*2)/(p6*64+p5))/SCALEF"

"l1=FACTOR1*SCALEF"



#   ifdef CALC_SPOFFS

"spoff2=bf1*(cnst21/1000000)-o1"

#   else

#   endif /*CALC_SPOFFS*/
```

1 ze

2 30m

20u pl1:f1 BLKGRAD

30m pl9:f2

d1 cw:f2 ph29

4u do:f2

50u UNBLKGRAD

(p1 ph1):f1

3u

p16:gp1

d16 pl0:f1

p12:sp2:f1 ph2:r

3u

p16:gp1

d16 pl10:f1

(p17 ph26)

;begin MLEV17

4 (p6 ph22 p7 ph23 p6 ph22)

(p6 ph24 p7 ph25 p6 ph24)

(p6 ph24 p7 ph25 p6 ph24)

(p6 ph22 p7 ph23 p6 ph22)

(p6 ph24 p7 ph25 p6 ph24)

(p6 ph24 p7 ph25 p6 ph24)

(p6 ph22 p7 ph23 p6 ph22)

(p6 ph22 p7 ph23 p6 ph22)

(p6 ph24 p7 ph25 p6 ph24)

(p6 ph22 p7 ph23 p6 ph22)

(p6 ph22 p7 ph23 p6 ph22)

(p6 ph24 p7 ph25 p6 ph24)

(p6 ph22 p7 ph23 p6 ph22)

(p6 ph22 p7 ph23 p6 ph22)

(p6 ph24 p7 ph25 p6 ph24)

(p6 ph24 p7 ph25 p6 ph24)

(p5 ph23)

lo to 4 times l1

;end MLEV17

(p17 ph26)

```
  go=2 ph31
  30m mc #0 to 2 F0(zd)
  20u BLKGRAD
exit


ph1=0 2
ph2=0 0 1 1 2 2 3 3
ph22=0
ph23=1
ph24=2
ph25=3
ph26=1
ph29=0
ph31=0 2 2 0


;pl0 : 0W
;pl1 : f1 channel - power level for pulse (default)
;pl9 : f2 presaturation power
;pl10: f1 channel - power level for TOCSY-spinlock
```

;sp2: f1 channel - shaped pulse

;p1 : f1 channel - 90 degree high power pulse

;p5 : f1 channel - 60 degree low power pulse

;p6 : f1 channel - 90 degree low power pulse

;p7 : f1 channel - 180 degree low power pulse

;p12: f1 channel - 180 degree shaped pulse

;p16: homospoil/gradient pulse [1 msec]

;p17: f1 channel - trim pulse [2.5 msec]

;d1 : relaxation delay; 1-5 * T1

;d9 : TOCSY mixing time

;d16: delay for homospoil/gradient recovery

;cnst21: chemical shift for selective pulse (offset, in ppm)

;l1: loop for MLEV cycle: (((p6*64) + p5) * l1) + (p17*2) = mixing time

;ns: 2 * n, total number of scans: NS * TD0

;ds: 4

;phcor 2 : phasedifference between power levels sp1 and pl1

;choose p12 according to desired selectivity

;the flip-angle is determined by the amplitude

;set O1 on resonance on the multiplet to be excited or use spoffs

;use gradient ratio: gp 1

; 15

;for z-only gradients:

;gpz1: 15%

;use gradient files:

;gpnam1: SMSQ10.100

;$Id: selmlgp,v 1.18 2012/01/31 17:49:28 ber Exp $

awselroesyprf2

;awselroesy2prf2

; With CW presaturation on f2

;avance-version (12/01/11)

```
;1D ROESY with cw spinlock for mixing
;   using selective refocussing with a shaped pulse
;
;H. Kessler, H. Oschkinat, C. Griesinger & W. Bermel,
;   J. Magn. Reson. 70, 106 (1986)
;J. Stonehouse, P. Adell, J. Keeler & A.J. Shaka, J. Am. Chem. Soc 116,
;   6037 (1994)
;K. Stott, J. Stonehouse, J. Keeler, T.L. Hwang & A.J. Shaka,
;   J. Am. Chem. Soc 117, 4199-4200 (1995)
;A. Bax & D.G. Davis, J. Magn. Reson 63, 207-213 (1985)
;T.-L. Hwang & A.J. Shaka, J. Am. Chem. Soc. 114, 3157-3159 (1992)
;
;$CLASS=HighRes
;$DIM=1D
;$TYPE=
;$SUBTYPE=
;$COMMENT=



#include <Avance.incl>
#include <Grad.incl>
```

"l4=p15/(p25*2)"

ifdef CALC_SPOFFS

"spoff2=bf1*(cnst21/1000000)-o1"

else

endif /*CALC_SPOFFS*/

1 ze

2 30m

20u pl1:f1 BLKGRAD

30m pl9:f2

d1 cw:f2 ph29

4u do:f2

50u UNBLKGRAD

(p1 ph1):f1

```
  3u
  p16:gp1
  d16 pl0:f1
  p12:sp2:f1 ph2:r
  3u
  p16:gp1
  d16 pl27:f1
4 (p25 ph3):f1
  (p25 ph4):f1
  lo to 4 times l4
  go=2 ph31
  30m mc #0 to 2 F0(zd)
  20u BLKGRAD
exit


ph1=0 2
ph2=0 0 1 1 2 2 3 3
ph3=0
ph4=2
ph29=0
```

ph31=0 2 2 0

;pl0 : 0W

;pl1 : f1 channel - power level for pulse (default)

;pl9 : f2 presaturation power

;pl27: f1 channel - power level for pulsed ROESY-spinlock

;sp2: f1 channel - shaped pulse

;p1 : f1 channel - 90 degree high power pulse

;p12: f1 channel - 180 degree shaped pulse

;p15: f1 channel - pulse for ROESY spinlock

;p16: homospoil/gradient pulse [1 msec]

;p25: f1 channel - 180 degree pulse at pl27

;d1 : relaxation delay; 1-5 * T1

;d16: delay for homospoil/gradient recovery

;cnst21: chemical shift for selective pulse (offset, in ppm)

;l4: loop for spinlock = p15 / p25*2

;ns: 2 * n, total number of scans: NS * TD0

;ds: 4

;phcor 2 : phasedifference between power levels sp1 and pl1

;choose p12 according to desired selectivity

;the flip-angle is determined by the amplitude

;set O1 on resonance on the multiplet to be excited or use spoffs

;use gradient ratio: gp 1

; 15

;for z-only gradients:

;gpz1: 15%

;use gradient files:

;gpnam1: SMSQ10.100

;$Id: selrogp.2,v 1.16 2012/01/31 17:49:28 ber Exp $

Appendix B – Supplementary spectra

Sample #1

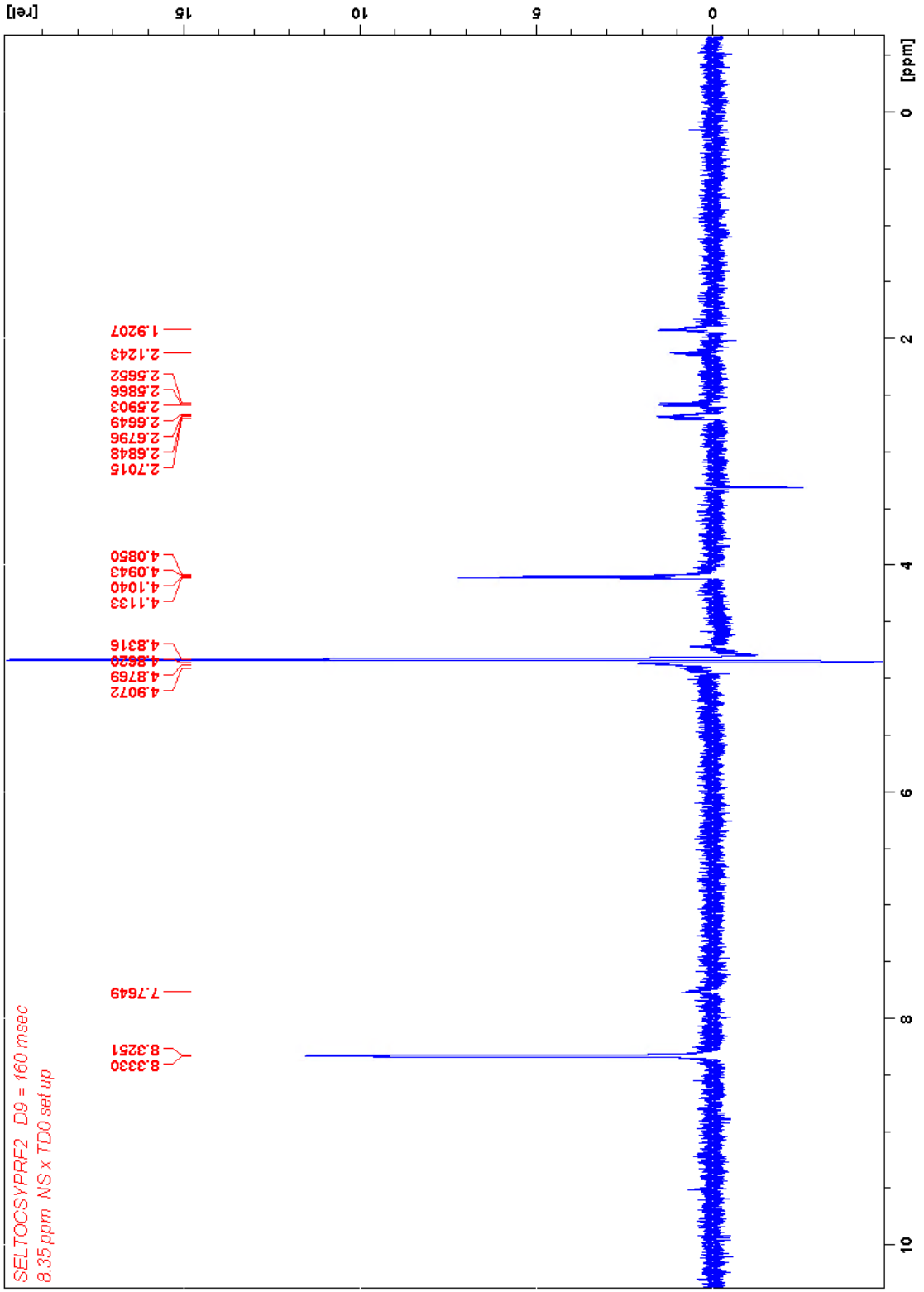

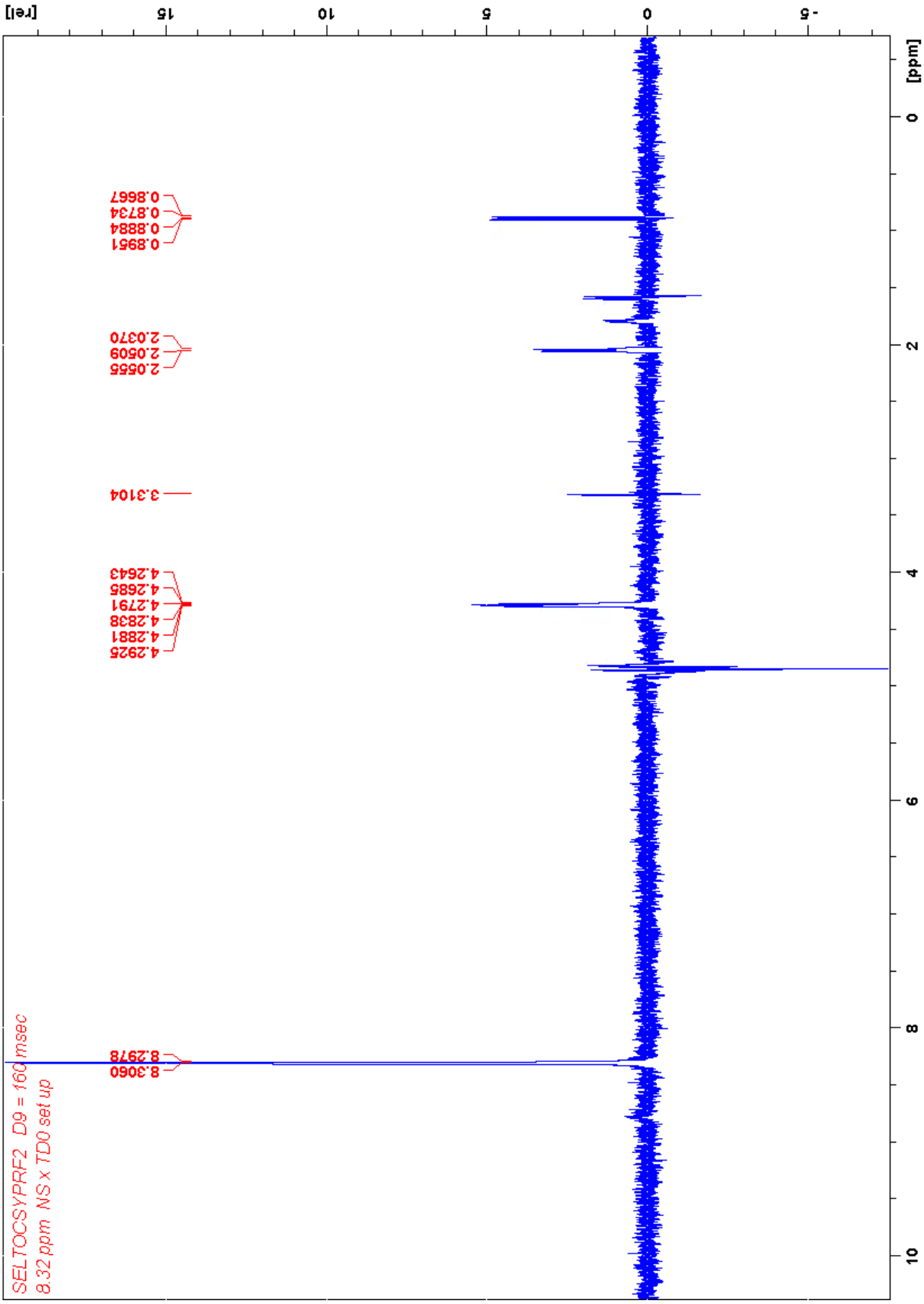
[rel]
15
10
5
0
-5
[ppm]
0
2
4
6
8
10
8.3060
8.2978
4.2925
4.2881
4.2838
4.2791
4.2685
4.2643
3.3104
2.0555
2.0509
2.0370
0.8951
0.8884
0.8734
0.8667
SELTOCSYPRF2 D9 = 160 msec
8.32 ppm NS x TD0 set up

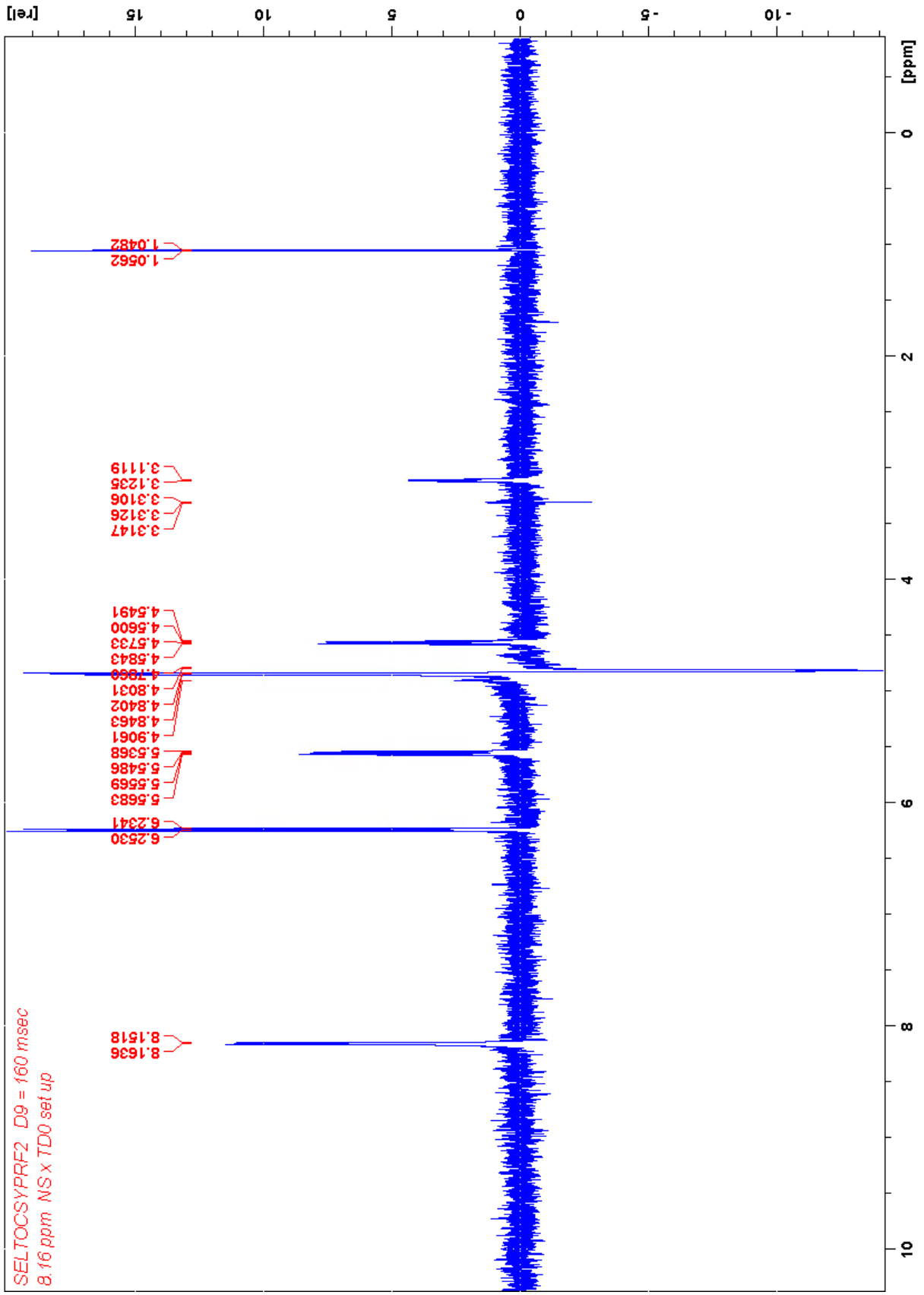
SELTOCSYPRF2 D9 = 160 msec
8.16 ppm NS x TD0 set up
[rel]
15
10
5
0
-5
-10
[ppm]
0
2
4
6
8
10
1.0562
1.0482
3.1119
3.1235
3.3106
3.3126
3.3147
4.5491
4.5600
4.5733
4.5843
4.7960
4.8031
4.8402
4.8463
4.9061
5.5368
5.5486
5.5569
5.5683
6.2341
6.2530
8.1536
8.1618

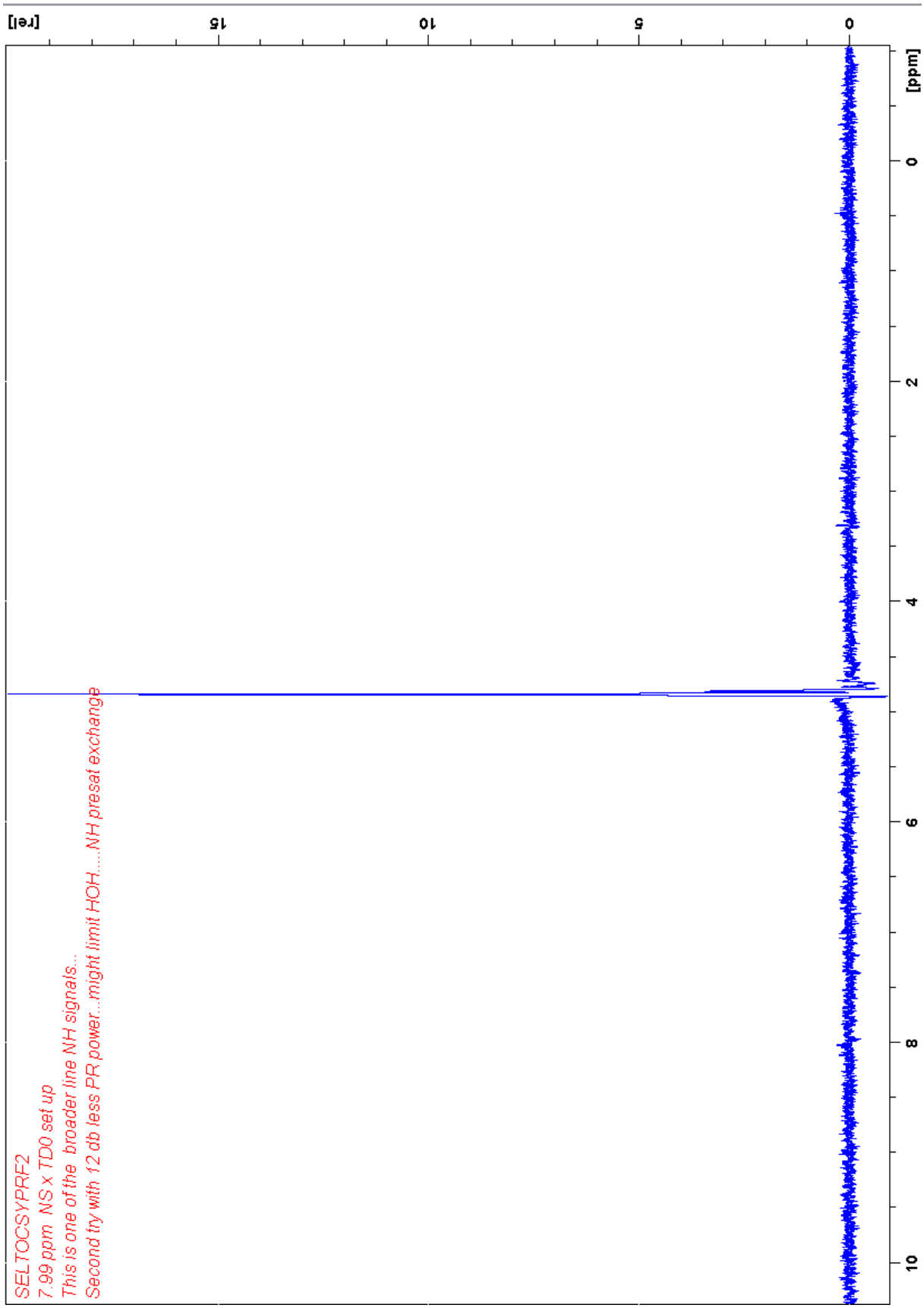
SELTOCSYPRF2
7.99 ppm NS x TD0 set up
This is one of the broader line NH signals...
Second try with 12 db less PR power...might limit HOH.....NH presat exchange
[rel]
15
10
5
0
[ppm]
0
2
4
6
8
10

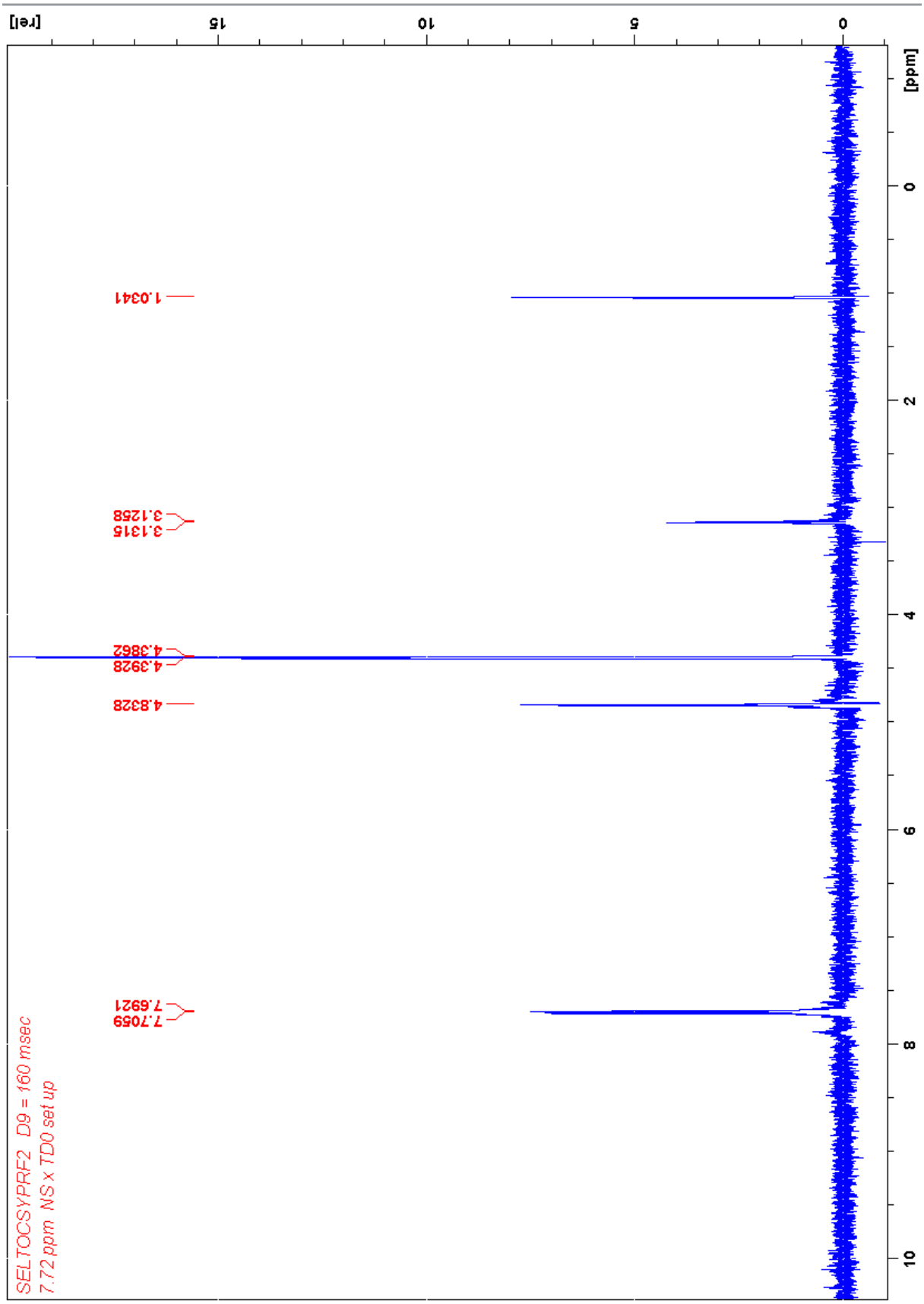
SELTOCSYPRF2 D9 = 160 msec
7.72 ppm NS x TD0 set up
7.7059
7.6921
4.8328
4.3928
4.3862
3.1315
3.1258
1.0341
[rel]
[ppm]

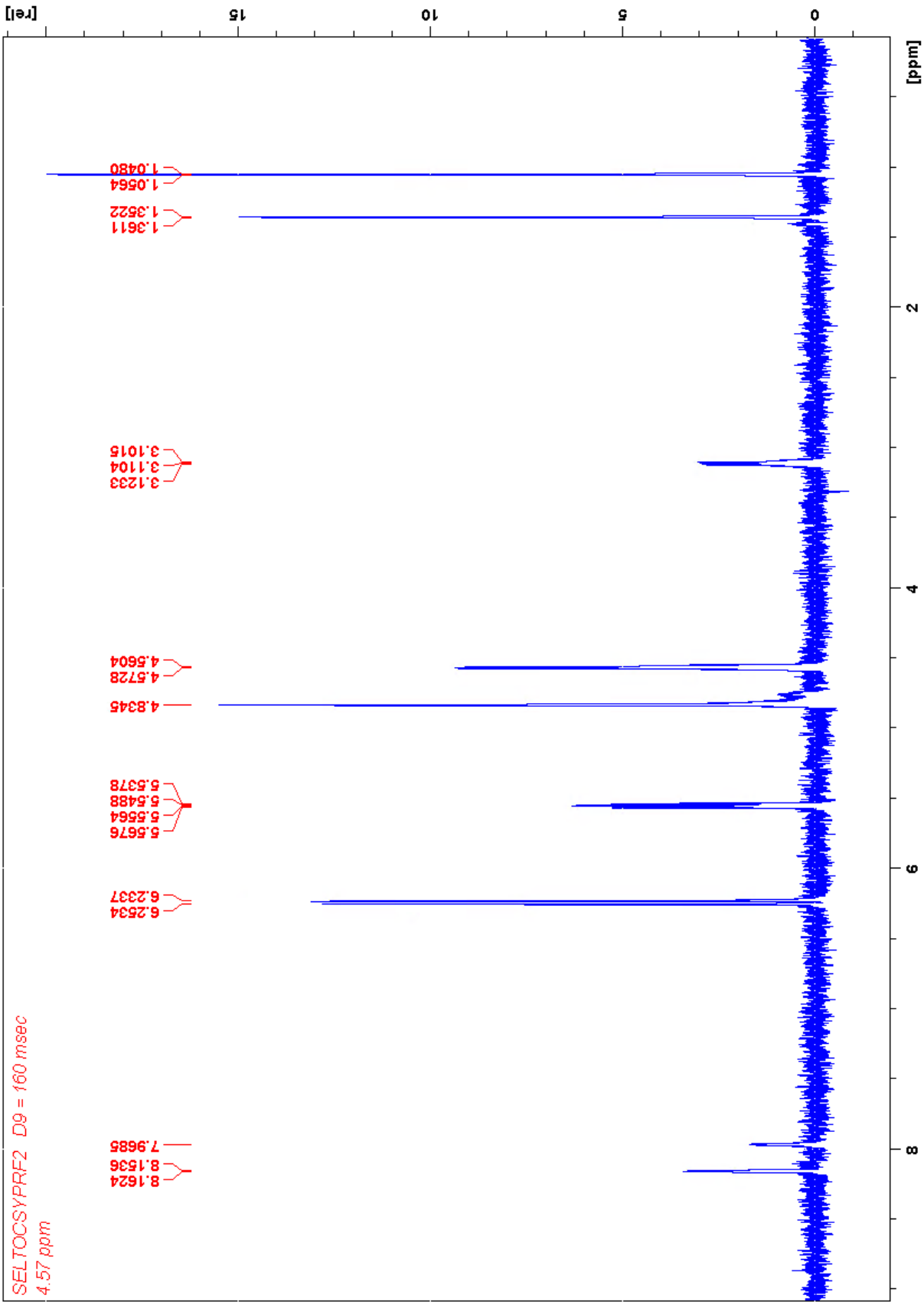
[rel]
15
10
5
0
[ppm]
2
4
6
8
1.0480
1.0564
1.3522
1.3611
3.1015
3.1104
3.1233
4.5604
4.5728
4.8345
5.5378
5.5488
5.5564
5.5676
6.2337
6.2534
7.9685
8.1536
8.1624
SELTOCSYPRF2 D9 = 160 msec
4.57 ppm

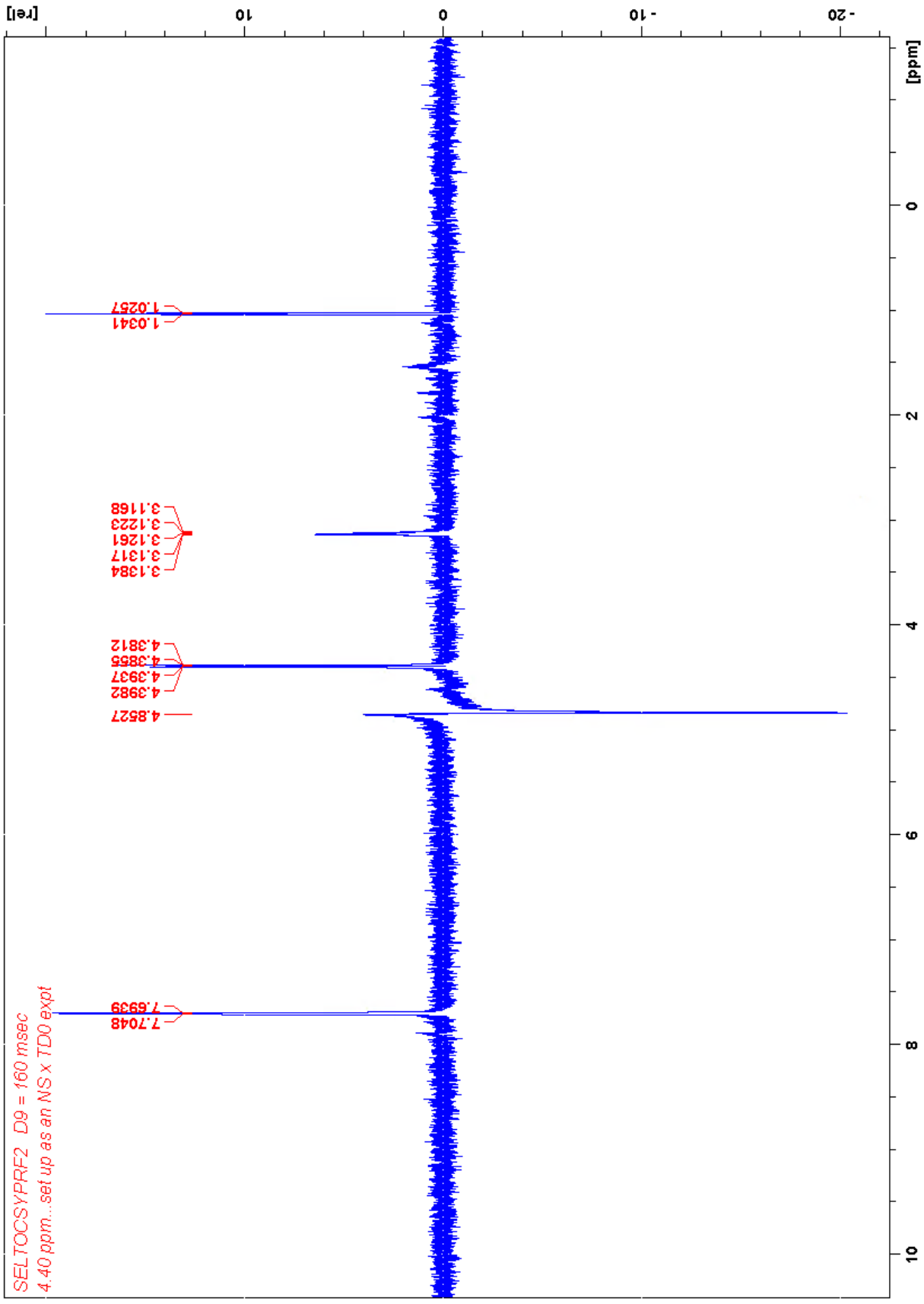
SELTOCSYPRF2 D9 = 160 msec
4.40 ppm...set up as an NS x TD0 expt
7.7048
7.6939
4.8527
4.3982
4.3937
4.3855
4.3812
3.1384
3.1317
3.1261
3.1223
3.1168
1.0341
1.0257
[rel]
10
0
-10
-20
[ppm]
0
2
4
6
8
10

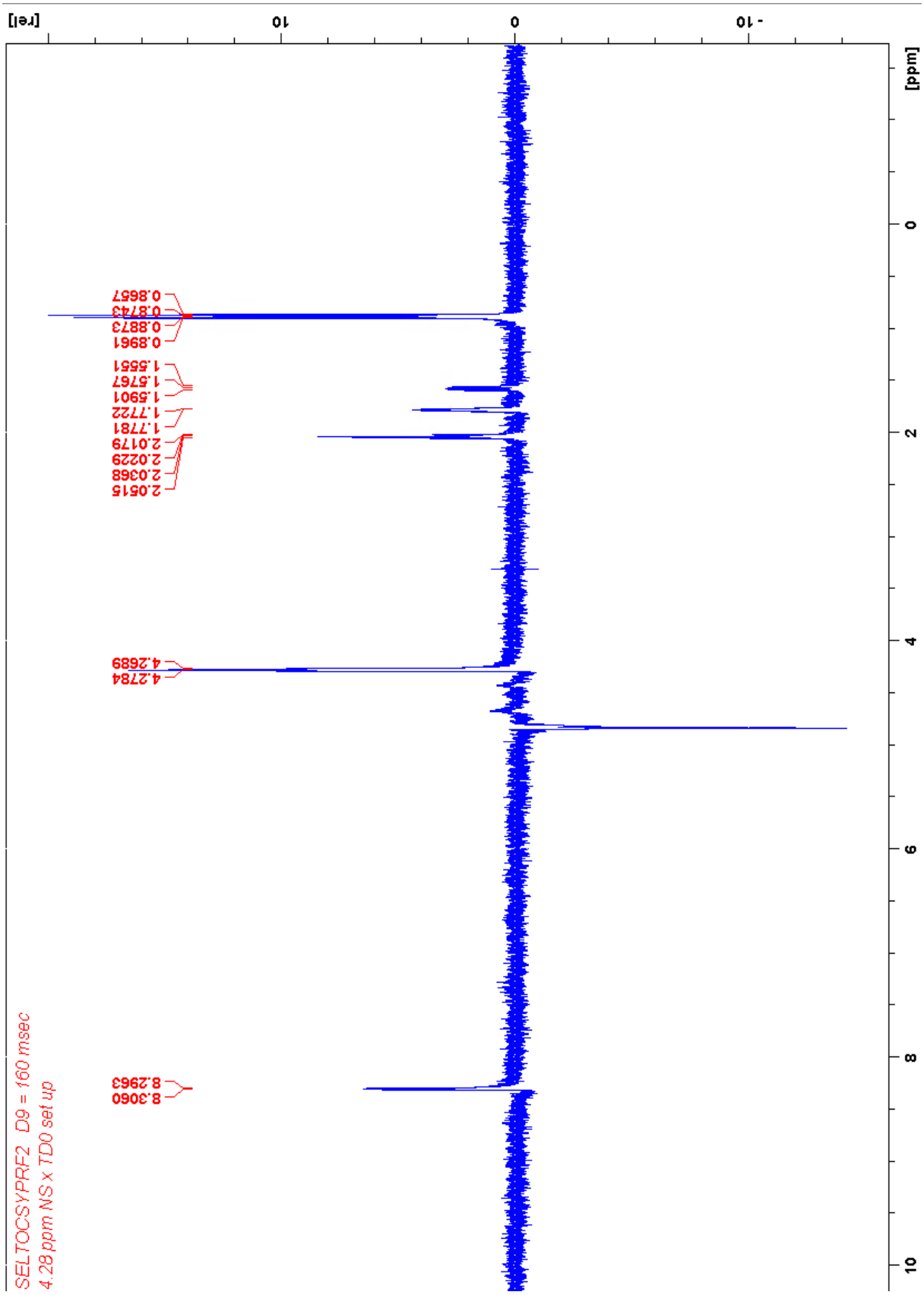
[rel]
10
0
-10
[ppm]
0
2
4
6
8
10
0.8657
0.8743
0.8873
0.8961
1.5551
1.5767
1.5901
1.7722
1.7781
2.0179
2.0229
2.0368
2.0515
4.2784
4.2689
8.3060
8.2963
SELTOCSYPRF2 D9 = 160 msec
4.28 ppm NS x TD0 set up

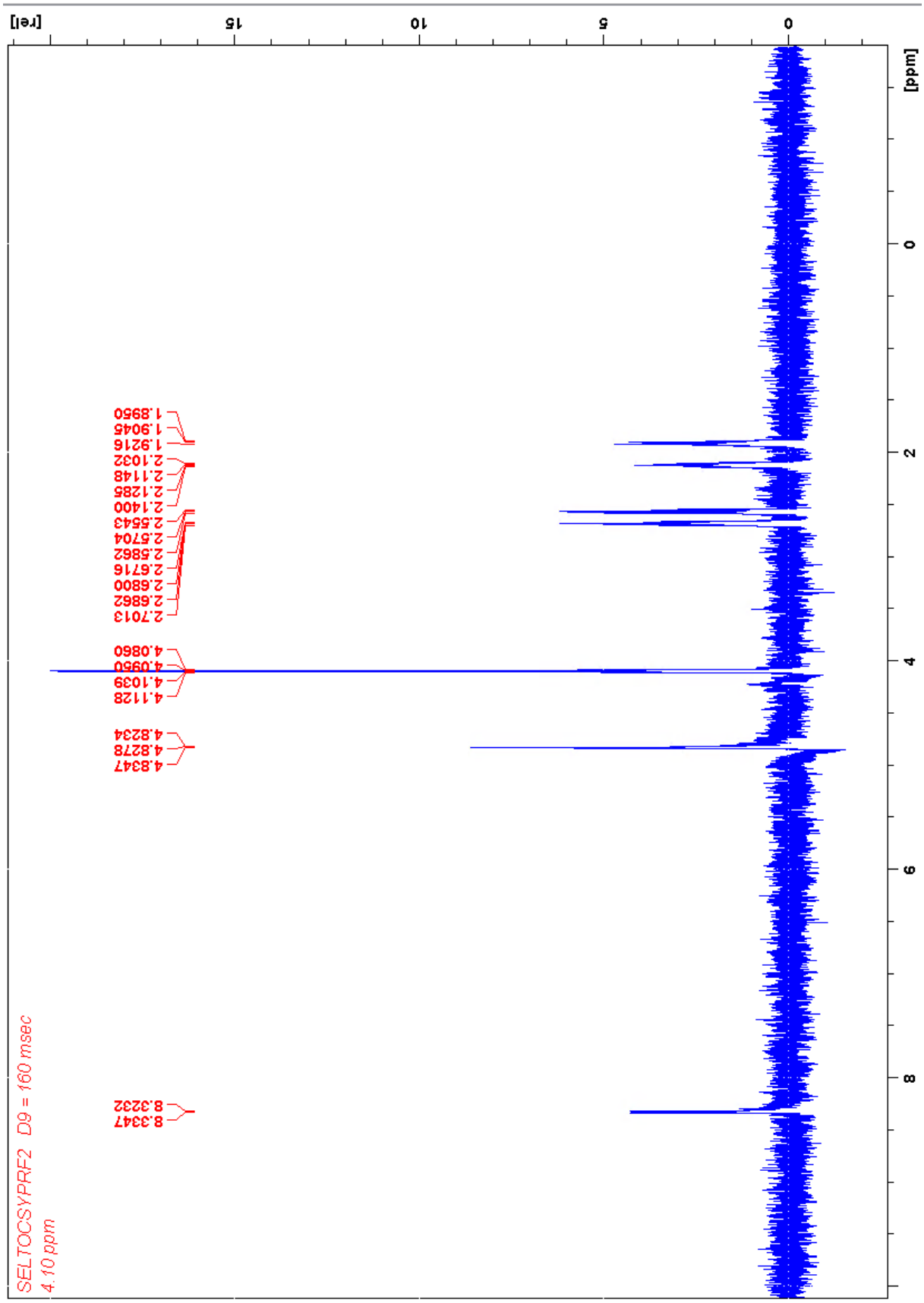
SELTOCSYPRF2 D9 = 160 msec
4.10 ppm
8.3347
8.3232
4.8347
4.8278
4.8234
4.1128
4.1039
4.0950
4.0860
2.7013
2.6862
2.6800
2.6716
2.5862
2.5704
2.5543
2.1400
2.1285
2.1148
2.1032
1.9216
1.9045
1.8950
[rel]
15
10
5
0
[ppm]
0
2
4
6
8

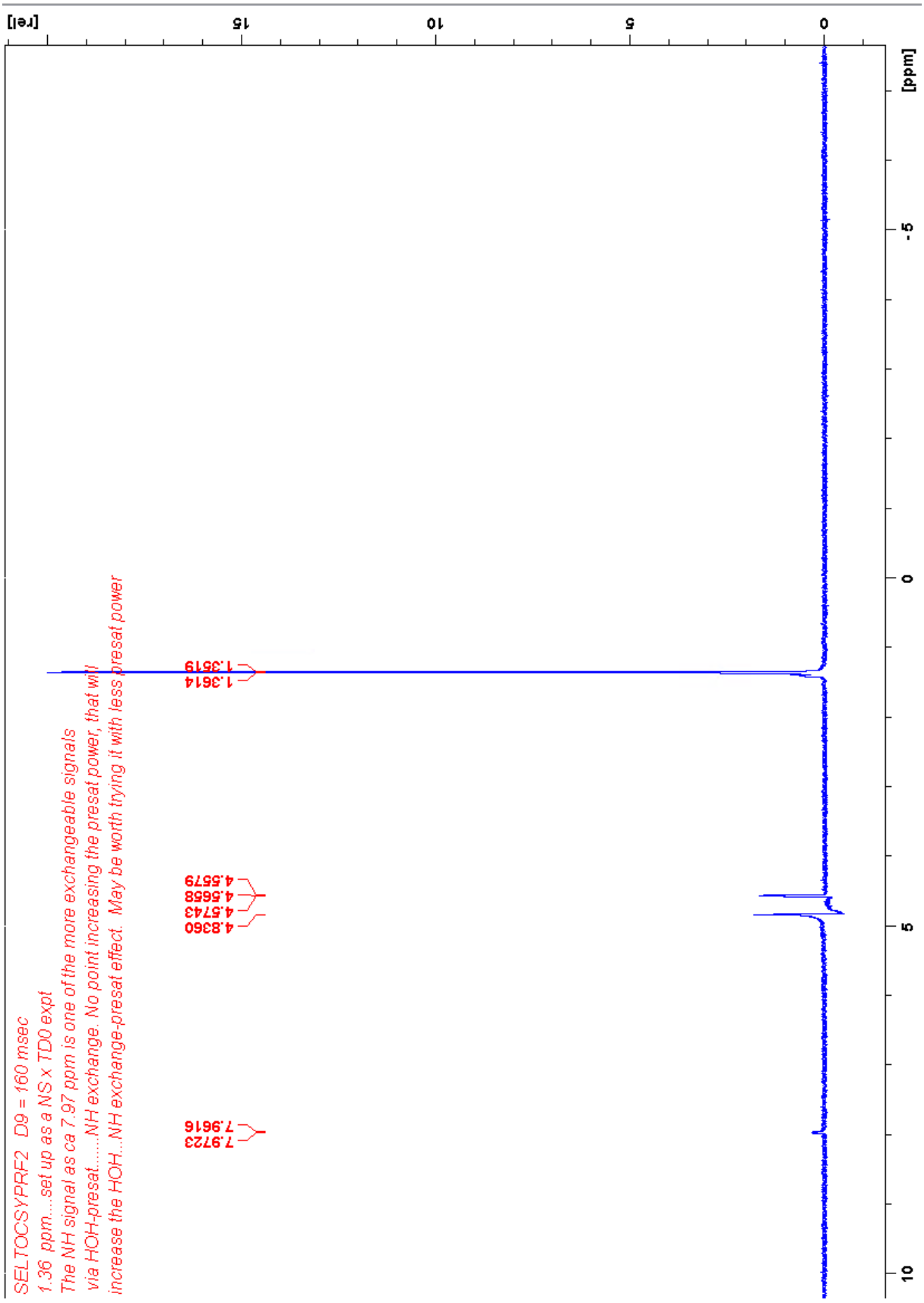
SELTOCSYPRF2 D9 = 160 msec
1.36 ppm....set up as a NS x TD0 expt
The NH signal as ca 7.97 ppm is one of the more exchangeable signals
via HOH-presat.....NH exchange. No point increasing the presat power, that will
increase the HOH...NH exchange-presat effect. May be worth trying it with less presat power
1.3614
1.3619
4.5579
4.5658
4.5743
4.8360
7.9723
7.9816
[rel]
15
10
5
0
[ppm]
-5
0
5
10

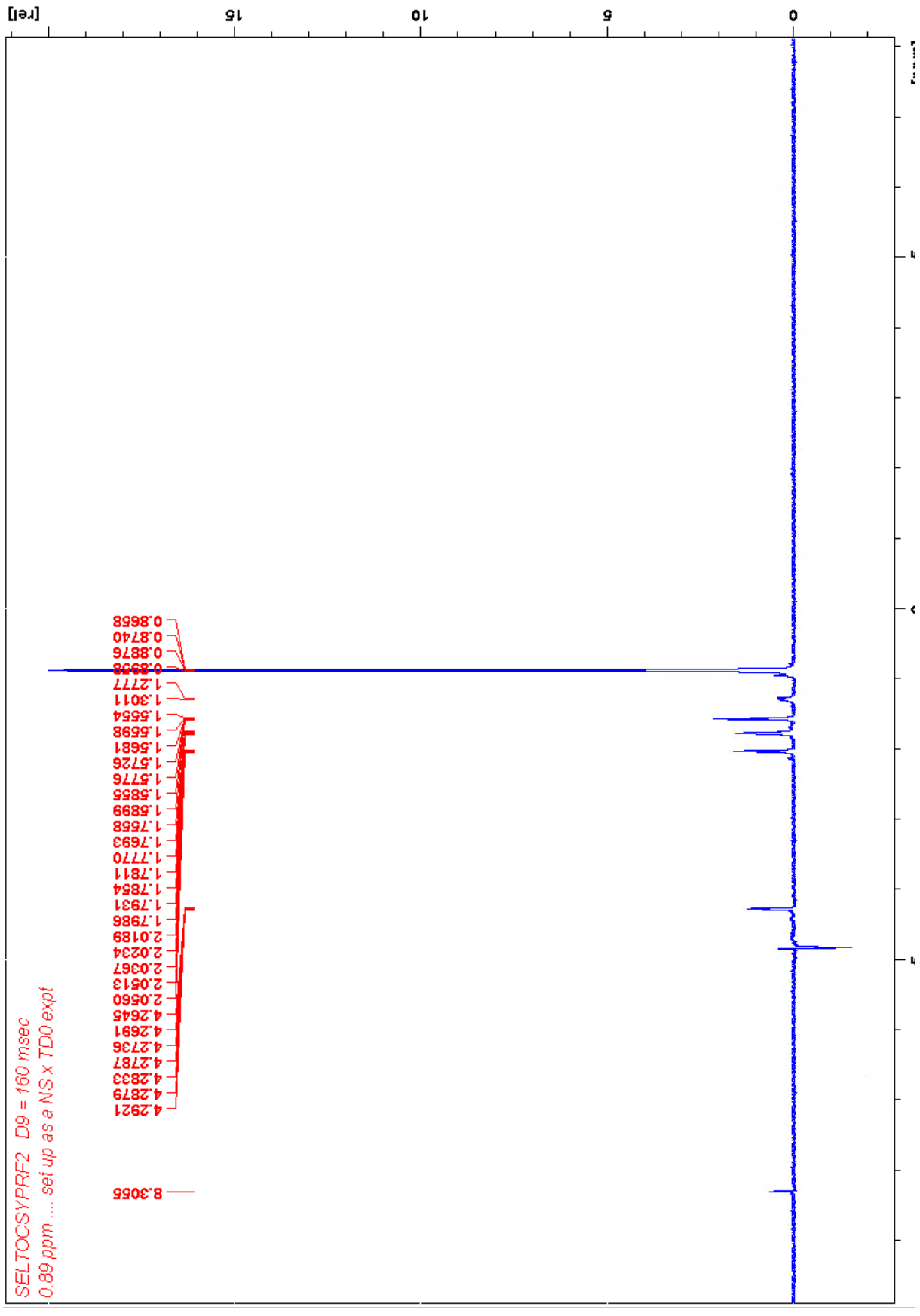
[rel]
15
10
5
0
SELTOCSYPRF2 D9 = 160 msec
0.89 ppm ..... set up as a NS x TD0 expt
8.3055
4.2921
4.2879
4.2833
4.2787
4.2736
4.2691
4.2645
2.0560
2.0513
2.0367
2.0234
2.0189
1.7986
1.7931
1.7854
1.7811
1.7770
1.7693
1.7658
1.5899
1.5855
1.5776
1.5726
1.5681
1.5598
1.5554
1.3011
1.2777
0.8938
0.8876
0.8740
0.8658

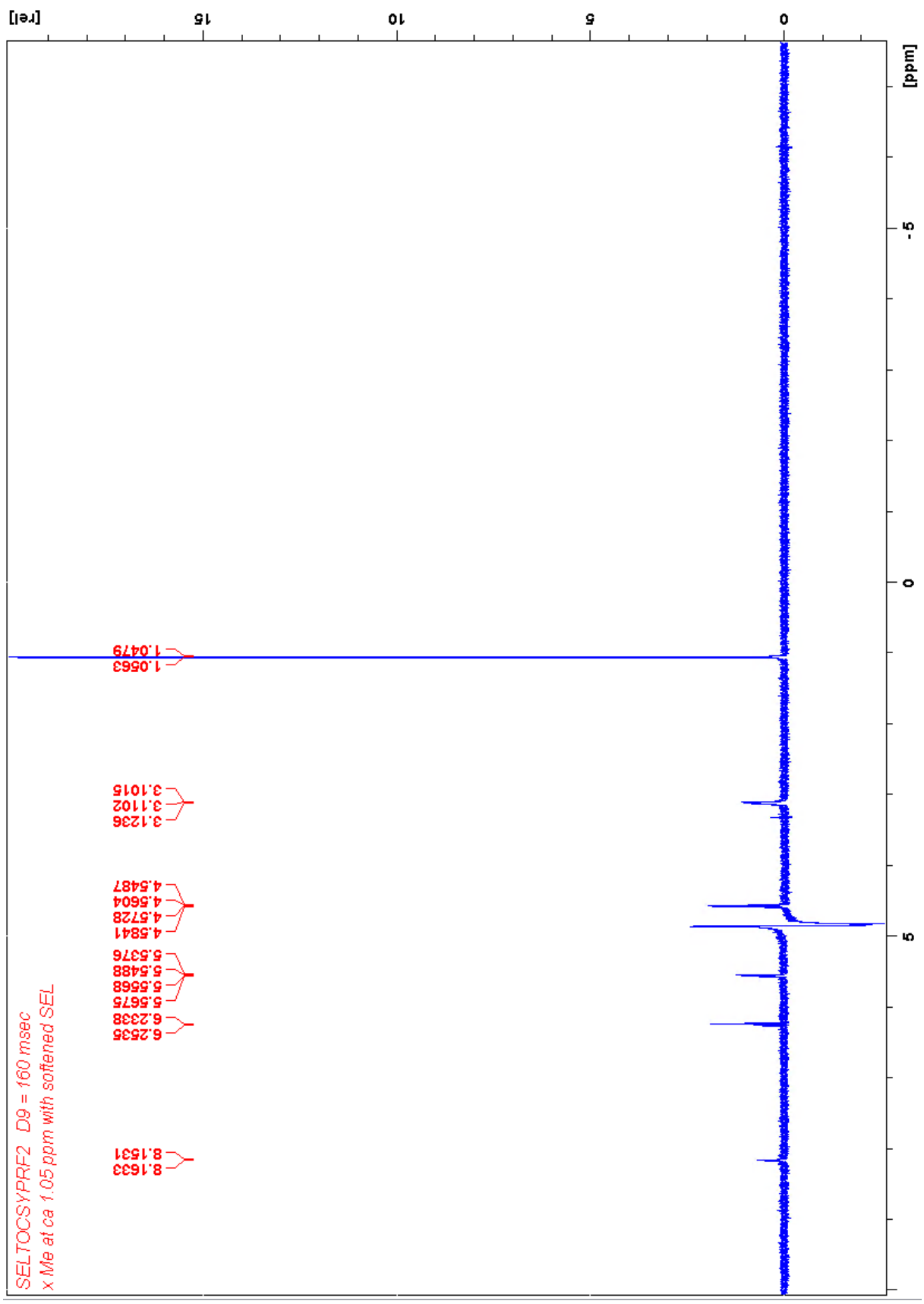
SELTOCSYPRF2 D9 = 160 msec
x Me at ca 1.05 ppm with softened SEL
8.1633
8.1531
6.2535
6.2338
5.5675
5.5568
5.5488
5.5376
4.5841
4.5728
4.5604
4.5487
3.1236
3.1102
3.1015
1.0563
1.0479
[rel]
15
10
5
0
[ppm]
-5
0
5

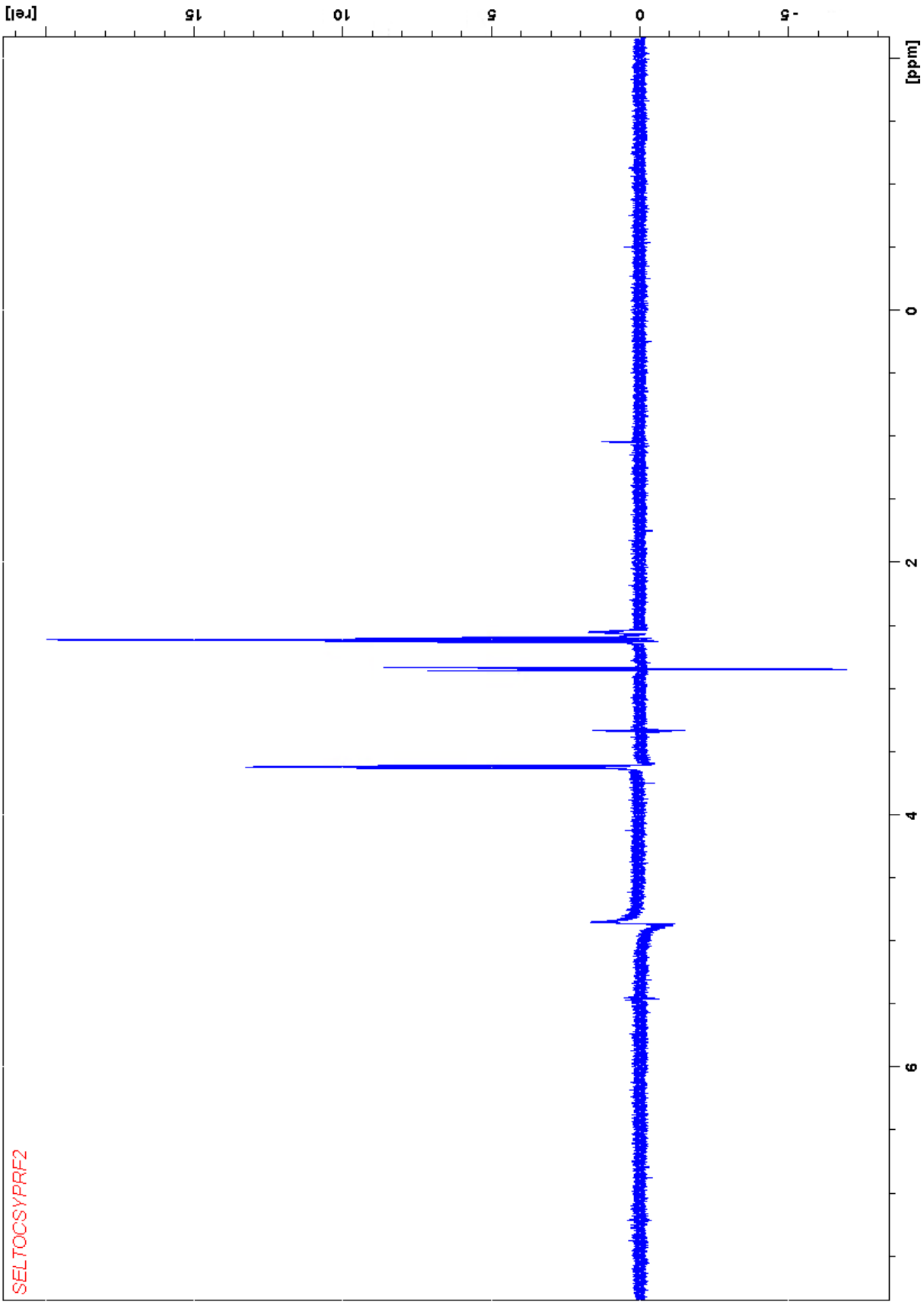

Irradiation of the resonance at 2.85 ppm.

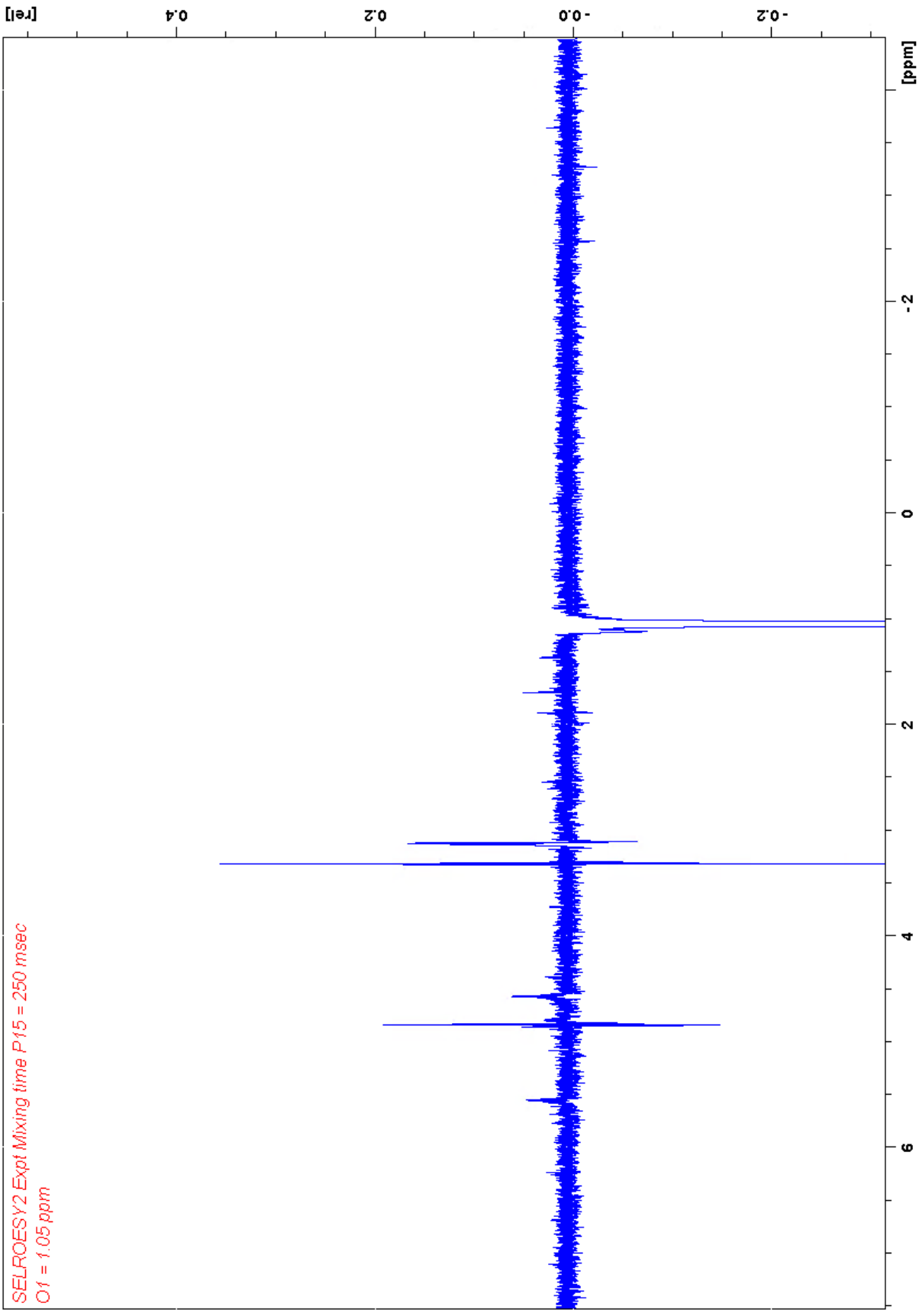
SELROESY2 Expt Mixing time P15 = 250 msec
O1 = 1.05 ppm
[rel]
0.4
0.2
0.0
-0.2
[ppm]
-2
0
2
4
6

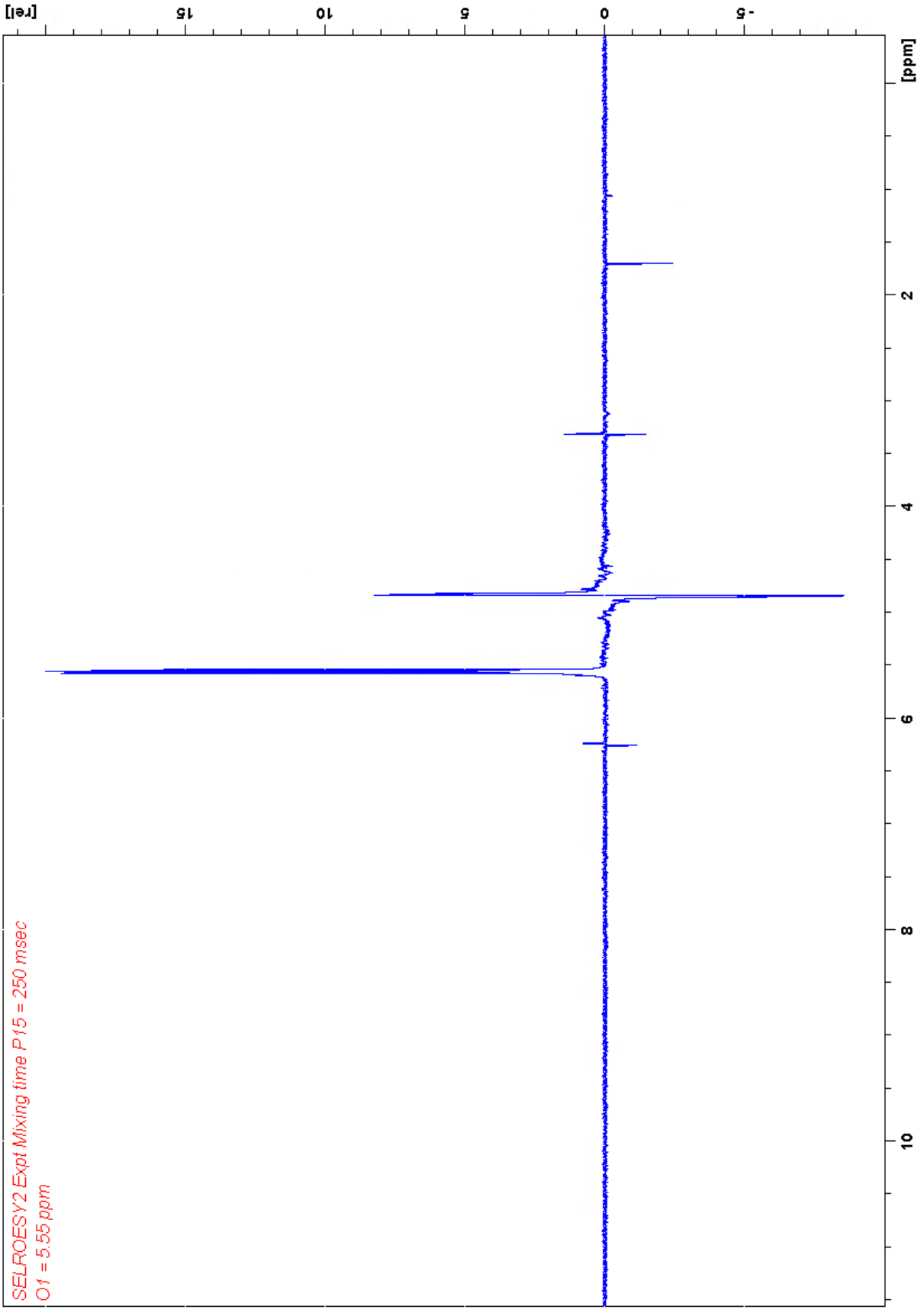
[rel]
15
10
5
0
-5
[ppm]
2
4
6
8
10
SELROESY2 Expt Mixing time P15 = 250 msec
O1 = 5.55 ppm

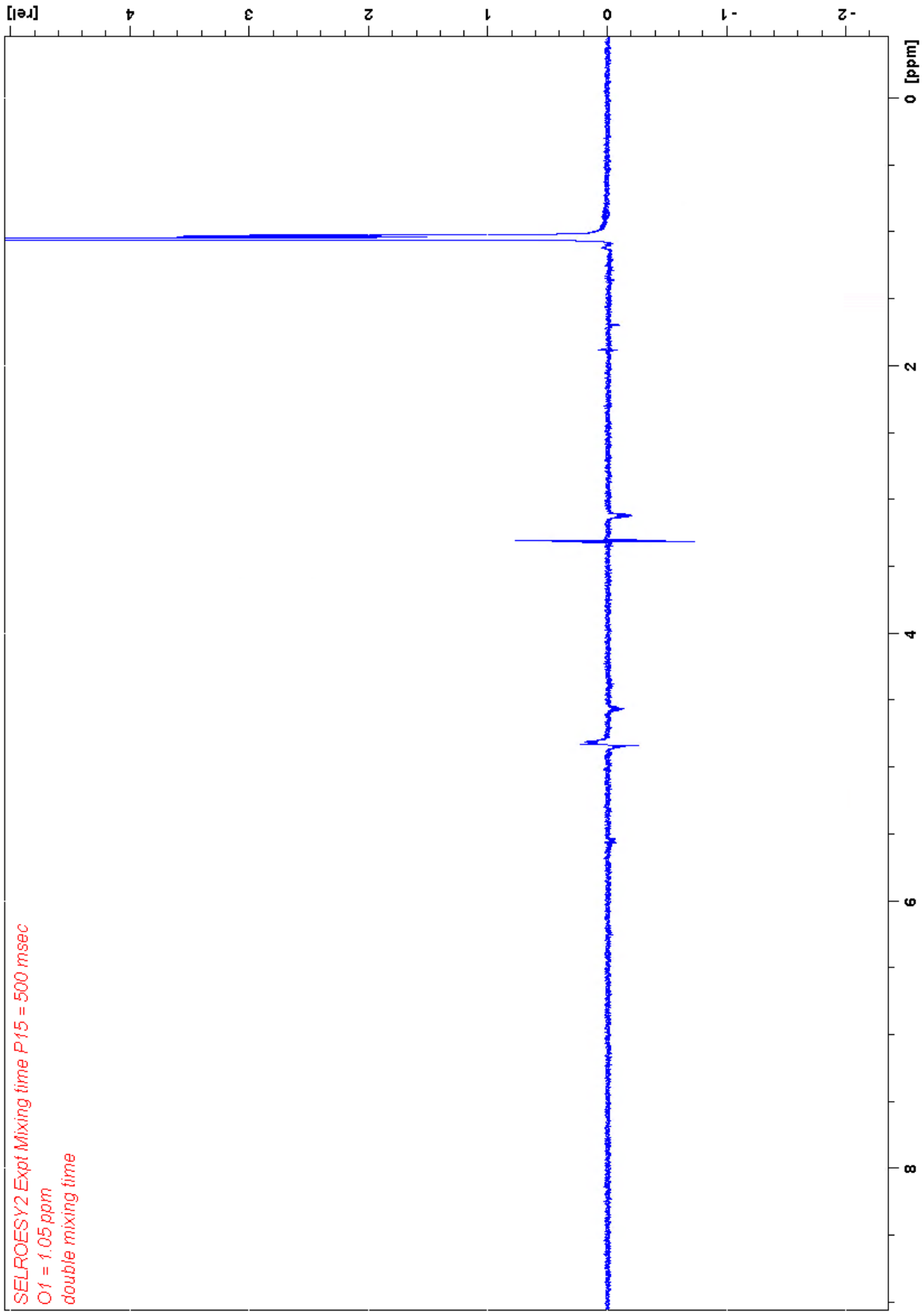
SELROESY2 Expt Mixing time P15 = 500 msec
O1 = 1.05 ppm
double mixing time
[rel]
4
3
2
1
0
-1
-2
0 [ppm]
2
4
6
8

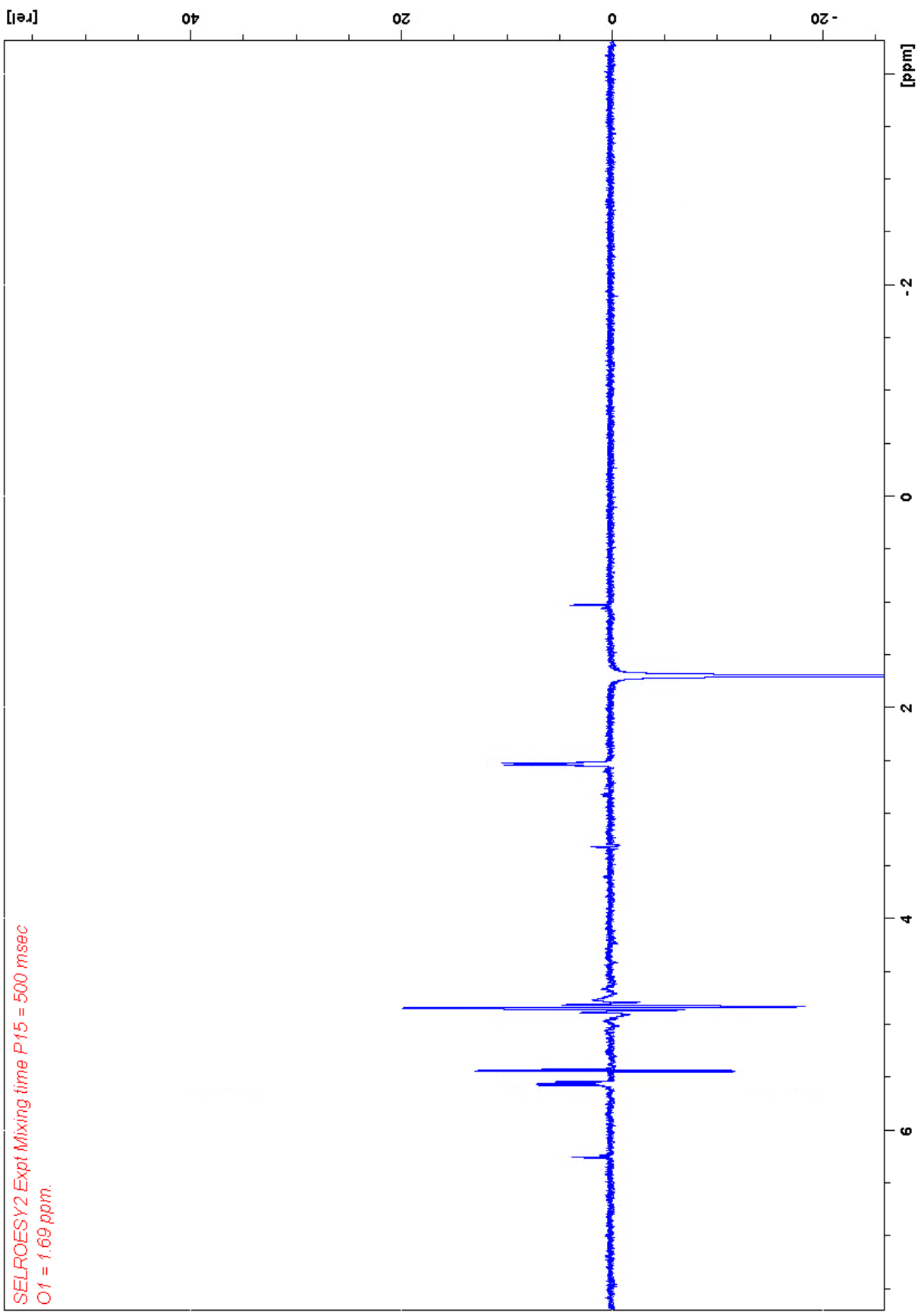
[rel]
40
20
0
-20
[ppm]
-2
0
2
4
6
SELROESY2 Expt Mixing time P15 = 500 msec
O1 = 1.69 ppm.

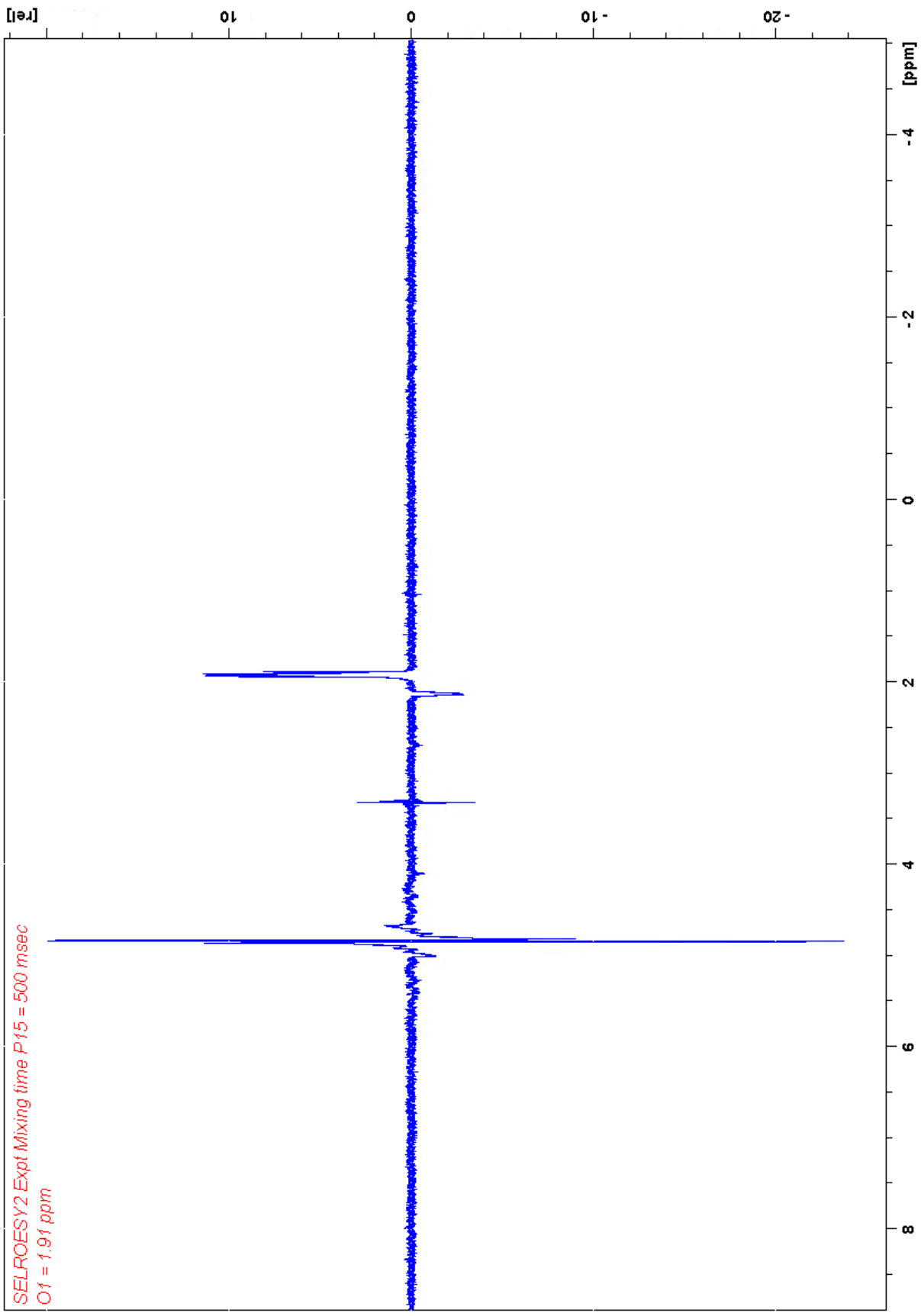
[rel]
10
0
-10
-20
[ppm]
-4
-2
0
2
4
6
8
SELROESY2 Expt Mixing time P15 = 500 msec
O1 = 1.91 ppm

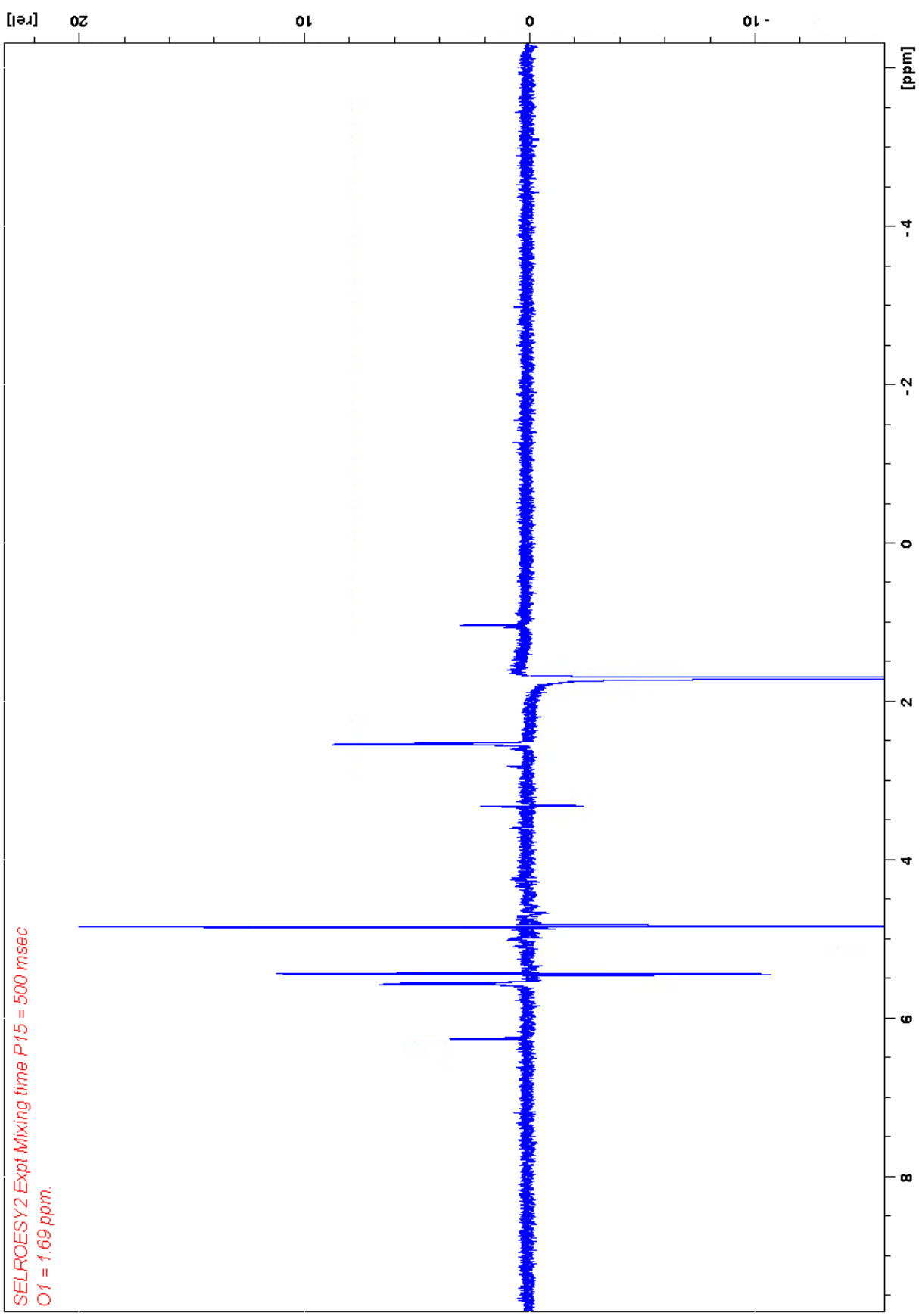
[rel]
20
10
0
- 10
[ppm]
-4
-2
0
2
4
6
8
SELROESY2 Expt Mixing time P15 = 500 msec
O1 = 1.69 ppm.

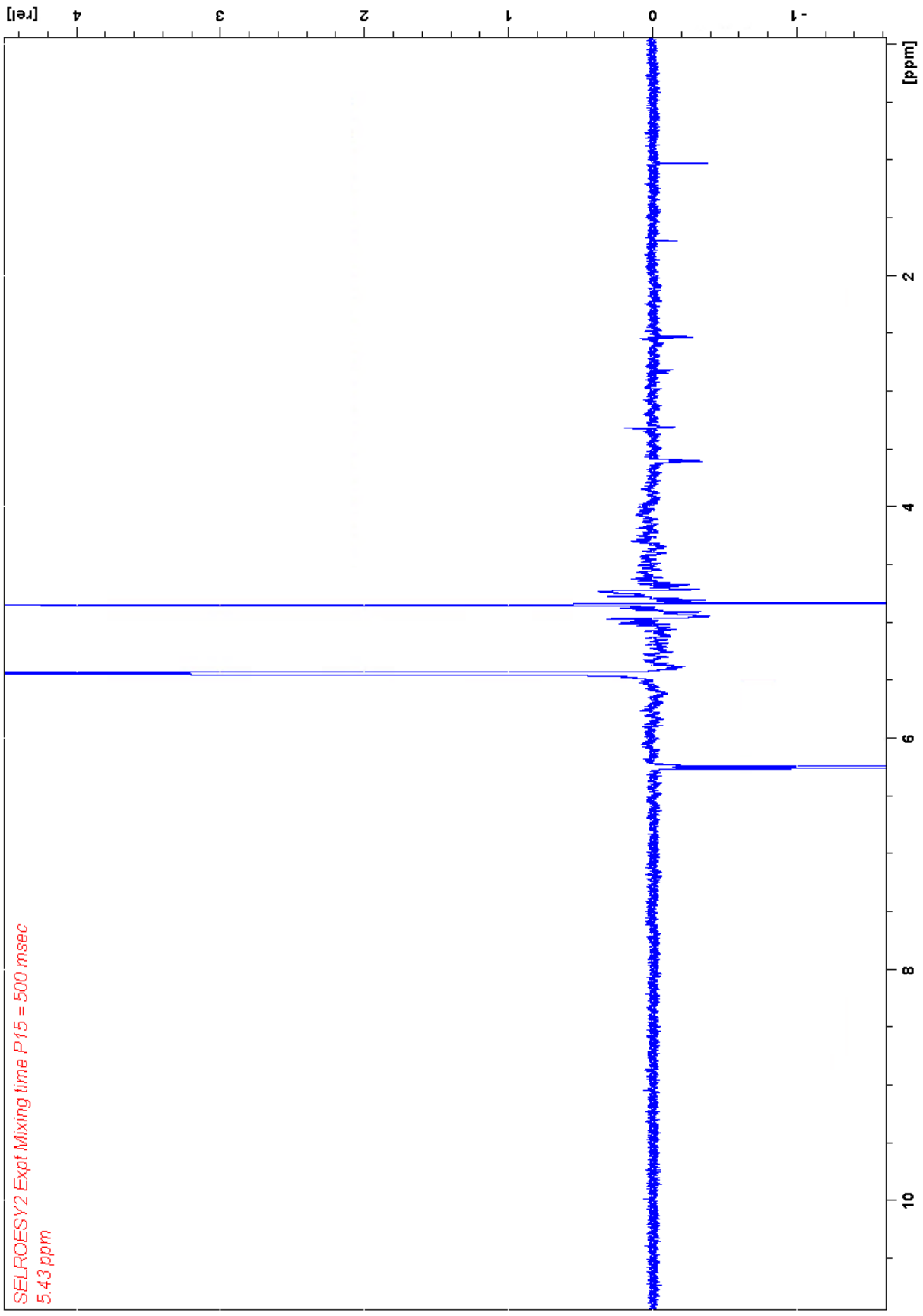
[rel]
4
3
2
1
0
-1
[ppm]
2
4
6
8
10
SELROESY2 Expt Mixing time P15 = 500 msec
5.43 ppm

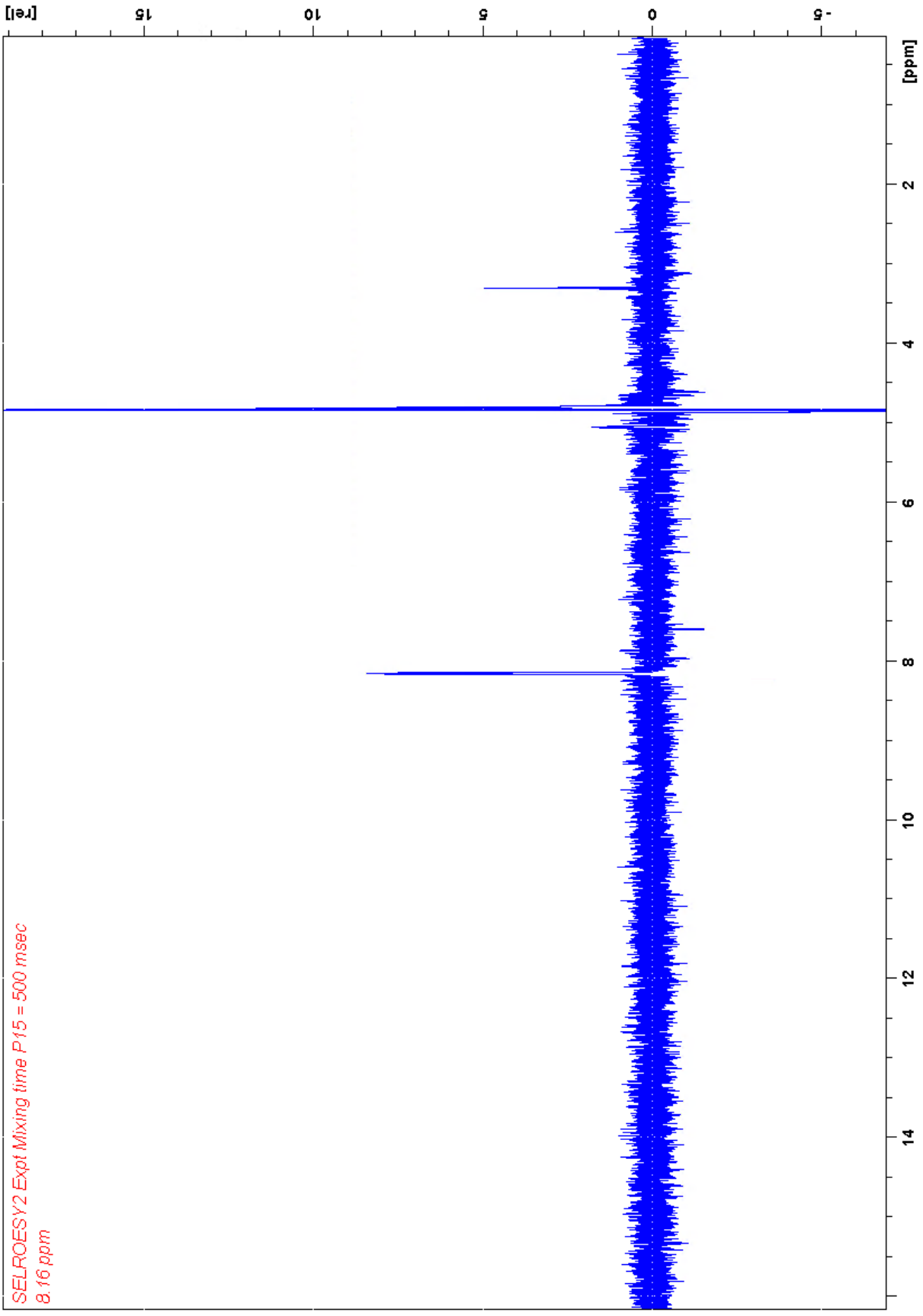
SELROESY2 Expt Mixing time P15 = 500 msec
8.16 ppm
[rel]
15
10
5
0
-5
[ppm]
2
4
6
8
10
12
14

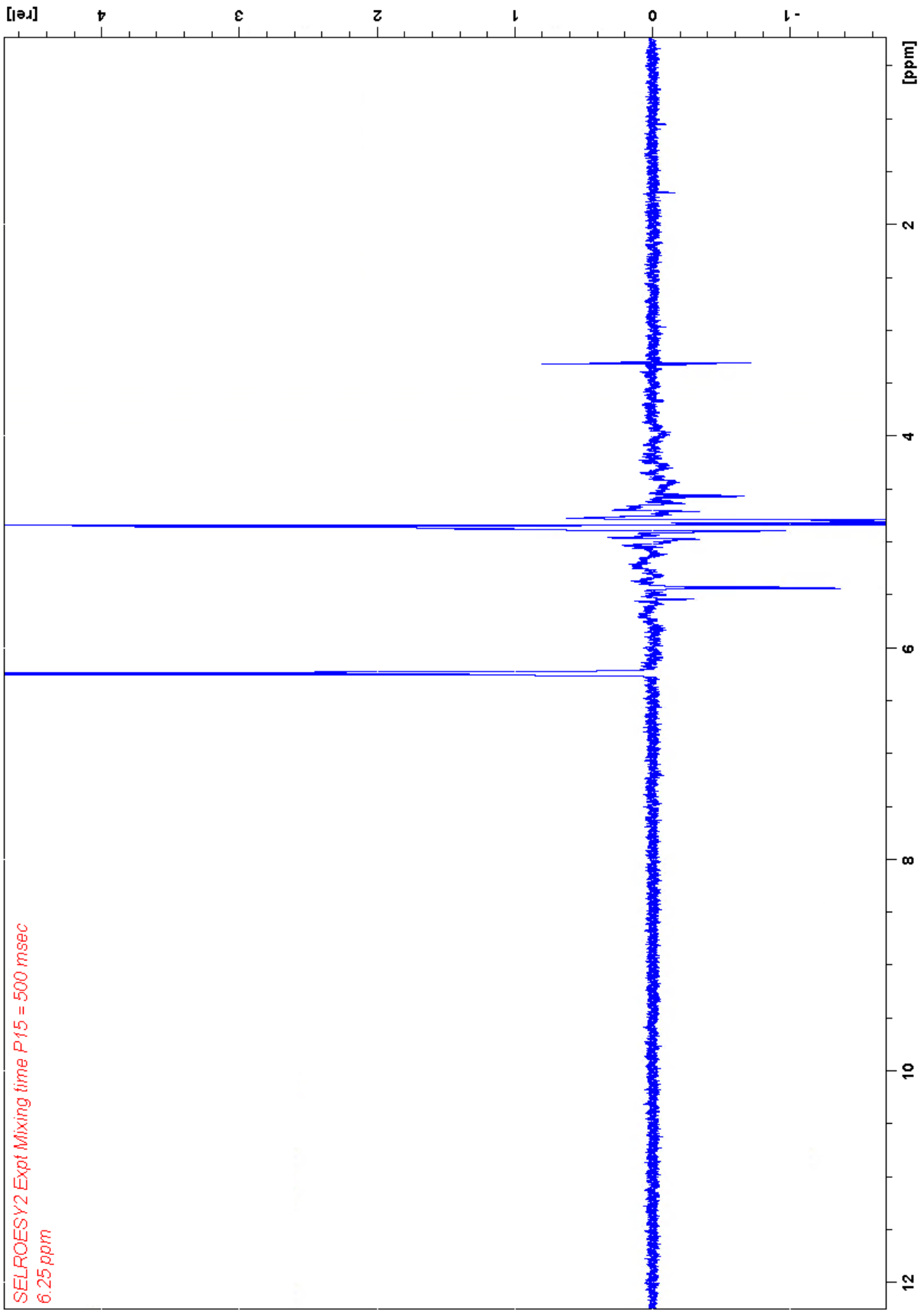
[rel]
4
3
2
1
0
-1
[ppm]
2
4
6
8
10
12
SELROESY2 Expt Mixing time P15 = 500 msec
6.25 ppm

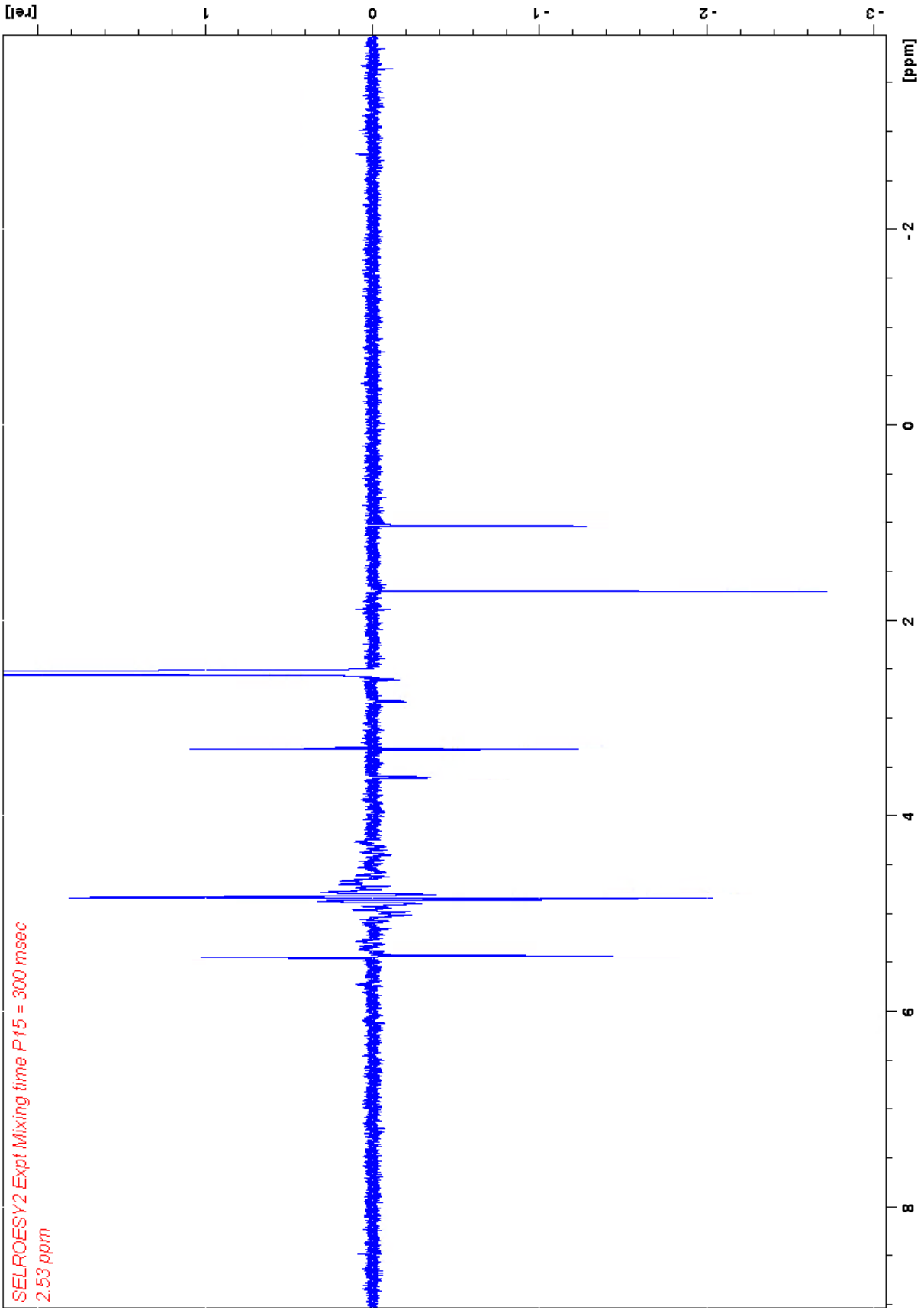
[rel]
1
0
-1
-2
-3
[ppm]
-2
0
2
4
6
8
SELROESY2 Expt Mixing time P15 = 300 msec
2.53 ppm

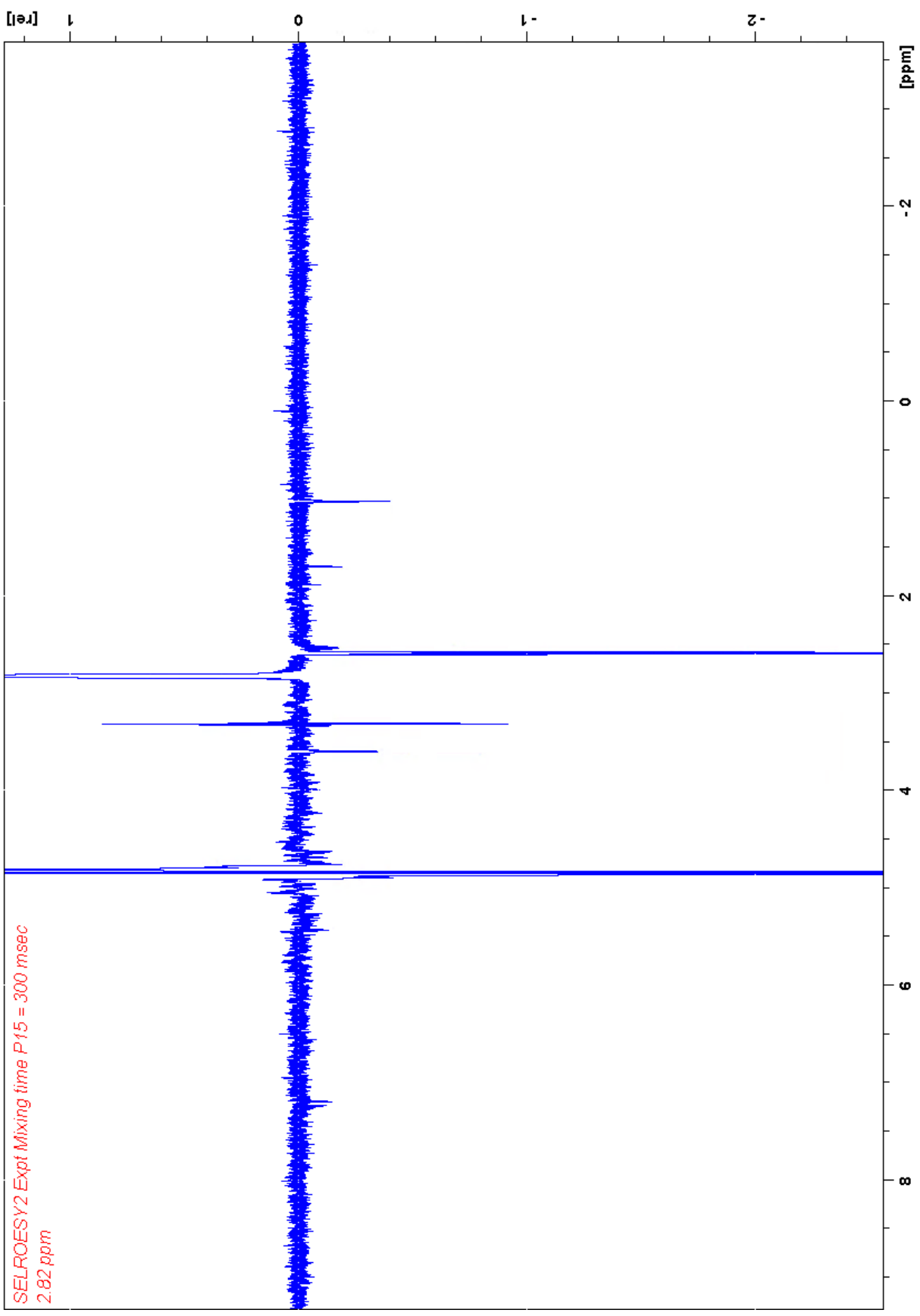
[rel]
1
0
-1
-2
[ppm]
-2
0
2
4
6
8
SELROESY2 Expt Mixing time P15 = 300 msec
2.82 ppm

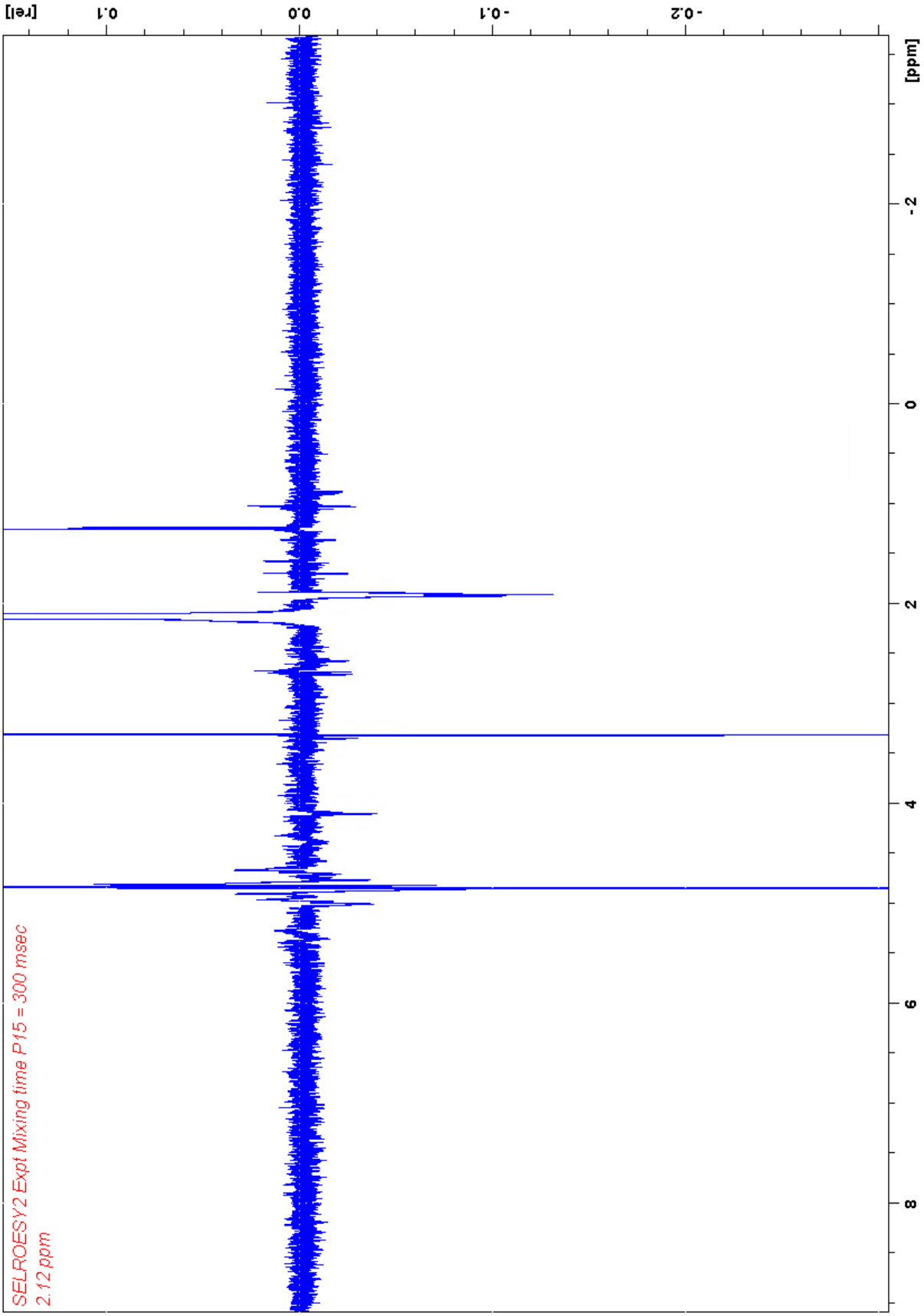
[rel]
0.1
0.0
-0.1
-0.2
[ppm]
-2
0
2
4
6
8
SELROESY2 Expt Mixing time P15 = 300 msec
2.12 ppm

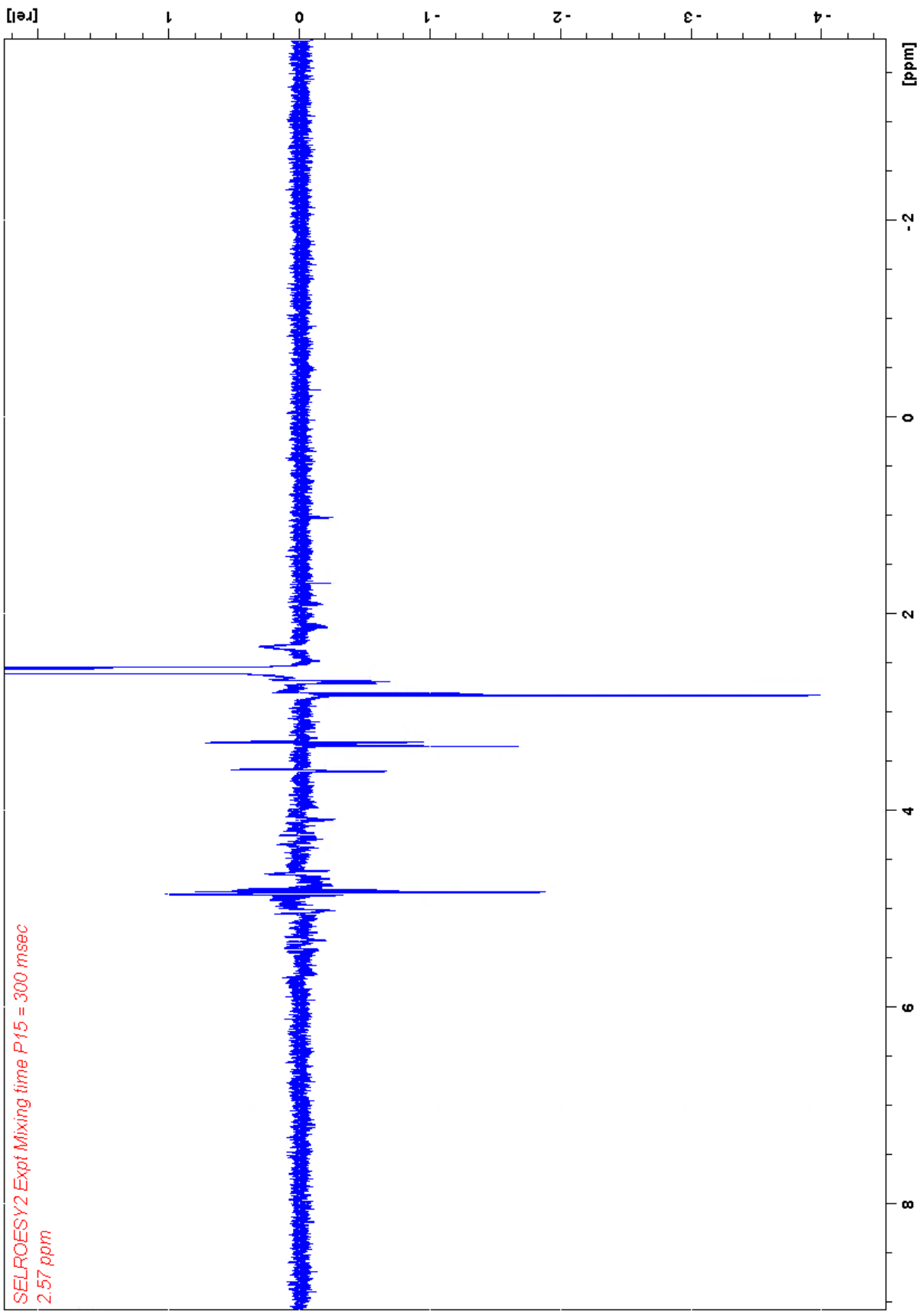
[rel]
1
0
-1
-2
-3
-4
[ppm]
-2
0
2
4
6
8
SELROESY2 Expt Mixing time P15 = 300 msec
2.57 ppm

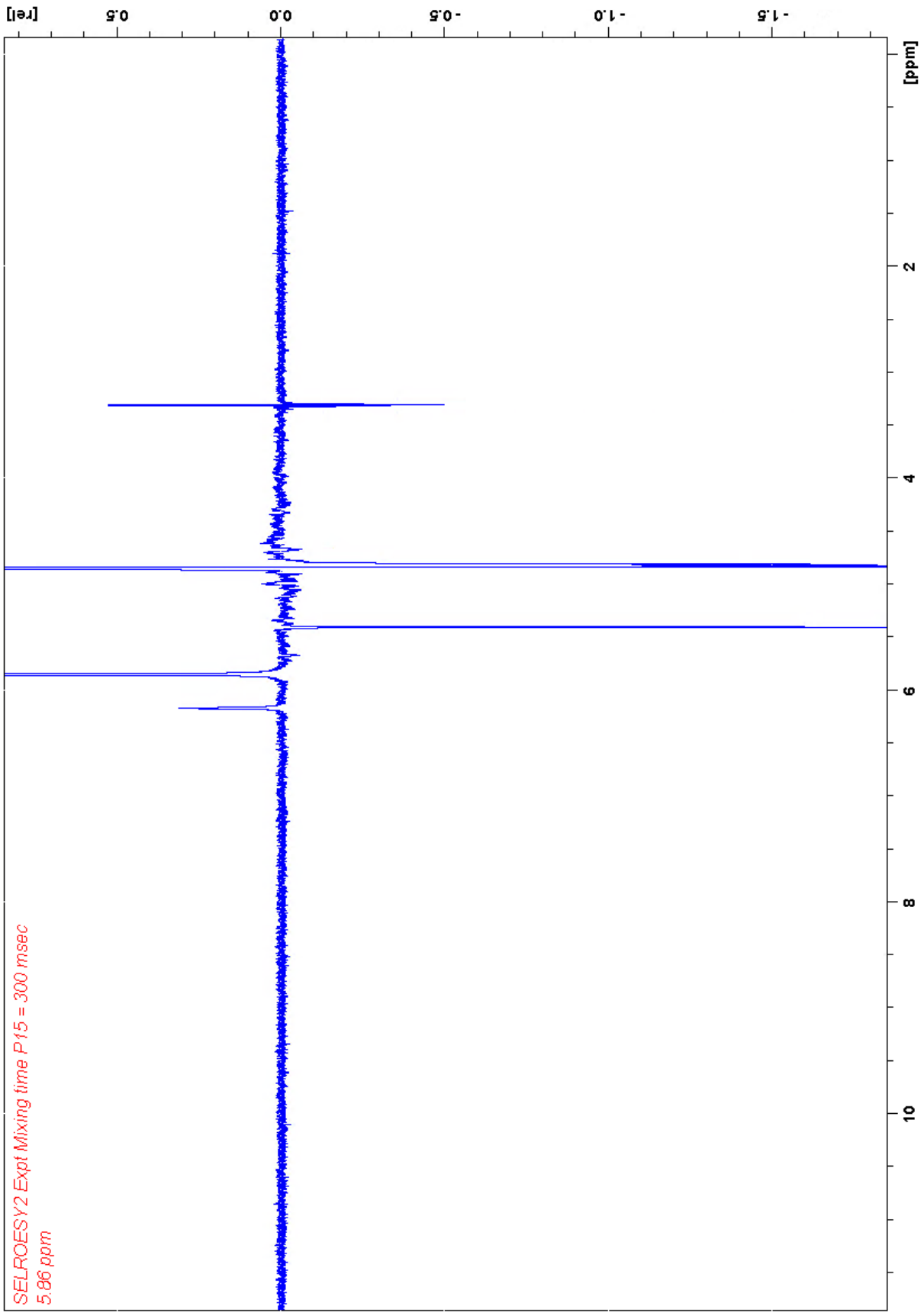
[rel]
0.5
0.0
-0.5
-1.0
-1.5
[ppm]
2
4
6
8
10
SELROESY2 Expt Mixing time P15 = 300 msec
5.86 ppm

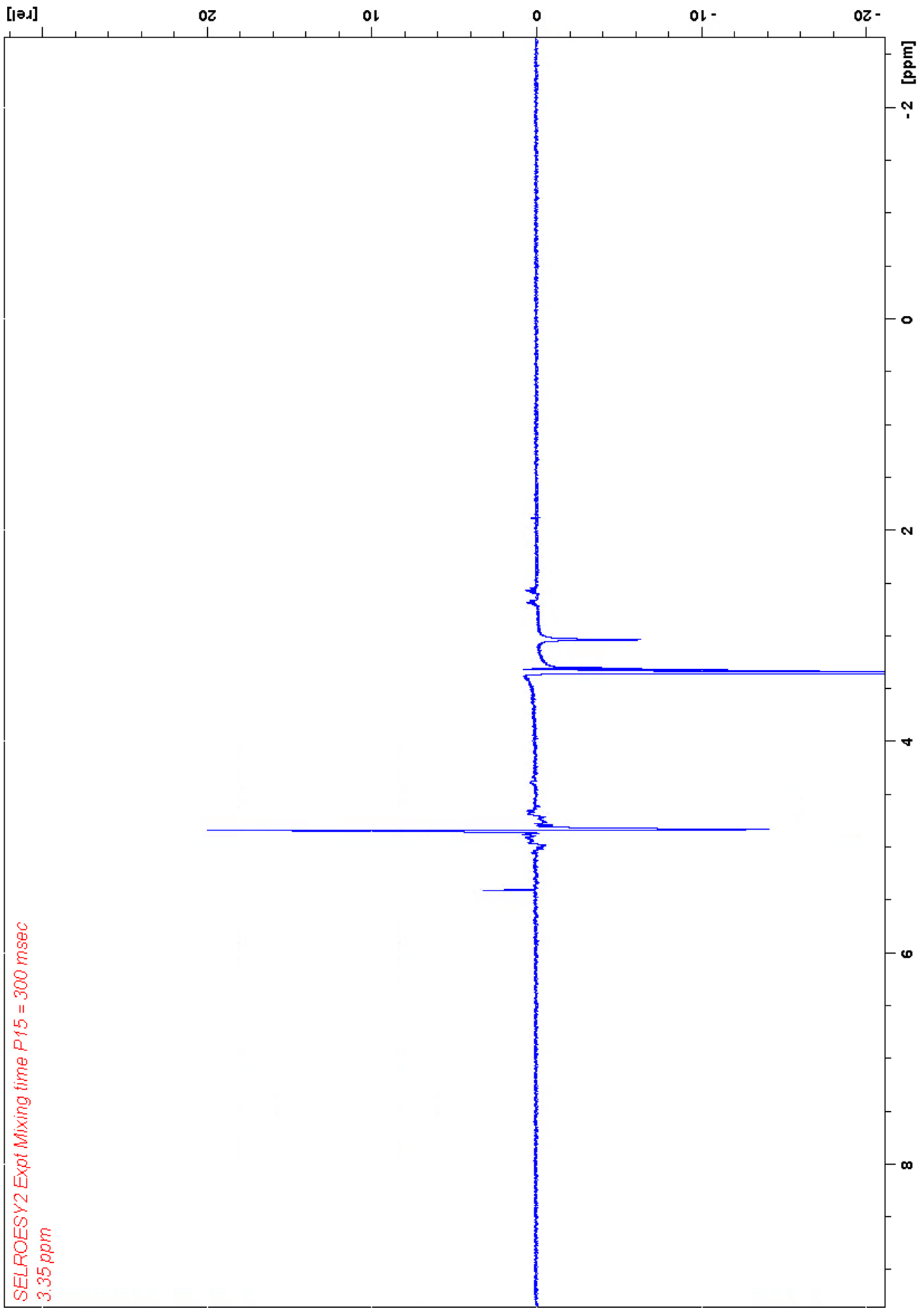
[rel]
20
10
0
-10
-20
-2
0
2
4
6
8
[ppm]
SELROESY2 Expt Mixing time P15 = 300 msec
3.35 ppm

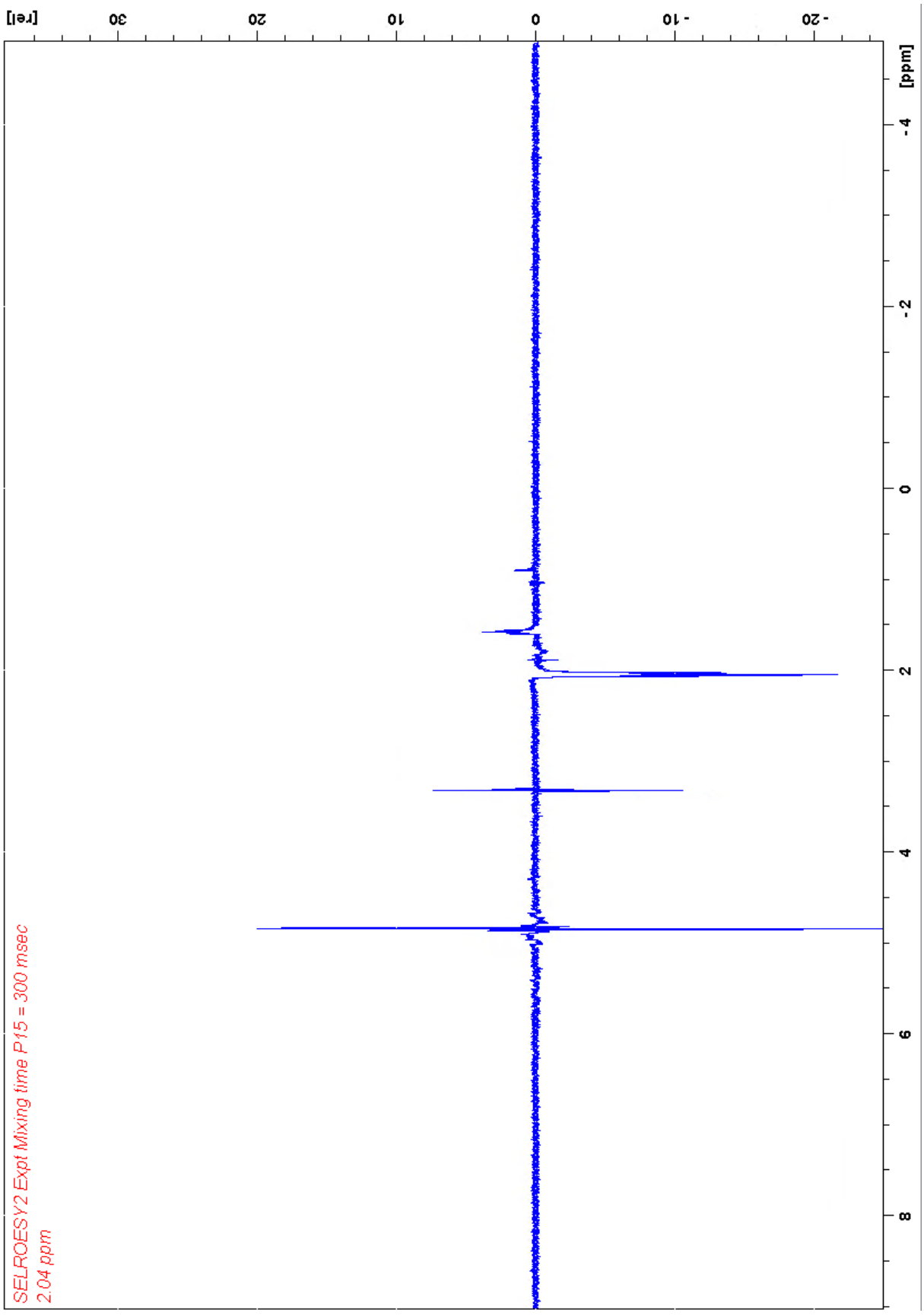
[rel]
30
20
10
0
-10
-20
[ppm]
-4
-2
0
2
4
6
8
SELROESY2 Expt Mixing time P15 = 300 msec
2.04 ppm

Sample #2

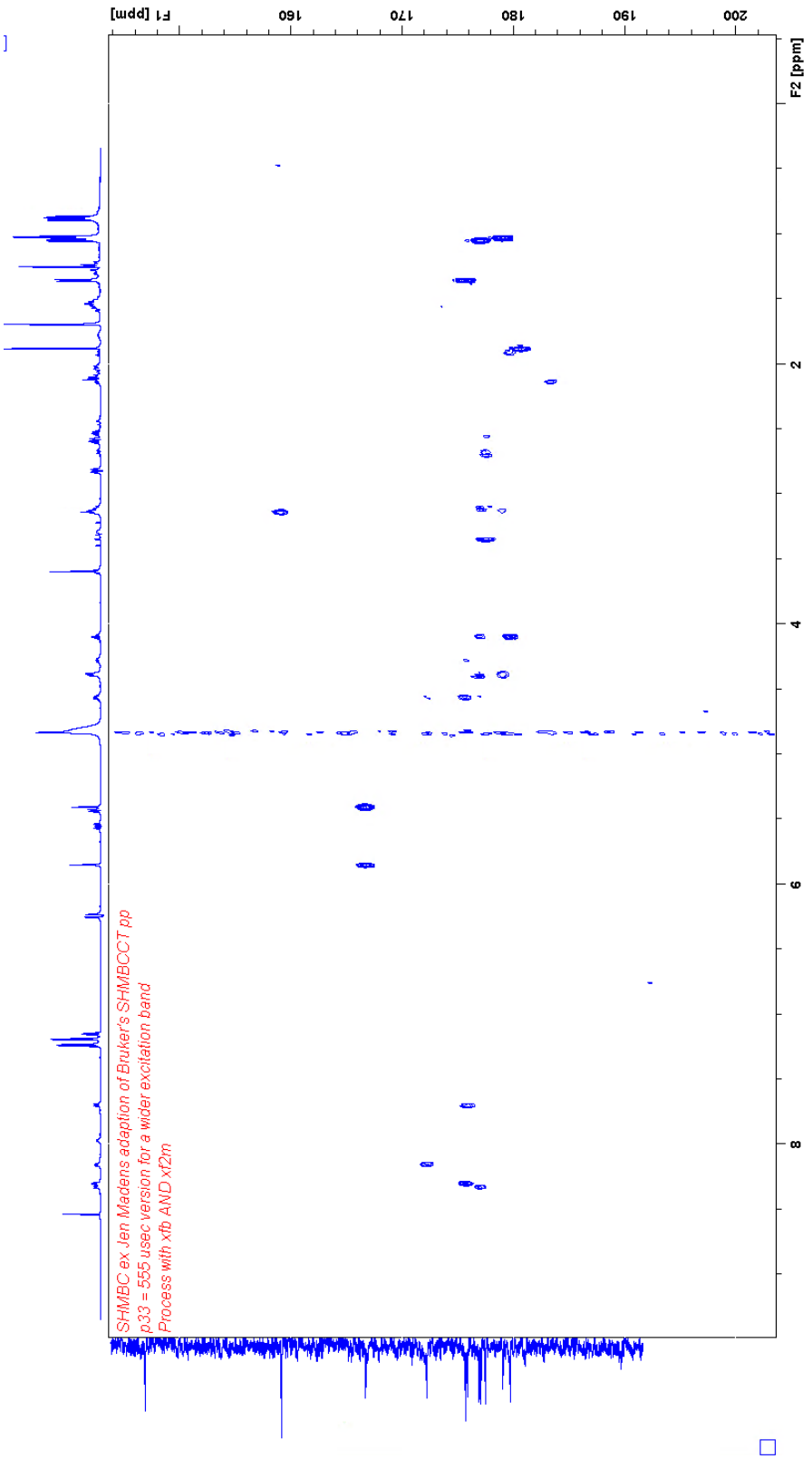
F1 [ppm]
160
170
180
190
200
F2 [ppm]
2
4
6
8
SHMBC ex Jen Madens adaption of Bruker's SHMBCCT pp
p33 = 555 usec version for a wider excitation band
Process with xfb AND xf2m

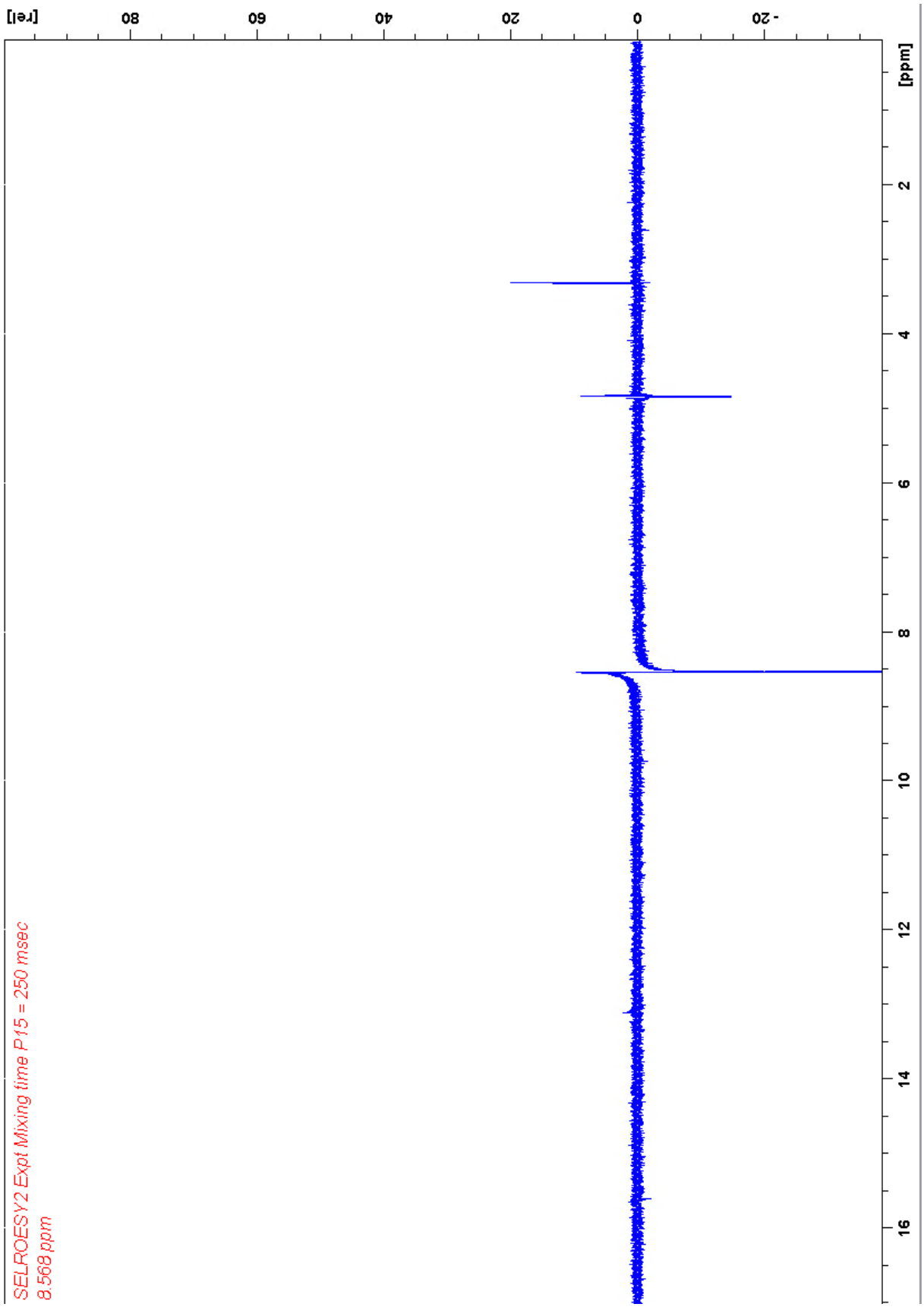
[rel]
80
60
40
20
0
-20
[ppm]
2
4
6
8
10
12
14
16
SELROESY2 Expt Mixing time P15 = 250 msec
8.568 ppm

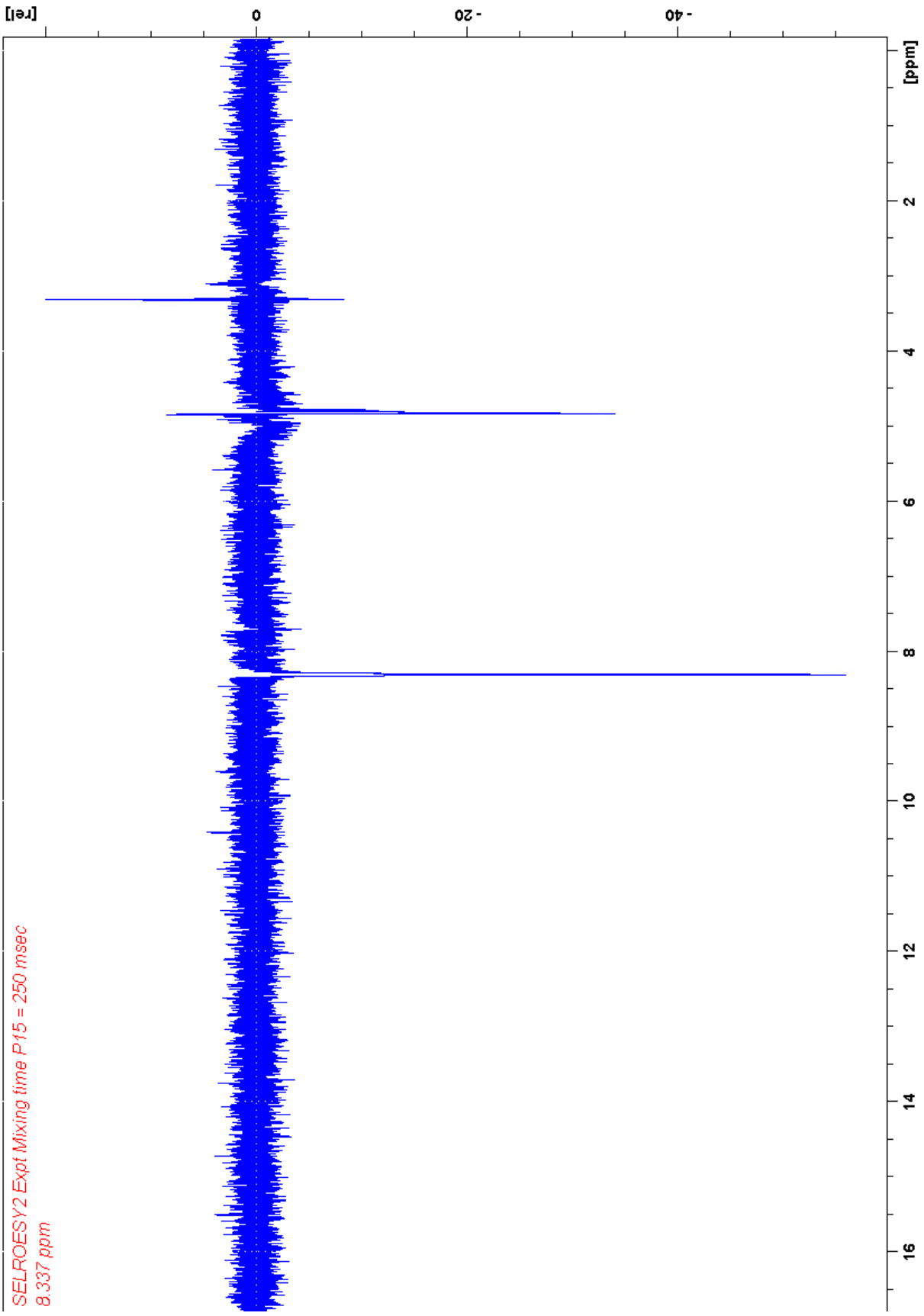
[rel]
0
-20
-40
[ppm]
2
4
6
8
10
12
14
16
SELROESY2 Expt Mixing time P15 = 250 msec
8.337 ppm

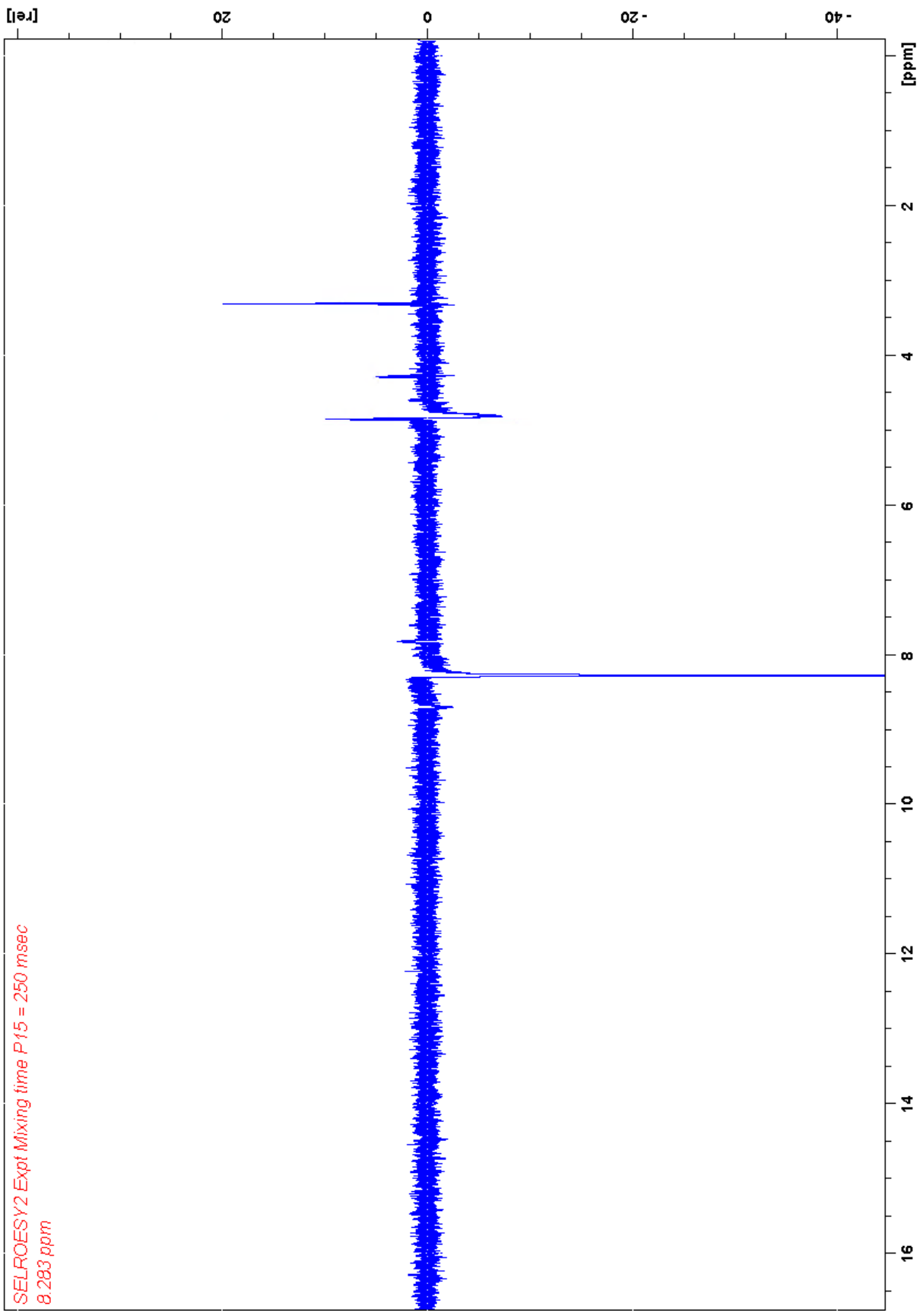
SELROESY2 Expt Mixing time P15 = 250 msec
8.283 ppm
[rel]
20
0
-20
-40
[ppm]
2
4
6
8
10
12
14
16

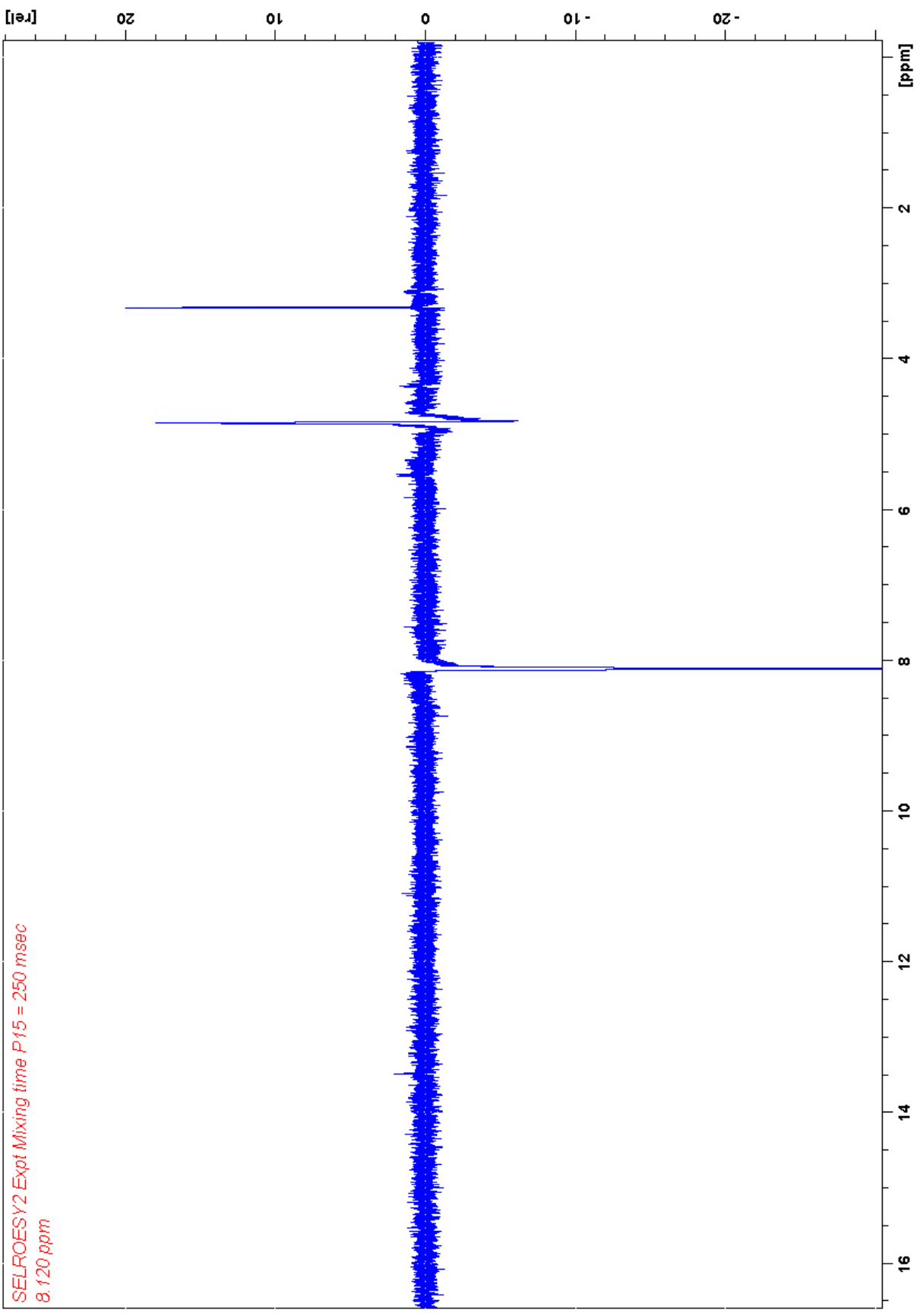
[rel]
20
10
0
-10
-20
[ppm]
2
4
6
8
10
12
14
16
SELROESY2 Expt Mixing time P15 = 250 msec
8.120 ppm

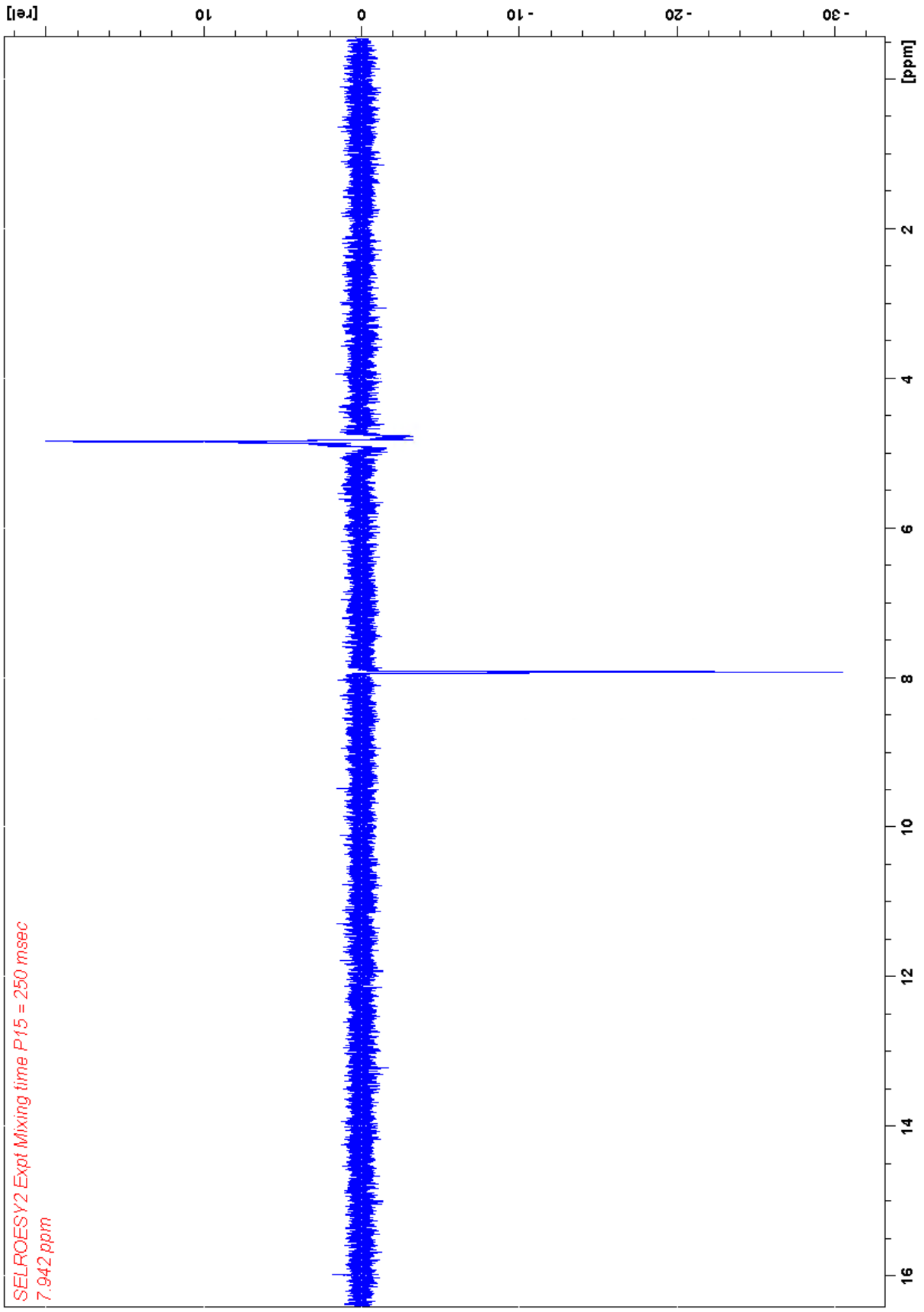
[rel]
10
0
-10
-20
-30
[ppm]
2
4
6
8
10
12
14
16
SELROESY2 Expt Mixing time P15 = 250 msec
7.942 ppm

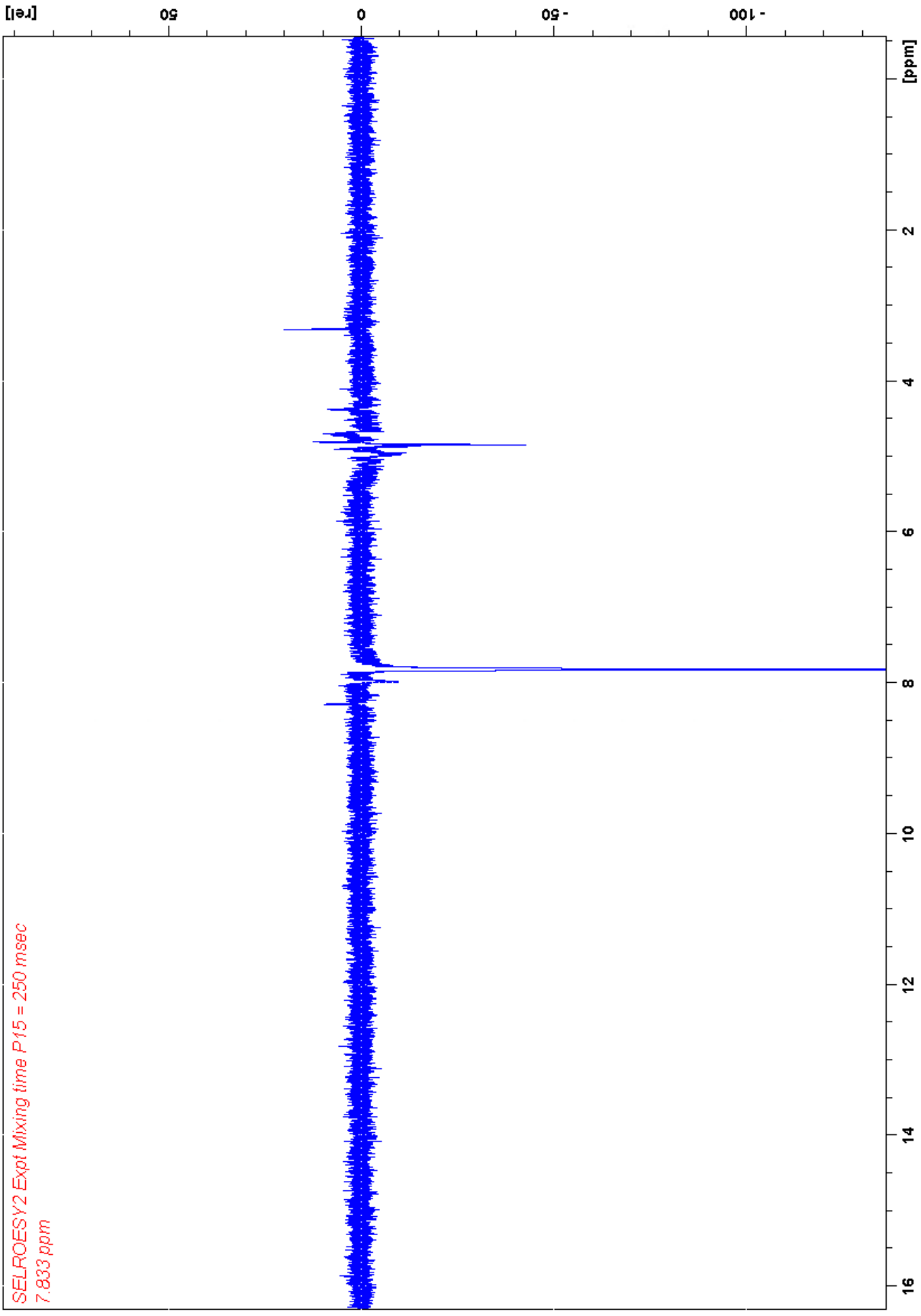
[rel]
50
0
-50
-100
[ppm]
2
4
6
8
10
12
14
16
SELROESY2 Expt Mixing time P15 = 250 msec
7.833 ppm

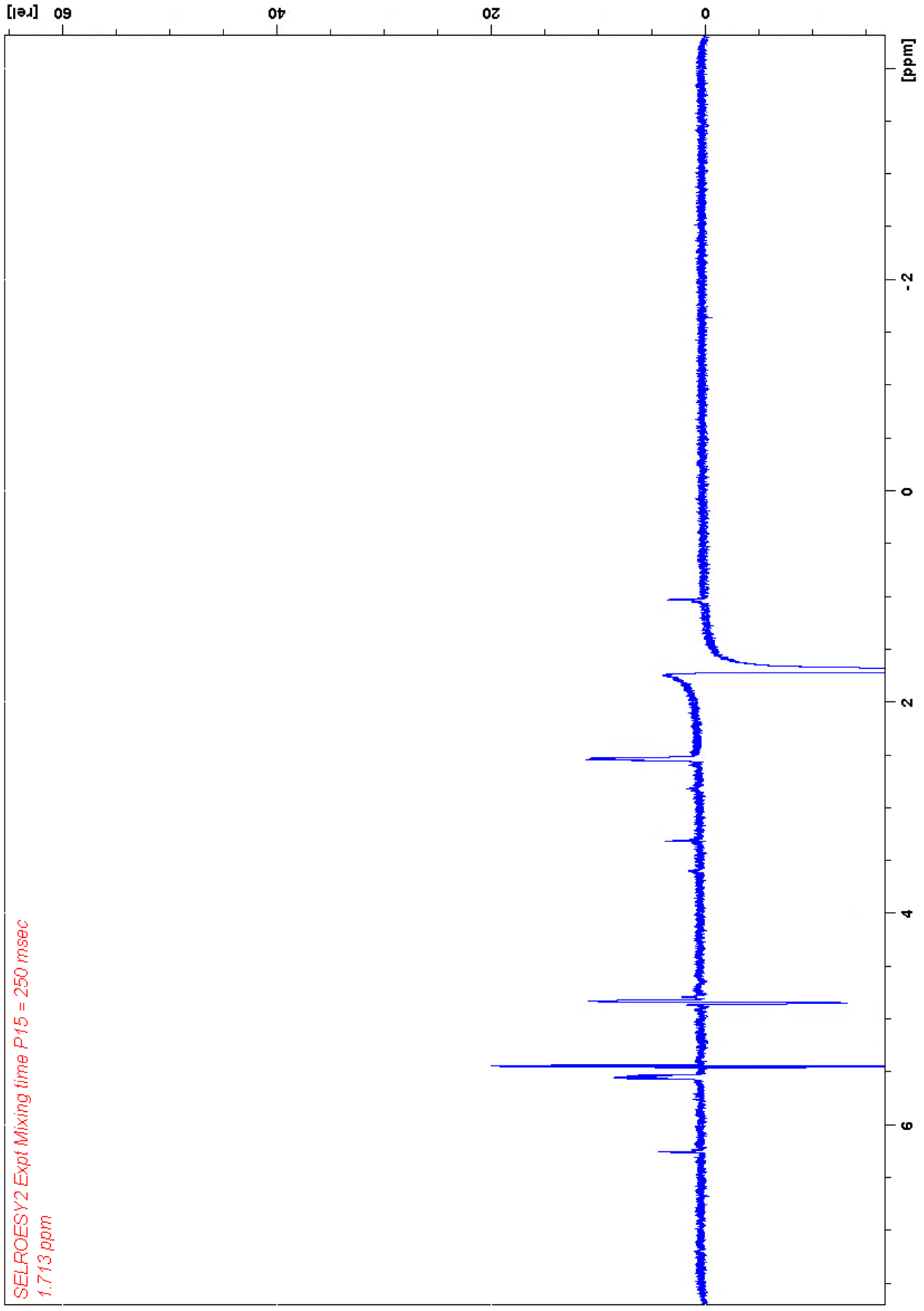
SELROESY2 Expt Mixing time P15 = 250 msec
1.713 ppm
[rel]
60
40
20
0
[ppm]
-2
0
2
4
6

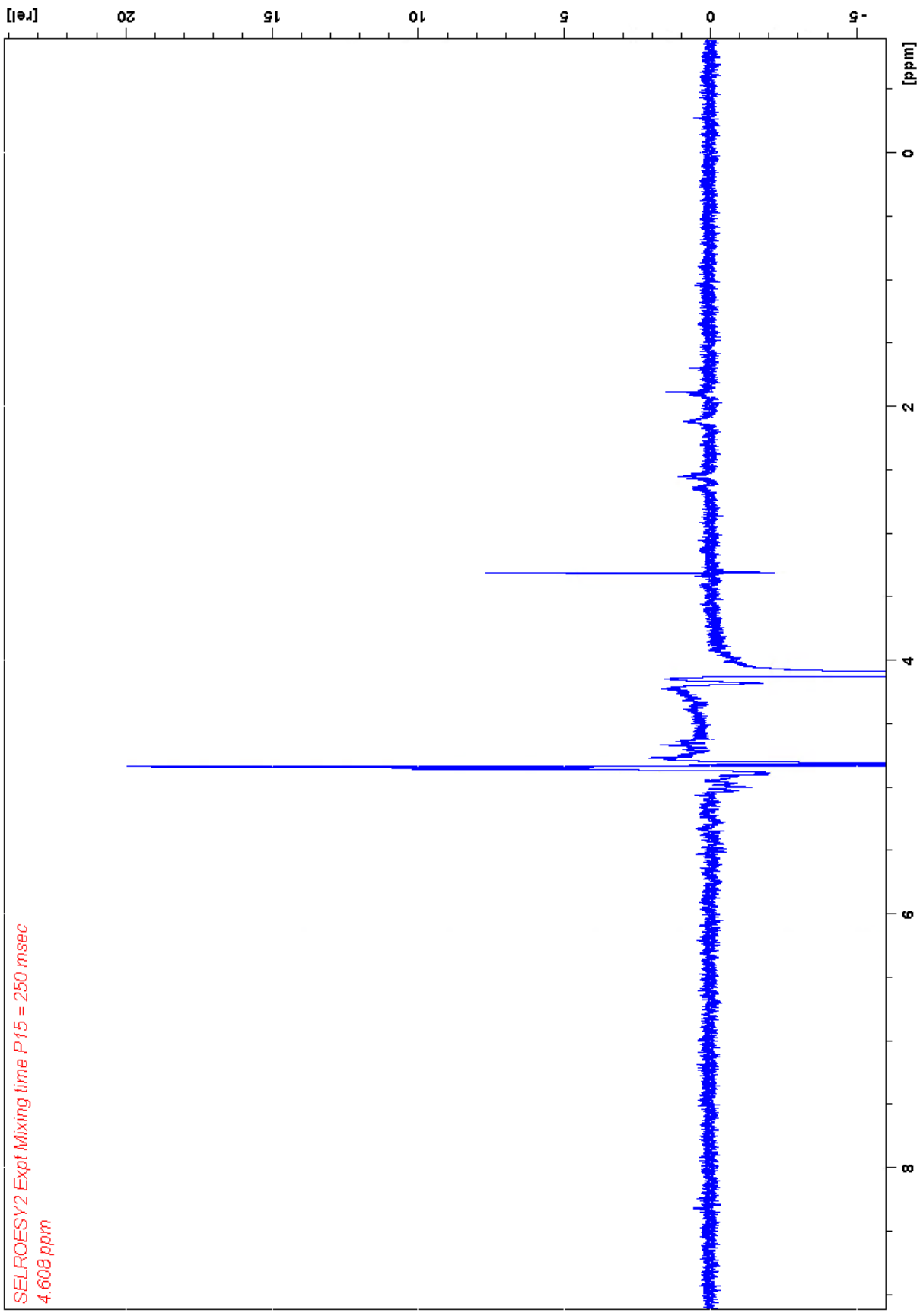
SELROESY2 Expt Mixing time P15 = 250 msec
4.608 ppm
[rel]
20
15
10
5
0
-5
[ppm]
0
2
4
6
8

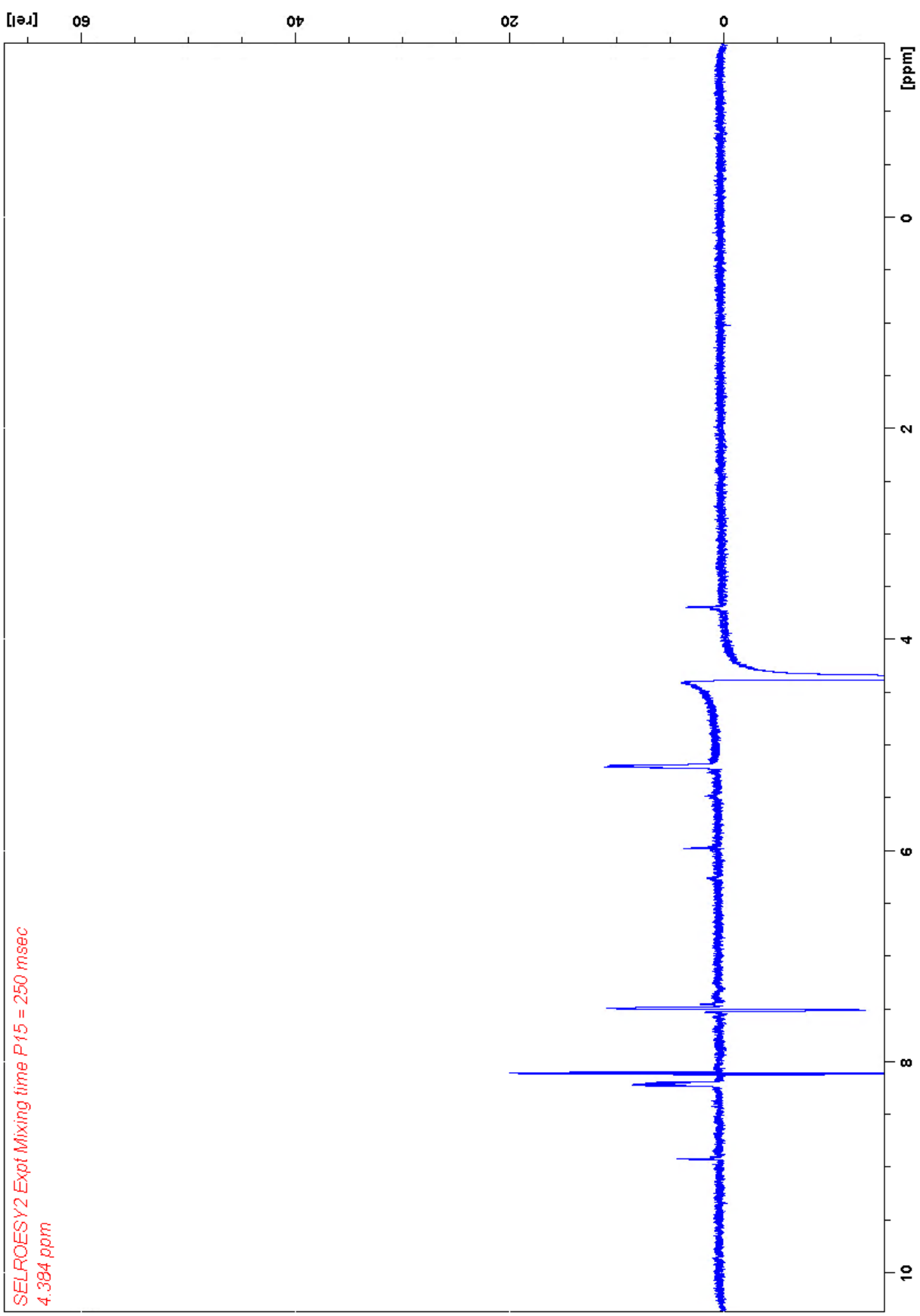
SELROESY2 Expt Mixing time P15 = 250 msec
4.384 ppm
[rel]
60
40
20
0
[ppm]
0
2
4
6
8
10

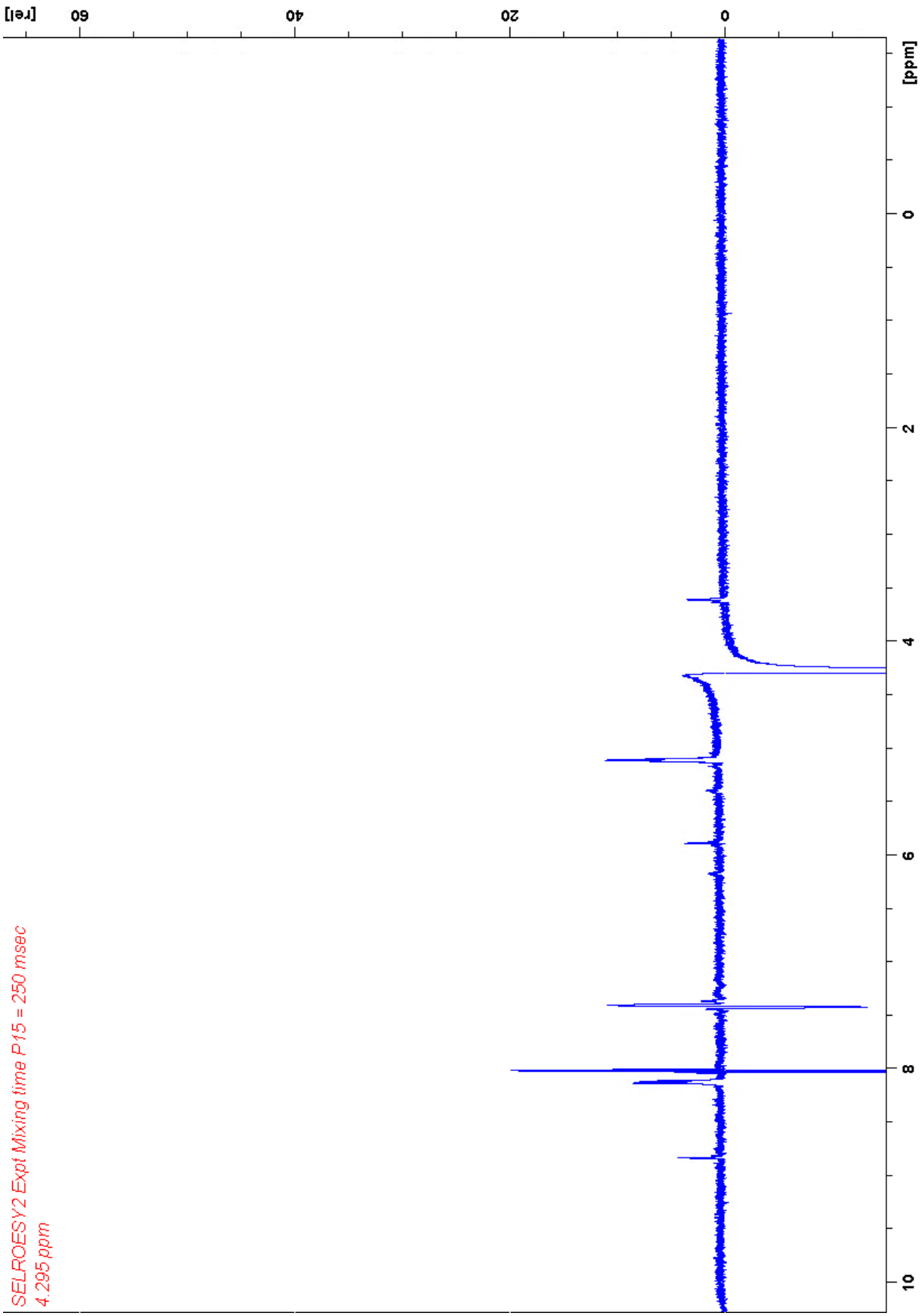
SELROESY2 Expt Mixing time P15 = 250 msec
4.295 ppm
[rel]
60
40
20
0
[ppm]
0
2
4
6
8
10

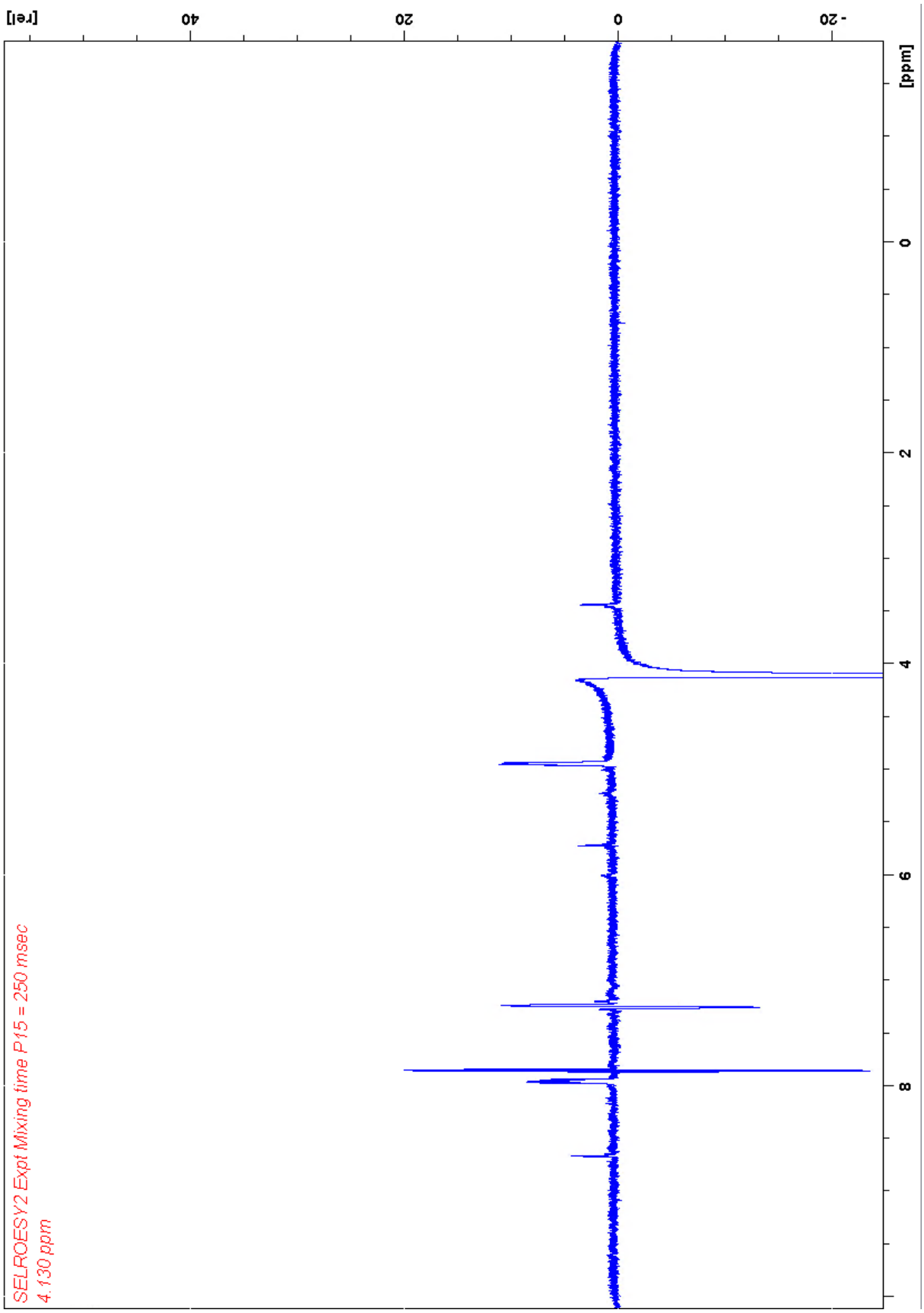
SELROESY2 Expt Mixing time P15 = 250 msec
4.130 ppm
[rel]
40
20
0
-20
[ppm]
0
2
4
6
8

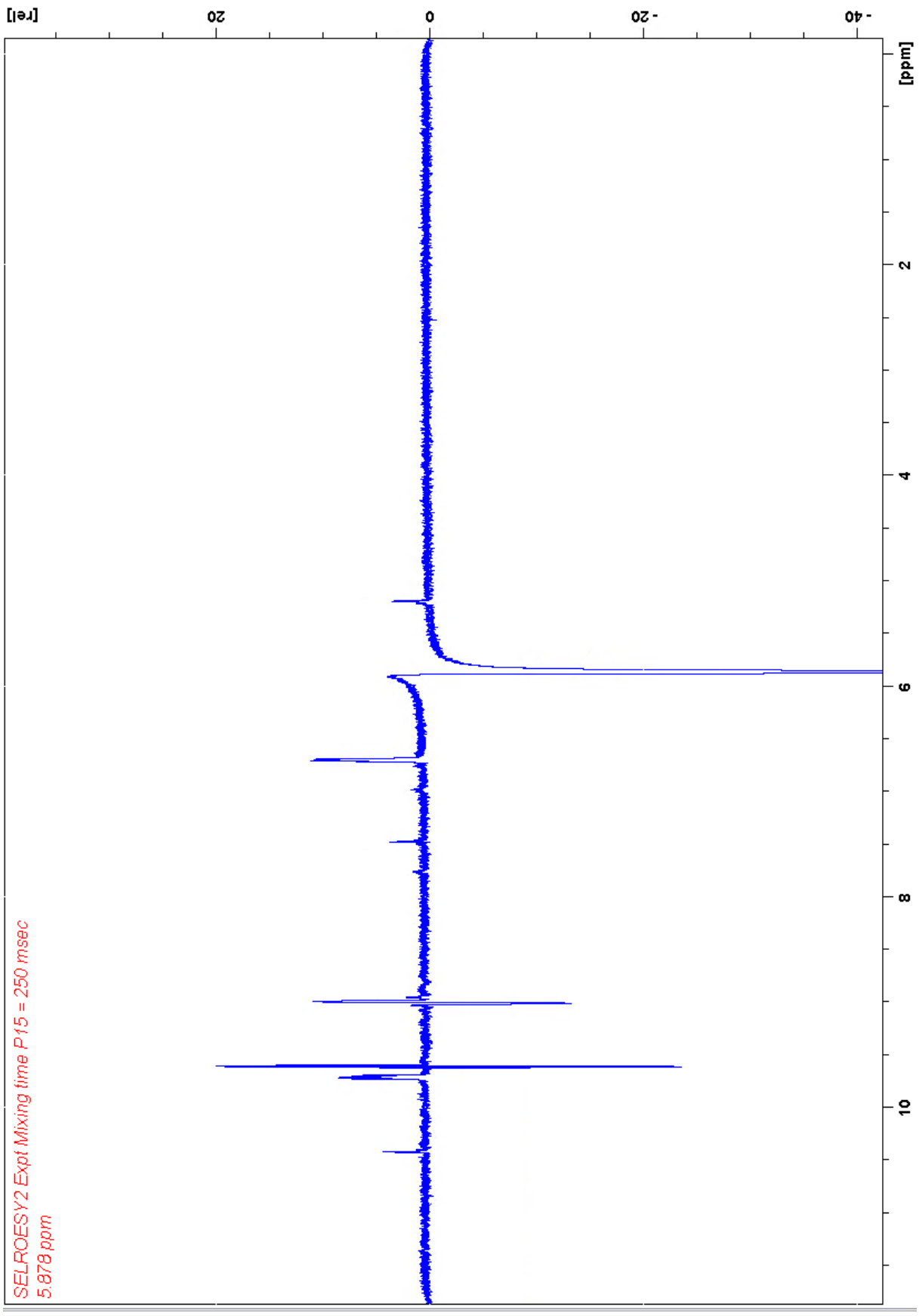
[rel]
20
0
-20
-40
[ppm]
2
4
6
8
10
SELROESY2 Expt Mixing time P15 = 250 msec
5.878 ppm

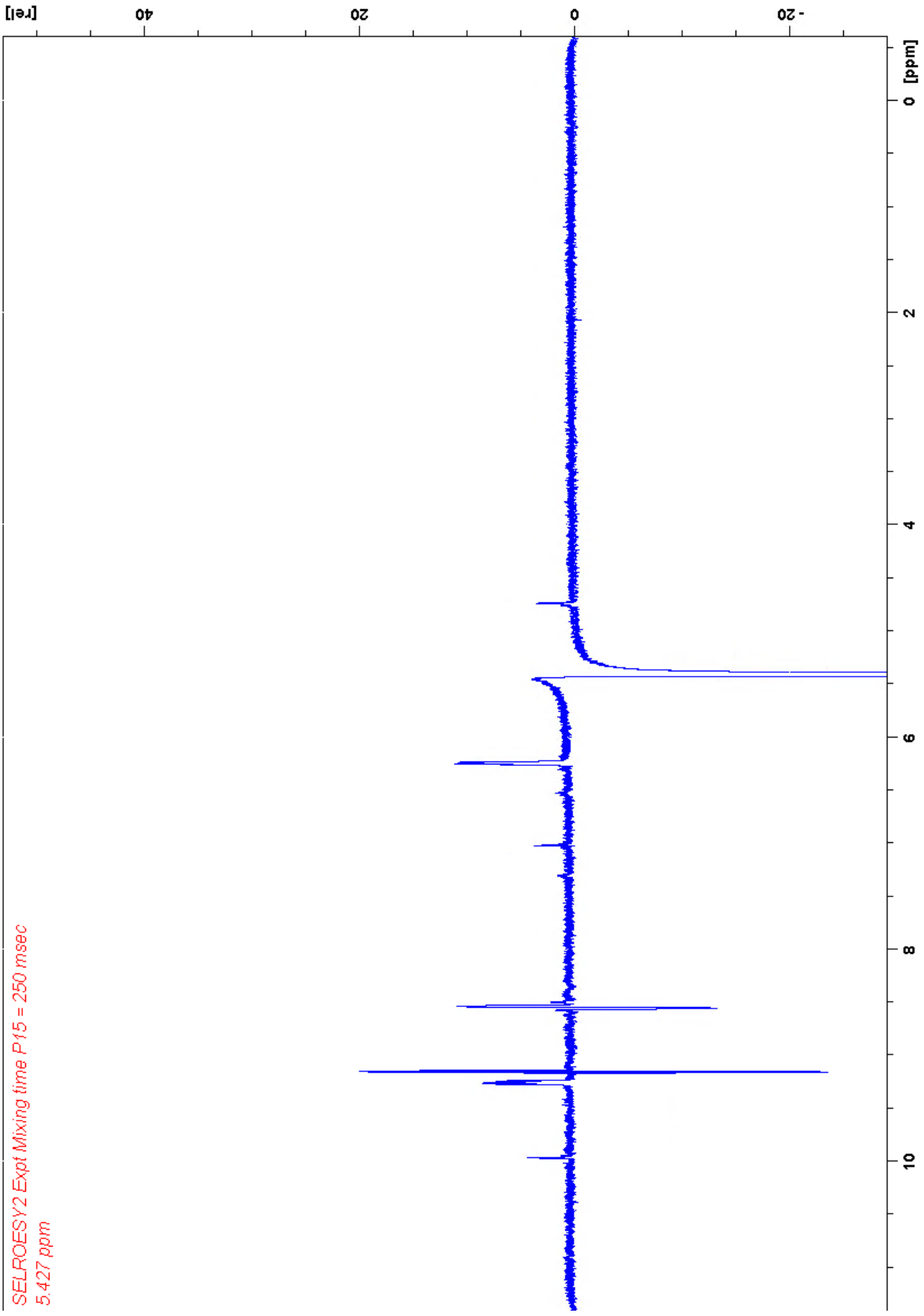
[rel]
40
20
0
-20
0 [ppm]
2
4
6
8
10
SELROESY2 Expt Mixing time P15 = 250 msec
5.427 ppm

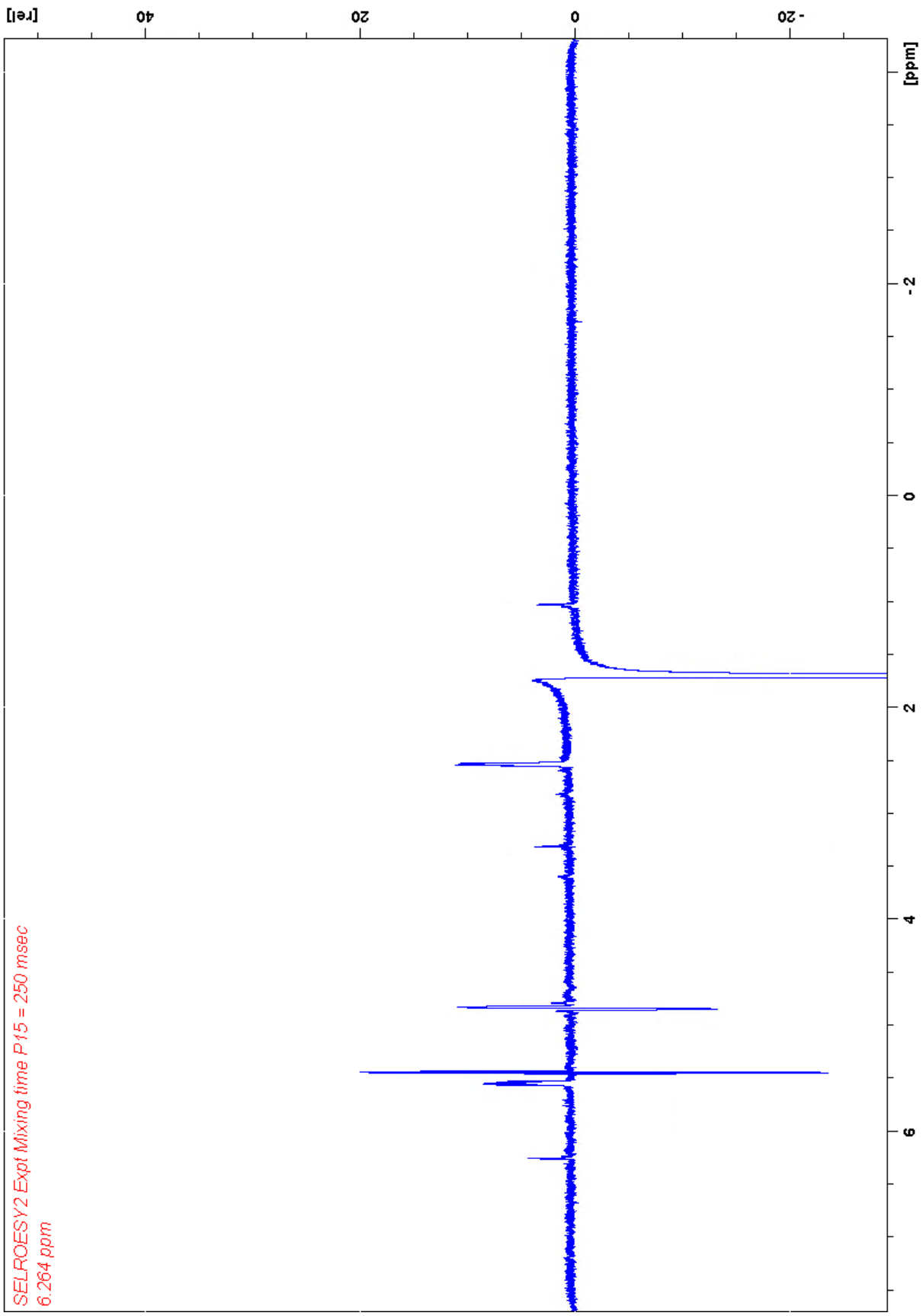
[rel]
40
20
0
-20
[ppm]
-2
0
2
4
6
SELROESY2 Expt Mixing time P15 = 250 msec
6.264 ppm

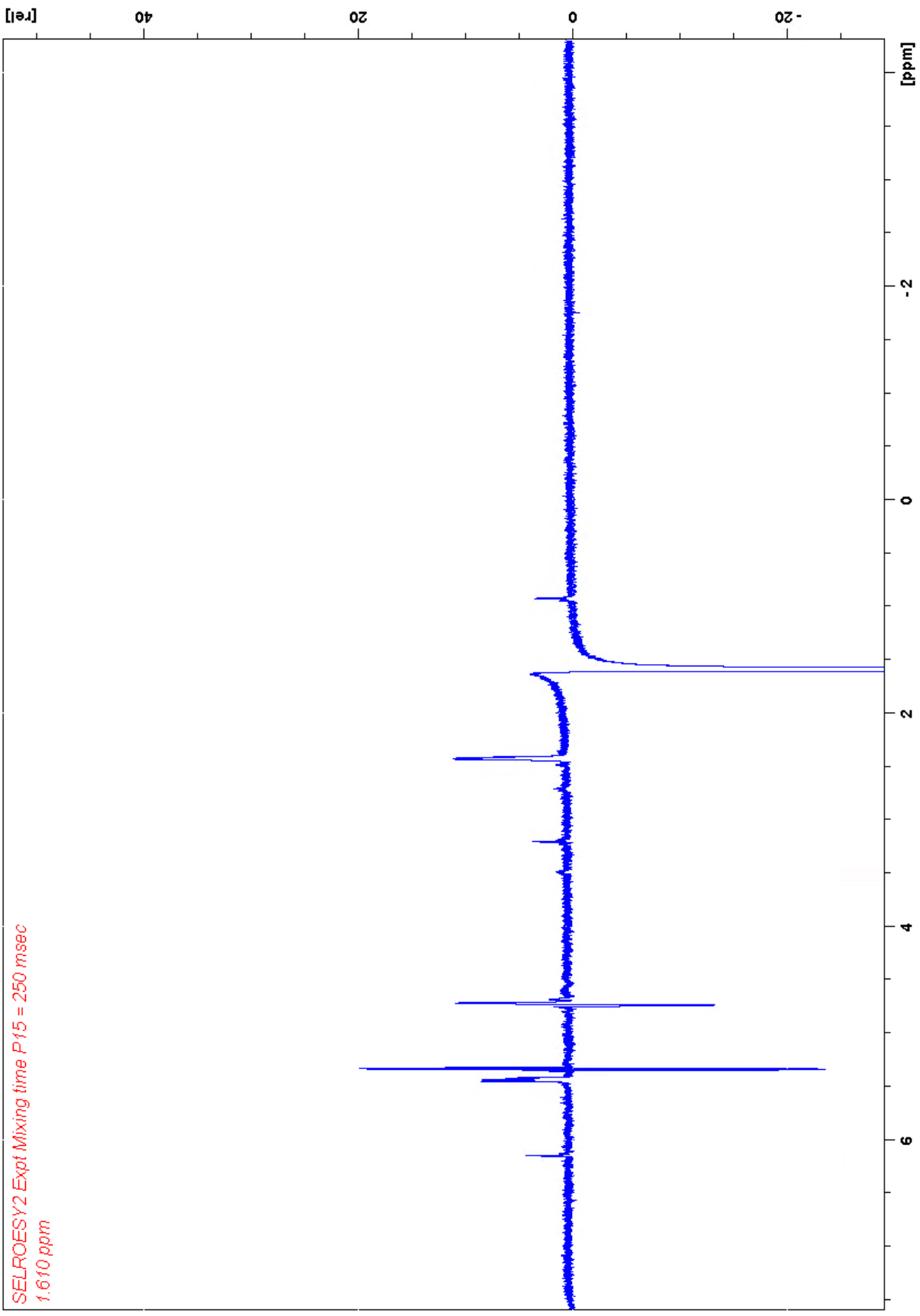
[rel]
40
20
0
-20
[ppm]
-2
0
2
4
6
SELROESY2 Expt Mixing time P15 = 250 msec
1.610 ppm

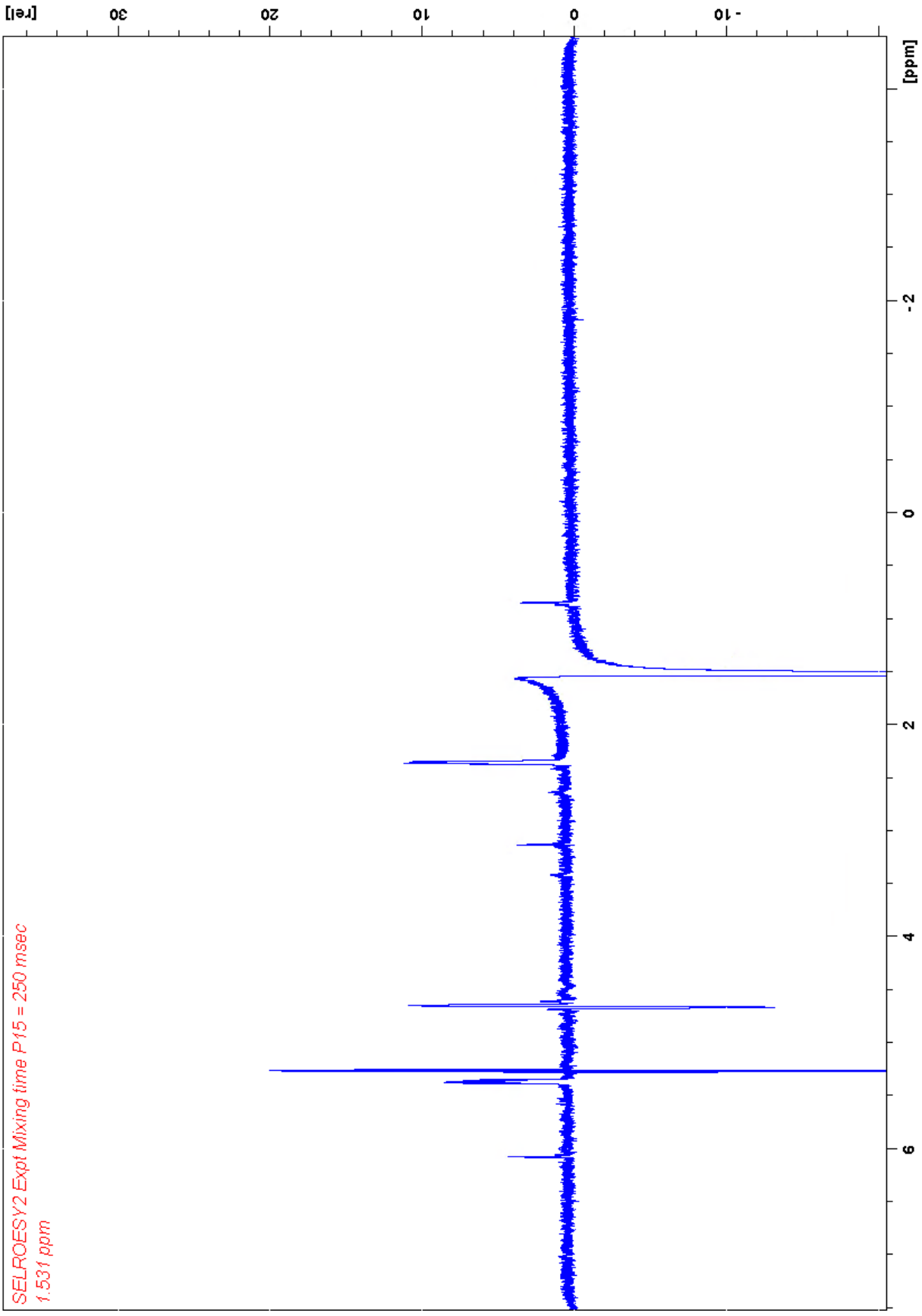
[rel]
30
20
10
0
-10
[ppm]
-2
0
2
4
6
SELROESY2 Expt Mixing time P15 = 250 msec
1.531 ppm

Appendix C – Excerpt: MS data from Miles

1	2	3	4	5	6	7	8	9	10	11	
							Formula and calculated *m/z*		Station 2		1
Amino acid origin							MC-LR		MC-LR		2
1	2	3	4	5	6	7	*m/z*	Formula	*m/z*	Difference	3
						■	84,0444	$C4H6NO^+$	84,0443	-0,0001	4
	■						68,0858	$(C5H12N^+)$-H2O	not seen		5
	■						86,0964	$C5H12N^+$	86,0963	-0,0001	6
				■			107,0855	$C8H11^+$	107,0854	-0,0001	7
			■				112,0869	$C5H10N3^+$	112,0868	-0,0001	8
■						■	127,0866	$C6H11N2O^+$	127,0865	-0,0001	9
				■			135,0804	$C9H11O^+$	135,0803	-0,0001	10
				■			135,1168	$C10H15^+$	135,1167	-0,0001	11
■						■	155,0815	C7H11N2O2+	155,0814	-0,0001	12
			■				157,1084	C6H13N4O+	157,1083	-0,0001	13
				■			163,1117	C11H15O+	163,1115	-0,0002	14
			■				174,1349	C6H16N5O+	174,1348	-0,0001	15
					■	■	213,0870	C9H13N2O4+	213,0867	-0,0003	16
■	■					■	250,1550	C13H20N3O2+	not seen		17
■	■					■	268,1656	C13H22N3O3+	268,1653	-0,0003	18
		■	■				269,1244	C11H17N4O4+	269,1247	0,0003	19
		■	■				286,1510	C11H20N5O4+	286,1505	-0,0005	20
				■	■	■	375,1914	C20H27N2O5+	375,1908	-0,0006	21
	■	■	■				364,1979	C17H26N5O4+	not seen		22
	■	■	■				382,2085	C17H28N5O5+	382,2080	-0,0005	23
■	■	■				■	379,1976	C18H27N4O5+	not seen		24
■	■	■				■	397,2082	C18H29N4O6+	397,2076	-0,0006	25
			■	■			397,2598	C23H33N4O2+	397,2575	-0,0023	26
	■	■	■				381,2245	C17H29N6O4+	not seen		27
	■	■	■				399,2350	C17H31N6O5+	399,2346	-0,0004	28
■				■	■	■	446,2286	C23H32N3O6+	446,2277	-0,0009	29
			■	■			470,3126	C26H40N5O3+	470,3118	-0,0008	30
■	■	■	■				452,2616	C20H34N7O5+	not seen		31
■	■	■	■				470,2722	C20H36N7O6+	470,2720	-0,0002	32
■	■	■	■			■	553,3093	C24H41N8O7+	553,3085	-0,0008	33
■	■	■	■			■	570,3358	C24H44N9O7+	570,3355	-0,0003	34
			■	■	■		599,3552	C31H47N6O6+	599,3546	-0,0006	35
			■	■	■	■	682,3932	C35H52N7O7+	682,3967	0,0035	36
		■	■	■	■		710,3872	C36H52N7O8+	710,3844	-0,0028	37
		■	■	■	■		728,3978	C36H54N7O9+	728,3971	-0,0007	38
■	■	■	■	■	■	■	844,4563	C40H62N9O11+	844,4568	0,0005	39

							854,4771	C42H64N9O10+	854,4765	-0,0006	40
							861,4829	C40H65N10O11+	861,4820	-0,0009	41
							866,5135	C44H68N9O9+	866,5137	0,0002	42
							866,5135	C44H68N9O9+	866,5137	0,0002	43
							995,5560	C49H75N10O10+	995,5551	-0,0009	44
									Calculated	995,5560	45